

The Regulation of Self-Renewal in Normal Human Urothelial Cells

Lisa A. Kirkwood

PhD

University of York

Department of Biology

April 2012

Abstract

The urinary tract is lined by a mitotically-quiescent, but highly regenerative epithelium, the urothelium. The mechanisms regulating urothelial regeneration are incompletely understood although autocrine stimulation of the Epidermal Growth Factor Receptor (EGFR) signalling pathway has been implicated. The hypothesis developed in this thesis is that urothelial homeostasis is regulated through resolution of interactive signal transduction networks downstream of local environmental cues, such as cell:cell contact. Here, canonical Wnt signalling was examined as a candidate key pathway due to the pivotal role of β -catenin in both nuclear transcription and intercellular adherens junctions.

Normal human urothelial (NHU) cells isolated from surgical biopsies were grown as finite cell lines in monolayer culture. mRNA analysis from proliferating cultures inferred all components for a functional autocrine-activated canonical Wnt cascade were present. In proliferating cells, β -catenin was nuclear and Axin2 expression provided an objective hallmark of β -catenin/TCF transcription factor activity. This endogenous activity was not mediated by Wnt receptor activation, as Wnt ligand was produced in inactive (non-palmitylated) form in serum-free culture, but instead β -catenin activation was driven via EGFR-mediated phosphorylation of GSK3 β and inhibition of the β -catenin destruction complex. In quiescent, contact-inhibited cultures, β -catenin was seen to re-localise to the adherens junctions and GSK3 β activity was re-established. Knock-down of β -catenin using RNA interference led to significant changes in p-ERK and p-AKT activity as well as an increase in E-cadherin protein expression. The results presented in this thesis identifies β -catenin as a central component of a bi-directional feedback loop between growth factor-mediated cell signalling and cell:cell contact and provides preliminary evidence that de-regulation of the mechanisms that control β -catenin regulation and EGFR signalling are important in neoplastic growth.

Contents

1	Introduction	21
1.1	The urinary system	21
1.2	The kidneys	22
1.2.1	The ureters	23
1.2.2	The bladder	24
1.3	The Human Urothelium	26
1.3.1	Tissue Architecture	26
1.3.2	Origins of the human urothelium	26
1.3.3	Characteristics of the urothelium <i>in situ</i>	28
1.3.4	Function of the urothelium	30
1.4	Urothelial tissue homeostasis	31
1.5	Cancer: When tissue homeostasis goes wrong	33
1.5.1	Bladder Cancer	34
1.6	Factors regulating human urothelial tissue homeostasis	38
1.6.1	Cell signalling	38
1.6.2	Cell environment	43
1.7	The canonical Wnt pathway	44
1.8	Wnt/ β -catenin signalling in the bladder	46
1.9	Urothelial cells <i>in vitro</i>	48
1.9.1	Isolation and propagation	48
1.9.2	NHU cell phenotype	48
1.9.3	NHU growth and proliferation	49
1.9.4	NHU cell differentiation	50
1.10	Thesis Aims	51

2	Materials and Methods	53
2.1	General	53
2.2	Suppliers	53
2.3	Dissection equipment, glassware and disposable plasticware.....	53
2.4	Stock solutions.....	53
2.5	Reagents.....	54
2.5.1	Antibodies.....	54
2.5.2	Agonists/Antagonists.....	54
2.6	Tissue Culture	57
2.6.1	General	57
2.6.2	Primary Urothelial Cell Culture.....	57
2.6.3	Differentiation of human urothelial cell lines	59
2.6.4	Culture of established carcinoma cell lines.....	60
2.6.5	Mycoplasma testing	62
2.6.6	Genotyping	63
2.7	Molecular Biology	64
2.7.1	General	64
2.7.2	Plasticware	65
2.7.3	Plasmids.....	65
2.7.4	Amplification of plasmid DNA.....	66
2.7.5	Molecular cloning.....	68
2.7.6	Genetic manipulation of NHU cells.....	70
2.8	Gene Expression Analysis	73
2.8.1	General	73
2.8.2	RNA Extraction	73

2.8.3	DNase treatment of RNA	74
2.8.4	RNA precipitation using sodium acetate	74
2.8.5	Reverse Transcriptase Polymerase Chain Reaction	75
2.8.6	First-strand cDNA synthesis -Reverse transcription (RT).....	75
2.8.7	Primer design for PCR	76
2.8.8	PCR primer testing.....	76
2.8.9	PCR.....	77
2.8.10	Quantitative Polymerase Chain Reaction (RTqPCR) using SYBR® - Green I technology	77
2.8.11	Primer design for qPCR	78
2.8.12	RTqPCR primer testing	78
2.8.13	RTqPCR.....	78
2.8.14	Affymetrix™ analysis.....	80
2.9	Protein Analysis.....	80
2.9.1	Indirect immunofluorescent labelling of cultured cells	80
2.9.2	Western blotting.....	82
2.10	Cell based assays	85
2.10.1	Cell viability assay.....	85
2.10.2	Luciferase Reporter assays	86
2.10.3	Flow Cytometry	92
2.11	Statistical analysis.....	92
3	Screening for components of the canonical Wnt pathway in Normal Human Urothelial cells	93
3.1	Aims	93
3.2	Experimental Design.....	94

3.3	Results	98
3.3.1	Quality control assessment	98
3.3.2	Assessment of the proliferation signature	100
3.3.3	Assessment of differentiation	102
3.3.4	Ontology analysis	106
3.3.5	In depth analysis of Wnt associated genes	111
3.3.6	RT-PCR analysis	120
3.3.7	RT-qPCR.....	123
3.4	Discussion	125
3.4.1	Analysis of the proliferative NHU culture	126
3.4.2	Comparison between quiescent and proliferating NHU cells.....	127
3.4.3	The Wnt pathway in differentiated NHU cells.....	128
4	Pharmacological activation of the Wnt canonical cascade in Normal Human Urothelial cells	130
4.1	Introduction.....	130
4.2	Hypothesis.....	131
4.3	Aim.....	131
4.4	Experimental Design	131
4.5	Results	133
4.5.1	Effect of GSK3 inhibitors on cell viability	133
4.5.2	Effect of GSK3 β inhibition on cell morphology	142
4.5.3	Effect of GSK3 β inhibition on β -catenin localisation.....	142
4.5.4	TCF transcription factor activity.....	146
4.6	Discussion	152
4.6.1	Toxicity of GSK3 inhibitors.....	152

4.6.2	β -catenin nuclear translocation	153
4.6.3	TCF activity.....	154
4.6.4	Conclusions.....	155
5	The interrelationships of different signalling mechanisms and cell:cell contact in modulating urothelial tissue homeostasis	156
5.1	Rationale	156
5.2	Wnt-independent β -catenin activation:The role of pathway crosstalk.	158
5.2.1	Signalling Crosstalk.....	158
5.2.2	Crosstalk with the Wnt pathway	158
5.2.3	GSK-dependent crosstalk mechanisms	158
5.2.4	GSK-independent crosstalk mechanisms.....	159
5.2.5	Rationale	159
5.2.6	Hypothesis.....	159
5.2.7	Aim	159
5.2.8	Objectives.....	160
5.2.9	Experimental Design (Objective 1).....	160
5.2.10	Results (Objective 1).....	163
5.2.11	Summary	180
5.2.12	Experimental design (Objective 2)	181
5.2.13	Results	183
5.2.14	Summary	194
5.3	The role of cell:cell contacts in modulating β -catenin activity.....	195
5.3.1	Cell:cell interactions.....	195
5.3.2	β -catenin sequestration at the adherens junction	198
5.3.3	Rationale	200

5.3.4	Hypothesis.....	200
5.3.5	Aim	200
5.3.6	Objectives.....	200
5.3.7	Experimental design.....	201
5.3.8	Results	202
5.3.9	Summary	214
5.4	The role of β -catenin signalling in NHU cell proliferation	214
5.4.1	Rationale	214
5.4.2	Aim	214
5.4.3	Objectives.....	214
5.4.4	Experimental design.....	215
5.4.5	Results	217
5.5	Discussion	231
5.5.1	Wnt-independent β -catenin activation via signalling crosstalk	231
5.5.2	The role of cell:cell contact.....	233
5.5.3	The role of β -catenin in NHU proliferation	234
6	Wnt ligand activation of the canonical Wnt cascade in NHU cells.....	238
6.1	Introduction.....	238
6.1.1	Wnt ligand	238
6.1.2	Processing of Wnt ligand	238
6.1.3	Secretion of Wnt ligand	239
6.1.4	Receptor binding and activation	239
6.2	Rationale	243
6.3	Aims	243
6.4	Experimental Plan.....	244

6.4.1	Wnt ligand choice	244
6.4.2	Verification of Wnt secreting L-cell lines	244
6.4.3	Assessing the effect of exogenous Wnt ligand on NHU cells	245
6.4.4	Assessing the impact of low serum concentrations on the production of active Wnt ligand	245
6.4.5	Assessing the effect of palmitic acid on the production of active Wnt ligand	246
6.4.6	Assessing the production of Wnt ligand in NHU cells.....	246
6.4.7	Assessing NHU autocrine response to Wnt ligand	247
6.5	Results	248
6.5.1	Verification of Wnt secreting L-cells	248
6.5.2	Testing CM from L Wnt-3a and L Wnt 5a cells on SaOS-2 cells ..	248
6.5.3	Effect of adding exogenous Wnt 3a and Wnt 5a ligand to NHU cells	254
6.5.4	The effect of reduced serum on the production and secretion of Wnt ligand	259
6.5.5	The role of palmitic acid in the production and secretion of Wnt Ligand.....	262
6.5.6	Assessing the production of Wnt ligand in NHU cells.....	269
6.5.7	Autocrine Wnt signalling	275
6.6	Discussion	277
6.6.1	Response to exogenous Wnt ligand	277
6.6.2	The role of serum in the processing and secretion of Wnt ligand	277
6.6.3	Secretion of Wnt ligand from urothelial cells	278
6.6.4	Autocrine Wnt signalling in NHU cells.....	279
6.6.5	Further work	279

7 Thesis overview and conclusions	280
7.1 Concluding Remarks	286
Appendix I.....	288
List of Suppliers	288
Appendix II.....	290
Stock solutions.....	290
Appendix III	293
Y-Number Tissue Information.....	293
Appendix IV.....	294
Genotyping.....	294
Appendix V	298
Primers	298
Appendix VI.....	299
Dissociation curves.....	299
Appendix VII.....	303
FACS analysis	303
Appendix VIII	309
TOPFLASH/FOPFLASH promoter sequence	309
Appendix IX.....	310
Western blots	310
Appendix X.....	311
β -catenin shRNA sequence.....	311
Appendix XI.....	312
Verification of the β -Catenin shRNA pSIREN RetroQ retroviral vector	312
Appendix XII.....	313

β-catenin expression in NHU cultured in physiological calcium and PD153035	313
Glossary	315
Bibliography.....	319

Figures

Figure 1-1 Schematic representation of the human urinary system	21
Figure 1-2 Schematical representation of a Nephron	22
Figure 1-3 Cross-section through a Normal Human Ureter	23
Figure 1-4 Schematical representation of the human bladder and urethra	25
Figure 1-5 Schematic representation and actual cross-section through Normal Human Urothelium	27
Figure 1-6 Structure of the uroplakin proteins	29
Figure 1-7 Schematic illustrating the link between dysregulated tissue homeostasis and cancer progression	33
Figure 1-8 The 20 most commonly diagnosed human cancers in the UK.....	34
Figure 1-9 Schematic illustrating autocrine, juxtacrine and paracrine signalling	38
Figure 1-10 EGFR signalling pathways	42
Figure 1-11 Schematic illustrating the canonical Wnt pathway	45
Figure 1-12 Phase-contrast micrograph of NHU cells in culture.....	49
Figure 2-1 pSIREN RetroQ plasmid.....	71
Figure 2-2 TOPFLASH/FOPFLASH vectors.....	87
Figure 2-3 pRL-CMV reporter construct.....	88
Figure 2-4 Dual Luciferase reporter assay	91
Figure 3-1 Schematic representing the experimental design for the microarray time course experiment.....	95
Figure 3-2 Cell cycle and associated proliferation marker gene expression	96
Figure 3-3 Spiked hybridisation controls.....	99
Figure 3-4 Affymetrix array analysis box and whisker plots	100
Figure 3-5 Expression of proliferation markers.....	101
Figure 3-6 Expression of urothelial differentiation- associated markers.....	104
Figure 3-7 Ontologies of genes up- and down-regulated in quiescent NHU cells compared to proliferating NHU cells <i>in vitro</i>	108
Figure 3-8 Ontologies of genes up- and down-regulated in TZ/PD treated NHU cells compared to proliferating NHU cells <i>in vitro</i>	109

Figure 3-9 Ontologies of genes up- and down-regulated in ABS/Ca ²⁺ treated NHU cells compared to proliferating NHU cells <i>in vitro</i>	110
Figure 3-10 Schematical representation of the components present from the canonical Wnt cascade in proliferating NHU cells	112
Figure 3-11 Schematical representation of the gene changes within the canonical Wnt pathway in quiescent NHU cells	113
Figure 3-12 Schematical representation of the gene changes within the canonical Wnt pathway in TZ/PD differentiated cultures	115
Figure 3-13 Schematical representation of the gene changes within the canonical Wnt pathway in ABS/Ca ²⁺ differentiated cultures.....	116
Figure 3-14 mRNA expression of Wnt signalling components in NHU cells <i>in vitro</i> and <i>in vivo</i>	121
Figure 3-15 mRNA expression of Wnt components in proliferative, quiescent and differentiated NHU cultures	124
Figure 4-1 Effect of SB415286 on SaOS-2 cell viability.....	134
Figure 4-2 SaOS-2 dose response curve to SB415286.....	135
Figure 4-3 Effect of SB415286 on NHU cell viability.....	136
Figure 4-4 NHU dose response curve to SB415286.....	137
Figure 4-5 Effect of LiCl on NHU cell viability	138
Figure 4-6 NHU dose response curve to LiCl.....	139
Figure 4-7 Effect of LiCl on SaOS-2 cell viability	140
Figure 4-8 SaOS-2 dose response curve to LiCl.....	141
Figure 4-9 Effect of GSK3 inhibitors on cell morphology of SaOS-2 and NHU cells <i>in vitro</i>	143
Figure 4-10 Expression and localisation of β -catenin after GSK3 β inhibition in SaOS-2 and NHU cells <i>in vitro</i>	144
Figure 4-11 Nuclear translocation of β -catenin in SaOS-2 and NHU cells after GSK3 inhibition	145
Figure 4-12 TCF transcription factor activity in SaOS-2 cells after GSK3 inhibition	147

Figure 4-13 TCF transcription factor activity in NHU cells after GSK3 inhibition	148
Figure 5-1 Experimental design used to assess potential EGFR and β -catenin crosstalk.....	162
Figure 5-2 Expression and localisation of β -catenin in NHU cells	164
Figure 5-3 Expression and localisation of β -catenin when NHU cells were cultured without exogenous rhEGF.....	165
Figure 5-4 Quantification of nuclear and cytoplasmic active β -catenin over 72 hours in normal growth medium (KSFMc) and without exogenous rhEGF.....	166
Figure 5-5 Wnt-independent expression of β -catenin via inhibition of GSK3 β	167
Figure 5-6 Expression and localisation of active β -catenin in NHU cells after EGFR tyrosine kinase inhibition	169
Figure 5-7 Quantification of nuclear and cytoplasmic active β -catenin in NHU cells when cultured with EGFR tyrosine kinase inhibitor	170
Figure 5-8 Effect of EGFR tyrosine kinase inhibition on expression of Wnt signalling components	171
Figure 5-9 Expression and sub-cellular location of active β -catenin after MEK1/MEK2 inhibition.....	173
Figure 5-10 Effect of MEK1/MEK2 inhibition on components of the Wnt signalling pathway.....	174
Figure 5-11 Expression and localisation of active β -catenin in NHU after treatment with LY294002	176
Figure 5-12 Effect of PI3K inhibition on components of the Wnt signalling pathway	177
Figure 5-13 Effect of EGF signalling on β -catenin/TCF mediated transcription	179
Figure 5-14 Experimental design to assess the effect of combined EGF and GSK3 inhibition on β -catenin signalling	182
Figure 5-15 Effect of combined EGFR and GSK3 inhibition on morphology	184
Figure 5-16 The effect of combined GSK3 and EGFR pathway inhibition on active β -catenin localisation.....	186

Figure 5-17 Quantification of nuclear active β -catenin in NHU cells treated with combined EGFR signalling and GSK3 inhibitors	187
Figure 5-18 Effect of combined EGFR and GSK3 inhibition on NHU cell viability	189
Figure 5-19 Effect of combined MEK1/MEK2 and GSK3 inhibition on NHU cell viability	190
Figure 5-20 Effect of combined PI3K and GSK3 inhibition on NHU cell viability	191
Figure 5-21 TCF transcription factor activity after co-treatment with EGFR signalling and GSK3 inhibitors.....	193
Figure 5-22 Cell:cell junctions.....	195
Figure 5-23 Schematic representation of an adherens junction between two adjacent cells.....	198
Figure 5-24 Expression and localisation of β -catenin in NHU cells over time when seeded at low plating density.....	203
Figure 5-25 Quantification of nuclear and cytoplasmic active β -catenin in NHU cells over time when seeded at low density.....	204
Figure 5-26 Expression and localisation of β -catenin in NHU cells over time when seeded at high plating density.....	205
Figure 5-27 Quantification of nuclear and cytoplasmic active β -catenin in NHU cells over time when seeded at high plating density.....	206
Figure 5-28 Expression and localisation of β -catenin in NHU cells over a 72 hour time course in KSFMc supplemented with physiological calcium.....	208
Figure 5-29 Quantification of nuclear and cytoplasmic active β -catenin in NHU cells over time when cultured in KSFMc supplemented with physiological calcium concentrations.....	209
Figure 5-30 Effect of calcium on components of the Wnt signalling pathway.	210
Figure 5-31 Effect of adherens junction formation on β -catenin/TCF-mediated transcription	212
Figure 5-32 Morphological characteristics of β -catenin knock-down cells after antibiotic selection.....	218

Figure 5-33 Effect of β -catenin shRNA on β -catenin protein expression and localisation in HU cells	220
Figure 5-34 Effect of β -catenin knock –down on NHU cell viability	221
Figure 5-35 Effect of β -catenin knock-down on the localisation of P-ERK and P-AKT in human urothelial cells.....	223
Figure 5-36 Effect of β -catenin knock-down on the expression of P-ERK, P-AKT and E-cadherin in human urothelial cells.....	224
Figure 5-37 Effect of β -catenin knock-down on the localisation of P-ERK and P-AKT in human urothelial cells when cultured in 2mM CaCl_2	225
Figure 5-38 Effect of EGFR tyrosine kinase inhibition on the viability of human urothelial with reduced β -catenin expression	227
Figure 5-39 Effect of MEK1/MEK2 inhibition on the viability of human urothelial cells with reduced β -catenin expression	228
Figure 5-40 Effect of PI3K inhibition on the viability of human urothelial cells with reduced β -catenin expression	229
Figure 5-41 Effect of EGFR, MAPK and PI3K inhibitors on the viable biomass of β CATKD cells	230
Figure 5-42 β -catenin and EGFR/MAPK crosstalk.....	232
Figure 5-43 A schematic diagram summarising the proposed positive feedback loop between Wnt and ERK signalling.....	236
Figure 5-44 Schematic illustrating the potential role of signalling crosstalk and cell:cell contact in modulating NHU cell proliferation.....	237
Figure 6-1 The three domains of Fzd and the approximate binding sites for Wnt and Dsh	240
Figure 6-2 Activation and inhibition of the canonical Wnt pathway by Wnt 5a	241
Figure 6-3 Cross contamination analysis of Wnt secreting L-cells using RT-PCR	250
Figure 6-4 Effect of L Wnt-3a and L Wnt-5a CM on SaOS-2 cell morphology .	251
Figure 6-5 Effect of L Wnt-3a and L Wnt-5a CM on β -catenin expression and localisation in SaOS-2 cells	252

Figure 6-6 TCF activity in SaOS-2 cells after treatment with L Wnt 3a or L Wnt-5a CM	253
Figure 6-7 Effect of Wnt 3a and Wnt5a CM on NHU cell morphology.....	256
Figure 6-8 Effect of Wnt 3a and Wnt5a CM on β -catenin expression and localisation in EGF responsive and EGFR blocked NHU cells.....	257
Figure 6-9 TCF activity in EGF responsive and EGFR blocked NHU cells after treatment with L Wnt 3a and L Wnt-5a CM	258
Figure 6-10 Effect of culturing Wnt secreting L-cells in low serum.....	260
Figure 6-11 TCF assay from SaOS-2 cells after treatment with CM from L-cells grown in low serum	261
Figure 6-12 Assessing the effect of palmitic acid on Wnt ligand production...	263
Figure 6-13 Normalised densitometry from western blots assessing the effect of palmitic acid on Wnt ligand production	264
Figure 6-14 Assessing activation of the canonical Wnt pathway in SaOS-2 cells after treatment with CM from L Wnt 3a 1% cells cultured in the presence of palmitic acid	266
Figure 6-15 Assessing activation of the canonical Wnt pathway in SaOS-2 cells after treatment with CM from L Wnt 3a 1% cells cultured in the presence of palmitic acid	267
Figure 6-16 Assessing TCF activity in SaOS-2 cells after treatment with CM from L Wnt 3a 1% cells cultured in the presence of palmitic acid	268
Figure 6-17 Morphology of NHU cells after a 3-day incubation in KSFMc supplemented with palmitic acid	271
Figure 6-18 Assessing the production of Wnt ligand in NHU cells	272
Figure 6-19 Assessing Wnt ligand production in NHU cells	274
Figure 6-20 Assessing autocrine Wnt signalling in NHU cells.....	276
Figure 7-1 The role of β -catenin in NHU proliferation.....	287

Tables

Table 1-1 UC grading using the 1973 WHO classification system	36
Table 1-2 UC grading using the 2004 WHO/ISUP classification system	36
Table 1-3 Staging of a urothelial primary tumour using the WHO 2002 TNM staging system.....	37
Table 2-1 Primary antibodies	55
Table 2-2 Secondary antibodies	56
Table 2-3 Agonists/Antagonists.....	56
Table 2-4 Plasmids	65
Table 3-1 Affymetrix internal controls	99
Table 3-2 Ranking non-differentiated NHU cultures according to expression of proliferation markers	102
Table 3-3 Ranking TZ/PD treated NHU cultures over time according to their expression of urothelial markers of terminal differentiation	105
Table 3-4 Ranking ABS/Ca ²⁺ treated NHU cultures over time according to their expression of urothelial markers of terminal differentiation	105
Table 3-5 Number of Wnt related genes up- and down-regulated in quiescent and differentiated NHU cultures compared to proliferating NHU cell cultures.	107
Table 3-6 Summary of Affymetrix™ microarray results for changes in the canonical Wnt pathway	119
Table 3-8 Summary of Affymetrix™ microarray and RT-PCR results for changes in the canonical Wnt pathway	122
Table 4-1 Potential transcription factor binding sites within the TCF promoter of TOPFLASH.....	150
Table 4-2 Potential transcription factor binding sites within the mutant TCF promoter of FOPFLASH	151
Table 6-1 Human Wnt genes	242
Table 6-2 Genes necessary for production of functional Wnt ligand.....	269

Acknowledgements

I would firstly like to thank my supervisors, Professor Jennifer Southgate at the University of York and Dr Nikolaos Georgopoulos from the University of Huddersfield, for their advice, guidance and support throughout this project. Thanks also go to members of my training committee, Drs Paul Genever and Marjan van der Woude for their helpful advice. Thanks must also go to my colleagues at the Jack Birch Unit for Molecular Carcinogenesis and throughout the Department of Biology for their technical assistance, encouragement, and above all, friendship.

I would also like to thank my family and friends, especially my husband, William Kirkwood, and father, Derek Clements, for their love, support and patience during the preparation of this thesis and throughout my University studies.

Finally, I would like to acknowledge York Against Cancer (YAC) for their funding.

Authors Declaration

The candidate confirms that the work submitted is her own and that appropriate credit has been given where reference has been made to the work of others.

1 Introduction

1.1 The urinary system

The urinary system secretes and excretes the nitrogenous waste products of metabolism and regulates the amount of water in our bodies. In mammals, this system consists of two kidneys, two ureters, a bladder and a urethra (Figure 1-1) (1).

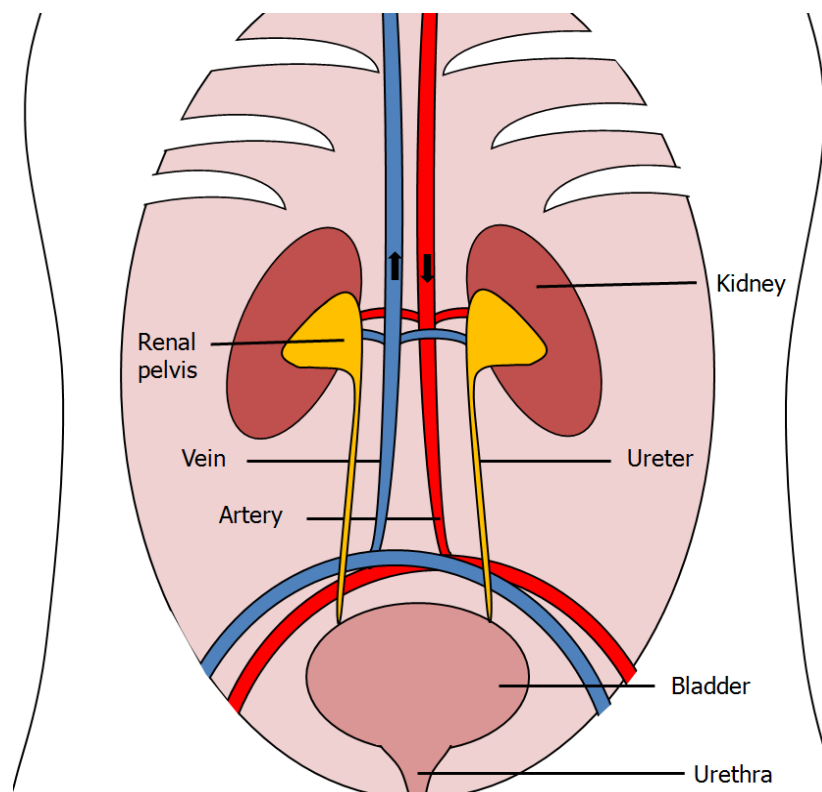


Figure 1-1 Schematic representation of the human urinary system

Schematic of the human urinary system depicting kidneys, ureter, bladder and urethra.

1.2 The kidneys

In the functional unit of the kidney, the nephron, blood is filtered under high pressure into an ultra-filtrate via the highly permeable glomerular capillaries. This process of glomerular filtration removes water, excess solutes, glucose and urea, the main nitrogenous waste product of amino acid deamination and the ornithine cycle, from the blood. The filtrate passes along the renal tubules where active re-absorption of glucose and sodium ions occurs prior to passive reabsorption of water in the loop of Henlé. Active secretion of unwanted ions is undertaken in the distal convoluted tubule, before a final cycle of passive water reabsorption in the collecting ducts (renal papillary ducts) and transport to the bladder via the ureters (Figure 1-2) (1).

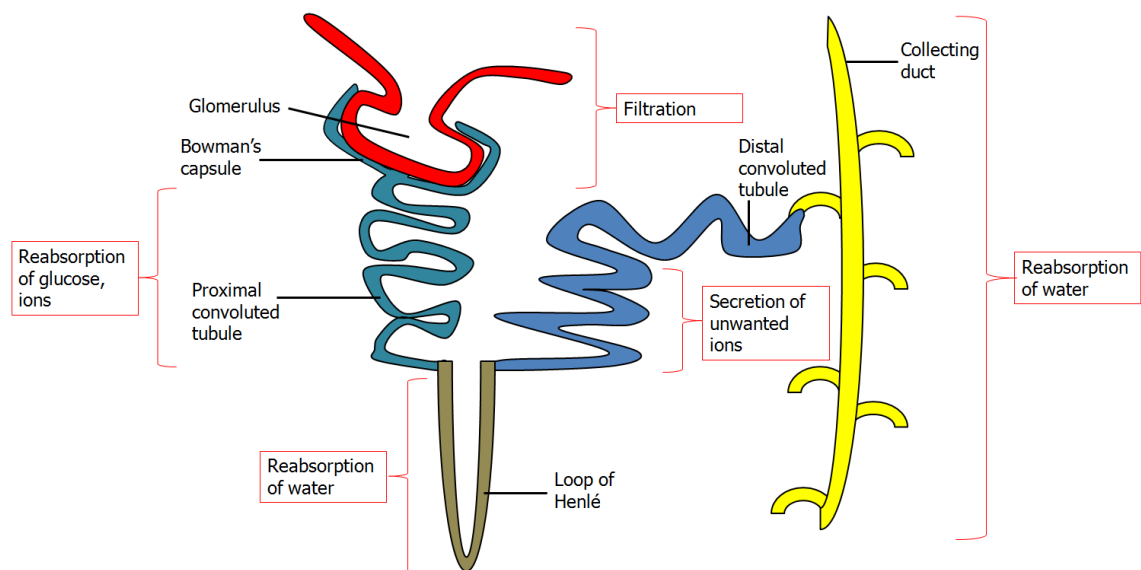


Figure 1-2 Schematical representation of a Nephron

Illustration depicting the functional unit of the kidney, the nephron, where filtration, passive and active reabsorption and secretion occur to produce urine.

1.2.1 The ureters

Urine leaves the kidneys via the collecting ducts and enters the renal pelvis and ureters. The ureters transport urine by peristalsis from the kidneys to the bladder via the ureterovesical junction. In adult humans, the ureters are approximately 25-30cm in length, 3-5mm in diameter and when analysed cross-sectionally can be divided into three layers: fibrous connective tissue (adventitia), smooth muscle (muscularis) and urothelium. On the luminal surface of the urothelium, specialised hinged plaques known as asymmetric unit membrane can be found (Figure 1-3; reviewed in section 1.3).

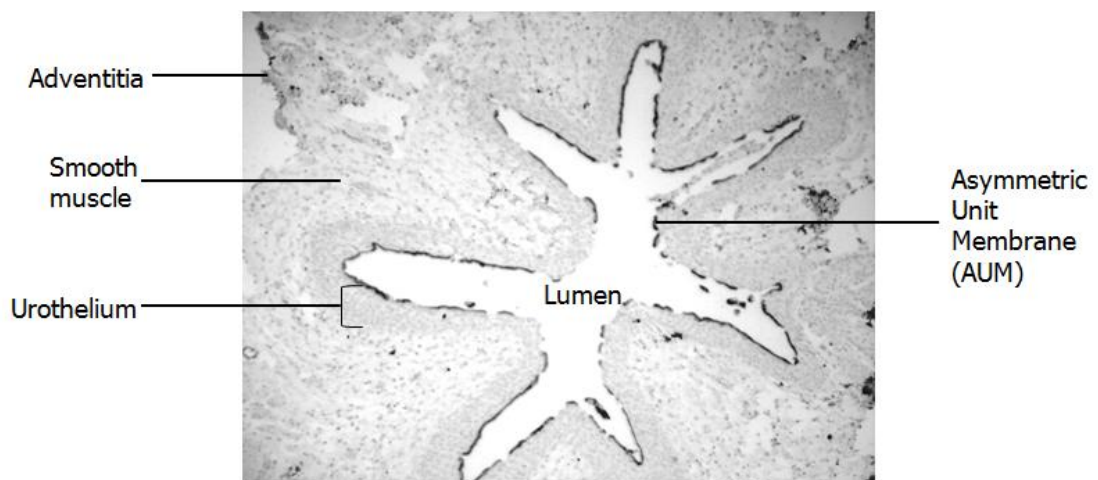


Figure 1-3 Cross-section through a Normal Human Ureter

Tissue section through a normal human ureter. Three morphologically distinct layers can be observed: adventitia (fibrous connective tissue), smooth muscle and urothelium. Tissue section has been immunolabelled with anti-asymmetric unit membrane (AUM) antibody (AU1) to highlight the specialised plaques found on the luminal surface of the urothelium and counterstained with haematoxylin to illustrate tissue architecture. Micrograph taken by L. A. Kirkwood (unpublished data).

1.2.2 The bladder

The main role of the urinary bladder is to store urine at low pressure (and thus avoid reflux back to the kidneys), as well as maintain urine composition prior to excretion via the urethra.

The adult human bladder can accommodate up to 500ml of urine and may fill and void several times a day. Successful micturition is dependent on a coordinated response between the bladder and the smooth muscle of the bladder neck and urethra (2). As the bladder fills and distends, stretch receptors excite sacral parasympathetic nerve fibres and results in detrusor muscle fibre contraction, while concurrently inhibiting somatic motor neurones supplying the external sphincter of the urethra. This increase in internal bladder pressure and external sphincter relaxation leads to urine release via the urethra (3).

Cross-sectionally, the bladder can be divided into several layers which are depicted in Figure 1-4. The bladder wall (also known as the peritoneum) covers the outer surface of bladder, inside this is the muscularis detrusor which is composed of smooth muscle bundles, the lamina propria or stroma; a layer of connective tissue containing blood and nerves in a collagen matrix, the basement membrane, and then, lining the lumen, a transitional epithelium known as the urothelium can be found (Figure 1-4) (1).

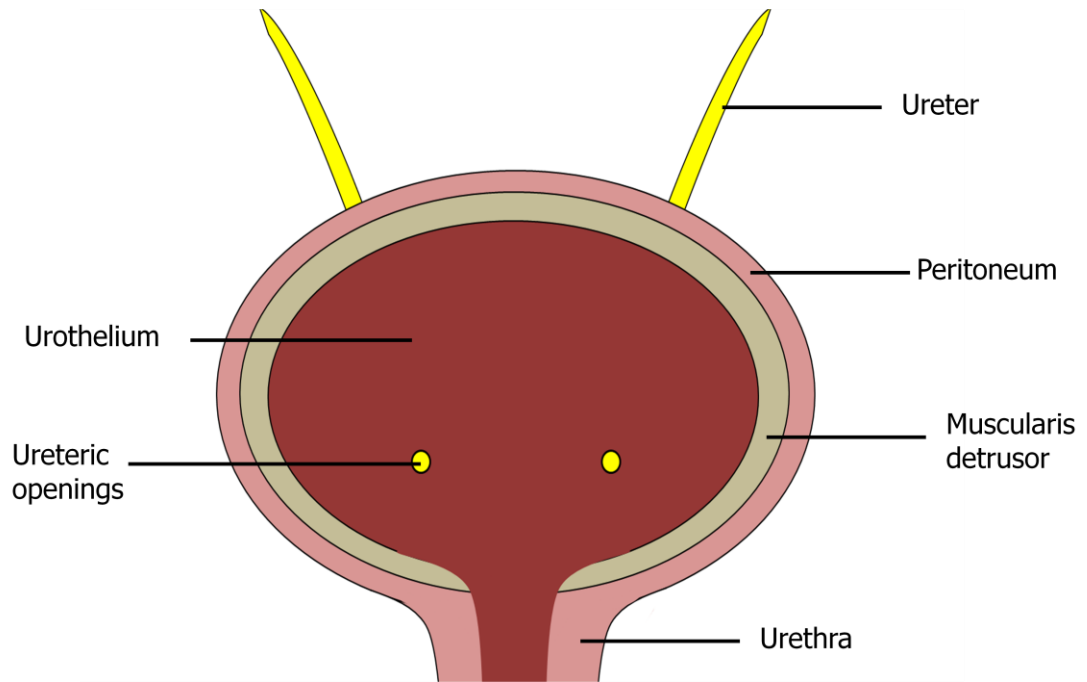


Figure 1-4 Schematical representation of the human bladder and urethra

Illustration depicting multiple layers of muscle and connective tissue within the human bladder. Lining the lumen is a transitional epithelium known as the urothelium.

1.3 The Human Urothelium

1.3.1 Tissue Architecture

Urothelium lines the majority of the lower urinary tract, including the renal pelvis, ureters, bladder and proximal urethra. Cross-sections through this tissue reveal it is multilayered and stratified into discrete cell layers which “transition” between simple columnar through to stratified squamous epithelia and can be divided into three distinct zones: basal, intermediate and superficial (4) (Figure 1-5). These morphologically-distinct layers increase in specialisation from basal through to the highly specialised superficial cells which line the luminal surface (4). The basal cell layer is composed of a single layer of small cuboidal cells which are anchored in place via a basement membrane to the lamina propria. On top of these, lies a layer 1-4 cells thick, of larger, polygonal shaped intermediate cells and then, towards the luminal surface, the terminally differentiated, large and often binucleate superficial cells reside which are characterised by “scallop-like” rigid plaques known as asymmetric unit membrane (AUM) (4, 5).

1.3.2 Origins of the human urothelium

The urothelium is unusual in that it develops from both embryological mesoderm and endoderm. Urothelium that lines the renal pelvis, ureters and bladder trigone develops in conjunction with the kidneys and is derived from mesoderm. The urothelium of the bladder and proximal urethra develop from the urogenital sinus and are derived from endoderm (reviewed by (6)). Although the urothelium that lines the bladder and bladder trigone evolve from two different lineages, morphologically they appear to be identical (4).

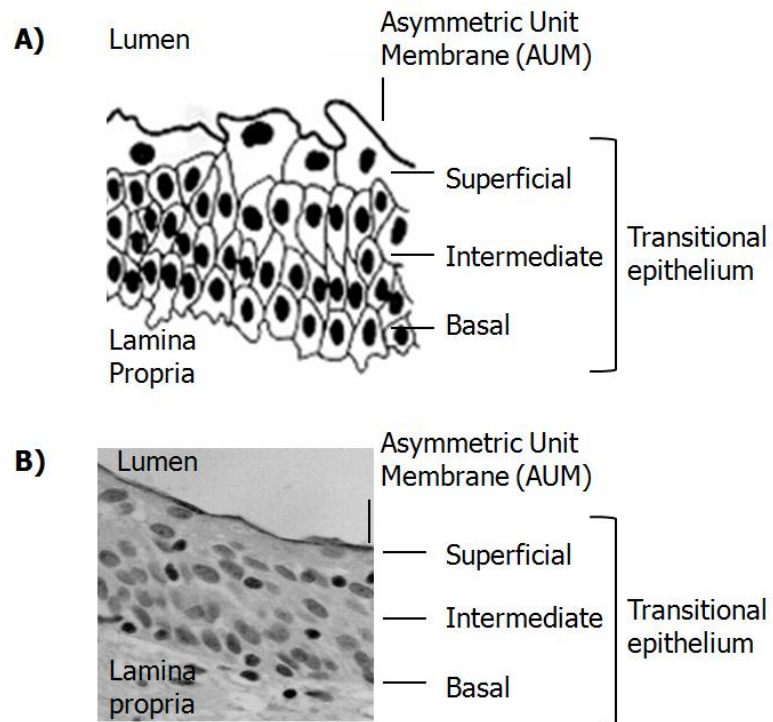


Figure 1-5 Schematic representation and actual cross-section through Normal Human Urothelium

Illustration depicting a cross-section through normal human urothelium (A; adapted from (7)) and a tissue section of human bladder immunolabelled with anti-AUM antibody and counterstained with haematoxylin to illustrate tissue architecture (B). Micrograph taken by L. A. Kirkwood (unpublished data).

1.3.3 Characteristics of the urothelium *in situ*

1.3.3.1 Uroplakin (UPK) expression

Uroplakins (UPK) are highly conserved glycoproteins which were first isolated from the bovine urothelium and identified as important transcriptional targets of urothelial differentiation by T.T Sun and colleagues in the 1990s (8-11). In humans, five uroplakin proteins have been cloned (UPK1a, UPK1b, UPK2, UPK3a and UPK3b) (12, 13). UPK1a, UPK2 and UPK3a/b have been shown to be expressed only by the specialised superficial cells of the urothelium making them ideal markers of terminal differentiation (14). UPK1b is less differentiation-specific and is expressed by the intermediate cells of the urothelium, as well as by several other human tissues (12, 14). Genetically and structurally, uroplakins can be split into two groups: UPK1a and UPK1b are members of the tetraspanin family of transmembrane proteins, whereas UPK2, UPK3a and UPK3b are single transmembrane-domain proteins (Figure 1-6 (10)). In the cow, uroplakins have been shown to heterodimerise in the endoplasmic reticulum (ER) (UPK1a with UPK2 and UP1b with UPK3a or UPK3b), and then combine in the Golgi apparatus to form polygonal AUM plaques which are transported to the apical cell surface via the exocytosis pathway (15, 16). These plaques are expressed on the apical surface of superficial cells in several mammals including cow, human, monkey, sheep, pig, dog, rabbit, rat, and mouse (9). Results from mouse knockout studies imply the uroplakins are important in the trans-cellular permeability barrier of the urothelium (17-19).

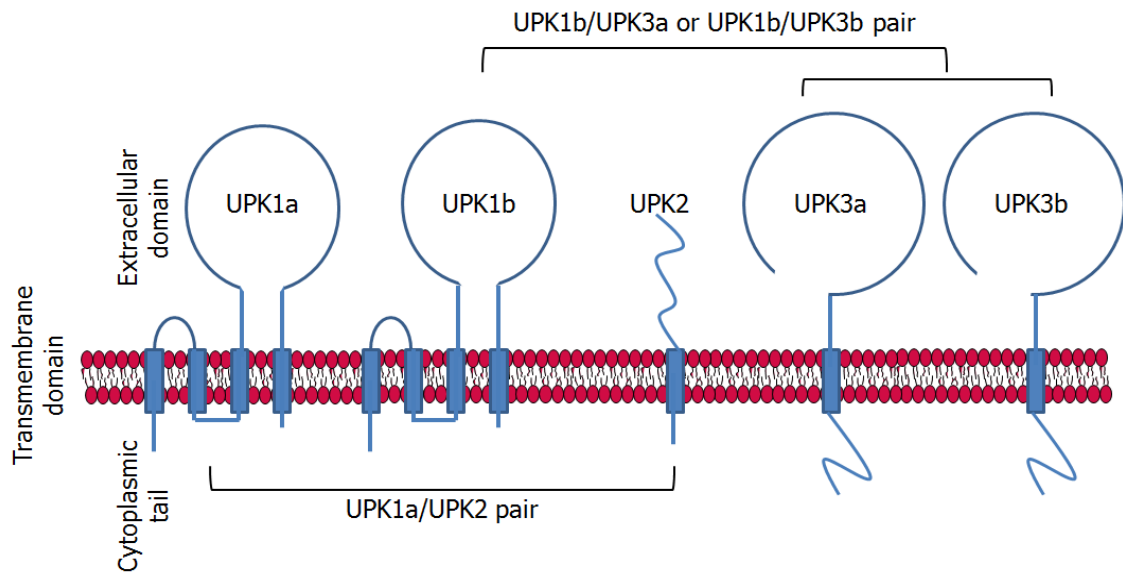


Figure 1-6 Structure of the uroplakin proteins

UPK1a and UPK1b are members of the tetraspanin family which possess 4 transmembrane domains. UPK2, UPK3a and UPK3b are single transmembrane proteins. In the endoplasmic reticulum, uroplakins heterodimerise as shown (UPK1a with UPK2 and UPK1b with UPK3a or UPK3b). Adapted from (13).

1.3.3.2 Tight Junctional proteins

A further specialised differentiation-associated feature of urothelium is the highly developed terminal tight junctions between adjoining superficial cells. Intracellular tight junctions (TJ) control para-cellular diffusion of water and ions (reviewed in (20)) and are a specific form of cell-cell contact found between the lateral membranes of adjacent cells. Tight junctions are composed of several types of proteins including cytoplasmic plaque proteins such as the zonula occludens (ZO), as well as transmembrane proteins including occludins, junctional adherens molecule (JAM) and the claudins (CLDN), which anchor the cell-cell junction to the cytoskeleton. The type of claudins expressed account for the tightness of the epithelium. In human urothelium, CLDN3, CLDN4, CLDN5, CLDN7, ZO1 and occludin are expressed, with CLDN3, CLDN5 and ZO1

confined to either “kissing points” (CLDN3 and ZO1) or basolaterally (CLDN5) between superficial cells of the urothelium (21)

1.3.3.3 Cytokeratin (CK) expression

Cytokeratins are the polypeptides that form the cytoskeletal intermediate filaments in epithelial cells. In humans, there are 20 known CK proteins but the urothelium only expresses a subset of these (reviewed by (22)). In normal human urothelium, CK7, CK8, CK18 and CK19 can be found throughout all layers (23, 24). CK13 expression is found only in the basal and intermediate cells of the urothelium, whereas CK5 and CK17 expression is restricted to the basal cells (24). CK20 is only found in the terminally differentiated superficial cells of the urothelium making it an ideal marker of urothelial terminal differentiation (25)(reviewed by (22)).

1.3.4 Function of the urothelium

1.3.4.1 Storage of urine

During the initial stages of bladder filling, superficial cells can be seen to elongate by up to ten times their normal size (26). This is achieved via folding and unfolding of the luminal surface made possible by “hinge-like” narrow bands of normal plasma membrane that lie between the rigid AUM plaques (5). Supplemental to this, fusiform vesicles containing AUM enter and exit the apical membrane during the bladders expansion/contraction cycle (5, 27, 28). This ability to alter the surface area of the urothelium helps maintain a low hydrostatic pressure and thus avoid damage to the upper urinary tract during the micturition cycle (reviewed in (5)).

1.3.4.2 Barrier function

The bladder has two primary roles: to accommodate large fluctuations in urine volume during the micturition cycle, and to act as a barrier between the hypertonic excretory products (urine) and isotonic blood that bathes the underlying tissue (5). AUM found on the apical surface of superficial cells is thought to minimise trans-cellular permeability (18), and in partnership with the tight junctions, which limit para-cellular transport (4) they make the urothelium the tightest of all known epithelial barriers (29). Loss of barrier function is associated with several painful bladder diseases, such as interstitial cystitis (30, 31).

1.4 Urothelial tissue homeostasis

Loss of cells through normal cell turnover or through tissue damage must be replaced to maintain tissue function and is termed tissue homeostasis.

In many epithelial tissues such as the skin and gut, tissue homeostasis is achieved via a constitutive program of self-renewal and replacement; this however is not seen in the bladder urothelium. Under normal conditions, urothelial cells are long-lived and mitotically quiescent, with only ~1% of cells in the cell cycle at any one time (32, 33). Urothelium does however have a high capacity for renewal, which is evident in response to injury (34). During such a response, cells from all layers of the urothelium are seen to re-enter the cell-cycle and contribute to the proliferative pool (5). This results in rapid repair of the damaged tissue and thought to be critical in maintaining urinary barrier function. It has been suggested that stem cells and their progenitors may be key to this responsive program of self-renewal. Tissue-specific stem cells were first described in the hematopoietic system (35), but since then, many other organs have disclosed resident stem cell populations, including brain, lung, and

heart, as well as many epithelial tissues, including liver, colon and skin (reviewed by (36)). The fact that many of the morphogenic signalling pathways present in embryonic development are also active during tissue repair helps support this hypothesis. Sonic Hedgehog (Shh) and Wnt for example are both active during epithelial repair of the gut lining (37, 38). In 2007, Fierabracci and colleagues successfully established self-replicating human urothelial spheroids which were shown to express markers of progenitor cells (CD34+ and CD45-)(39). Research into urothelial stem cells is ongoing, but so far, no resident stem cell population has been conclusively identified in the human urothelium (40). Research into urothelial stem cells has however been more fruitful in the rodent urothelium. In the rat, a sub-population of highly clonogenic, BrdU label-retaining (i.e., long lived) basal cells were identified and shown to express markers consistent with stem cells in other tissues (e.g., Bcl, p63, CK14 and β 1-integrin) (41). In the mouse bladder, a subset of CK5+ basal urothelial cells have been shown to express Sonic hedgehog (Shh), a ligand important during embryological development. Upon bacteria-induced injury, Shh was shown to act as a paracrine signal on the underlying stromal cells of the lamina propria leading to stromal release of Wnt ligand that induced basal urothelial cell proliferation (42). The relevance of this work to human urothelium still remains unclear, as human and rodent urothelium *in vivo* differ significantly in their expression of markers of terminal differentiation as well as ki67 expression, suggesting there may be fundamental difference in the regulation of urothelial regeneration between the two (43).

1.5 Cancer: When tissue homeostasis goes wrong

Cancer is a disease associated with an imbalance in the mechanisms that control normal tissue homeostasis (Figure 1-7). According to the Office for National Statistics, 309,527 new cases of cancer (excluding non-melanoma skin cancer) were diagnosed in the UK in the year 2008 equating to 504 cases per 100,000 people (44).

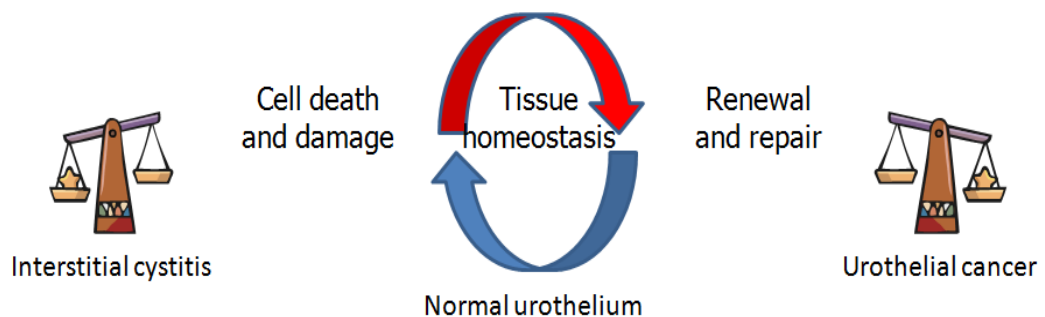


Figure 1-7 Schematic illustrating the link between dysregulated tissue homeostasis and cancer progression

Imbalances in the control of normal tissue homeostasis can result in two very different outcomes in the bladder. If the urothelium is damaged and not repaired, barrier function is lost causing conditions such as interstitial cystitis. However, bladder cancer may develop if repair mechanisms allow urothelial cells to proliferate too much.

1.5.1 Bladder Cancer

1.5.1.1 Epidemiology

According to the latest UK cancer statistics published in December 2011, bladder cancer is the 7th most common cancer in the UK, with 10,335 new cases diagnosed in 2008 (Figure 1-8 (44)). In the UK, bladder cancer affects over twice as many men (7390 new cases in the UK in 2008) as women (2945 new cases in the UK in 2008) and is the 4th most common cancer in males after prostate, lung and colorectal cancer. Like most cancers, bladder cancer is a disease of the elderly, with two thirds of all new cases diagnosed in people over the age of 70. In 2009, bladder cancer accounted for 5011 deaths, 3% of the total cancer related deaths in the UK (44).

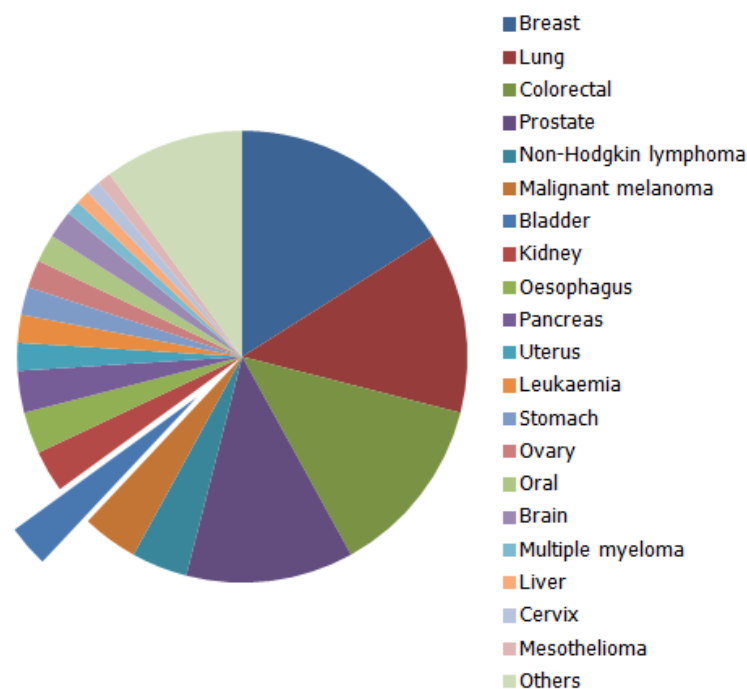


Figure 1-8 The 20 most commonly diagnosed human cancers in the UK

Pie-chart illustrating the 20 most commonly diagnosed human cancers in the UK in 2008. Bladder cancer accounts for 3% (10,335) of all newly diagnosed cancers making it the 7th most prevalent cancer in the UK. Adapted from data published in (44).

1.5.1.2 Aetiology

Symptoms of bladder cancer include but are not limited to, blood in the urine (haematuria), a burning sensation on voiding, pelvic pain and the need to pass urine more frequently.

90% of all bladder cancers develop from neoplastic changes in the urothelial lining of the bladder and are termed urothelial carcinoma (UC). The other 10% include the much rarer squamous carcinoma (SC), which arises from cells which have obtained a squamous phenotype (usually after chronic infection with the parasitic worm *Schistosoma haematobium* (reviewed by (45)) and adenocarcinoma (reviewed by (46)).

Upon diagnosis, all tumours undergo histopathological assessment using clearly defined criteria set out by the World Health Organisation (WHO) and the International Society for Urological Pathology (ISUP) in 2004 (47). Tumours are biopsied and classified according to their grade and stage. Grade gives an indicator of the differentiation status of the cells involved and uses two concurrent grading systems. These are the 1973, WHO classification system and the 2004 WHO/ISUP classification system which is currently being validated in clinical trials and is reviewed in (48) (Table 1-1, Table 1-2). Stage determines the degree of invasion into the underlying tissue and currently uses the 2002 Tumour, Node Metastasis (TNM) staging system (Table 1-3) (49).

Approximately 75-85% of newly diagnosed UC presents as a superficial tumour involving only the mucosa and lamina propria (Ta-Tis). Of these, most are papillary, highly recurrent, but non-invasive in nature, whereas those that are classified as Tis, are flat, carcinomas in situ (CIS) which are high grade (i.e., poorly differentiated) and have high metastatic potential (50). The remaining 15-25% of patients present with invasive tumours which have already invaded the muscularis (and beyond) and have a poor clinical outcome (51).

Grade	Appearance
G1	well differentiated, have an existing papillary architecture, fine chromatin, and a little indication of nucleoli or mitoses
G2	moderately differentiated, usually have a papillary architecture, granular chromatin, and a stronger indication of nucleoli and mitoses
G3	Poorly differentiated, least likely to have a papillary architecture, have coarse chromatin, and have many examples of nucleoli and mitoses.

Table 1-1 UC grading using the 1973 WHO classification system

Adapted from (52).

	Grade
0	Urothelial papilloma
i	papillary urothelial neoplasia of low malignant potential (PUNLMP)
ii	low-grade urothelial carcinoma
iii	high-grade urothelial carcinoma

Table 1-2 UC grading using the 2004 WHO/ISUP classification system

Adapted from (52).

Stage	Appearance
TX	Primary tumour cannot be assessed
T0	No evidence of primary tumour
Ta	Superficial, non-invasive papillary tumour
Tis	Superficial, non-invasive, flat tumour, carcinoma <i>in situ</i> (CIS)
T1	Tumour has invaded subepithelial connective tissue ie Lamina propria
T2a	Tumour has invaded superficial muscle
T2b	Tumour has invaded deep muscle
T3a	tumour has invaded perivesical tissue microscopically
T3b	tumour has invaded perivesical tissue macroscopically
T4a	Tumour has invaded prostate, uterus or vagina
T4b	Tumour has invaded pelvic wall, abdominal wall

Table 1-3 Staging of a urothelial primary tumour using the WHO 2002 TNM staging system

Adapted from (52).

1.5.1.3 Molecular pathways involved in the development of UC

Genetic mutations in chromosome 9, such as loss of 9p or 9q are frequently seen in all types of UC and thus believed to be an early initiating event involved in neoplastic transformation (53, 54) reviewed by (55). UC can clearly be segregated into two clinically distinct forms: superficial papillary and CIS. Certain genetic mutations have been shown to correlate with one or the other of these two forms giving rise to the hypothesis that Ta and CIS tumours arise from different molecular mechanisms (56). Activating mutations in the fibroblast growth factor receptor 3 (FGFR3) or HRAS genes are found in approximately 70% of all low grade (Ta) superficial tumours compared to only 20% of high grade invasive tumours (57). Both of these mutations lead to increased proliferation, driven via the MAPK/ERK and PI3K/STAT pathways (58). In comparison to this, p53 and Retinoblastoma (Rb) inactivating mutations are closely associated with high grade, invasive tumours and are markers of poor prognosis (53).

1.6 Factors regulating human urothelial tissue homeostasis

1.6.1 Cell signalling

Mitogenic polypeptide growth factors are important mediators of tissue homeostasis and can exert their effect via several mechanisms: autocrine signalling (self stimulation by secreting growth factor and expressing the appropriate receptor to respond), juxtacrine signalling (where ligand is an integral part of the cell membrane and only adjacent cells that express the appropriate receptor can respond) or paracrine signalling (where ligand is released in soluble form to act on distant receptor-expressing cells of the same or different type) (Figure 1-9).

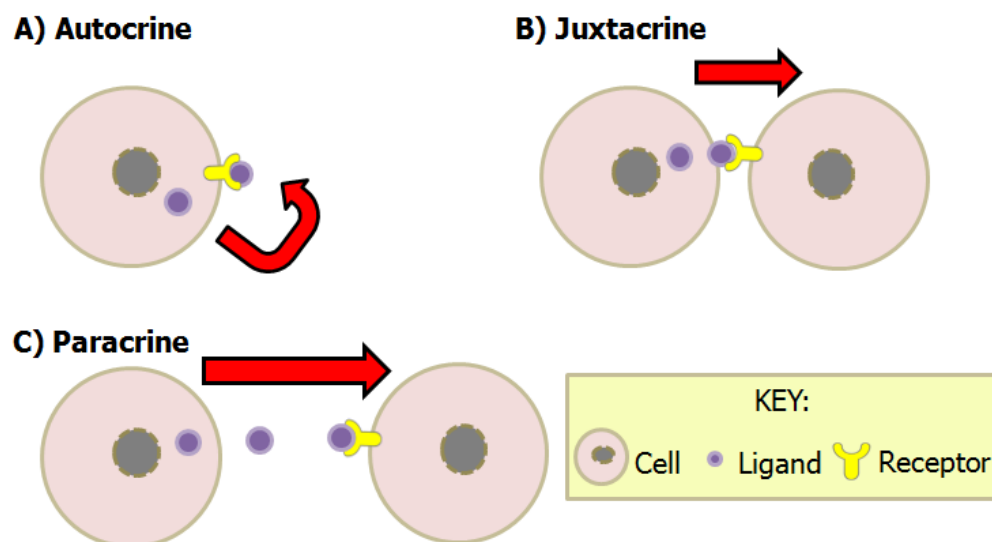


Figure 1-9 Schematic illustrating autocrine, juxtacrine and paracrine signalling

Growth factors can activate their receptor via an autocrine (A), juxtacrine (B) or paracrine mechanism (C) to regulate cell size, cell survival and cell cycle progression.

Although there is evidence that urothelial regeneration is responsive to paracrine signalling via the stromal compartment (42), there is also evidence for autocrine and juxtacrine growth factors in urothelial tissue regeneration. Best characterised is autocrine activation of the EGFR-family of receptors (reviewed in 1.6.1.1) which has been intensively researched using normal human urothelial cells *in vitro* (33, 59-62).

1.6.1.1 Expression of EGFR-family receptors in the human urothelium

THE EGFR-family of receptors consists of four members: EGFR (synonym; HER1), ERBB2 (synonym; HER2), ERBB3 (synonym; HER3) and ERBB4 (synonym; HER4). ERBB2 lacks a ligand binding domain and ERBB3 has no tyrosine kinase activity, therefore both must heterodimerise with either EGFR or ERBB4 to elicit a signal transduction pathway. *In vitro*, urothelial cells predominantly express EGFR which has been shown to drive self-renewal via juxtacrine amphiregulin engagement and MAPK/ERK-mediated gene transcription (33). *In situ* and upon culture confluence, ERBB2 and ERBB3 expression is also found but the relevance of their expression still remains to be fully explored (33, 61). Varley and colleagues have proposed that modulation of ERBB2 and ERBB3 expression and subsequent heterodimerisation with EGFR, may be an important mechanism modulating EGFR signalling upon confluence and contact-induced quiescence (33).

1.6.1.2 Expression of EGF-family ligands in the human urothelium

The EGF-family of ligands consists of several low molecular weight mitogenic polypeptide growth factors that bind with high affinity to the EGFR-family of tyrosine kinase receptors. In normal human urothelial cells, heparin-binding EGF (HB-EGF) (33, 60) transforming growth factor α (TGF α) (59, 61) and amphiregulin (33, 59, 61) have all been proposed as endogenous autocrine-ligands.

1.6.1.3 EGFR signalling

Upon ligand activation, EGFR dimerises, causing a conformational change and auto-phosphorylation of several C-terminal tyrosine residues (Y992, Y1045, Y1068, Y1148 and Y1173) in its extracellular domain. Auto-phosphorylated EGFR dimer can then activate downstream signalling via 3 main signalling cascades: mitogen-activated protein kinase (MAPK) pathway, phosphatidylinositol 3 kinase (PI3K) pathway and the signal transducers and activators of transcription (STAT) pathway (Figure 1-10 and reviewed by (63)).

1.6.1.4 MAPK pathway

The auto-phosphorylated EGFR dimer is recognised by the adaptor protein Grb2, which contains specific phosphotyrosine binding domains, Src homologue 2 (SH2) and Src homologue 3 (SH3). In turn, this binding leads to the recruitment of guanine nucleotide exchange factors (GEFs) such as, Son of Sevenless (SOS), a GTPase-activating protein which triggers downstream Ras proteins by facilitating the exchange of guanosine diphosphate (GDP) for guanosine triphosphate (GTP). Once Ras is activated the signal is transduced via phosphorylation through the MAPK cascade, starting with the phosphorylation of Raf which in turn phosphorylates MEK and finally extracellular signal regulated-kinase (ERK). ERK then translocates to the

nucleus and initiates transcription of cell cycle regulatory genes such as cyclin D and c-MYC.

1.6.1.5 PI3K pathway

The P13K/AKT pathway is an important pathway in controlling cell proliferation, cell survival and cell growth (reviewed in (64)) and can be activated via two separate mechanisms downstream of the EGFR.

In the first cascade, auto-phosphorylation of EGFR dimers allows direct recruitment of phosphatidylinositol 3 kinases (PI3K) to the plasma membrane through interactions of the SH2 domains on the EGFR dimer with the regulatory unit (p85) of PI3K (or indirectly via the adaptor proteins IRS1 or IRS2). This results in a conformational change in PI3K, releasing the inhibitory effect of p85 on the catalytic subunit (p110) of PI3K. Active PI3K can then convert its substrate, membrane bound phosphatidylinositol (4,5) triphosphate (PIP₂) into phosphatidylinositol (3,4,5) triphosphate (PIP₃). PIP₃ recruits AKT to the plasma membrane where phosphorylation of residues threonine 308 and serine 473 occur via the kinases, phosphoinositide dependent kinase-1 (PDK1) and integrin-linked kinase (ILK), respectively. Once phospho-activated, AKT can positively regulate cell growth by phosphorylation of mammalian target of rapamycin (mTOR), mediate cell survival via direct inhibition of pro-apoptotic signals such as Bad and regulate cell proliferation by translocating to the nucleus and up-regulating transcriptional targets such as p21 and p27, two cyclin dependent kinase inhibitors (CDKs).

In the second cascade, the catalytic domain of PI3K is activated via binding to Ras which results in the same downstream cascade as above (65).

1.6.1.6 STAT pathway

Auto-phosphorylated EGFR dimer activates the phosphorylation of signal transducers and activators of transcription (STAT) STAT1, STAT3 and STAT5 via the tyrosine kinase JAK (66, 67). Activated STATs can then translocate to the nucleus and exert their effect on gene transcription.

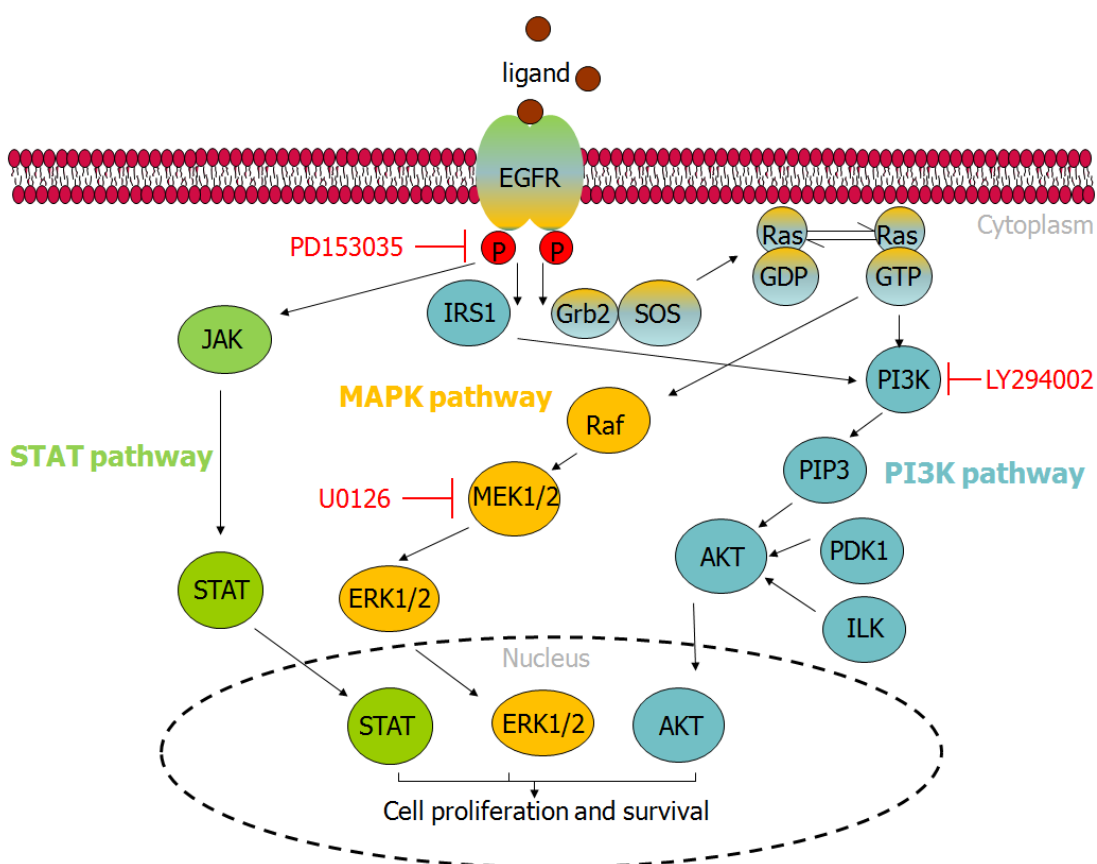


Figure 1-10 EGFR signalling pathways

Illustration depicting the three main signalling cascades downstream of EGFR. Each pathway is highlighted in a separate colour: The MAPK pathway in orange, the PI3K pathway in blue and the STAT pathway in green. Component shared by more than one pathway are shaded accordingly. Pharmacological inhibitors are shown in red.

1.6.2 Cell environment

In vitro, the cellular microenvironment can dramatically affect a cell's response to growth promoting signals. At confluence, normal human urothelial (NHU) cells are seen to down regulate EGFR expression and up-regulate ERBB2 and ERBB3 (33), but how this is coordinated still remains unclear. Upon confluence, cell spread is curtailed and several types of cell:cell junctions form. These interactions abrogate any response to proliferation-promoting signals and force the cell into growth arrest, a process known as contact inhibition or contact-induced quiescence (68). Wounding a confluent urothelial monolayer allows cells at the wound edge to spread, break cell:cell contact and respond to growth promoting signals (33).

One such cell:cell junction which may be involved in modulating a cell's response to growth promoting signals is the adherens junction (AJ). Adherens junctions are cell:cell anchoring junctions which form via calcium-dependent homophilic interactions between epithelial-cadherin (CDH1) and are anchored internally to the actin cytoskeleton via α - and β -catenins (69). These junctions not only mediate cell adhesion but also transmit signals from the plasma membrane to the nucleus where they regulate gene expression (68, 70).

The dynamics between growth factor signalling and cell:cell contact are clearly involved in urothelial self-regeneration, but how they fully interconnect and regulate each other to allow close coordination of gene expression with cell contact still remains uncertain. Research has focused on proteins that localise to both sites of cell:cell contact and to the nucleus in the hope of finding the key mediators of this process. One such protein that may be important is β -catenin, as it is a pivotal component of the canonical Wnt signalling cascade (reviewed in section 1.7), as well as an intrinsic component of the adherens junction (reviewed by (71) and in section 5.3). As yet, little research has been undertaken to explore the role of β -catenin in normal human urothelial

homeostasis although several studies have looked at the potential role of β -catenin in human bladder tumours (reviewed in section 1.8).

1.7 The canonical Wnt pathway

In the absence of Wnt ligand (Figure 1-11), β -catenin exists in two forms: one form is membrane-bound to α -catenin and E-cadherin where it is involved in maintaining cell-cell adhesion, the other is also cytoplasmic, but bound to a clustered group of proteins including the scaffold protein axin, glycogen synthase kinase 3 β (GSK3 β), the tumour suppressor protein APC and casein kinase Ia (CKIa), collectively known as the "destruction complex". When bound to this structure, β -catenin is phosphorylated by CKIa at the amino acid serine 45 allowing GSK3 β to phosphorylate serine/threonine residues 41, 37, 33. Phosphorylation of amino acids 37 and 33 triggers ubiquitination of β -catenin by the phospho-recognising protein β -transducin repeat-containing protein (β -TrCP) and ultimately results in β -catenin proteasome degradation (104).

Canonical Wnt signalling begins with the binding of Wnt ligand to its G-protein coupled receptor, Frizzled (Fzd) and co-receptor, low density lipoprotein receptor (LRP). Ligand activation results in several phosphorylation events but the exact mechanism(s) involved have yet to be fully elucidated. Fzd receptor is thought to trigger the phosphorylation of Dsh by activating the serine/threonine kinases, CKI ϵ , CK2 and PAR1 (105-107). Once primed, Dsh recruits Frat1 and together they bind as a complex to Axin and GSK3 resulting in the release of β -catenin (108). Free, cytoplasmic, non-phosphorylated β -catenin can then translocate to the nucleus where it acts as a co-activator of TCF/LEF driven transcription by recruiting members of the chromatin remodeling complex and ultimately drives cell cycle progression (Figure 1-11).

Canonical Wnt signalling is tightly regulated with agonists and antagonists acting on almost all parts of the signalling cascade. Several antagonists have been shown to inhibit Wnt signalling outside the cell by sequestering Wnt ligand

and include: secreted frizzled related protein (sFrp), Cerberus and Wnt inhibitory factor-1 (Wif1). Even if bound to Fzd, Dickkopf (DKK) can block ligand access to its co-receptor LRP5/6 by inducing endocytosis of LRP5/6 via Kremen (109-112). Within the nucleus, β -catenin signalling can be blocked via Nemo-like kinase (NLK) phosphorylation of TCF or binding of β -catenin to ICAT (113, 114).

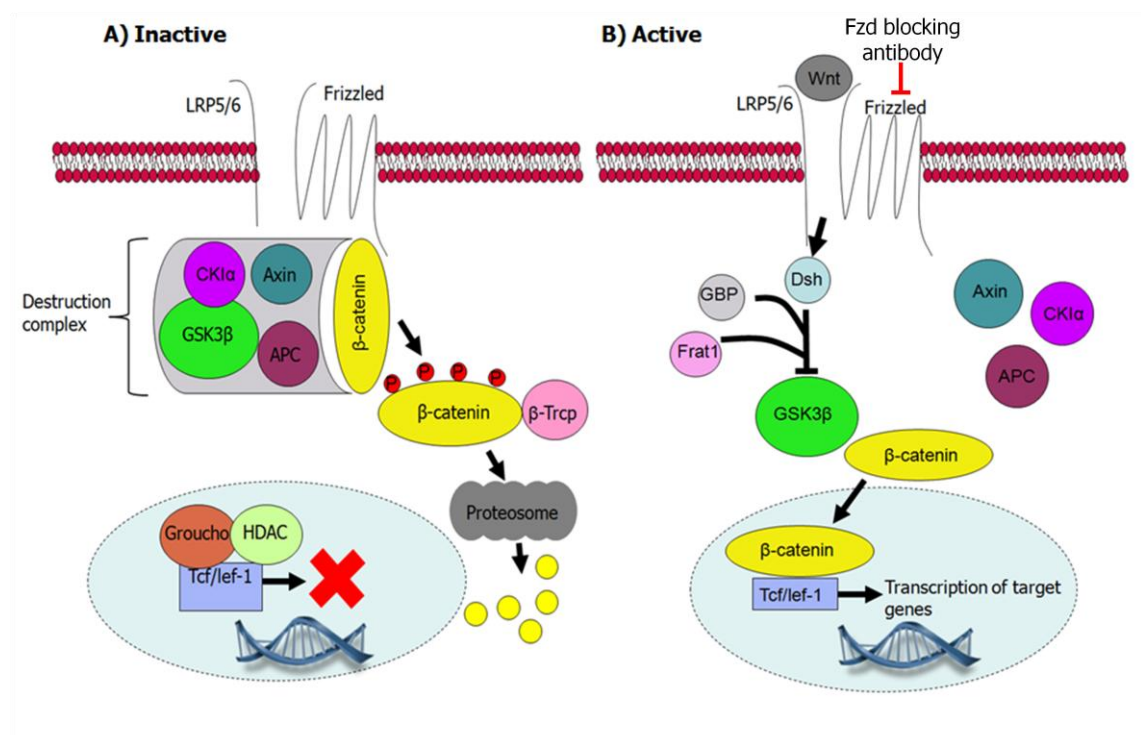


Figure 1-11 Schematic illustrating the canonical Wnt pathway

A) Inactive pathway: Without Wnt stimulation, β -catenin is held within a complex of proteins called the “destruction complex” and is targeted for proteasome degradation. (B) Active pathway: Wnt ligand binds to Fzd and LRP5/6 and leads to activation of Dsh and phospho-inhibition of GSK3 β , destroying the “destruction complex.” Non-phosphorylated β -catenin accumulates and translocates to the nucleus where it activates Tcf/Lef-1 transcription factors leading to target gene expression and cell cycle progression. Inhibitors (blocking antibodies) are shown in red.

1.8 Wnt/ β -catenin signalling in the bladder

Early work in 2003 by Thievensen and colleagues concluded there was no Wnt/ β -catenin signalling in normal human urothelium or in seven human urothelial cancer cell lines using a luciferase TCF reporter assay (72). Many research groups have however found an increase in nuclear β -catenin protein expression in UC biopsies compared to normal urothelium using immunohistochemistry (73-76). More recently, APC missense mutations and/or nuclear β -catenin accumulation has been shown to be associated with shorter disease free intervals and poor clinical outcome in a cohort of patients with invasive UC, suggestive of a role for deregulated Wnt/ β -catenin signalling in cancer progression (77). In support of this, epigenetic studies have shown a number of Wnt antagonists to be silenced in UC, for example, secretory frizzleds (sFrp) were shown to be promoter hypermethylated in a cohort of patients with invasive disease (78), while research undertaken by Urakami and colleagues has shown CpG hypermethylation of Wnt inhibitory factor 1 (Wif1), sFrp2 and Dickkopf-3 (DKK-3) correlating with higher levels of nuclear β -catenin in UC (79, 80). In support of a role for Wif-1 in UC, Tang and colleagues saw growth inhibition via G₁ cell cycle arrest when human bladder cancer cell lines T24 and TSU-PR1 were incubated in the presence of Wif-1 (81).

The role of Wnt/ β -catenin signalling has been more widely studied in rodent urothelium than in human and has been found to play an important role in tissue homeostasis. In the mouse, proliferation in response to bacterial or chemical induced injury is regulated by signal feedback between the basal urothelial cells and the underlying stromal cells (42). After injury, basal urothelial cells were seen to secrete Sonic Hedgehog (shh) evoking expression of Wnt2 and Wnt4 (via Gli1) from the underlying stroma. Both stromal and urothelial cells proliferated in response to Wnt ligand, restoring urothelial integrity (42).

Genetically engineered mouse models harbouring mutations found in human bladder cancer have helped advanced our understanding of the disease and have implicated deregulated Wnt/ β -catenin signalling in the process. *In vivo* experiments investigating deregulated Wnt/ β -catenin signalling by expression of a GSK3 resistant mutant form of β -catenin (missing exon 3) driven by a UPK2 promoter led to localised urothelial hyperplasia but did not develop into cancer (82). These lesions contained elevated levels of phosphatase and tensin homologue (PTEN), known to inhibit the PI3K pathway by dephosphorylating phosphatidylinositol-3,4,5-trisphosphate (82). In contrast, *in vivo* experiments where PTEN was deleted alongside constitutively active β -catenin went on to form papillary carcinoma and displayed high levels of P-AKT (S473), suggesting the tumour suppressor PTEN blocked cancer progression and implied β -catenin activity and PTEN loss were both required before bladder cancer would develop (82). Alongside this work, Ahmad and colleagues also investigated the potential interaction between H-Ras activating mutations and deregulated Wnt/ β -catenin signalling. Addition of constitutively active HRas (using the HRasQ61L mutant) alongside activated β -catenin also resulted in low grade UC but these lesions were dependent on the MAPK/ERK pathway and showed little activation of the AKT pathway, indicating both mutations in the AKT and MAPK pathways could synergise with deregulated Wnt/ β -catenin signalling to drive tumorigenesis in the mouse bladder (83). As yet, it is unclear what actual role Wnt signalling plays in the development of bladder cancer. Published data would however imply that the Wnt pathway could be deregulated on both the genetic and epigenetic level and thus does not follow the trend seen in bowel cancer where a specific mutation in APC is responsible for cellular transformation.

1.9 Urothelial cells *in vitro*

1.9.1 Isolation and propagation

The capacity of the human urothelium to regenerate can be exploited to propagate normal human urothelial (NHU) cells *in vitro* and provide a valuable research tool to investigate the mechanisms involved in urothelial homeostasis. Using well-defined methodologies developed by Southgate and colleagues, viable NHU cells can be isolated and propagated from small surgical specimens (84, 85). Using this technique, urothelium is dissociated, intact, from the basement membrane (using a calcium-chelating EDTA solution to limit stromal contamination) and then disaggregated using collagenase to form a single-cell suspension. Cultures are maintained in low calcium keratinocyte serum-free medium (KSFM) to discourage the growth of non-epithelial cells which is supplemented with recombinant human epidermal growth factor (rhEGF), bovine pituitary extract (BPE) and cholera toxin (CT; to aid plating efficiency (84)). Primaria™ tissue culture flasks are used as the plastic is coated with a mixture of negative, positive, and nitrogen containing functional groups which aid cellular attachment (86).

1.9.2 NHU cell phenotype

In serum-free, low calcium (0.09mM) culture medium, NHU cells adopt a highly proliferative “wound healing” phenotype, form non-stratified monolayers with a typical epithelial “cobblestone” morphology and undergo contact inhibited G₁ growth arrest upon attaining confluence (Figure 1-12 (33, 84, 85)). Under normal growth conditions, NHU cells express a non-differentiated, basal/intermediate cytokeratin profile with expression of CK7, CK8, CK17, CK18, CK19 and low levels of CK13 (84). CK20 and uroplakin protein expression (except for UPK1b) is absent under normal culture conditions (12, 84). Increasing the extracellular calcium concentration from 0.09mM to 2mM

induces stratification, desmosome formation and E-cadherin adherens junction formation, but does not permit urothelial cytodifferentiation (12, 84).

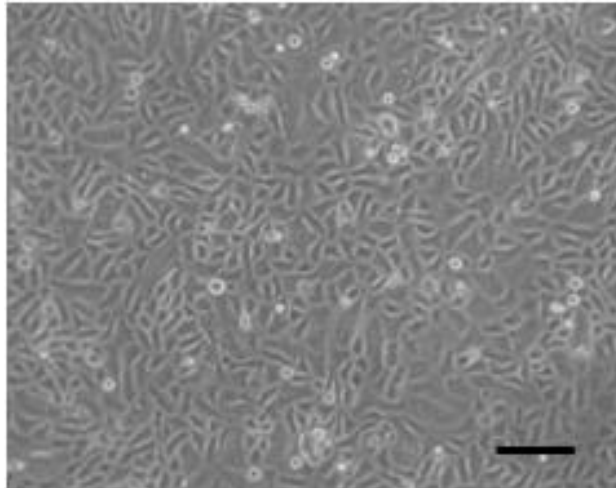


Figure 1-12 Phase-contrast micrograph of NHU cells in culture

NHU cells exhibiting a typical epithelioid "cobble-stone" morphology when cultured in KSFMc. Scale bar 100 μ m.

1.9.3 NHU growth and proliferation

In KSFMc, NHU cells display a high rate of proliferation with a mean population doubling time of 14.7 ± 1.8 hours (84). NHU cells can be sub-cultured for ~ 12 passages before they undergo replicative senescence (87, 88). Over-expression of telomerase (hTERT) can immortalise urothelial cells but results in compromised differentiation and functional capacity (89-91). Proliferation is an autonomous process driven primarily by autocrine epidermal growth factor (EGF) activation of EFGR and leads to transcription of genes that promote G_1 -S phase transition (33).

1.9.4 NHU cell differentiation

Cultured NHU cells retain their ability to undergo differentiation. Initial evidence of this was first reported when NHU cells were combined in organ-culture with de-epithelialised stroma and formed a stratified transitional urothelium identical to that seen *in situ* (92). Since these early experiments, two methods for induction of differentiation have been developed. In the first method, NHU cells are treated with a peroxisome proliferator activated receptor- γ (PPAR- γ) agonist, troglitazone, which induces differentiation but only when the EGFR pathway is concurrently blocked with EGFR tyrosine kinase antagonist, PD153035 (protocol hereafter termed TZ/PD)(21, 93). TZ/PD treatment induces epithelial differentiation by heterodimerisation of activated PPAR γ with retinoid X receptor α (RXR α) to form a transcription factor complex and transcription of genes with peroxisome proliferator response elements (PPRE) within their promoters. This method induces transcription of urothelial cytodifferentiation-associated genes, but does not result in organisation of a functional barrier.

In the second method, NHU cells are grown in KSFMc, pre-treated with serum and then sub-cultured in the presence of physiological calcium concentrations (hereafter referred to as ABS/Ca)(94). These cultures form a biomimetic urothelial tissue facsimile which displays many functional properties of the native urothelium including stratification, polarisation and barrier function (94).

Irrespective of method, induction of differentiation results in transcriptional up-regulation of terminal differentiation-associated genes, such as the uroplakins, CK13 and CK20 (93-95).

1.10 Thesis Aims

The overall aim of this project was to build on the current understanding of how urothelial regeneration is regulated to maintain tissue homeostasis. The dynamics between growth factor signalling and cell:cell contact clearly play an important role in regulating self-renewal mechanisms, but to date, it remains unclear how this is coordinated. Research has focused on proteins that localise to both sites of cell contact and to the nucleus in the hope of finding the key mediators of this process. In this thesis, the canonical Wnt signalling cascade was examined as a potential key pathway due to the pivotal role of β -catenin in both gene transcription and cell:cell contact.

The role of Wnt/ β -catenin signalling in urothelial homeostasis was investigated by meeting the following objectives:

- To utilise previously generated MicroarrayTM data to assess whether key components and regulators of the canonical Wnt signalling pathway were present at the mRNA level in NHU cells.
- To use pharmacological inhibitors of the destruction complex to ascertain whether there was a functional Wnt signalling cascade present in urothelial cells.
- To assess if NHU cells could respond canonically to Wnt ligand and determine whether this might be an alternate paracrine or autocrine signalling mechanism utilised by NHU cells to drive transcription of cell cycle associated genes and thus the regenerative phenotype seen during tissue repair.
- To utilise EGFR signalling antagonist, shRNA knock down and exogenous calcium modulation to address whether urothelial proliferation is

regulated through the resolution of multiple interacting signal transduction pathways downstream of cell:cell contact.

2 Materials and Methods

2.1 General

All practical work was carried out in the Jack Birch Unit for Molecular Carcinogenesis, or within the central Technology Facility, at the Department of Biology, University of York.

2.2 Suppliers

Commercial suppliers and manufacturer are indicated at the first mention of the reagent or equipment in the text. A full list of all suppliers can be found in Appendix I.

2.3 Dissection equipment, glassware and disposable plasticware

Metal dissection instruments, glassware, Pasteur glass pipettes (SLS), as well as disposable centrifuge tubes and pipette tips (Starlab) were sterilised by autoclaving in a Harvard/LTE Series 100 autoclave at 121°C (1 bar) for 15 minutes and then air dried at 80°C in a drying oven. Single use sterile plasticware was purchased from Sterilin (SLS), except for RNase/DNase-free pipette tips which were from (Axygen; Fisher Scientific), RNase-free tubes (Applied Biosystems), and serological pipettes (Starstedt).

2.4 Stock solutions

All chemical reagents were either of analytical or tissue culture grade, as appropriate for the experiment and were supplied by Sigma Aldrich unless otherwise stated. General laboratory stock solutions were prepared with deionised water (dH₂O). Solutions for use in tissue culture were prepared with ultra-pure water from a Purelab Ultra Genetic (Elga) ultra violet purification unit. Heat stable solutions were sterilised by autoclaving at 121°C (1 bar) for

15 minutes or filter-sterilised using an Acrodisc low-protein binding Tuffryn® HT syringe filter with a pore size of 0.2µm (VWR). Recipes for all stock solutions can be found in Appendix II.

2.5 Reagents

2.5.1 Antibodies

Primary antibodies used in this study are listed in Table 2-1. Antibodies were titrated on known positive controls to establish optimal concentrations prior to use. Primary antibodies were aliquoted and stored as recommended by the manufacturer. Working stocks were diluted in Tris buffered saline (TBS; appendix II) with 0.1% (v/v) bovine serum albumin (BSA; Sigma), 0.1% (w/v) sodium azide (Sigma), and stored at 4°C.

Fluorochrome-conjugated secondary antibodies were titrated prior to use and stored in the dark at 4°C (Table 2-2).

2.5.2 Agonists/Antagonists

Agonists/antagonists were reconstituted in either tissue culture grade dimethyl sulphoxide (DMSO; Sigma) or sterile H₂O according to the manufacturer's instructions and stored in single use aliquots at -20°C. Prior to use, compounds were titrated to determine the effective dosage and solvent-balanced dilutions were made from the stock solutions into growth medium (Table 2-3).

Antigen	Clone/catalogue number	Host	Supplier	Use	Molecular weight of antigen
Active β -catenin	8E7(dephosphorylated on Ser 37 and Thr 41)	Mouse	Kind gift from Prof. H.Clevers	WB, IIF	92 (KDa)
AKT	7	Mouse	BD Bioscience	WB, IIF	59
β -actin	AC-15	Mouse	Sigma	WB	42
β -catenin	C2206 (raised against amino acids 768-781)	Rabbit	Sigma Aldrich	WB, IIF, IHC	92
E-cadherin	HECD-1	Mouse	Abcam	WB, IIF, IHC	110
ERK	16	Mouse	Transduction Laboratories	WB, IIF	42/44/54/ 90
MKI67	MM1	Mouse	Novacastra Laboratories	IIF, IHC	N/A
Phospho-473 AKT	D9E	Rabbit	Cell Signalling	WB, IIF	60
Phospho-9 GSK3 β	AB30619	Rabbit	Abcam	WB	47
Phospho 42/44 MAPK	D13.14.4E	Rabbit	Cell Signalling	WB, IIF	42/44
Wnt 3a	3A6	Mouse	Santa Cruz	WB	39
Wnt 5a	C-16	Goat	Santa Cruz	WB	41

Table 2-1 Primary antibodies

Table listing primary antibodies used throughout this study and their use (WB: western blotting, IIF: indirect immunofluorescence, IHC: immunohistochemistry, N/A not applicable). Antibodies used for western blotting also include molecular weight of protein.

Antigen	Conjugate	Host	Supplier	Application
Mouse IgG	Alexa 488	Goat	Molecular Probes	IF
Rabbit IgG	Alexa 594	Goat	Molecular Probes	IF
Mouse IgG	Alexa 680	Goat	Invitrogen	WB
Rabbit IgG	Alexa 800	Goat	Invitrogen	WB
Goat IgG	Alexa 680	Donkey	Invitrogen	WB

Table 2-2 Secondary antibodies

Compound	Target	Published IC ₅₀ /EC ₅₀	Supplier	Stock conc.	Effective concentration in NHU cells
PD153035	EGFR Inhibitor	25pM*	Calbiochem	1mM (DMSO)	1μM
U0126	MEK1 and MEK2	72/58nM*	Calbiochem	5mM(DMSO)	5μM
LY294002	PI3K inhibitor	1.4μM	Calbiochem	5mM(DMSO)	5μM
SB415286	GSK3 inhibitor	2.9μM	Sigma Aldrich	10mM(DMSO)	10μM
Lithium Chloride	GSK3 inhibitor	15mM	Sigma Aldrich	10M(H ₂ O)	25mM
Troglitazone	PPARγ agonist	-	Parke Davis	1μM (DMSO)	1μM

Table 2-3 Agonists/Antagonists

*published IC/EC₅₀ in cell-free system.

2.6 Tissue Culture

2.6.1 General

All tissue culture work was undertaken using aseptic technique within a class II laminar flow safety cabinet with HEPA filtration. For routine tissue culture, a recycling class II safety cabinet (Medical Air Technology), or an externally ducted (Envair) cabinet was used. Before and after use, cabinets were cleaned with 70% (v/v) ethanol (Fisher) and once weekly with Mikrozid[®] AF disinfectant (SLS). Culture media was replenished every 2-3 days, unless otherwise stated. Waste cells and medium were aspirated into a Buchner flask containing 10% (w/v) Virkon[®] and left for a minimum of 30 minutes prior to disposal. All cell culture reagents were of tissue culture grade and were from Sigma, unless otherwise stated.

All centrifuge steps were carried out in a bench top centrifuge (Sigma) at 400g for 5 minutes, unless otherwise stated. Cells were counted in single cell suspension using an "improved Neubauer" haemocytometer (VWR) prior to re-seeding. Cells were then incubated in a HeraCell 240 incubator (Thermo Scientific) at 37°C in a humidified atmosphere of either 5% CO₂ in air for cells cultured in Keratinocyte Serum-Free Medium (KSFM; Invitrogen) or 10% CO₂ in air for other media.

2.6.2 Primary Urothelial Cell Culture

2.6.2.1 Tissue specimens

Specimens of human bladder, ureter and renal pelvis were provided by surgeons from York District Hospital, St James' University Hospital, Leeds and Guy's and St Thomas' NHS Foundation Trust, London. Tissue biopsies were taken for research purposes with fully informed consent from patients with no history of urothelial neoplasia and with the permission of the relevant Local Research Ethics Committee. Biopsies were collected in sterile 25ml polystyrene

Universal tubes containing 15mls of sterile transport medium (Appendix II) and where possible were stored at 4°C until processing. Prior to isolation, each sample was given an arbitrary laboratory record number (Y-number) and the patient's age, sex and operation were recorded. Each Y-number used in the study, along with the patients age, sex and operation details can be found in Appendix III).

2.6.2.2 Isolation of primary human urothelial cells

Primary urothelial cultures were established as previously describes (84, 85). Specimens were dissected in sterile Petri dishes (Nunc) using scissors and forceps to remove unwanted fat and connective tissue. Ureters were split longitudinally to allow access to the urothelium. Where possible, a small cross-section was removed and fixed overnight in 10% (v/v) formalin in PBSc (appendix II) for routine histological analysis. The remaining tissue was incubated in 5mls of stripper medium (Appendix II) for 4 hours at 37°C to dissociate the urothelium from the basement membrane. Urothelial sheets were detached from the underlying stroma using forceps and pelleted via centrifugation. A single cell suspension was achieved via incubation in 2mls (400U) of Collagenase IV (Appendix II) for 20 minutes at 37°C. Cells were then collected via centrifugation and counted prior to seeding into Primaria[®] flasks or Petri dishes (Falcon; BD Biosciences). NHU primary cell cultures were established in KSFM, supplemented with 50µg/ml bovine pituitary extract (BPE; Invitrogen), 5ng/ml epidermal growth factor (rhEGF; Invitrogen) and 30ng/ml cholera toxin (Sigma) termed complete KSFM (KSFMc).

2.6.2.3 Subculture of human urothelial cell lines

NHU cells were sub-cultured when approximately 90% confluent. Cell monolayers were incubated in 0.1% (w/v) in Ethylenediaminetetra-acetic acid disodium salt (EDTA) in PBS for 5 minutes at 37°C to chelate calcium and

promote dissociation. Cells were then incubated in 0.5ml of Hank's balanced salt solution (HBSS; Invitrogen) containing 0.25% (w/v) trypsin and 0.02% (w/v) EDTA for <1 minute at 37°C. Cells were resuspended in 10ml of KSFMc containing 2mg of Soya bean trypsin inhibitor (Sigma) and collected by centrifugation prior to reseeding at a ratio of 1:3. Cells were used for experiments between passage 0-7 (P0-P7).

2.6.3 Differentiation of human urothelial cell lines

2.6.3.1 Induction of differentiation with Troglitazone and PD153035 (21, 95)

NHU cells were seeded into T25 flasks at a concentration of 4×10^5 /flask and incubated in 5ml of KSFMc until approximately 70% confluent. The PPAR γ agonist troglitazone was added at a final concentration of 1 μ M (Day -1). After 24 hours, medium was replaced with fresh KSFMc containing 1 μ M PD153035 and cultures incubated at 37°C (day 0). RNA was harvested at day 3 post PD153035 addition, whilst protein and immunofluorescence analysis were carried out at day 6. Medium was replaced with fresh PD153035 at day 3 if cells were to be cultured for longer than three days. Control cells were treated as above except no Troglitazone or PD153035 was added but instead were solvent-balanced with DMSO and harvested as above.

2.6.3.2 Induction of differentiation by ABS and 2mM CaCl₂ (94)

NHU cells were seeded at a concentration of 4×10^5 /T25 flask and incubated in KSFMc until approximately 80% confluent. KSFMc medium was supplemented with batch tested Adult Bovine Serum (Harlan Sera-lab) at a final concentration of 5% (v/v) and incubated until confluent. Cultures were trypsinised and passaged 1:2 into fresh flasks with KSFMc + 5% (v/v) ABS. After 24 hours, CaCl₂ was adjusted to 2mM to induce stratification. Cell sheets were incubated

for a further 7 days, with the medium being replaced every 3 days. Control samples were untreated in KSFMc and harvested at the same time point.

2.6.4 Culture of established carcinoma cell lines

2.6.4.1 Human urothelial carcinoma cell lines

Three established urothelial cell carcinoma (UC) cell lines; RT4, RT112 and EJ (T24) were obtained from the Health Protection Agency Culture Collection (HPACC; Porton Down). Prior to use, all UCC cell lines were genotyped to verify pedigree. Cells were cultured in Dulbecco's Modified Eagle's Medium (DMEM) supplemented with 5% (v/v) fetal bovine serum (FBS; Harlan Sera-Lab) and 1% (v/v) L-glutamine in Iwaki tissue culture flasks (SLS) at 37°C in 10% CO₂ in air. UCC cell lines were passaged as for NHU cells, except the addition of trypsin inhibitor was omitted due to the presence of serum in the medium. Cells were passaged using a split ratio of between 1:10 and 1:60. Genotyping data for all carcinoma cell lines used in this study can be found in Appendix IV.

2.6.4.2 Osteoblast SaOS2 cell line

The osteosarcoma cell line SaOS2 was obtained from American Type Culture Collection (ATCC; Manassas). SaOS2 cells were cultured in McCoy's 5A medium (ATCC) supplemented with 15% (v/v) FBS at 37°C in 5% CO₂ in air. Cells were passaged as for UC cell lines and were split at a ratio of 1:3, for a maximum of 10 passages.

2.6.4.3 Wnt3a and Wnt5a secreting L-cell lines

Parental L cells, L Wnt-3a and L Wnt-5a lines were kindly provided by Dr. P. Genever, University of York. All three lines are derived from the mouse fibroblast cell line LM(TK-) and were stably transfected with a Wnt3a or Wnt5a phosphoglycerate kinase (PGK) driven expression vector (96, 97). These lines

are used for the production of conditioned medium containing either mouse Wnt3a or Wnt5a ligand, with parental L-cell conditioned medium as a control. All three lines were cultured in DMEM (11966; Invitrogen) containing 4mM L-glutamine, 4.5g/L glucose and 10% (v/v) FBS. The antibiotic G418 was added to the medium to maintain selection pressure at the following concentration; Wnt3a L-cells 0.4mg/ml; Wnt5a L-cells 0.6mg/ml.

2.6.4.4 Production of secreted Wnt 3a or Wnt 5a ligand

Confluent cultures were split at a ratio of 1:15 into 10ml of fresh growth medium without antibiotics and incubated for 4 days at 37°C in 10% CO₂ in air. Conditioned media was harvested (batch 1) and the growth medium was replenished. Cells were then cultured for a further three days prior to harvesting of the second batch of conditioned medium and then discarded. Both batches of conditioned medium were mixed and filtered through a 0.2µm Tuffryn[®] filter (Acrodisc) prior to immediate use or storage at 4°C for up to 3 months.

2.6.4.5 Retropack[™] PT67 Packaging Cell Line

The Retropack PT67 cell line (Clontech) is a NIH3T3 fibroblast derived cell line which has been genetically engineered to stably produce the retroviral gag, pol and env genes. Once transfected with retroviral vector, cells produce a replication-defective retrovirus, with a broad (amphotrophic) mammalian host range. Cells were routinely cultured in DMEM supplemented with 10% (v/v) FBS and were passaged as for UC cell lines. Cells were split at a ratio of between 1:5-1:15. Prior to transfection, cells were subjected to Hypoxanthine Aminopterin Thymidine (HAT; Invitrogen) medium re-selection as recommended by the supplier. PT67 cells were firstly cultured in normal growth medium supplemented with 100nm aminopterin for 5 days, and then 5 days in DMEM-HAT medium (30nm hypoxanthine, 1M aminopterin, 20mM

thymidine), and then finally 5 days in DMEM-HT medium (30mM hypoxanthine, 20mM thymidine). Immediately after HAT re-selection, PT67 cells were either cryo-preserved or transfected.

2.6.4.6 Cryo-preservation and thawing of cell lines

Cells were cryo-preserved and stored in liquid nitrogen in a Statebourne storage dewar at -196°C. For cryopreservation of cell lines, cultures were harvested as for passaging and collected by centrifugation. The cell pellet was resuspended in the appropriate ice-cold growth medium containing 10% (v/v) FBS and 10% (v/v) dimethylsulphoxide (DMSO) at a cell density not less than 1×10^6 cells/ml. Cells were aliquoted into 1ml polypropylene cryovials (Greiner) and transferred to an ice-cold "Mr Frosty" (Nalgene) containing 250ml of isopropanol (SLS) to control the cooling rate to 1°C per minute. The cells were then placed within a -80°C freezer for 4-6 hours prior to transfer to liquid nitrogen. Cells were thawed rapidly at 37°C and 5mls of pre-warmed growth medium was immediately added. Cells were centrifuged at 400g for 5 minutes and then plated as required.

2.6.5 Mycoplasma testing

Mycoplasma *spp.* contamination is a huge problem in eukaryotic cell culture and can lead to unreliable experimental results (98). All cell lines were routinely tested for intracellular bacteria Mycoplasma *spp.* prior to cryopreservation. The presence of extra-nuclear staining with the DNA-intercalator bisbenzimidazole (Hoechst 33258) is highly suggestive of Mycoplasma *spp.* contamination and was employed as a simple screening tool for such infection. Autoclaved 12-well Teflon-coated glass slides (Hendley-Essex) were placed into the chambers of a sterile Hereaus box (Sartorius). Cells were seeded at a density of 1×10^4 cells per well and allowed to attach for 4 hours at 37°C. Each chamber was flooded with 5ml of complete growth medium and the cells were then left to grow overnight at 37°C. Medium was removed and slides were washed with 5ml of

PBS prior to fixing in methanol:acetone (50:50) for 30 seconds and air drying. Cells were stained with Hoechst 33258 (0.1µg/ml (w/v) in PBS) for 5 minutes in the dark, washed in PBS, air-dried and mounted in DABCO/glycerol antifade (appendix II). Once dry, slides were examined using an Olympus BX60 microscope using epifluorescence and the appropriate filter set.

2.6.6 Genotyping

Cross-contamination of cell lines is a serious and costly problem in today's laboratory and can lead to confusion in the literature as well as retraction of previously published manuscripts (reviewed by (98)). To reduce the chances of this, strict tissue culture practice was adhered to as well as routine authentication of each cell line prior to use. Cell lines were genotyped using a PCR-based short tandem repeat (STR) analysis system to verify cell line pedigree. STR's are distributed throughout the genome and are highly polymorphic in number. By counting the number of alleles for 9 different loci, one can determine with a high degree of certainty whether two cell lines are of the same origin. The Powerplex® 1.2 system (Promega) allows identification of 9 independent loci (Penta E, D18S51, D21S11, TH01, D3S1358, FGA, TPOX, D8S1179 and vWA) from freshly isolated genomic DNA.

2.6.6.1 Isolation of genomic DNA from cultured cells

Genomic DNA (gDNA) was purified from cultured cells using a DNeasy Blood and Tissue Kit (Qiagen). 1×10^6 cells were collected into a universal, centrifuged at 400g for 5 minutes and resuspended in 200µl of PBS prior to genomic DNA extraction as recommended by the manufacturer (Qiagen). In brief, samples were lysed using proteinase K and the genomic DNA (gDNA) was bound to a DNeasy mini column. Each column was then washed to remove contaminants and the resulting gDNA eluted in 200µl of AE buffer (Qiagen). DNA was quantified using a Nanodrop™ ND-1000 spectrophotometer (Thermo Fisher) and stored at 4°C until use.

2.6.6.2 STR genotyping using the Powerplex[®] 2.1 System (Promega)

Genomic DNA was diluted to 0.4ng/μl using nuclease free water (Promega). A PCR reaction was assembled on ice in a thin-walled 0.5ml PCR tube containing 2.5μl of test gDNA (1ug), 2.5μl of Powerplex 1.2[®] 10x primer pair mix, 0.45μl of AmpliTaq Gold[®] DNA polymerase I and 17.05μl of nuclease free water. A positive PCR reaction containing 1μg of K562 DNA was also assembled along with a no template negative control. The PCR was then cycled in a GeneAmp[®] PCR system 9700 (Applied Biosystems) as described by the manufacturer. To each sample 9μl of Hi-Di[™] formamide (Applied Biosystems) and 1μl internal lane standard (Promega) was added and mixed by vortexing. 10μl was then added to a well of a 96-well optical plate (Applied Biosystems) and was sealed with optical adhesive tape. The sample was injected into a Beckman CEQ 8000 fragment analyzer capillary electrophoresis system along with an Allelic ladder (Promega). Results were analysed using GeneMapper[®] 4.0 software (Applied Biosystems) and the STR profile for each sample was compared to that found on the Health Protection Agency Culture Collection (HPACC) or American Type Culture Collection (ATCC) website (Appendix IV).

2.7 Molecular Biology

2.7.1 General

All microbiological culture work was undertaken using aseptic technique and within the guidelines set out by the University of York for Good Microbiological Practice. Before and after use, benches were cleaned with 2% (w/v) Virkon[®] and then 70% (v/v) ethanol (Fisher). Waste cells and growth medium were treated with 2% (w/v) Virkon[®] overnight prior to disposal down the sink. Contaminated glassware was completely immersed in 2% (w/v) Virkon[®] overnight, after which it was rinsed and washed as normal. Contaminated solids were autoclaved prior to disposal.

2.7.2 Plasticware

Liquid cultures were grown overnight in 500ml glass Buchner flasks containing Luria Broth (LB; Appendix II). Luria-Broth Agar plates (LBA; Appendix II) were poured into 9cm UV-irradiated Petri dishes and allowed to set prior to use. Sterilin single use inoculating loops and T-shaped spreaders were purchased from VWR.

2.7.3 Plasmids

Full details including vector map can be found in the appropriate section of use. Table 2-4 outlines all plasmids used in this study and the relevant supplier.

Vector name	Supplier	Size (Kb)	Promoter	Use
pSIREN- RetroQ	Clontech	6.4	U6	shRNA knock-down (section 2.7.6)
TOPFLASH	Millipore	5.5	TK and TCF	Firefly luciferase reporter (section 2.10.3)
FOPFLASH	Millipore	5.5	TK and mutant TCF	Firefly luciferase reporter (section 2.10.3)
pRL-CMV	Promega	4.1	CMV	Renilla luciferase reporter (section 2.10.3)
pBabe-EGFP	Gift from Dr. N.Georgopoulos	5.0	LTR	Cell sorting-FACS analysis (section 2.10.4)

Table 2-4 Plasmids

2.7.4 Amplification of plasmid DNA

2.7.4.1 Transformaton of competent E-coli cells

Amplification of previously established plasmid DNA: 20ng of plasmid DNA was transformed into a 50µl aliquot of DH5aTM ultracompetent *E.coli* cells (genotype: *F- mcrA (mrr-hsdRMS-mcrBC) 80lacZM15 lacX74 recA1 ara139 (ara-leu)7697 galU galK rpsL (StrR) endA1 nupG>*) (Invitrogen). Plasmid was gently mixed with cells and incubated on ice for 30 minutes. Cells were then heat shocked at 42°C for 30 seconds and returned to ice for 2 minutes. 250µl of S.O.C medium (Invitrogen) was added and the cells were incubated in an orbital shaker at 225rpm for 1 hour at 37°C. 100µl of the cell suspension was spread onto an LBA plate (appendix II) containing 100µg/ml ampicillin and incubated, inverted at 37°C, overnight. A single colony was picked using a sterile single use loop and used to inoculate 5ml of LB containing 100µg/ml ampicillin and incubated at 37°C with shaking at 225rpm for 4 hours. The culture was then used to inoculate a further 50ml of LB containing 100µl/ml ampicillin and incubated for 16 hours at 225rpm, 37°C.

Amplification of ligated product (section 2.7.5.5): 5µl of ligated product was added to one 50µl thawed vial of TOP10[®] *E.coli* (genotype: *F- mcrA Δ(mrr-hsdRMS-mcrBC) ϕ 80lacZ Δ M15 Δ lacX74 nupG recA1 araD139 Δ(ara-leu)7697 galE15 galK16 rpsL(Str^R) endA1 λ*). DNA and bacteria were gently mixed and incubated on ice for 30 minutes prior to heat-shocking at 42°C for 30 seconds. Bacteria were then placed on ice for 2 minutes. 250µl of pre-warmed (37°C) S.O.C medium was added and the cell suspension was incubated at 37°C with shaking (220rpm) for 1 hour. Between 20-200µl of cell suspension was then spread onto an LBA plate (appendix II) containing 100µg/ml ampicillin and incubated, inverted at 37°C, overnight. Single colonies were picked using a sterile single use loop and used to inoculate 5ml of LB containing 100µg/ml ampicillin and incubated at 37°C with shaking at 225rpm for 16 hours.

2.7.4.2 Purification of plasmid DNA

Plasmid DNA was recovered from overnight cultures using a Midi Endotoxin-free plasmid extraction kitTM (Qiagen). Bacteria were harvested from the overnight cultures by centrifugation at 4000g for 10 minutes at 4°C. The pellet was resuspended in 4ml of P1 buffer (50 mM Tris-Cl [pH 8.0], 10mM EDTA, 100µg/ml RNase A) and vortexed until in suspension. 4ml of buffer P2 (200mM NaOH, 1% SDS) was added, inverted 6 times and incubated at ambient temperature for 5 minutes. 4ml of chilled buffer P3 (3.0 M potassium acetate, pH 5.5) was added and inverted several times to stop the lysis reaction. The lysate was poured into the barrel of a QIAfilter cartridge and left for 10 minutes at ambient temperature to settle. The cap was removed from the QIAfilter and the plunger was gently depressed. The resulting flow through was collected into a 50ml polypropylene centrifuge tube and 1ml of ER buffer (proprietary recipe; Qiagen) was added, inverted ten times and then incubated on ice for 30 minutes. A Qiagen tip-100 was equilibrated by adding 10ml of QBT buffer (750mM NaCl, 50mM MOPS [pH 7.0], 15% isopropanol, 0.15% Triton X-100) and allowed to flow through under gravity. The chilled lysate was added to the filter and allowed to enter the resin via gravity flow and then washed twice with 10ml of QC buffer (1.0M NaCl, 50mM MOPS [pH 7.0], 15% (v/v) isopropanol). DNA was eluted into an autoclaved Corex 30ml tube (Gentaur) using 5ml of QF buffer (1.25 M NaCl, 50mM Tris-Cl [pH 8.5], 15% isopropanol). DNA was precipitated by adding 3.5ml of isopropanol, mixed and centrifuged at 15000g for 30 minutes at 4°C. The resulting DNA pellet was washed in 5ml of 70%(v/v) ethanol, air dried and resuspended in nuclease free water. Plasmid DNA was quantified using a NanodropTM Spectrophotometer and stored at -20°C.

2.7.4.3 Glycerol stocks

Glycerol stocks were made from overnight LB cultures. 750µl of culture was aliquoted into a 1.5ml cryovial[®] and 250µl of sterile 80% (v/v) glycerol was added and mixed prior to long term storage at -80°C. To recover bacteria, 5µl was streaked onto an LBA plate containing 100µg/ml ampicillin and incubated overnight at 37°C.

2.7.5 Molecular cloning

2.7.5.1 Restriction enzyme digestion

Plasmid DNA was restriction enzyme digested to check for the presence of insert DNA. Restriction enzyme digestion was typically carried out in a total volume of 20µl. 5µl (2-3µg) of DNA was digested with 5 units of restriction enzyme (New England Biolabs) in the appropriate buffer and at the temperature recommended by the supplier for 1-2 hours.

2.7.5.2 Preparation of analytical agarose gels

A clean plastic gel rig (100mm x 100mm) was sealed at the ends with autoclave tape to form a mould. Combs were inserted into appropriate slots in the gel rig. 500mg of high purity agarose (Invitrogen) was mixed with 50ml of TBE buffer (Appendix II) and was heated in a microwave oven for 2 minutes, or until all of the agarose had dissolved. The solution was then allowed to cool to around 45°C, after which, 1.2µl of ethidium bromide solution (5mg/ml) was added and mixed gently. The solution was carefully poured into the gel rig and all bubbles were removed with a pipette tip. The gel was allowed to set for at least 30 minutes prior to the combs and tape being carefully removed. The gel rig was lowered into an Horizon[®] 58 electrophoresis gel tank (Gibco[®]; Invitrogen) with enough TBE buffer (appendix II) to cover the gel by about 3-5mm.

2.7.5.3 Agarose gel electrophoresis

DNA samples were diluted in 6x loading buffer (Blue:orange loading dye; Promega) and loaded into the wells of a pre-cast agarose gel. 5µl of Hyperladder I (Bioline) was loaded alongside. DNA fragments were resolved by applying a voltage of 100V for approximately 45 minutes and visualised using a Gene Genius bio-imaging system and Genesnap 7.07 software (Syngene).

2.7.5.4 Annealing of oligonucleotides

10µl of each oligonucleotide at a concentration of 100pmol/µl were mixed in a microcentrifuge tube and the volume made up to 20µl with nuclease-free water. The mixture was heated to 95°C for 30 seconds, 72°C for two minutes, 37°C for two minutes, 25°C for two minutes and then cooled on ice. Annealed oligo pairs were either used immediately for ligation or stored at -20°C.

2.7.5.5 Ligation

Ligations were typically carried out in a total volume of 20µl. 50µl of pre-cut vector was ligated with 3x (w/w) of insert DNA. 2µl of 10x ligation buffer (50mM Tris-HCl [pH7.8], 10mM MgCl₂, 20mM dithiothreitol, 10mM ATP, 50mg/ml of bovine serum albumin; Promega) was used per ligation, together with 1µl (200 units) of T4 DNA ligase (Promega). The reaction was incubated at ambient temperature for 3 hours prior to transformation into One Shot[®]TOP10 *E.coli*.

2.7.5.6 Sequencing

Dye terminator cycle sequencing was undertaken by Cogenics (Beckman Coulter). The resulting sequences were viewed using Chromas v1.45 (Technelysium Pty Ltd) and were aligned using Fasta3 and the EMBL library.

2.7.6 Genetic manipulation of NHU cells

2.7.6.1 Retroviral transduction

The infection efficiency of retroviruses can be employed to rapidly and stably express a transgene of interest within a population of mitotically active cells. Transduction is much more efficient than many transfection protocols as it results in less cellular stress and subsequent cell death and is thus the method of choice when using finite cell lines.

2.7.6.2 RNAi delivery plasmid

RNAi ready pSIREN RetroQ (Clontech) is a self-inactivating retroviral expression vector designed to express shRNAs via a U6 promoter. The vector encodes a 5' long terminal repeat (LTR) containing a cytomegalovirus type 1 (CMV) enhancer region and a mouse sarcoma virus (MSV) promoter to drive transcription of the RNA packaging signal $\Psi+$, shRNA of interest and puromycin resistance cassette in eukaryotic cells. When expressed in the packaging cell line, PT67, the plasmid produces infectious but replication-incompetent viral particles, which can infect a wide host range but cannot replicate (Figure 2-1).

2.7.6.3 shRNA design

shRNA sequences were designed using the Clontech online design tool and incorporating *Bam*HI and *Eco*R1 overhangs as well as an internal *Mlu*I restriction site to aid in selection of positive clones.

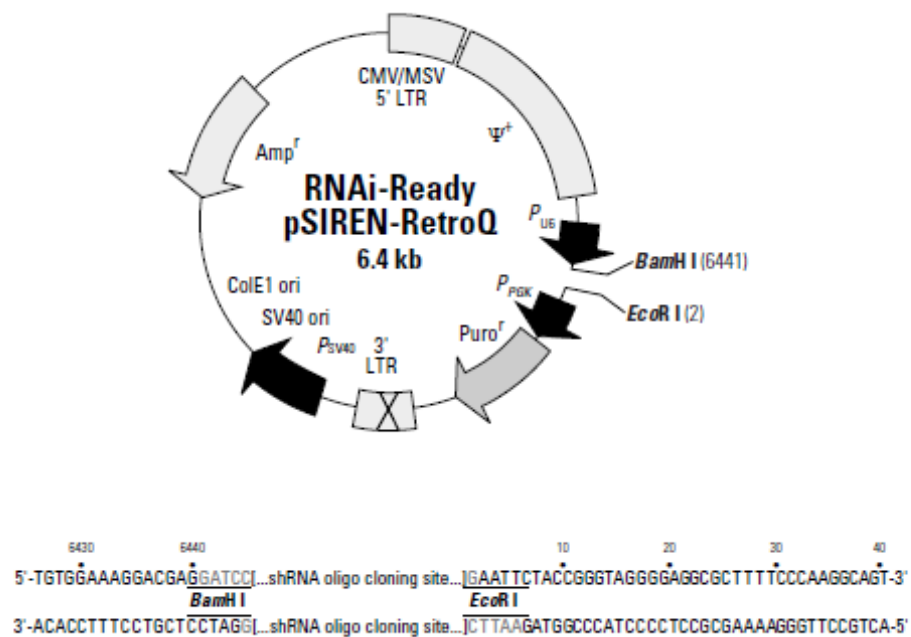


Figure 2-1 pSIREN RetroQ plasmid

pSIREN RetroQ plasmid is based on the Moloney mouse leukemia virus (MMLV) and can be used for targeted gene silencing using RNAi. Oligonucleotides encoding short-hairpin RNA sequences can be cloned between the *Bam*HI and *Eco*RI restriction enzyme sites. Plasmid is then propagated in competent *E. coli* bacteria using the ColE1 origin of replication (ColE1^{ori}) and successfully transformed cells are selected via expression of the ampicillin resistance gene (*Amp*^r). Upon transfection into the packaging cell line, PT67, the RNA packaging signal (Ψ +), shRNA of interest and puromycin resistance cassette (*Puro*^r) is transcribed via a 5' long terminal repeat (LTR) containing a cytomegalovirus type 1 (CMV) enhancer region and a mouse sarcoma virus (MSV) promoter. During reverse transcription of the retroviral RNA, the 3' LTR is copied and replaces the 5' LTR, resulting in inactivation of the 5' LTR CMV enhancer sequences. Vector is then packaged and the resulting retroviral particles can be utilised to infect a variety of mammalian cells. In target cells, expression of the short hairpin RNA and *Puro*^r is driven via a U6 promoter, an RNA Polymerase III-dependent promoter. Image reproduced from the Clontech pSIREN RetroQ manual PT3737-5.

2.7.6.4 Transfection of the packaging cell line PT67

All procedures involving transfected PT67 cells were carried out in a class II externally vented tissue culture hood. The packaging cell line PT67 was maintained in DMEM (Invitrogen) supplemented with 10% (v/v) FBS and 1% (v/v) L-glutamine until 60% confluent. Cells were transfected using Effectene (Qiagen), a lipid-based transfection reagent according to the manufacturer's instructions. In brief, 5µg of endotoxin-free plasmid DNA was mixed with 150µl of buffer EC and 40µl of enhancer, vortexed for one second and incubated at ambient temperature for 5 minutes. 50µl of Effectene transfection reagent was added, vortexed for 10 seconds and incubate at ambient temperature for a further 10 minutes. To this, 1ml of complete growth medium (DMEM with 10% (v/v) FBS and 1% (v/v) L-glutamine) was added, gently mixed and then added drop-wise to the flask. A negative control culture where the plasmid DNA was omitted was included in all experiments. Cultures were incubated for 16 hours, after which the medium was replaced with fresh, pre-warmed complete growth medium and the cells were left to reach confluence. At confluency, the transfected PT67 cells and negative control flask were harvested as with routine passaging and reseeded at a split ratio of 1:2 into complete medium supplemented with 4µg/ml of puromycin (Autogen Bioclear). A 100% stably transfected cell population was assumed in the test flask when all cells in the untransfected negative control flask had perished. Transfected PT67 cells were maintained under puromycin selection pressure until viral particles were harvested.

2.7.6.5 Retroviral transduction of urothelial cells

Stably transfected PT67 cells were grown to 100% confluence when the medium was changed to 10ml DMEM:RPMI (50:50) supplemented with 5% (v/v) FBS (no antibiotics) for 16 hours. Conditioned virus-containing medium was harvested and filtered through a 0.45µm Tuffryn[®] filter (Acrodisc) to

remove any cellular debris and 8µg/ml polybrene (Sigma) was added. Medium was removed from 2 T75 flasks of passage 1 (P1) NHU cell cultures at approximately 50% confluence. 8ml of virus-containing medium was added to one culture. The remaining culture was treated with 8mls of DMEM:RPMI (50:50)+5% (v/v) FBS to serve as a negative control. Both cultures were then incubated at 37°C for 4-6 hours after which the medium was replaced with 15ml KSFMc. At 48 hours post transduction, both cultures were trypsinised and passaged 1:3 into KSFMc supplemented with 2mg/ml puromycin. A 100% stably transduced cell population was assumed in the test flask when all cells in the untransduced negative control flask had perished. Puromycin selection pressure was then maintained at a reduced concentration of 0.5mg/ml.

2.8 Gene Expression Analysis

2.8.1 General

Before working with RNA, all surfaces and pipettes were cleaned with RNase Zap® (Ambion). Glassware and 13ml polypropylene tubes and caps (Starstedt) were incubated at ambient temperature, overnight with 0.1% (v/v) diethyl pyrocarbonate (DEPC) (Sigma) to inactivate RNase activity. Glass and plasticware was then autoclaved and air-dried prior to use. Only DNase and RNase free pipette tips (Axygen;Fisher Scientific) and nuclease-free microcentrifuge tubes (Ambion) were used. RNA was reconstituted in nuclease-free H₂O (Promega).

2.8.2 RNA Extraction

Cell lysates were prepared from cultures *in situ* using TRIzol™ reagent (Invitrogen). Growth medium was removed and the cell monolayer was washed in 10ml of PBSc. 5ml of TRIzol™ was added for 5 minutes on a rotary shaker and lysates were collected into 13ml polypropylene tubes using a cell scraper (Greiner) and either extracted as outlined below or stored at -80°C.

Frozen lysates were thawed on ice and total RNA was extracted by the addition of 1ml of chloroform (BDH). Tubes were vortexed for 15 seconds and incubated for 5 minutes at ambient temperature prior to centrifugation at 12,000g, 4°C in a refrigerated centrifuge (Sorvall RC-5, Du-Pont) for 15 minutes. The upper aqueous phase was carefully removed to a fresh 13ml tube and the RNA was precipitated using an equal volume of isopropanol for 10 minutes at ambient temperature. Precipitate was collected by centrifugation at 12,000g for 10 minutes at 4°C and was washed with 5ml 70% (v/v) ethanol. The resulting pellet was air-dried and resuspended in 30µl of nuclease-free H₂O prior to transfer into a 0.5ml nuclease-free tube.

2.8.3 DNase treatment of RNA

Residual genomic DNA contamination was removed by DNase I digestion. RNA was incubated with 1µl of DNase I (DNA-freeTM; Ambion) and an appropriate volume of 10x DNase I buffer for 30 minutes at 37°C. 5µl or 1/10th volume (whichever was greater) of DNase inactivating reagent was added to terminate the reaction. After a 2 minute incubation at ambient temperature, the DNase inactivating reagent was removed by centrifugation at 10,000g for 1 minute. RNA supernatant was collected and transferred to a fresh nuclease-free tube and stored at -80°C. RNA quality and quantity was assessed using a NanodropTM ND-1000 Spectrophotometer (Thermo Fisher).

2.8.4 RNA precipitation using sodium acetate

To remove contaminants such as ethanol and salt (evident by a low 260nm:230nm ratio), RNA was cleaned using alcohol and salt precipitation. 1/9th volume of 3M Sodium Acetate and 2.5 x volume of ethanol was added, vortexed, and left at -80°C for at least 16 hours. Tubes were centrifuged at maximum speed in a benchtop refrigerated centrifuge (Hettich; SLS) for 30 minutes at 4°C and washed with 500µl of 70% (v/v) ethanol, air-dried and

resuspended in an appropriate volume of nuclease-free H₂O. RNA was then re-quantified using a Nanodrop spectrophotometer and stored, aliquoted at -80°C.

2.8.5 Reverse Transcriptase Polymerase Chain Reaction

RT-PCR is a powerful technique used to detect the presence of a specific mRNA transcript in a population of cells. RT-PCR involves two steps; the reverse transcription of mRNA and subsequent PCR amplification. mRNA transcripts are converted to complementary DNA (cDNA) using RNA-dependant DNA polymerase. The resulting thermostable cDNA is then used as a template for PCR amplification using specific primers targeted to the gene of interest. The amplified product can then be visualised using agarose gel electrophoresis.

2.8.6 First-strand cDNA synthesis - Reverse transcription (RT)

cDNA was synthesised using 1µg of total RNA, 50ng of random hexamer primers and a Superscript™ II first-strand cDNA synthesis kit (Invitrogen). After incubation at 65°C for 10 minutes the RNA/hexamer mix was snap-cooled on ice for 1 minute and 7µl of a "master mix" containing the following was added to each reaction: 2µl of Reverse transcription buffer, 2µl of 25mM MgCl₂, 2µl of 0.1mM Dithiothreitol (DTT) and 1µl of 10µM dinucleotide triphosphate (dNTP) mix. Tubes were gently mixed and incubated at 25°C for 2 minutes prior to addition of 1 unit of Superscript™ II reverse transcriptase enzyme. Samples were incubated at 25°C for 10 minutes prior to transfer to a 42°C heatblock for 50 minutes. The reaction was then inactivated at 70°C for 10 minutes and the resulting cDNA was stored at -20°C until use. For each RNA sample a negative control reaction was included where the reverse transcription enzyme was omitted (RT negative).

2.8.7 Primer design for PCR

mRNA coding sequences for genes of interest were obtained from the Ensembl database (99). Where more than one transcript variant was found, the sequences were aligned and primers designed to regions of homology. Primers of between 18-27bp in length were designed using Primer3 version 04.0 software (Whitehead Institute for Biomedical Research, USA) and default parameters, except GC content was restricted to between 40-60%, and melting temperature (T_m) was set to between 56-63°C. Amplicon size was restricted to 300-400bp and was always within one exon. Primers were selected against primer dimer formation or strong secondary structure. Specificity was checked using an NCBI primer BLAST[®] search prior to ordering (Eurofins). On arrival, primers were reconstituted in nuclease free H₂O to a concentration of 100mM and stored at -20°C. Primer sequences are detailed in Appendix V.

2.8.8 PCR primer testing

Primer binding efficiency and optimal annealing temperatures for each primer set were determined using a gradient PCR. A 10-reaction master mix was assembled on ice as follows: 50µl of 20ng/µl human genomic DNA (Promega), 25µl of 10x reaction buffer (Agilent), 2µl of dNTP mix (25mM each dATP, dCTP, dGTP, dTTP; Invitrogen), 10µl of each primer (10mM stock), 2µl (1 Unit) SureStart Taq DNA Polymerase (Agilent) and 151µl of nuclease-free H₂O. 8 x 25µl reactions were then assembled in thin-walled PCR tubes (Axygen;Fisher Scientific) and subjected to the following PCR conditions with a gradient annealing temperature present across the PCR block (Left-Right); 9 minutes at 94°C, 26 cycles of denaturation for 30 seconds at 94°C, annealing for 30 seconds at 50-60°C and a 1 minute extension at 72°C. A final elongation phase of 10 minutes at 72°C was then followed by a 4°C hold. 10µl of each PCR reaction was analysed via agarose gel electrophoresis. The annealing temperature which produced the strongest band at the expected size was then

chosen for RT-PCR. If specific product yield was poor or secondary bands were present, primers were redesigned.

2.8.9 PCR

All PCR reactions were undertaken in thin-walled 8-well strip PCR tubes (Axygen; Fisher Scientific) using a PCR Express® thermocycler (Hybaid). For each experiment a PCR mastermix was prepared on ice to minimise pipetting error. Each reaction contained as follows: 5µl of cDNA (or 5µl of 20ng/µl human genomic DNA (Promega)), 2.5µl of 10x reaction buffer (Agilent), 0.2µl of dNTP mix (25mM each dATP, dCTP, dGTP, dTTP; Invitrogen), 1µl of each primer (10mM stock), 0.2µl (1 Unit) SureStart® Taq DNA Polymerase (Agilent) and 15.1µl of nuclease-free H₂O. Each experiment included the following controls: an RT negative control for each test sample to assess for genomic DNA contamination, a genomic DNA positive control (100ng) to verify the PCR reaction had been successful and a β-actin control PCR for each test sample to verify the integrity of the cDNA. A hotstart Taq polymerase was used in all experiments to reduce background noise and increase efficiency. cDNA template was denatured and Surestart® Taq polymerase activated with a 9 minute, 94°C pre-heat step. This was followed by 30 cycles of denaturation at 94°C for 30 seconds, annealing for 30 seconds at 50-55°C (depending on primer pair) and a 1 minute/Kb extension at 72°C. A final elongation phase of 10 minutes at 72°C was then followed by a 4°C hold. PCR products were analysed using agarose gel electrophoresis.

2.8.10 Quantitative Polymerase Chain Reaction (qPCR) using SYBR® -Green I technology

Quantitative PCR (qPCR) measures the accumulation of PCR products over time and allows the measurement of amplicon product throughout the experiment not just at a predetermined end-point. This is achieved by addition of SYBR®-Green I Dye, a DNA intercalator which binds to double stranded DNA formed

during the PCR reaction. Once bound to DNA, SYBR[®]-Green I emits a fluorescent signal which is proportional to the amount of PCR product present and can be excited using a tungsten halogen lamp or argon laser (at 488nm) and detected using a charged coupled device (CCD) image sensor. A well optimised reaction is essential for accurate results, as SYBR[®]-Green I dye will bind to all double stranded DNA including non-specific product. Therefore it was essential that all primer pairs were tested for specificity as outlined in section 2.8.12.

2.8.11 Primer design for qPCR

Primes were designed using Primer Express Software v.3 (Applied Biosystems) and default parameters. Primers were of 16-27bp in length with an optimal T_m of 58-60°C. Amplicons were of 100-150bp in length and were always within an exon. Specificity was checked using NCBI primer BLAST[®] prior to ordering from Eurofins. Primers were reconstituted in nuclease free H₂O and stored frozen at -20°C. All Primer sequences can be found in appendix V.

2.8.12 qPCR primer testing

RTqPCR primers were tested for specificity and primer binding efficiency prior to use. A dissociation curve or melt curve was used to determine the number of products generated within a reaction. dsDNA product was melted into ssDNA by an increase in temperature over time. The magnitude of the reduction in fluorescence at each increment was then plotted as a dissociation curve. For each dissociation curve, an RT negative and water only control was included. If more than one major peak (one PCR product) was detected, primers were redesigned. Dissociation plots for primer pairs can be found in appendix VI.

2.8.13 qPCR

Reactions were prepared with SYBR[®]-Green I PCR Master mix (Applied Biosystems) containing the SYBR[®]-Green I Dye, AmpliTaq Gold[®] DNA

polymerase, dNTPs, buffer components, and a passive ROX reference to allow for background correction. Reactions were assembled as follows on ice in a 96-well optical reaction plate (ABI): 5µl of template cDNA, 12.5µl of 2x SYBR[®]-green I PCR Master mix, 400nm of each primer and 5.5µl of nuclease free H₂O. The plate was sealed with an optical adhesive cover (ABI) and run on an ABI 7300 sequence detection system using the following thermal cycle profile: 2-minute hold at 50°C, incubation at 95°C for 10 minutes, followed by 40 cycles of denaturation at 95°C for 15 seconds and elongation at 60°C for 1 minute. Each sample was run in triplicate alongside an RT negative control sample from which the reverse transcriptase enzyme had been omitted. A water only (no template) control was included on each plate. Loading controls targeted to GAPDH were included for each sample. Data was collected using ABI Sequence detection software v1.2.3f2 and normalised against the passive reference fluorophore ROX. Data was analysed using the comparative cycle threshold (CT) method as described by the manufacturer (100). Thresholding was set in the region of exponential amplification and cycle threshold values (CT) were calculated as the cycle number required to cross the threshold. Data was expressed as relative quantification (RQ) using GAPDH as the loading control:

Each sample was calculated relative to loading control to give Δ CT;

Δ CT values (CT target-CT reference gene GAPDH)

Δ CT was expressed as relative to the calibrator sample;

$\Delta\Delta$ CT values (Δ CT test sample- Δ CT calibrator)

$\Delta\Delta$ CT was converted to relative quantification;

$RQ = 2^{-\Delta\Delta CT}$

Results were then expressed as log (base2) from calibrator sample.

2.8.14 Affymetrix™ analysis

Affymetrix .CEL files were analysed using Arrayassist™ 5.5.1 software (Agilent). Background was removed and chips were normalised using the Microarray suite 5 (MAS5) algorithm before an absolute calls database was generated (101). Signal intensities were transferred to Excel® and Ingenuity® Pathway Analysis (IPA) software (Ingenuity Systems Inc) for further analysis.

2.9 Protein Analysis

2.9.1 Indirect immunofluorescent labelling of cultured cells

Immunolabelling of cells uses the specificity of antibody-antigen interactions to visualise the distribution of a protein within a fixed cell population. Indirect immunofluorescence uses two antibodies, the first or primary antibody targets the protein of interest, whereas the secondary antibody is conjugated to a fluorophore and binds specifically to the primary antibody. The fluorophore can then be excited using an appropriate wavelength and the resulting emission visualised using a fluorescent microscope.

2.9.1.1 Slide preparation

Teflon® coated 12-well multispot slides (CA Hendley) were wiped with 70% (v/v) ethanol and autoclaved prior to use. Slides were placed into a sterile 4-chambered Hereaus box using sterile forceps. Cells in culture were seeded at a density of 5×10^3 – 2×10^4 cells/well, depending on the experiment. Slides were then incubated at 37°C for 3 hours to allow cell attachment prior to flooding with 5ml of the appropriate medium. At designated time points, cells were fixed using either methanol:acetone (50:50) or 10% (v/v) formalin depending on the antigen of interest.

2.9.1.2 Methanol:Acetone fixation

Cells were fixed by immersion in 5ml of 50:50 (v/v) methanol:acetone for 30 seconds, air dried and stored desiccated at -20°C until required. Once thawed to ambient temperature, wells were delineated using a delineating pen (DakoCytomation).

2.9.1.3 Formalin fixation

Slides were fixed in 10% (v/v) formalin in PBSC for 15 minutes and then washed with PBS for 5 minutes. Cells were permeabilised and blocked with 0.5% (v/v) Triton-X + 5% (v/v) FBS in PBS for 1 hour at ambient temperature. Wells were then delineated using a delineating pen.

2.9.1.4 Fluorescent immunolabelling of cultured cells

50µl of primary antibody at a predetermined dilution was added to each well and incubated for 16 hours at 4°C. No primary antibody negative controls (TBS only) were included in each experiment. Slides were washed 3x in TBS (appendix II) for 5 minutes. 50µl of appropriate Alexa 488/Alexa 594-conjugated secondary antibody was applied to each well and incubated in the dark, at ambient temperature for 1 hour. Slides were then washed five times with TBS on an orbital shaker for five minutes each. To aid visualisation, the cell nuclei were stained with Hoechst 33258 (0.1µg/ml) in the penultimate wash. Slides were air-dried, mounted in DABCO/glycerol antifade (appendix II) to reduce photo-bleaching and sealed with nail varnish.

2.9.1.5 Photomicroscopy of immunofluorescent labelled cells

Cells were visualised on an Olympus BX60 microscope under epifluorescent illumination using x20, x40 and x60 oil immersion objectives. The microscope was equipped with the appropriate excitation and emission filters for

bisbenzimidazole, dual and specific filters for FITC and Texas Red. Images were taken using an Olympus DP50 digital camera and analysed with Image-Pro[®] Plus software (MediaCybernetics) and Photoshop CS4 (Adobe) as outlined in section 2.9.1.6.

2.9.1.6 Calculating nuclear and cytoplasmic protein expression from immunofluorescent images

Nuclear and cytoplasmic labelling was quantified using Photoshop CS4 (Adobe) as described by Kirkeby and colleagues (102). In brief, Hoechst images were superimposed onto the adjacent fluorescent image to be quantified. Background labelling was normalised and the Hoechst image was used as a mask to calculate mean nuclear intensity from the histogram. Selection was then inverted to give cytoplasmic and membrane labelling intensities. One should note that if images are over-saturated Photoshop[™] will not be able to make any distinction between saturated and over-saturated pixels and inaccuracies in the quantification of mean nuclear intensity will result.

2.9.2 Western blotting

Western blotting is a powerful and widely used analytical technique to detect specific proteins within a cell lysate. The principle of western blotting involves size fractionation of a cell lysate using gel-electrophoresis and subsequent transfer onto a solid membrane prior to addition of an antibody specific to the target protein of interest. A near-infrared (NR) fluorophore-conjugated secondary antibody raised against the primary antibody is then added to the membrane and the membrane is scanned using an infrared scanner.

2.9.2.1 Protein extraction

Cell cultures were lysed *in situ* at approx 70% confluence unless otherwise stated. Medium was aspirated and cell sheets were washed 2x in ice-cold D-PBS (Appendix II). 100µl of 2x sodium dodecyl sulphate (SDS) buffer (appendix II) containing 2mg/ml DTT and 0.2%(v/v) protease inhibitor cocktail set 3 (Calbiochem) was pipetted onto the cell monolayer and the cells were scraped using a cell scraper (Greiner) into a chilled microcentrifuge tube. Samples were sonicated using an ultrasonic probe (Jencons Scientific) for three 10-second bursts and then rested on ice for 30 minutes. The lysates were centrifuged at 18,500g, 4°C for 30 minutes to pellet the insoluble material before aliquoting the supernatant and storing at -20°C.

2.9.2.2 Protein Quantification

Total protein content of each sample was determined using a Coomassie protein reagent assay kit (Pierce). Samples were diluted 1:12.5 in dH₂O and 10µl was aliquoted in duplicate into a 96-well flat bottomed plate. A seven point standard curve of 0-1mg/ml BSA (Pierce) was included on each plate. 200µl of ambient temperature Coomassie reagent was added to each well and mixed gently by pipetting. Absorbance was measured using a Multiskan Ascent[®] V1.25 plate reader (Thermo Fisher) at 570nm (test) and 630nm (reference) against a dH₂O control. Ascent software 2.6 (Thermo Fisher) was used to plot a standard curve for the BSA and to estimate the protein concentration for each lysate.

2.9.2.3 SDS-Polyacrylamide gel Electrophoresis (SDS-PAGE)

20µg of protein lysate was made up to 13µl with 2x SDS-lysis buffer. 5µl of 4x lithium dodecyl sulfate sample buffer (LDS; Invitrogen) and 2µl of 10x reducing agent (Invitrogen) was added and the sample denatured by heating to 70°C for 10 minutes in a heatblock. 10-well NuPAGE[™] Novex electrophoresis pre-cast

gels (Invitrogen) were placed into an *Xcell* Surelock™ mini-cell upright electrophoresis tank (Invitrogen). 200ml and 600ml of 1x NuPAGE™ SDS running buffer (Invitrogen) was poured into the inner and outer chambers, respectively. 500µl of NuPAGE™ antioxidant (Invitrogen) was added to the inner chamber prior to loading of the samples. 5µl of All-Blue Precision Plus Protein™ standard (Bio-Rad) was loaded alongside as a marker of protein size and the gel was run at 150V for 90 minutes.

2.9.2.4 Electrophoretic membrane transfer

Electrophoretically-separated proteins were transferred onto Immobilon-P™ polyvinylidene difluoride membrane (PVDF; Millipore) using an *Xcell* II™ blot module (Invitrogen). PVDF membrane was dipped in methanol, rinsed in dH₂O and then soaked in 0.5x "Towbin" transfer buffer with 20% (v/v) methanol (appendix II) along with the required number of blotting pads and Whatman™ filter paper (SLS) for 30 minutes. The gel membrane sandwich was assembled cathode to anode as follows; 2x blot pads, filter paper, gel, PVDF membrane, filter paper, 2x blot pads. The blot module was secured into the *Xcell* SureLock™ Mini-Cell and filled with transfer buffer. The outer chamber was filled with dH₂O and the transfer was performed at 25V for 2 hours on ice.

2.9.2.5 Ponceau Red staining

Protein transfer was visualised on the PVDF membrane by reversible Ponceau red staining. The PVDF membrane was soaked in 42mM Ponceau red in 3% (v/v) trichloroacetic acid for 5-seconds and then washed in dH₂O.

2.9.2.6 Immunolabelling of PVDF membrane using Li-Cor Odyssey

To minimise non-specific binding, membranes were blocked in 50:50 (v/v) Odyssey blocking buffer (Li-Cor):10mM TBS pH 7.6 at ambient temperature on an orbital shaker for 1 hour. Membranes were then probed for 16 hours at 4°C with 5-8ml of pre-titrated primary antibody diluted in 50:50 Odyssey blocking buffer:TBS+0.2% (v/v)Tween-20 (Table 2-1). Membranes were washed 5x 5 minutes in TBS+0.1% (v/v)Tween-20 prior to addition of 5ml of appropriate Alexa Fluor[®] -conjugated secondary antibody (Table 2-2) for 1 hour at ambient temperature with shaking. Membranes were washed as for primary antibody and then washed 1x for 5 minutes with TBS prior to visualisation using an Odyssey[™] Infra-red Imaging system (Li-Cor). Equal loading was verified using an antibody raised against the house keeping gene, β -actin. Densitometry was performed using Odyssey V1.1 software (Li-Cor) and protein expression was normalised relative to β -actin.

2.9.2.7 Membrane stripping and re-probing

PVDF Membranes were incubated in 5mls of 1x western blot recycling reagent (Autogen Bioclear) for 20-30 minutes at ambient temperature on an orbital shaker. Membranes were then washed in TBS, re-blocked with 50:50 (v/v) Odyssey blocking buffer:TBS and re-probed up to 4 times.

2.10 Cell based assays

2.10.1 Cell viability assay

Cell viability was measured using a Methylthiazolyldiphenyl-tetrazolium bromide (MTT) assay. MTT is reduced to an insoluble formazan purple crystal by the activity of the mitochondrial enzyme, dehydrogenase. The amount of formazan purple crystal produced over a set time period can be measured by dissolving in a suitable solvent and performing a spectrophotometric analysis. The amount

of formazan crystal produced is generally proportional to the amount of mitochondrial activity and is assumed to be comparable to viable cell number.

NHU cells were seeded into a 96-well Primaria™ plate at a density of 2×10^3 cells per well in 200µl of KSFMc and were incubated for 24 hours at 37°C (day - 1). Plates were treated with inhibitors in triplicate wells (day 0) and assayed at day 0, 1, 3 and 6. A solvent balanced control was included at each timepoint. To assay, medium was removed and 200µl of 0.5mg/ml MTT was incubated on the cells for 4 hours at 37°C. MTT solution was then removed and the resulting formazan crystals were dissolved in 200µl of spectrophotometric grade DMSO. Absorbance was measured at 570nm (test) and 630nm (reference) against a DMSO control using a Multiskan Ascent® V1.25 plate reader (Thermo Fisher) and Ascent software 2.6 (Thermo Fisher). Absorbance is directly proportional to mitochondrial activity in each sample, which in turn is assumed to be proportional to viable cell biomass and cell number.

2.10.2 Luciferase Reporter assays

Reporter assays are used to assess the activity of a signal transduction pathway by assessing the functional status of the downstream transcription factor (TF). Luciferase (Luc) reporter constructs contain the TF binding site of interest, upstream of a luciferase reporter gene. The vector can be transfected into cells and the activity of the reporter gene measured using a chemiluminescent assay.

2.10.2.1 TOPFLASH/FOPFLASH TCF reporter plasmids

TOPFLASH TCF reporter plasmid (Millipore) is a luciferase reporter of β -catenin mediated transcription first described by Korinek and colleagues (103). Activation of the three TCF-binding sites upstream of a thymidine kinase (tk) minimal promoter leads to transcription and translation of the encoding Firefly luciferase (*Photinus pyralis*) gene (Figure 2-2) and can be quantified via a dual luciferase reporter assay (section 2.10.3.6). The negative control plasmid,

FOPFLASH (Figure 2-2), has an identical backbone and minimal promoter but contains a mutated TCF binding site which does not bind TCF transcription factor and is used to assess basal activity from the minimal promoter.

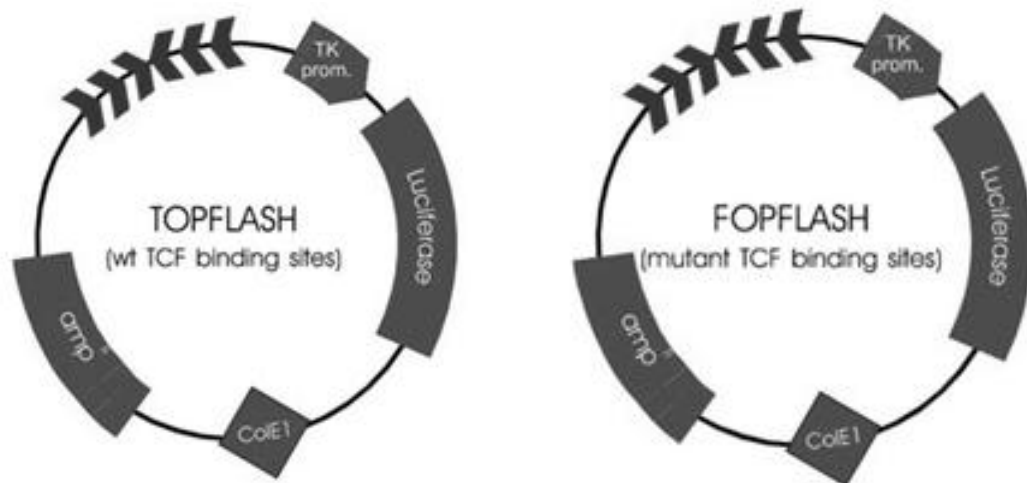


Figure 2-2 TOPFLASH/FOPFLASH vectors

Schematic representation of the luciferase reporter constructs TOPFLASH and FOPFLASH used for assessing TCF transcription factor activity. In bacteria, plasmid is replicated using the ColE1 origin of replication (ColE1^{Ori}) and successfully transformed cells are selected via expression of the ampicillin resistance cassette (Amp^r). In mammalian cells, Firefly luciferase expression is driven via the thymidine kinase minimal promoter (TK prom.) and potential TCF binding sites. Image reproduced from Millipore catalogue number 1-285.

2.10.2.2 pRL-CMV internal control plasmid

The pRL-CMV vector (Figure 2-3; Promega) is a normalising transfection control reporter for use in combination with the Firefly luciferase reporter construct, (TOPFLASH/FOPFLASH). pRL-CMV contains a CMV promoter to drive high-level expression of Renilla luciferase (*Renilla Reniformis*) which can be measured in conjunction with Firefly luciferase using a Dual luciferase reporter assay.

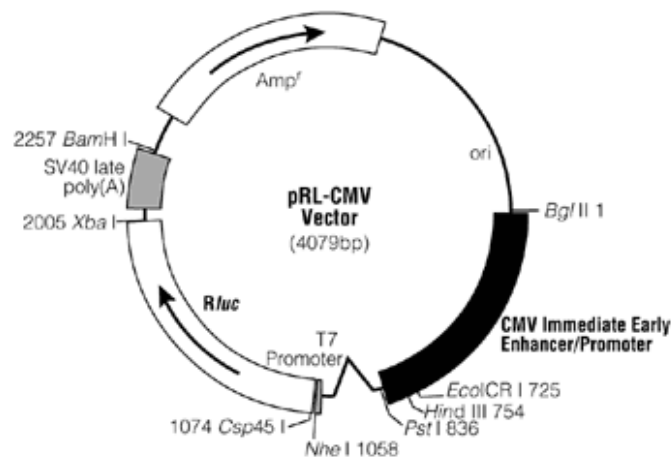


Figure 2-3 pRL-CMV reporter construct

pRL-CMV is intended for use as an internal control reporter vector in combination with a *Firefly* luciferase reporter vector such as TOPFLASH/FOPFLASH. pRL-CMV Vector can be propagated in competent *E.coli* bacteria using the ColE1 origin of replication (*Ori*). Successfully transformed cells can be selected via expression of the ampicillin resistance gene (Amp^r). pRL-CMV contains the cytomegalovirus (CMV) immediate/early enhancer/promote to drive high-level expression of *Renilla* luciferase (*Rluc*) in mammalian cells. An SV40 Late Polyadenylation Signal (SV40 late poly(A)) enhances RNA stability and translation via the addition of a poly A-tail. Image reproduced from catalogue E2261 (Promega).

2.10.2.3 Transfection

The transfection of NHU cells using liposome-based gene transfer was optimised using a GFP reporter plasmid and analysis by flow cytometry (FSC vs. SSC plots and histograms can be found in Appendix VII). Five different

transfection reagents were tested in parallel on NHU cells, alongside a non-transfected control to assess toxicity. Each reagent was tested at the manufacturer's recommended ratio of lipid to DNA. Of the five reagents tested, Fugene[®]HD (Roche) was chosen as the most effective reagent for liposome mediated gene delivery as it was tolerated well by NHU cells and yielded the highest transfection rate (Appendix VII).

2.10.2.4 Transfection of NHU cells with Fugene[®]HD transfection reagent

NHU cells were seeded into a 24-well plate in KSFMc at a concentration of 4×10^4 cell/well and incubated overnight at 37°C in 5% CO₂ in air. The following day, 0.5µg of either TOPFLASH or FOPFLASH along with 0.01µg of pRL-CMV plasmid was mixed in 40µl of serum-free medium (Optimem; Invitrogen) containing 3µl of Fugene[®] HD transfection reagent and incubated at ambient temperature for 30 minutes. KSFMc was removed from the 24-well plate and replaced with 0.5ml of Optimem medium. DNA:Fugene complex was added dropwise to each well and gently mixed by rocking. The transfection was incubated at 37°C with 5% CO₂ in air for 16 hours, after which the medium was replaced with normal growth medium and the cells were treated with Wnt ligand or GSK3β inhibitor for 24-72 hours.

2.10.2.5 Cell lysis

Medium was removed and cells were rinsed in 1ml of PBS per well. 100µl of 1x passive lysis buffer (Promega) was incubated in each well for 15 minutes with gentle agitation. Lysate was transferred to a 1.5ml autoclaved microcentrifuge tube and stored at -20°C for no more than 2 weeks before analysis.

2.10.2.6 Dual luciferase reporter assay

All reagents were prepared as described by the manufacturer (Promega). In short, lyophilised Firefly luciferase assay substrate was reconstituted in 10ml of luciferase assay buffer II (LARII). Stop and Glo™ reagent was prepared by mixing 1:50 Stop and glo™ buffer to 50x Stop and Glo™ substrate. Both reagents were kept out of the light and on ice. 20µl of each sample to be tested was dispensed into a black flat-bottomed 96-well plate in triplicate. 100µl of LARII was dispensed into each well and luminescence from Firefly luciferase was measured using a BMG Labtech POLARstar Optima plate reader. 100µl of Stop and Glo™ reagent was then added to extinguish Firefly luciferase activity and activate Renilla luciferase. Luminescence from Renilla luciferase was recorded and used to normalise the experimental data for differences in transfection efficiency (Figure 2-4).

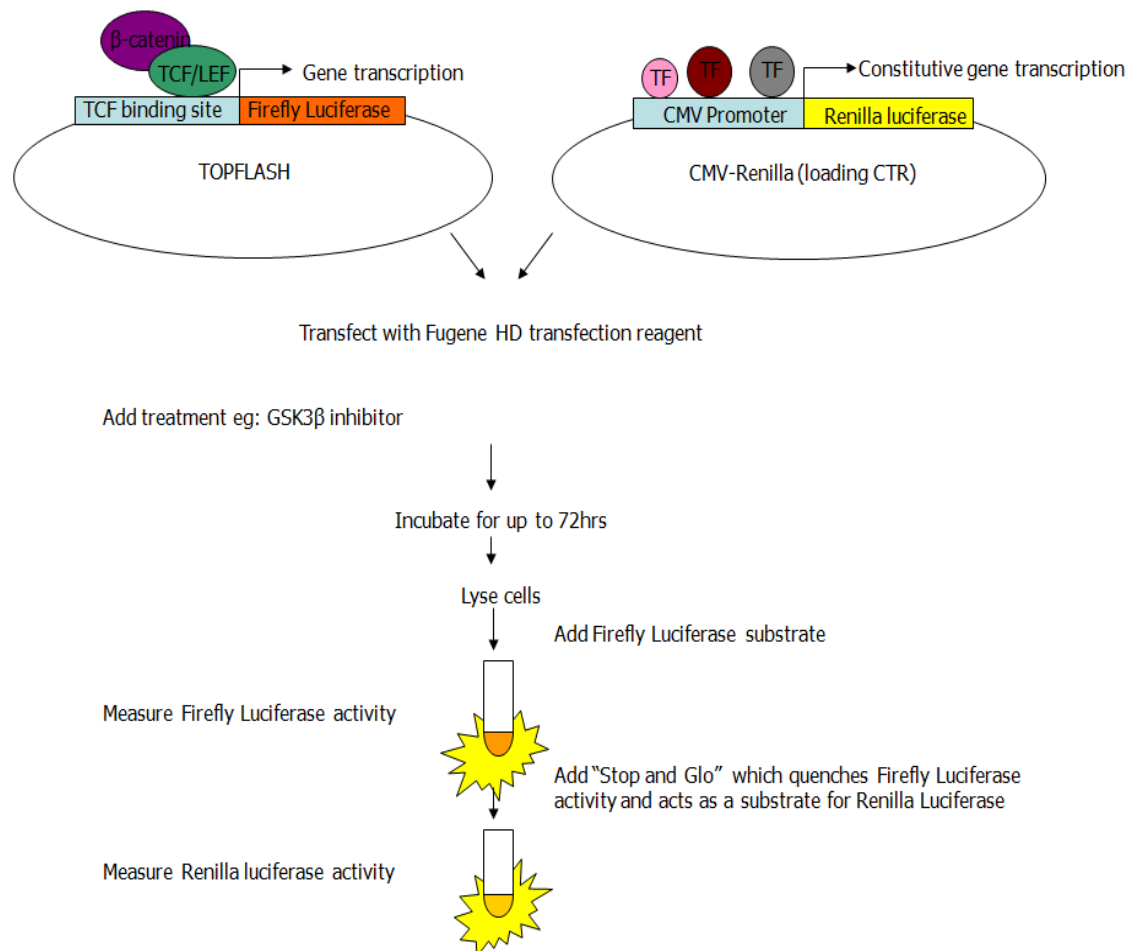


Figure 2-4 Dual Luciferase reporter assay

Schematical representation of a dual luciferase assay to measure Wnt signalling and downstream TCF activity. Adapted from Promega technical manual TM040.

2.10.3 Flow Cytometry

NHU Cells were harvested as for routine passaging, washed and re-suspended in 100µl of FACS buffer (PBS with 1% (v/v) FBS) prior to analysis on a Beckman Coulter Epics XL FACS machine. Untransfected cells were used as a control to gate the live cell population. Cells treated with transfection reagent alone (no plasmid) were used as a negative control. A total of 10,000 live cells were collected per analysis. Side scatter (SSC) was plotted against forward scatter (FSC) and GFP fluorescence was measured in the FITC channel. Scatter plots and histograms were analysed using Summit Software v4.3 (DakoCytomation).

2.11 Statistical analysis

Data was represented graphically using either Excel[®] (Microsoft) or Sigmaplot 11.0 (Systat Software). Where possible, data was presented as the mean of all replicates with error bars representing \pm one standard deviation. Statistical analysis was performed using GraphPad InStat software V3.05 (GraphPad) when at least three data points were obtained, in which case, the data were confirmed to be drawn from Gaussian distribution. One-way analysis of variance (ANOVA) tests were used to compare three or more sample means, along with the appropriate post-test. Bonferroni multiple comparison post-tests were used to test which treatments were significantly different from each other. A two-tailed, unpaired t-test was used to compare two sample means. Levels of significance are cited in the text and assumed to be significant where $P < 0.05$.

3 Screening for components of the canonical Wnt pathway in Normal Human Urothelial cells

3.1 Aims

The aims of this chapter were:

- To determine if fundamental components of the canonical Wnt signalling pathway were present at the mRNA level in NHU cells.
- To investigate the hypothesis that Wnt signalling is involved in the development and maintenance of the proliferative phenotype important in urothelial repair and regeneration.

Specific objectives of this sub-chapter were:

- To use mRNA Affymetrix™ genechip expression data to assess the presence of essential components of the canonical Wnt signalling cascade in proliferating NHU cells *in vitro*.
- To compare the mRNA expression profile of Wnt signalling components during proliferation, when quiescent and after differentiation.

3.2 Experimental Design

Affymetrix™ U133 plus 2 mRNA genechip files previously generated by Dr. J. Fleming (Jack Birch Unit; University of York) were used as a screening tool to assess the presence or absence of mRNA transcript from genes implicated in the Wnt canonical signalling cascade. The data set consisted of a six day time course (6 hours, 24 hours, 72 hours, and 144 hours) from a bladder-derived NHU cell line (Y676) that had been treated as outlined below and in Figure 3-1:

Maintained as a non-differentiated culture.

Induced to differentiate with 1µM troglitazone (PPARγ agonist) and concurrent EGFR blockade using 1µM PD153035 (TZ/PD).

Induced to differentiate with 5% (v/v) adult bovine serum (ABS) and 2mM calcium chloride (ABS/Ca²⁺).

Gene chip raw data files (.cel) were imported into Genespring GX v11.0. Background correction, normalisation and probe summarisation were performed using the MAS5 algorithm. Internal hybridisation controls were checked to assess the reliability of the data from each chip and unreliable chips were removed from the analysis. An absolute calls database was generated for each probe set using the background correction and MAS5 algorithm. Probe sets were assigned an absent, marginal or present call using the standard thresholding criteria within the MAS5 algorithm. Genes with no present call in any of the chips were omitted. A list of probe sets with at least one present call was compiled and exported into Microsoft Excel® as well as Ingenuity™ IPA software for further analysis.

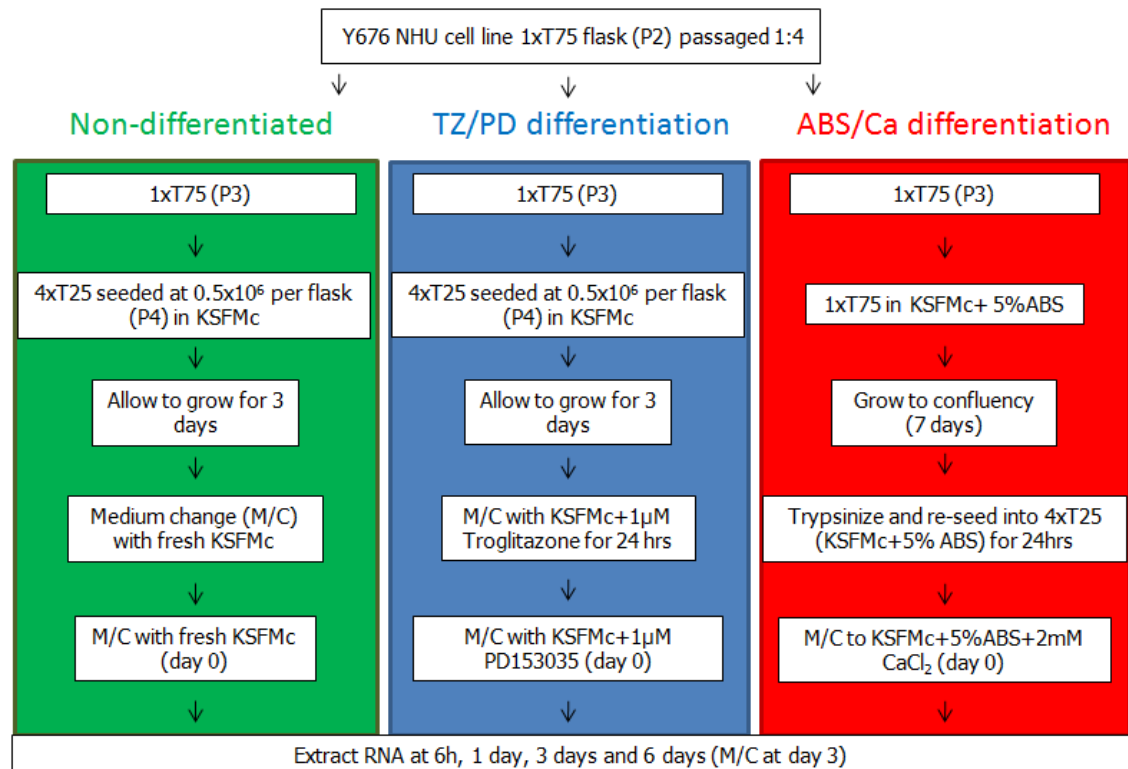


Figure 3-1 Schematic representing the experimental design for the microarray time course experiment

Bladder-derived NHU cell line (Y676) was passaged at a split ratio of 1:3 and grown as either a non-differentiated monolayer or induced to differentiate using two independent methods (TZ/PD or ABS/Ca²⁺). RNA was extracted using TRIzol at 4 time points over the course of 6 days to look at the changes in mRNA profile during the transition from proliferative to confluent monolayer, as well as during differentiation.

Each microarray was firstly interrogated for well-characterised markers of proliferation. This was achieved by assessing the expression of a subset of genes involved in the cell cycle, known as the “proliferation signature” (reviewed by (115)). Expression of the “proliferation signature” correlates well with the proliferation rate of cells in culture and can be used as a defined marker of cell cycle progression (115). This signature can vary between cell types but there is a core set of genes whose highest expression always correlates with a rapid proliferation rate. These genes are PLK1, BUB1 and TOP2A (all genes which contain a FOXM1 transcription factor binding site) and are important in initiating the transition from G₂ –M (Figure 3-2).

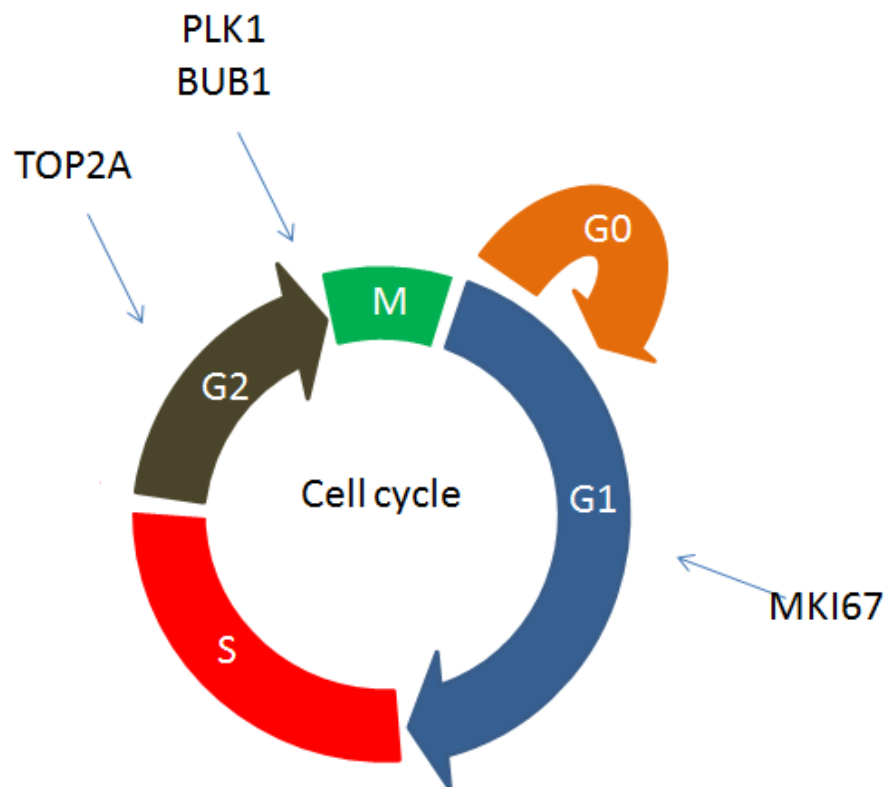


Figure 3-2 Cell cycle and associated proliferation marker gene expression

If a marker was represented by more than one probe set, the most specific and sensitive probe set (as ranked by Geneannot Microarray Gene Annotation, Weizmann Institute of Science (116)) was plotted. Each chip was ranked according to its expression of each proliferation marker. Each differentiated time series was validated manually using specific markers of terminal urothelial differentiation and ranked accordingly. The chip ranked as the most proliferative was then compared to the least proliferative (quiescent) and the most terminally differentiated. Changes greater than 2-fold were exported into Ingenuity™ IPA software and a gene ontology analysis was undertaken to establish which biological processes and signalling pathways were altered in the following scenarios:

- Quiescent cells vs. proliferating cells
- TZ/PD terminally differentiated cells vs. proliferating cells
- ABS/Ca 2+ terminally differentiated cells vs. proliferating cells

Specific changes in the Wnt pathway were interrogated manually using Excel®. Wnt ligands, receptors and downstream gene targets, as well as known agonists and antagonists were expressed as log₂ fold change and represented in schematic as well as tabular form.

Changes in gene expression were confirmed for 13 targets using RT-PCR and mRNA from the original Y676 cell line used to generate the Affymetrix Genechips. RNA from uncultured stripped urothelium (Y1043) was used to assess the presence of transcript *in vivo*. A genomic DNA positive control and a no template control were included in all experiments. Reverse transcriptase negative samples were included to verify samples were free from genomic DNA contamination. Primers targeted to UPK2 and MKI67 were used to assess differentiation and proliferation, respectively. Expression changes were then validated on differentiated and undifferentiated cultures from three independent NHU cell lines (Y878, Y372 and Y387) using SYBR-green I RT-qPCR and the appropriate controls.

3.3 Results

3.3.1 Quality control assessment

Quality control analysis of the MAS5 normalised data was undertaken in Genespring GX v11.0. Internal controls for housekeeping genes, GAPDH, β -actin, 18s rRNA and 28s rRNA were used to assess the quality of the hybridised cDNA by measuring the 3' to 5' ratio using C- and N-terminal probe sets. A ratio greater than 3 indicated either RNA degradation prior to cDNA synthesis or incomplete cDNA synthesis during reverse transcription. Two chips out of the 12 failed the acceptable 3-fold cut off for one gene (Table 3-1). These were data points TZ/PD 6h and TZ/PD 72 h.

Log₂ MAS5 normalised signal intensities for the externally spiked hybridisation controls; BioB, BioC, BioD (from the *E.coli* biotin synthesis pathway) and CreX (from the recombinase gene for P1 bacteriophage) were plotted and displayed as line graphs. BioB, bioC, bioD and CreX signal intensities increased as expected indicating hybridisation was acceptable for all chips except TZ/PD 6h (Figure 3-3).

Box and whisker plots were drawn from the median, 25th quartile and 75th quartile (Figure 3-4). One chip had a significantly higher than average median and spread of data. This was data point TZ/PD 6h. To enable accurate comparison between chips, data must be similar in range and quality. Hybridisation problems and quality issues could skew the results but as there were no technical replicates (N=1) within the experiment, chip substitutions were not possible. Time point TZ/PD 6h had quality control issues, signifying possible RNA degradation. It also had a larger than average spread of data, indicating high levels of background which would produce a skewed distribution of expression (i.e., was not normally distributed). Chip TZ/PD 6h was therefore removed from the data set and the data was normalised once again using the MAS5 algorithm.

	β -actin (X00351_at)	GAPDH (M33197_at)	18S rRNA (M10098_at)	28s rRNA (M27830_at)
Proliferating 6h	1.332	1.012	1.535	0.067
Proliferating 24h	1.414	1.014	1.665	0.068
Proliferating 72h	1.333	1.003	1.617	0.067
Proliferating 144h	1.439	0.990	1.385	0.084
TZ/PD 6h	1.421	1.033	4.742	0.997
TZ/PD 24h	1.614	0.992	1.129	0.025
TZ/PD 72h	3.354	1.060	0.956	0.071
TZ/PD 144h	2.423	1.228	1.263	0.073
ABS/Ca 6h	1.202	0.998	1.741	0.125
ABS/Ca 24h	1.549	1.025	1.613	0.081
ABS/Ca 72h	1.500	1.005	2.123	0.073
ABS/Ca 144h	1.557	1.037	1.451	0.263

Table 3-1 Affymetrix internal controls

Table of 3'/5' ratios for internal controls β -actin, GAPDH, 18S rRNA and 28S rRNA. A ratio higher than 3 indicates RNA degradation. Boxes highlighted in yellow indicate samples that failed the quality control check for RNA degradation.

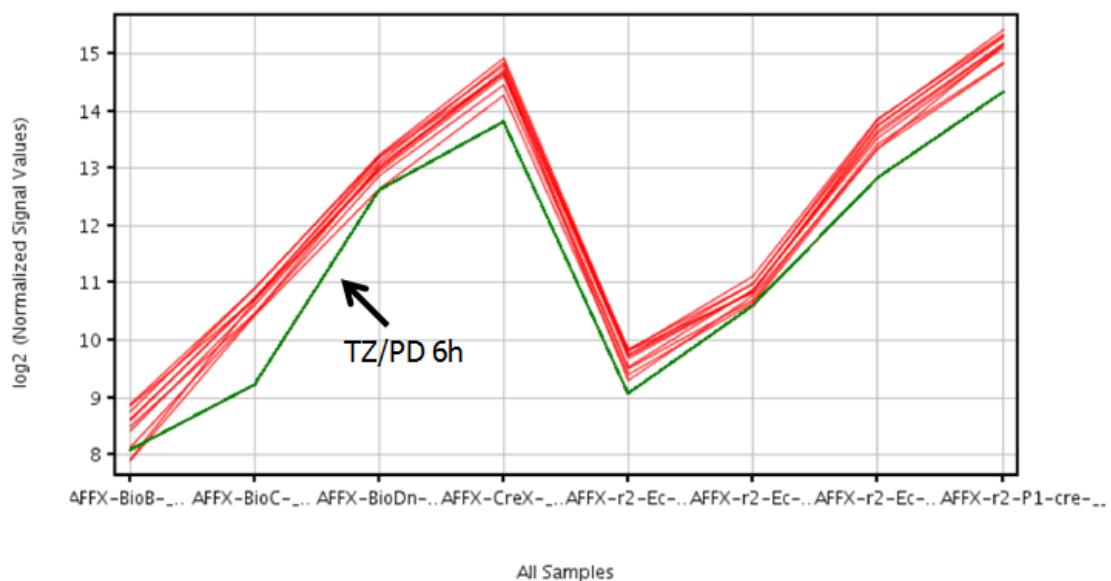


Figure 3-3 Spiked hybridisation controls

Log₂ normalised signal values for spiked biotin-labelled cRNA transcripts from bioB, bioC, bioD and cre at 1.5, 5, 25, and 100pm respectively. All chips show a similar level of hybridisation except chip TZ/PD 6h (labelled in green) which has a lower normalised signal value for bioB indicating an issue with cRNA hybridisation.

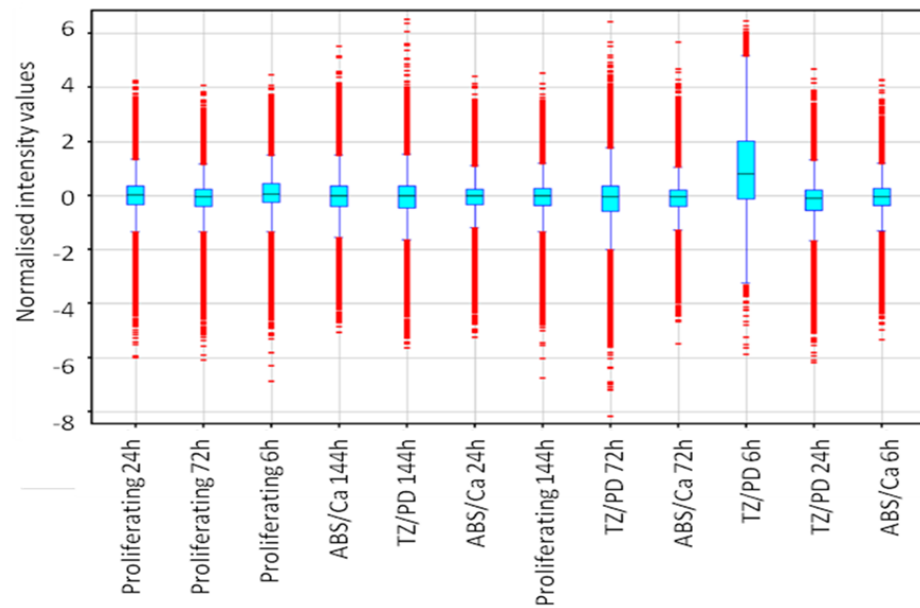


Figure 3-4 Affymetrix array analysis box and whisker plots

Normalised MAS5 intensity values for all probes within the U133 plus 2 chip were displayed as a box and whisker plot. Blue boxes indicate the median, 25th and 75th quartile, whiskers indicate the 5th and 95th quartile. Points in red indicate outliers. Chip TZ/PD 6h had a higher than average median intensity as well as a larger spread of data.

3.3.2 Assessment of the proliferation signature

PLK1, TOP2A and BUB1 mRNA expression was higher in the non-differentiated time series compared to the TZ/PD and ABS/Ca²⁺ treated cells (Figure 3-5). Within the non-differentiated time series, mRNA expression peaked at 24 hours for all three markers (Figure 3-5). MKI67 expression also correlated well, with its highest expression seen at the 24 hour time point (Figure 3-5). The 24 hour time point scored the highest for all four markers and was ranked as the most proliferative. The 144 hour time point was ranked as the least proliferative (Table 3-2).

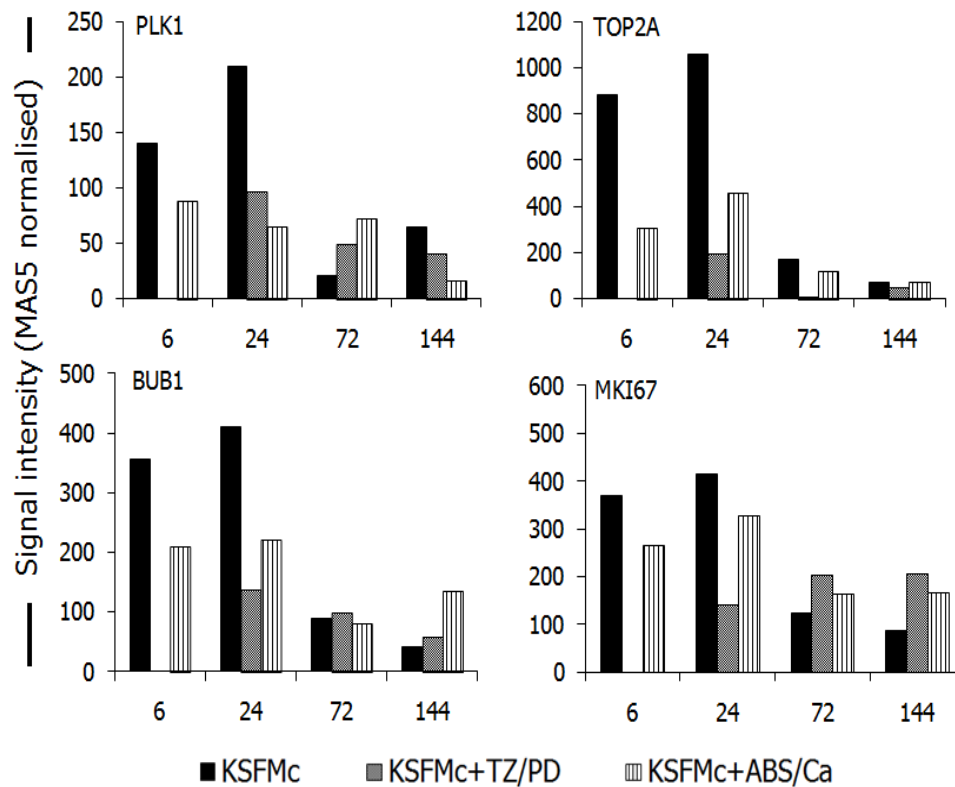


Figure 3-5 Expression of proliferation markers

Affymetrix™ mRNA microarray analysis of proliferation markers PLK1, TOP2A, BUB1 and MKI67 in cultures of non-differentiated and differentiated NHU cells over a 6 day time course. Data is expressed as arbitrary MAS5 normalised signal intensities. Black bars represent non-differentiated NHU cultures. Dotted bars represent NHU cultures induced to differentiate with the addition of TZ/PD. Striped bars represent NHU cultures induced to differentiated with ABS/Ca²⁺.

Time point	PLK1	TOP2A	BUB1	MKI67	Score	Rank
6	+++	+++	+++	+++	12	2nd
24	++++	++++	++++	++++	16	1st
72	+	++	++	++	7	3rd
144	++	+	+	+	5	4th

Table 3-2 Ranking non-differentiated NHU cultures according to expression of proliferation markers

Non-differentiated NHU cultures were ranked according to their expression of PLK1, TOP2A, BUB1 and MKI67 mRNA expression using Affymetrix™ microarray data from a 6 day time course. Key; + lowest expression over time, ++++ highest level of expression over time.

3.3.3 Assessment of differentiation

Each time series was assessed for markers of urothelial differentiation. With both differentiation protocols UPK2 and UPK3a were seen to accumulate over time with the final time point of 144 hours expressing the highest amount of UPK2 and UPK3a mRNA (Figure 3-6). Almost no UPK2 or UPK3 was detected in any of the non-differentiated cultures (KSFMc). KRT7 expression increased over time in the TZ/PD model but was relatively unchanged in the ABS/Ca²⁺ model (Figure 3-6). This was probably due to the fact that the ABS/Ca²⁺ cultures were pre-treated prior to commencement of the time course. Pre-treatment of cultures with 5% (v/v) ABS is a prerequisite to obtain a tight epithelial barrier in accordance with the published method (94). Because of this, KRT7 up-regulation had probably already occurred (evident from the high KRT7 expression at 6h) and thus was not observed as a change in the dataset.

Cultures induced to differentiated using either method express urothelial terminal differentiation markers, but only the ABS/Ca²⁺ model is known to result in a functional barrier (94). The factors that contribute to this are yet to be defined but both models are thought to activate the nuclear receptor PPAR γ . For this reason each differentiation procedure was compared separately to the proliferating culture with common changes compiled at the end.

CLDN4 expression varied significantly over the 144 hour time course with no real trend (Figure 3-6). CLDN4 was seen to increase in the non-differentiated (KSFMc) cultures by > 5-fold between time points 24-72 hours. Both systems of inducing differentiation were ranked according to expression of the four markers of urothelial differentiation. For both systems, the final time point of 144 hours was ranked the most "differentiated" within the data set (Table 3-3, Table 3-4).

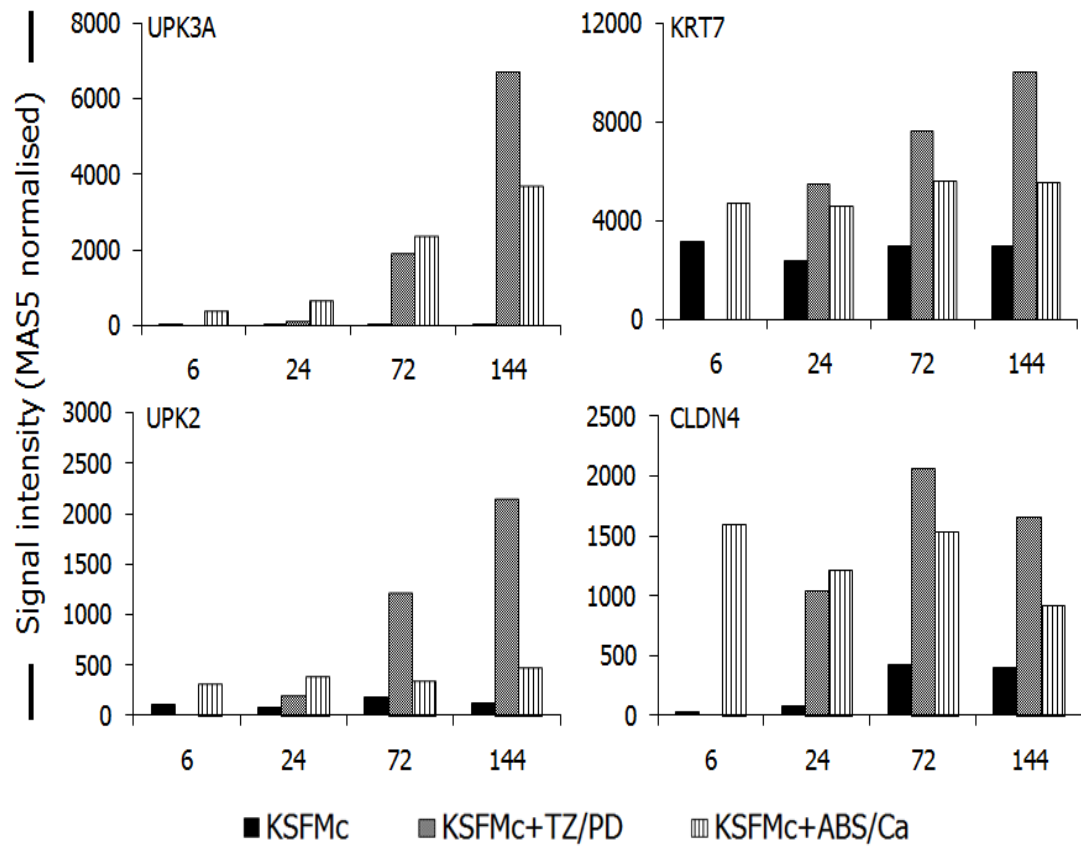


Figure 3-6 Expression of urothelial differentiation- associated markers

Affymetrix mRNA microarray analysis of urothelial specific markers of differentiation UPK3a, KRT7, UPK2 and CLDN4 in cultures of non-differentiated and differentiated NHU cells over a six day time course. Data is expressed as arbitrary MAS5 normalised signal intensities. Black bars represent non-differentiated NHU cultures. Dotted bars represent NHU cultures induced to differentiate with the addition of TZ/PD. Striped bars represent NHU cultures induced to differentiate with ABS/Ca²⁺.

Time point	UPK2	UPK3a	KRT7	CLDN4	Score	Rank
6	ND	ND	ND	ND		N/A
24	+	+	+	+	4	3rd
72	++	++	++	+++	9	2nd
144	+++	+++	+++	+++	11	1st

Table 3-3 Ranking TZ/PD treated NHU cultures over time according to their expression of urothelial markers of terminal differentiation

TZ/PD treated NHU cultures were ranked according to their expression of UPK2, UPK3a, KRT7 and CLDN4 mRNA expression using Affymetrix™ microarray data from a 6 day time course. Key; + lowest expression over time, ++++ highest level of expression over time. ND= no data as chip removed.

Time point	UPK2	UPK3a	KRT7	CLDN4	Score	Rank
6	+	+	++	++++	8	3rd/4th
24	+++	++	+	++	8	3rd/4th
72	++	+++	+++	+++	11	2nd
144	++++	++++	++++	+	13	1st

Table 3-4 Ranking ABS/Ca²⁺ treated NHU cultures over time according to their expression of urothelial markers of terminal differentiation

ABS/Ca²⁺ treated NHU cultures were ranked according to their expression of UPK2, UPK3a, KRT7 and CLDN4 mRNA expression using Affymetrix™ microarray data from a six day time course. Note induction of differentiation procedure for ABS/Ca contains pre-treatment). Key; + lowest expression over time, ++++ highest level of expression over time.

3.3.4 Ontology analysis

20,490 genes were termed “present” from the MAS5 normalised proliferating 24 hour time point. These genes were imported into ingenuity IPA software and a core functional analysis was undertaken. The highest ranked functions were gene expression, cell cycle control, RNA post transcriptional modification and cell growth.

Ontology analysis of the significant changes (2127 >2 fold) between quiescent and proliferating cultures revealed 18 signalling pathways significantly altered, of which Wnt was ranked 6th behind Notch, Sonic Hedgehog, mTOR, PTEN and p53 signalling (Figure 3-7). Further analysis of the Wnt-specific changes, revealed 6 Wnt related genes were up-regulated and 4 were down-regulated (Table 3-5).

Ontology analysis of the significant changes (2896 >2 fold) between TZ/PD differentiated and proliferating cultures revealed 22 signalling pathways were significantly altered of which Wnt signalling was ranked 17th (Figure 3-8). In total, 23 Wnt related changes were found, 8 of which were up-regulated and 15 down-regulated (Table 3-5).

Ontology analysis of the significant changes (2187 >2 fold) between ABS/Ca²⁺ differentiated and proliferating cultures revealed 22 signalling pathways were significantly altered of which Wnt signalling was ranked 16th (Figure 3-9). 21 Wnt pathway-associated changes were seen, with 9 components up-regulated and 12 down-regulated (Table 3-5).

	Quiescent	TZ/PD	ABS/Ca ²⁺
Wnt genes up-regulated (≥ 2 fold)	6	8	9
Wnt genes down-regulated (≥ 2 fold)	4	15	12
Total Wnt related changes (≥ 2 fold)	10	23	21
Total gene changes across chip	2127	2896	2187

Table 3-5 Number of Wnt related genes up- and down-regulated in quiescent and differentiated NHU cultures compared to proliferating NHU cell cultures

Number of Wnt signalling components altered by at least 2-fold in quiescent, TZ/PD differentiated and ABS/Ca²⁺ differentiated cultures when compared to proliferating NHU cell cultures.

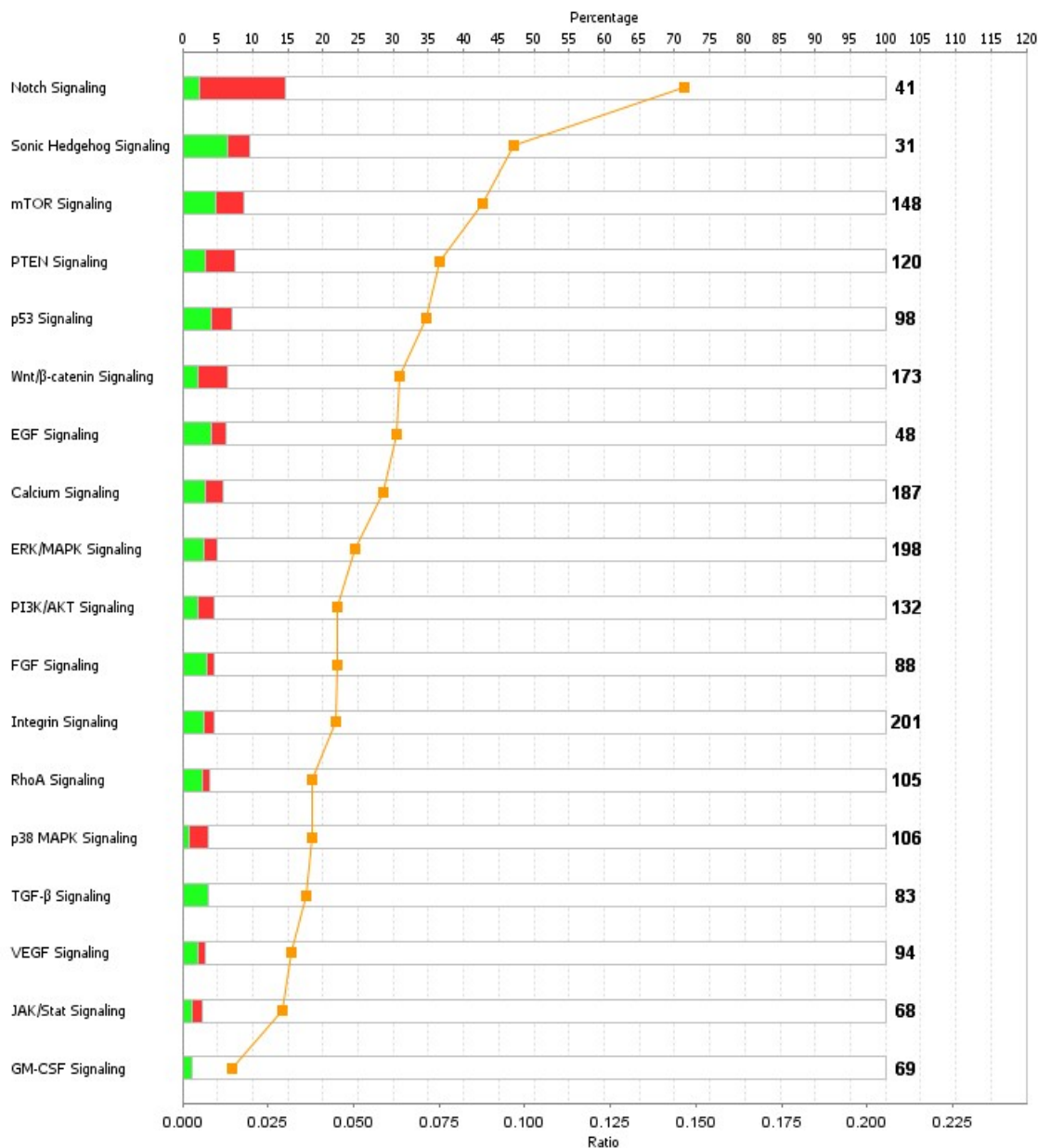


Figure 3-7 Ontologies of genes up- and down-regulated in quiescent NHU cells compared to proliferating NHU cells *in vitro*

Genes involved in signal transduction with at least a 2-fold change in mRNA expression (total gene changes 2127) were categorised according to the pathway in which they function. Up-regulated genes are expressed as red bars and down regulated as green bars. Signalling pathways were then ranked according to the percentage of gene altered within each pathway. Some genes may function in more than one pathway. Bar charts were drawn using Ingenuity™ IPA software.

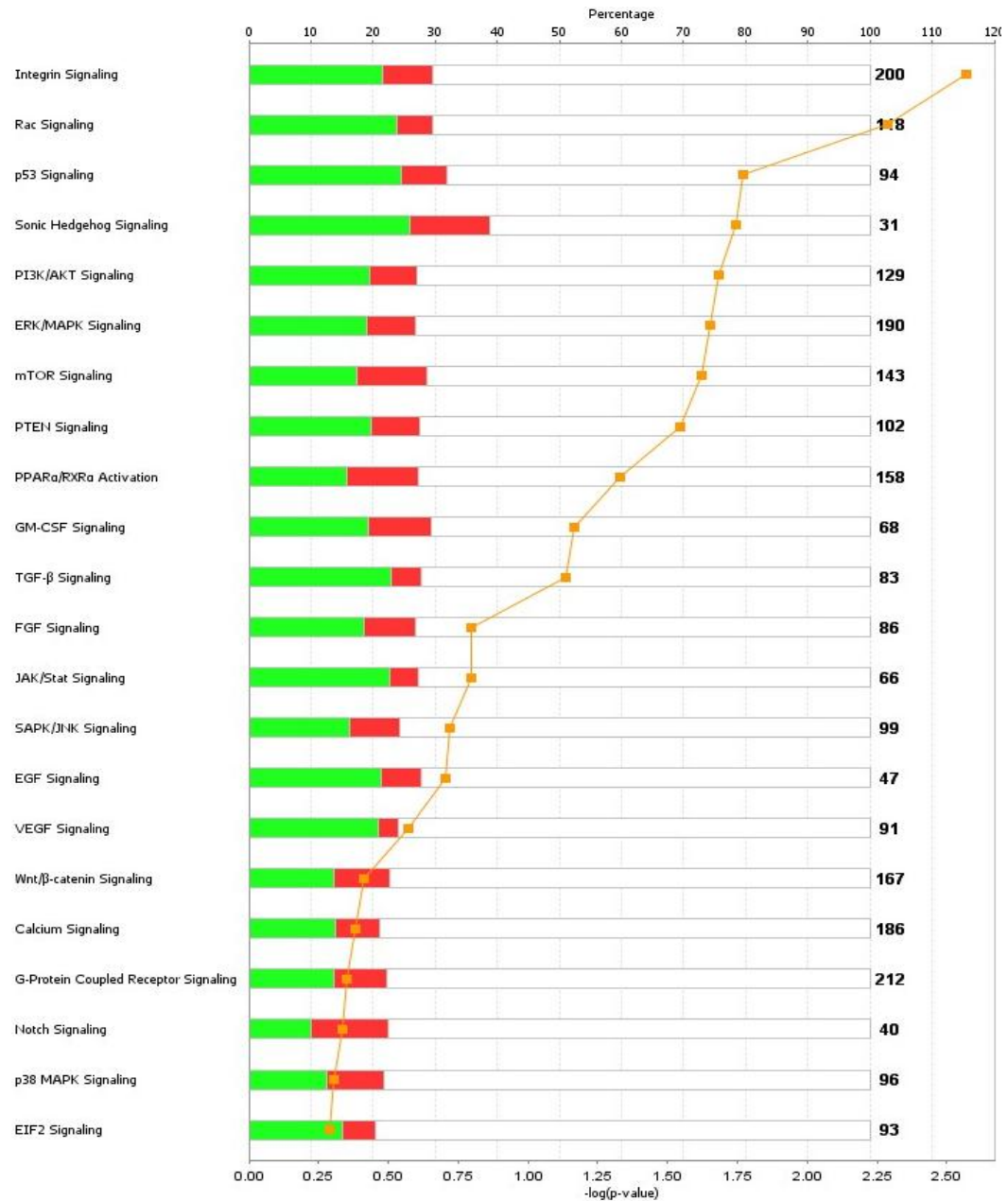


Figure 3-8 Ontologies of genes up- and down-regulated in TZ/PD treated NHU cells compared to proliferating NHU cells *in vitro*

Genes involved in signal transduction with at least a 2-fold change in mRNA expression (total gene changes 2127) were categorised according to the pathway in which they function. Up-regulated genes are expressed as red bars and down-regulated as green bars. Signalling pathways were then ranked according to the percentage of gene altered within each pathway. Some genes may function in more than one pathway. Bar charts were drawn using Ingenuity™ IPA software.



Figure 3-9 Ontologies of genes up- and down-regulated in ABS/Ca²⁺ treated NHU cells compared to proliferating NHU cells *in vitro*

Genes involved in signal transduction with at least a 2-fold change in mRNA expression (total gene changes 2127) were categorised according to the pathway in which they function. Up-regulated genes are expressed as red bars and down-regulated as green bars. Signalling pathways were then ranked according to the percentage of gene altered within each pathway. Some genes may function in more than one pathway. Bar charts were drawn using Ingenuity™ IPA software.

3.3.5 In depth analysis of Wnt associated genes

Wnt pathway related mRNA transcripts were comprehensively analysed using the normalised MAS5 data imported into Excel[®]. All fundamental components necessary for a functional Wnt cascade were present at the mRNA level in the proliferating NHU culture (Figure 3-10). All constituents downstream from the frizzled receptor to TCF/Lef transcription factors were categorised as present using the calls database generated through MAS5. For several components, more than one gene was expressed at the mRNA level and thus to aid visualisation, data was interpreted as a schematical Wnt cascade with present transcripts detailed alongside each component (Figure 3-10). Seven receptors, all of which were known to play a role in transducing the Wnt canonical signal, were present. 20 known transcriptional Wnt signalling targets were present in proliferating NHU cells. A number of intracellular as well as extracellular Wnt signalling antagonists were also expressed at the mRNA level including DKK, Kremen, CBY, CTNNBIP and NLK. mRNA transcript for four Wnt ligands were also present.

Manual interrogation of the fold change values from the quiescent vs. proliferating chips revealed 13 significant (>2 fold) Wnt pathway changes (Figure 3-11). Expression of four Wnt ligands significantly increased when the culture was quiescent. One Frizzled receptor, Fzd8 was also up-regulated in the quiescent population by 4.85-fold. Wif1, an extracellular Wnt signalling antagonist was up-regulated 6.53-fold in the quiescent population. Five downstream Wnt gene targets were down-regulated in the quiescent population including Axin2 (down 2.38-fold), Twist (down 7.9-fold) and Survivin (BIRC5 down 12.7-fold), although none are Wnt-specific.

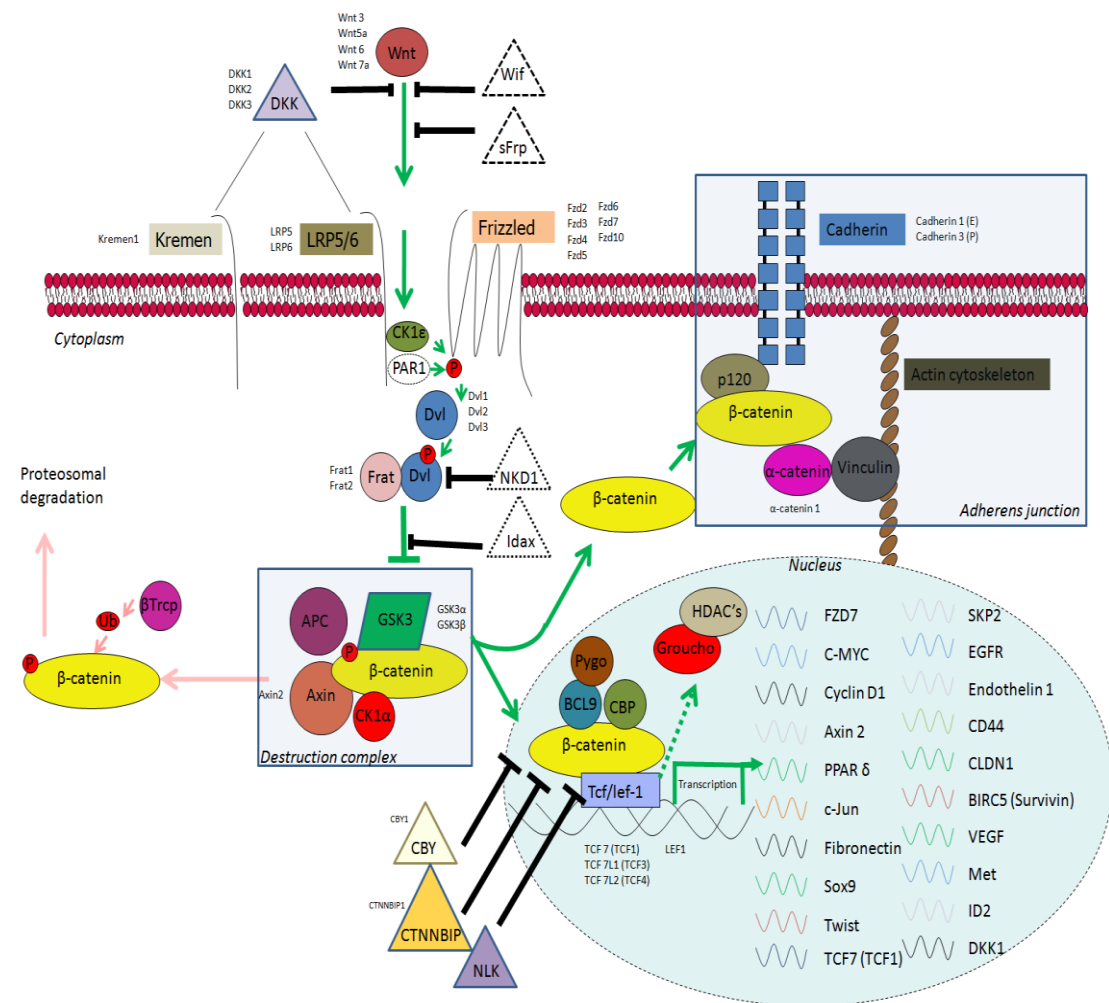


Figure 3-10 Schematic representation of the components present from the canonical Wnt cascade in proliferating NHU cells

All coloured components were classified as present from MAS5 normalised Affymetrix™ data taken from proliferating NHU cells *in vitro*. Components in white with dashed borders were classified as absent in the proliferating NHU culture. Components with more than one gene expressed are labelled at the side.

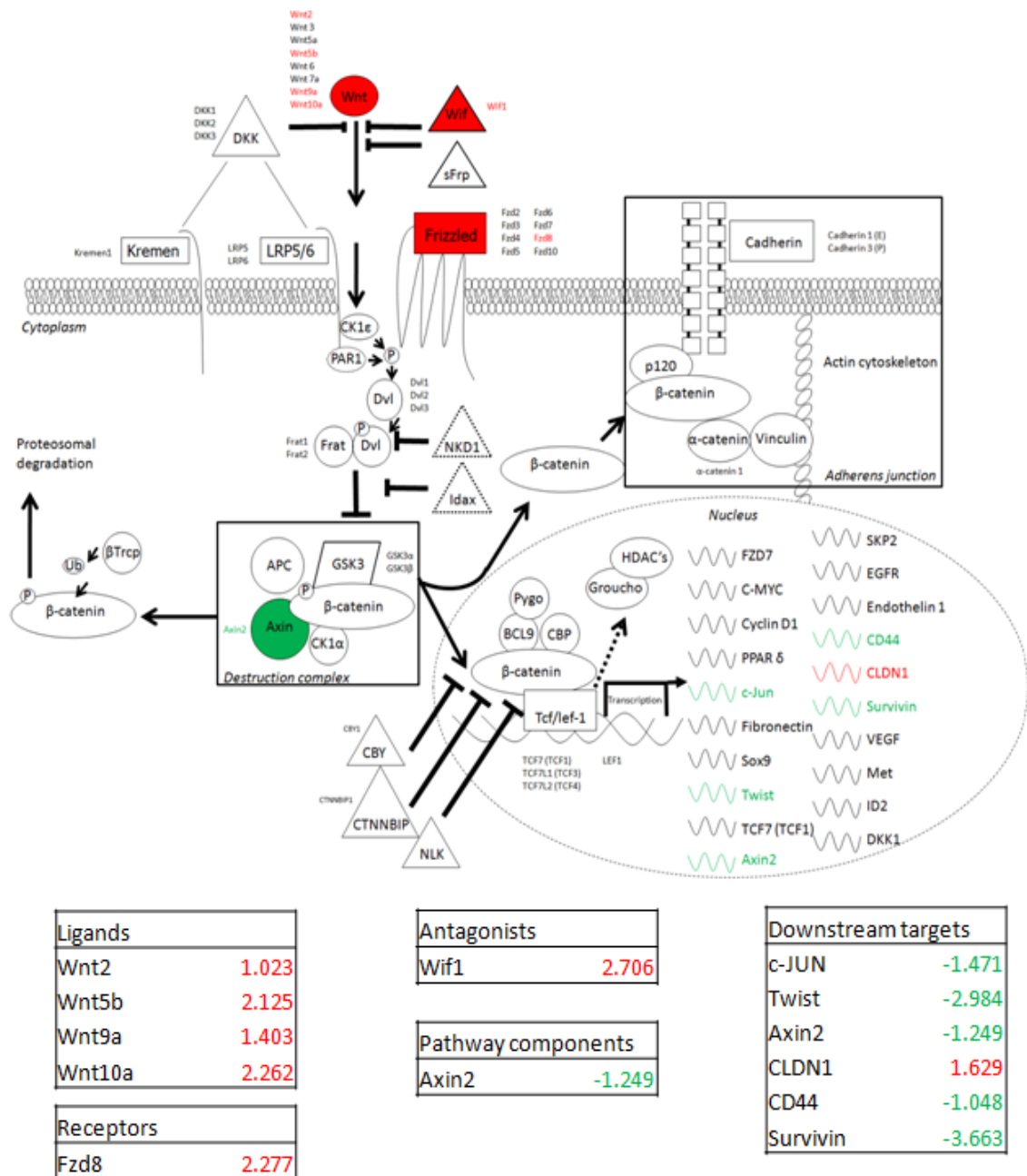


Figure 3-11 Schematic representation of the gene changes within the canonical Wnt pathway in quiescent NHU cells

Genes with at least a 2-fold change in expression compared to the proliferative culture are labelled as either red (up-regulated) or green (down-regulated). Actual changes in expression are detailed within the tables and are expressed as signal log ratios (log base 2).

Manual interrogation of the fold change differences between TZ/PD treated cultures and proliferating NHU cultures revealed 23 members of the Wnt pathway were significantly altered at the mRNA level. These gene changes were displayed as an overlay on top of a schematic Wnt pathway along with log₂ fold change values (Figure 3-12). Immediate attention was drawn to the fact that two Wnt antagonists were significantly up-regulated in the TZ/PD treated culture compared to the proliferating culture, these were; sFrp1 (up-regulated 2.29 fold) which was classed as absent at the mRNA level in the proliferating culture and Kremen1 which was up-regulated 3.23 fold. Noteworthy changes were also seen in four key Wnt pathway components, these were; Wnt7a (down-regulated 4.23 fold), Wnt7b (up regulated 2.64 fold) Fzd2 and Fzd4 (down-regulated 4.56 and 5-fold, respectively) as well as GSK3 β (down regulated 4.2 fold). Ten downstream Wnt targets were also significantly altered, with the majority down-regulated (7/10) (Figure 3-12).

A comparative analysis of the ABS/Ca²⁺ treated culture vs. the proliferative NHU culture showed no up-regulation of Wnt antagonists. One important difference between the TZ/PD and ABS/Ca²⁺ model is the need for a pre-treatment with 5% (v/v) ABS prior to passage into medium containing 5% (v/v) ABS and 2mM CaCl₂ (94) and therefore there is a time difference between the two methods of differentiation which may account for the dissimilarity. As with the TZ/PD model Fzd2 and Fzd4 were significantly down-regulated (3.92 and 3.41-fold, respectively). Wnt5a was significantly up-regulated (4.54 fold) and has been implicated as both an activator and inhibitor of the canonical Wnt pathway. Ten downstream targets were found to be significantly altered with the majority (7/10) down-regulated (Figure 3-13). In total 23 genes involved in either transducing the Wnt signal or direct gene targets of TCF/ β -catenin were significantly altered between the ABS/Ca²⁺ and the proliferating NHU cell cultures.

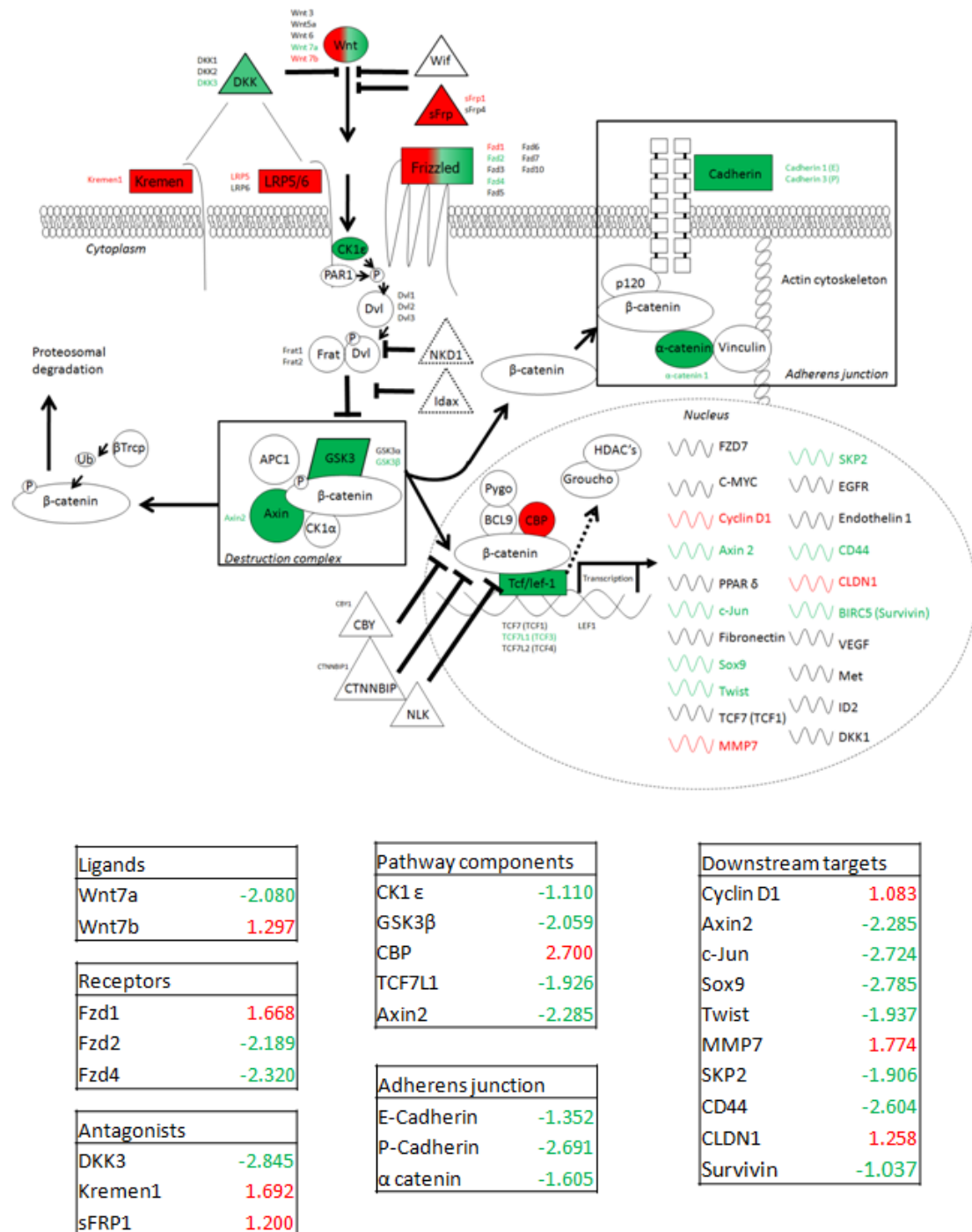
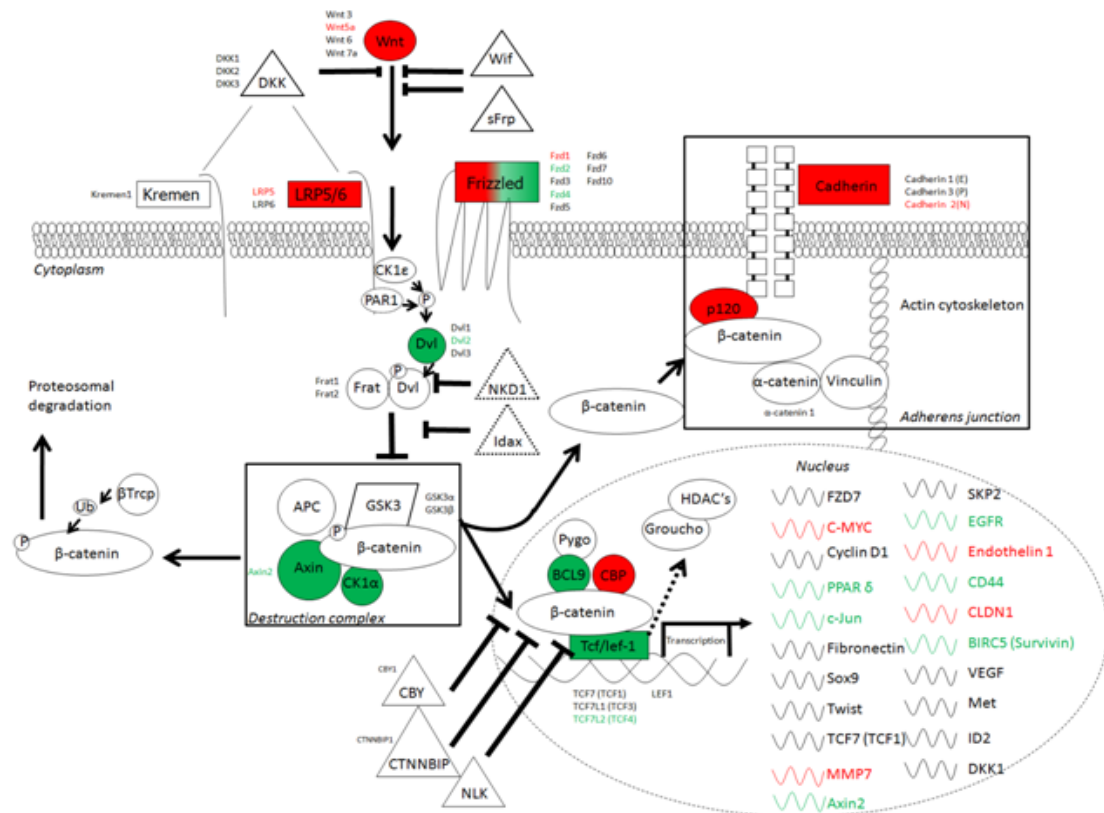


Figure 3-12 Schematic representation of the gene changes within the canonical Wnt pathway in TZ/PD differentiated cultures

Genes with at least a 2-fold change in expression are labelled as either red (up-regulated) or green (down-regulated). Actual changes in expression are detailed within the tables and are expressed as signal log ratios (log base 2).



Ligands	
Wnt5a	2.181

Receptors	
fzd1	1.072
fzd2	-1.970
fzd4	-1.770

Adherens junction	
p120	2.381
N-cadherin	3.489

Pathway components	
Lrp5	1.024
BCL9	-1.207
CBP	2.111
TCF4	-1.408
CK1α	-1.122
DVL2	-1.170
Axin2	-1.793

Downstream targets	
C-MYC	-1.010
PPARδ	-1.063
c-Jun	-1.211
EGFR	-1.429
Endothelin	1.325
MMP7	3.373
Axin2	-1.793
CD44	-1.619
CLDN1	2.302
Survivin	-4.461

Figure 3-13 Schematic representation of the gene changes within the canonical Wnt pathway in ABS/Ca²⁺ differentiated cultures

Genes with at least a 2-fold change in expression compared to the proliferative culture are labelled as either red (up-regulated) or green (down-regulated). Actual changes in expression are detailed within the tables and are expressed as signal log ratios (log base 2).

To facilitate analysis of all culture conditions, fold-change data was summarised in a table (Table 3-6). mRNA expression values for Wnt components within the quiescent and differentiated NHU cultures were compared to the proliferative culture and expressed as fold change. Changes greater than two fold were represented as a colour; red for a significantly up-regulated gene and green for a significantly down-regulated gene.

Different Wnt ligands were up and down regulated between the two methods of differentiation. No similarity in expression profile was observed. In the quiescent NHU cell culture, four Wnt ligands showed up-regulated expression. Fzd receptors showed a similar pattern of expression in the two differentiation methods. In both the TZ/PD and ABS/Ca²⁺ cultures, Fzd1 expression increased when compared to the proliferative culture. Both Fzd2 and Fzd4 were down-regulated in the TZ/PD and ABS/Ca²⁺ cultures when compared to the proliferative culture. Wnt signalling antagonists were seen to be altered in expression when NHU cells were differentiated with TZ/PD. DKK3 was down regulated, whereas Kremen1 and sFrp1 were both up-regulated. Expression of Wnt signalling antagonists did not alter in the ABS/Ca²⁺ model. Wif1 was up-regulated in the quiescent culture compared to the proliferative culture. Several components important in transducing a Wnt signal changed in expression when NHU cells were induced to differentiate. CBP, an important part of the β -catenin/TCF transcription complex increased in expression in both models of differentiation. Axin2, part of the destruction complex as well as a direct downstream target of the Wnt cascade, decreased in expression when cells were induced to differentiate, and also when the culture became confluent. Several downstream targets of the Wnt cascade were altered in expression when cultures were differentiated as well as confluent. Axin2, c-Jun, CD44 and Survivin were down-regulated in all conditions when compared to the proliferative NHU cell culture. Both TZ/PD and ABS/Ca²⁺ differentiation lead to expression changes in Fzd1, Fzd2, Fzd4 and CBY. Changes in expression of these genes as well as three well-characterised antagonists

(DKK3, sFrp1 and Wif1) and three transcriptional targets (c-Jun, Axin2 and CyclinD1) were verified using RT-PCR on the same RNA used to undertake the Affymetrix™ analysis. CyclinD1 expression was included in the panel of targets not because it showed any trend in expression in the Affymetrix™ analysis but because there is evidence of a correlation between β -catenin mutation in bladder cancer and over-expression of CyclinD1 (117). Three canonical Wnt ligands (Wnt3, 5a and 7a) were also interrogated using RT-PCR. Changes seen in the Affymetrix™ and RT-PCR were then verified using RT-qPCR on three independent cell lines.

	Gene	TZ/PD	ABS/Ca ²⁺	Quiescent
Ligands	Wnt2			Red
	Wnt5a		Red	
	Wnt5b			Red
	Wnt7a	Green		
	Wnt7b	Red		
	Wnt9a			Red
	Wnt10a			Red
Receptors	Fzd1	Red	Red	
	Fzd2	Green	Green	
	Fzd4			
	Fzd8			Red
Antagonists	DKK3	Green		
	Kremen1	Red		
	sFRP1			
	Wif1			Red
Pathway components	CBP	Red	Red	
	Axin2	Green		Green
	TCF4		Green	
	CK1 α		Green	
	DVL2		Green	
	TCF7L1	Green		
	Lrp5		Red	
	BCL9		Green	
	CK1 ϵ	Green		
	GSK3 β			
Adherens junction	E-Cadherin	Green		
	P-Cadherin	Green		
	α -catenin			
	p120		Red	
	N-cadherin			
Downstream targets	Axin2	Green	Green	Green
	c-Jun	Green	Green	Green
	Sox9	Green		
	Twist	Green		Green
	MMP7	Red	Red	
	EGFR		Green	
	CD44	Green	Green	Green
	CLDN1	Red	Red	Red
	Survivin	Green	Green	Green
	Endothelin		Red	
	C-MYC		Green	
	PPAR δ		Green	
	Cyclin D1	Red		
	SKP2	Green		

Table 3-6 Summary of AffymetrixTM microarray results for changes in the canonical Wnt pathway

Changes in mRNA expression are labelled as red (up-regulated >2-fold) or green (down-regulated >2-fold).

3.3.6 RT-PCR analysis

RT-PCR was used to verify the changes seen in the Affymetrix™ array analysis. UPK2 was only expressed in the ABS/Ca²⁺ treated NHU cell culture, TZ/PD treated culture and freshly isolated (P0) urothelium as expected (Figure 3-14). MKI67 was expressed in the proliferating NHU culture. A faint band was also visualised in the freshly isolated urothelium. RT-PCR confirmed the presence of Wnt3, Wnt5a and Wnt7a in proliferating culture, quiescent and both differentiation procedures. Interestingly, both Wnt3 and Wnt7a were absent from freshly isolated urothelium. Fzd1 did not appear to be expressed in culture with only a very faint product in the freshly isolated urothelium. Fzd2 expression matched that observed in the Affymetrix™ analysis: mRNA was detected in the proliferative and quiescent culture but was absent from differentiated cultures. Fzd2 was also detected in the P0 urothelium. Fzd4 was expressed in all samples and gave no hint of a possible down-regulation upon differentiation as observed in the Affymetrix™ array data. DKK3 was expressed in all samples including the P0 urothelium. sFrp1 was absent in all samples. Wif1 expression was very weak with only a very faint band visible in the quiescent culture. This agreed with the results obtained from the Affymetrix analysis. Axin2 mRNA was found in the proliferative culture as well as the P0 urothelium. A faint band for Axin2 was observed in the quiescent culture but no mRNA for Axin2 was observed in either model of differentiation. Expression of CyclinD1 was evident in all culture conditions as well as in the P0 urothelium. c-Jun mRNA was expressed in all culture conditions but appeared to be down regulated upon differentiation. CBY RT-PCR failed with the genomic DNA positive control and was therefore not taken forward.

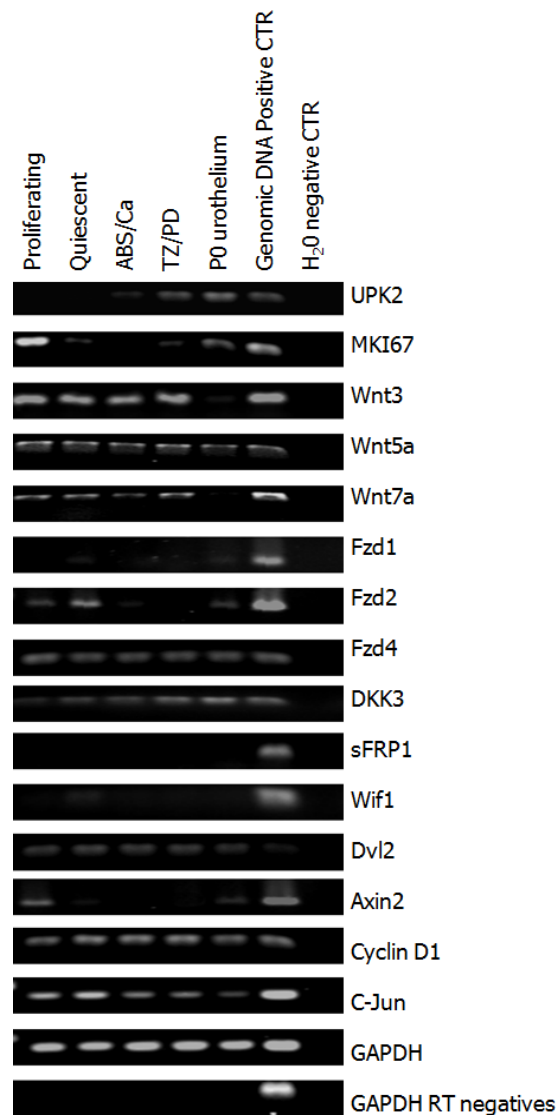


Figure 3-14 mRNA expression of Wnt signalling components in NHU cells *in vitro* and *in vivo*

RT-PCR analysis of Wnt signaling components from Y676 NHU cells grown in culture as a proliferative monolayer, quiescent culture or differentiated using TZ/PD or ABS/Ca²⁺ as well as expression in uncultured stripped urothelium (Y1043). Human genomic DNA was used as a template control. Water only was used as a no-template negative control. GAPDH was used as a positive control to verify intact cDNA. RT negatives were included to verify lack of gDNA contamination in the cDNA.

Although the RT-PCR data was not quantitative, it provided back up data to the Affymetrix™ analysis and is summarised in table 3-7. From the RT-PCR and Affymetrix™ data, seven targets revealed a convincing change in expression between treatments and were taken forward for quantitative analysis on three independent NHU cell lines. These were Wnt3, Wnt5, Wnt7a, Fzd2, Fzd4 and Axin2.

	Expression in proliferating sample		Regulation					
			Quiescent		ABS/Ca ²⁺		TZ/PD	
	Affymetrix	RT-PCR	Affymetrix	RT-PCR	Affymetrix	RT-PCR	Affymetrix	RT-PCR
UPK2	A	A						
MKI67	P	P						
Wnt3	P	P						
Wnt5a	P	P						
Wnt7a	P	P						
Fzd1	A	A						
Fzd2	P	A						
Fzd4	P	P						
DKK3	P	A						
sFrp1	A	A						
Wif1	A	A						
Dvl2	ND	P	ND		ND		ND	
Axin2	P	P						
Cyclin D1	P	P						
c-Jun	P	P						

Table 3-7 Summary of Affymetrix™ microarray and RT-PCR results for changes in the canonical Wnt pathway

Changes in mRNA expression are labelled as red (up-regulated) or green (down-regulated) in each of the labelled conditions. A=Absent transcript, P=Present transcript, ND=No data available.

3.3.7 RT-qPCR

Quantitative PCR using SYBR-green was performed on three independent NHU cell lines (Y878, Y372 and Y387) to validate the changes in mRNA expression seen between proliferating, quiescent and differentiated NHU cultures using Affymetrix™ microarray analysis and RT-PCR. RTq-PCR for UPK2 and UPK3a verified that the cultures treated with TZ/PD and ABS/Ca²⁺ were expressing markers of urothelial differentiation (P<0.001 and P<0.05, respectively for UPK2 as well as UPK3a; Figure 3-15). MKI67 mRNA expression verified the confluent cultures had reduced expression of the proliferation marker (P<0.01) and were deemed quiescent (Figure 3-15). Of the three Wnt ligands tested, only Wnt5a significantly changed in expression when proliferating and differentiated cultures were compared. Changes in mRNA expression for Wnt5a were statistically significant when TZ/PD differentiated cultures as well as ABS/Ca²⁺ differentiated cultures were compared to proliferating NHU cultures (P<0.001 and P<0.01, respectively). No significant change was observed with Wnt3 or Wnt7a. Of the two Fzd receptors highlighted in the Affymetrix™ array analysis, Fzd2 was significantly down-regulated in TZ/PD treated cultures (P<0.05) agreeing with the results seen from the Affymetrix™ analysis and RT-PCR. Fzd2 appeared to be down regulated in the ABS/Ca²⁺ treated cultures too, with a median down-regulation of 2.4-fold, however, this was not statistically significant. Fzd4 was unaffected by TZ/PD treatment or quiescence, but was down-regulated in the ABS/Ca²⁺ treated cultures (P<0.05). The Wnt antagonist, DKK3 was seen to be significantly up-regulated in the ABS/Ca²⁺ differentiated cultures (P<0.01) but remained unchanged in the TZ/PD and quiescent cultures. Expression of the Wnt signalling downstream gene target, Axin2, was significantly altered in both differentiation procedures (<0.001), but remained unchanged in quiescent cultures. In summary, no opposing regulatory expression changes were observed between the Affymetrix™ /RT-PCR screen and the RT-qPCR analysis.

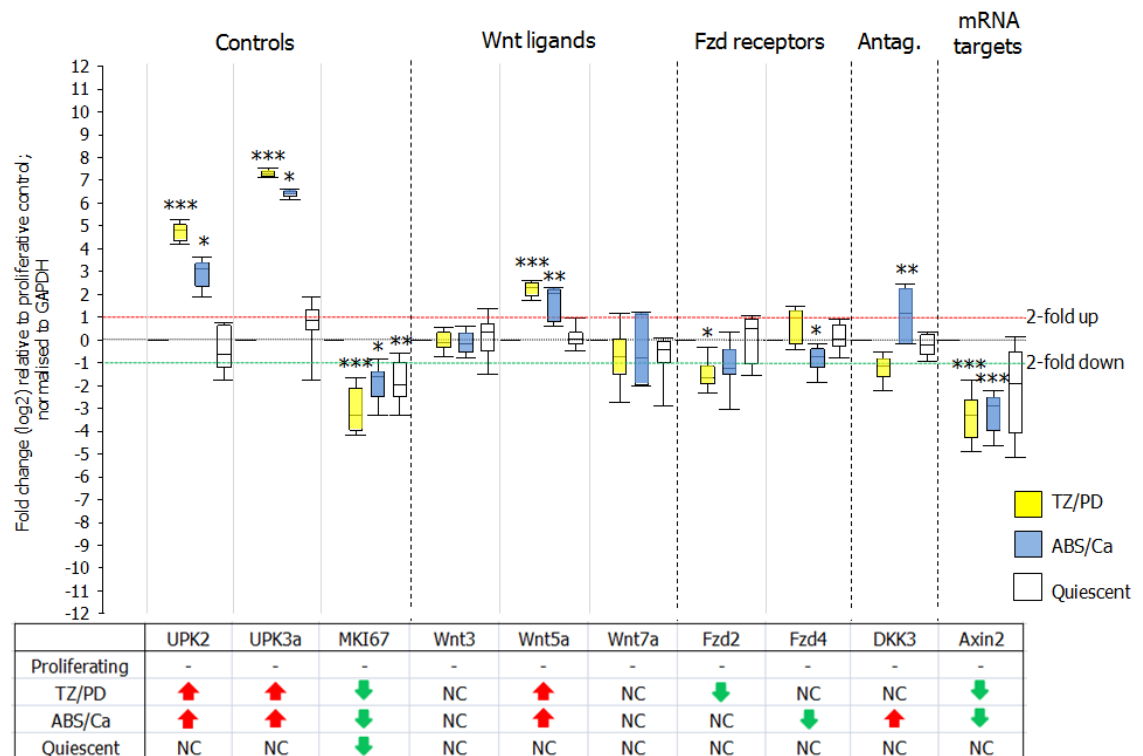


Figure 3-15 mRNA expression of Wnt components in proliferative, quiescent and differentiated NHU cultures

Expression of Wnt components as assessed by SYBR-green RT-qPCR and normalised to GAPDH. Changes in expression were measured as fold-change compared to the proliferative culture and data represented as a box and whisker plot. Boxes indicate the median, 25th and 75th quartile, whiskers denote the 5th and 95th quartile. Red and green arrows indicate a statistically significant up- and down-regulation, respectively. Statistical analysis was performed using a non-parametric ANOVA and Dunn's multiple comparison post test. *** indicate a P value of <0.001, ** indicate a P value of <0.01, * denotes a P value of <0.05. NC=No change. Data is from three independent NHU cell lines (Y878, Y372 and Y387) each assayed in technical triplicate (n=9).

3.4 Discussion

Affymetrix™ microarray analysis is a powerful and convenient method of analysing relative changes in gene expression. The dataset used in this study represented a differentiating time series and had been a widely used resource to study the vast but sometimes subtle changes that occur during *in vitro* urothelial differentiation over time (118). In this study, the data was not classically interrogated using clustering but was used as a screening tool for investigating changes within a specific pathway.

No technical replicates were present in the dataset (n=1). A second time series using an independent cell line derived from ureter was available but was not used in this study because markers of urothelial differentiation were poorly expressed. Technical replicates would have made the data more robust by compensating for anomalies in such things as hybridisation differences and background correction. Unfortunately one chip out of the 12-chip dataset was shown to have issues with RNA quality and hybridisation. As no technical replicates were available, this timepoint was removed from the dataset to prevent skewing of the results. Although the dataset was incomplete it still contained a vast amount of information and was used as a screening tool to direct further investigations.

As the canonical Wnt signalling pathway is important in driving proliferation one might expect components of the pathway as well as downstream targets to be expressed at a higher level in an actively dividing population than in a culture that was quiescent due to contact inhibition or differentiation. One might also expect that if the Wnt pathway was important during proliferation, antagonists would be more transcriptionally-active in a contact-inhibited culture or upon differentiation.

3.4.1 Analysis of the proliferative NHU culture

All components necessary for a functional Wnt cascade were present at the mRNA level in the proliferating NHU cell culture. Four Wnt genes were also transcribed in proliferative culture, these were: Wnt3, Wnt5a, Wnt6 and Wnt7a. Wnt3 is a well characterised canonical Wnt ligand which has been found to be up-regulated in several cases of primary breast and rectal cancer (119) and signals via Fzd7 (120), which was also present. Wnt7a has been found to drive proliferation in endometrial cells, the epithelial cells that line the uterus (121) and is thought to occur via binding to Fzd 5 (122) which was also present in the proliferating NHU cell culture. Wnt5a was initially classified as a non-canonical Wnt ligand as it activates the RAC-1 cell motility pathway via Fzd2 and ROR1/2, however, when Fzd4 is present, Wnt5a can activate the classical β -catenin signalling cascade (123).

Fzd receptor expression is an important regulator of the Wnt pathway. Seven Fzd receptors were classified as present (Fzd2, Fzd3, Fzd4, Fzd5, Fzd6, Fzd7 and Fzd10). Fzd2 and Fzd4 are interesting as they can bind Wnt3 and may be an important component of a possible autocrine/paracrine Wnt signalling loop in NHU cells (explored in chapter 6). Fzd7 was also a compelling target for further investigation because it also mediates the β -catenin/TCF canonical response via Wnt3 (120) and has been suggested as having an important role in the self-renewal of embryonic stem cells (124).

Several antagonists were transcriptionally-active in the proliferative culture including the Dickkopf (DKK) family of genes. DKK proteins primarily act as antagonists of the Wnt canonical pathway by blocking access to the Wnt co-receptor LRP5/6 and inducing endocytosis via Kremen (109, 110, 125). The role of DKK1 and DKK3 as inhibitors of the Wnt pathway is well established, but not all DKK proteins are antagonists. DKK2 was also present in the dataset and has been shown in the absence of Kremen2, to activate DVL via LRP6 and drive β -catenin mediated TCF transcription (126, 127). In the proliferative culture,

Kremen2 was absent suggesting DKK2 could potentially act as a driver of β -catenin mediated proliferation in NHU cells.

The fact that several Wnt extracellular antagonists such as Wif1 and sFrp were not transcribed in the proliferating culture was promising evidence for a functional cascade during urothelial regeneration. The same was not true for several intracellular Wnt signalling antagonists. Both Chibby (CBY), an intracellular trafficking molecule which shuttles β -catenin out of the nucleus (128) and ICAT, an inhibitor of β -catenin and TCF interaction (129) were present as transcripts in proliferating NHU cell cultures.

Although the presence of mRNA for several antagonists was not an encouraging sight, many of these inhibitors require post-translational modification and therefore their transcription does not necessarily imply activity. This is indeed the case for CBY which requires phosphorylation at serine 20 before it can form a tripartite bond between 14-3-3 ϵ/ζ and β -catenin (130).

Several downstream Wnt signalling target transcripts were expressed in the proliferative NHU cell culture. These included such targets as: Axin2, a feedback repressor of the Wnt pathway (131) and a downstream target of Wnt and pRB/E2F signalling (132, 133); Survivin (BIRC5)(134); Twist (135) and SKP2, a reported downstream target of the Wnt signalling pathway in bladder cancer cells (81). Another potential Wnt-associated transcript, CyclinD1 (136) was also present, but its link to the Wnt pathway is debatable (137).

3.4.2 Comparison between quiescent and proliferating NHU cells

If Wnt signalling was important in driving proliferation one might expect a number of expression changes within the cascade when a culture reached confluency and entered G₁ cell cycle arrest. Indeed, several changes in the expression of Wnt pathway components were evident between the proliferative and confluent dataset. The most interesting of these changes was the

induction of otherwise undetected Wnt2 and Wnt5b. The role of Wnt2 remains unclear but Wnt5b, a homologue of Wnt5a acts non-canonically in pre-adipocytes to stimulate adipogenesis via PPAR γ (138), the same type II nuclear receptor activated in urothelial differentiation (93, 95). Wnt inhibitory factor 1 (Wif1) was also an mRNA target not seen in the proliferative NHU dataset but present in confluent culture. Wif1 is interesting as it is a potent extracellular antagonist of Wnt signalling and has been shown to be frequently hypermethylated in bladder tumours. Knock-down of Wif1 in bladder cancer cells leads to an increase in cell proliferation rate, which is thought to be driven by the observed increase in c-MYC transcription and implies that Wif1 may regulate urothelial cell proliferation by inhibiting β -catenin/TCF-mediated transcription (79). The results presented here suggest contact inhibited NHU cells may also up-regulate Wif1, possibly to inhibit further Wnt signalling and maintain tissue quiescence.

3.4.3 The Wnt pathway in differentiated NHU cells

Both systems for inducing urothelial differentiation result in the up-regulation of well characterised markers of urothelial terminal differentiation, but only the ABS/Ca²⁺ model results in a functional barrier (94). The factors that contribute to this have yet to be defined, but both models are thought to result from the activation of the nuclear receptor PPAR γ . For this reason each model of differentiation was compared separately to the proliferative culture.

A comparison between TZ/PD differentiated and proliferating NHU cultures revealed a down regulation in Wnt7a, as well as a significant down-regulation in Fzd2 and Fzd4, both of which are important in transducing the signal from Wnt3 and Wnt5a (120, 123). The fact that both of these receptors were down-regulated along with Wnt7a implied that Wnt signalling (if active) would likely be diminished upon differentiation.

Analysis of the ABS/Ca²⁺ differentiated dataset revealed different changes in components of the Wnt pathway compared to the TZ/PD model. After ABS/Ca²⁺ differentiation, Wnt5a ligand was seen to be significantly up-regulated. This increase in Wnt5a expression coincided with a reduction in its canonical receptor Fzd4, suggesting that in this situation, Wnt5a may be acting as an antagonist via ROR1/2.

In summary, AffymetrixTM mRNA expression analysis of NHU cells under proliferative and differentiated conditions revealed several changes within the Wnt pathway. In this study, previously generated microarray data was used as a screening tool to assess the presence of the Wnt canonical pathway at the mRNA level in NHU cells. The results indicated that all components necessary for a functional cascade were present in proliferating NHU cells.

In conclusion, analysis of the AffymetrixTM dataset provided preliminary evidence for a functional Wnt pathway during proliferation and suggested that it may be differentially regulated upon differentiation.

4 Pharmacological activation of the Wnt canonical cascade in Normal Human Urothelial cells

4.1 Introduction

GSK3 is a proline directed serine-threonine kinase that plays a crucial role in glycogen metabolism as well as other tissue-specific signalling roles throughout the human body. GSK3 has two isoforms, α and β which are encoded on two separate genes at 19q13.2 and 3q13.3, respectively. The two isoforms of GSK3 share 98% amino acid homology within their kinase domain (139), but it remains unclear as to whether these isoforms are functionally interchangeable. Both α and β isoforms appear to have some overlapping roles in Wnt signalling. Over expression of GSK3 α or GSK3 β have both been shown to result in a reduction in β -catenin nuclear translocation and TCF activity (140) but, as demonstrated in the GSK3 β embryonic lethal knock-out mouse, GSK3 α and GSK3 β are not functionally redundant (141, 142).

Together, GSK3 α and GSK3 β are known to phosphorylate over 40 targets, including signalling proteins, transcription factors as well as structural proteins. Inhibitors of GSK3 are widely used as crude activators of the Wnt signalling cascade, even though they have the potential to affect several other signalling pathways.

To date there are roughly 30 known inhibitors of GSK3 which are reviewed in detail elsewhere (143). Most inhibitors are not GSK3-specific and affect the activity of other protein kinases at similar IC_{50} concentrations (e.g., hymenialdisine, flavopiridol and kenpaullone)(143).

4.2 Hypothesis

The canonical Wnt pathway is functional in NHU cells and may be utilised to drive proliferation *in vitro*.

4.3 Aim

The aim of this chapter was to determine if the canonical Wnt pathway was functional in NHU cells and to assess its ability to initiate self-renewal.

Specific objectives of this chapter were:

- To inhibit the destruction complex using antagonists targeted to GSK3 and assess activation of the Wnt cascade by monitoring active (non-phosphorylated) β -catenin nuclear accumulation.
- To assess the effect of pharmacological activation of the Wnt pathway on NHU cell morphology and proliferation.
- To utilise the TOPFLASH TCF reporter assay in NHU cells to assess TCF transcription factor activity before and after GSK3 inhibition.

4.4 Experimental Design

Two GSK3 β antagonists were used in this study: SB415286, a DMSO-soluble inhibitor with a published IC₅₀ of 2.9 μ M (144) and LiCl salt, a widely used, water-soluble but less specific GSK antagonist with a published IC₅₀ of between 2mM-15mM (145). Both inhibitors were titrated in the well-characterised Wnt-responsive osteosarcoma cell line, SaOS-2 (146, 147) and in NHU cells. Cytotoxicity was assessed by comparison to vehicle control in a 6-day cell viability assay using MTT and by phase contrast photomicroscopy.

The effect of GSK3 inhibition on β -catenin nuclear translocation was assessed using indirect immunofluorescence on formalin-fixed cultures. Nuclear and cytoplasmic signal intensities for β -catenin were quantified from each

micrograph using Hoechst 33258 stain to delineate the nucleus and Adobe® Photoshop™ software as previously described (section 2.9.1.6).

The effect of GSK3 inhibition on the TCF activity of NHU cells was assessed in triplicate cultures using the TOPFLASH Firefly luciferase reporter plasmid and a dual luciferase reporter kit. NHU cells were cultured for 24-hours ± SB415286. SaOS-2 cells were included alongside as a positive Wnt-responsive control. Results were normalised to a constitutively-active Renilla luciferase loading control plasmid. The mutant TCF Firefly luciferase plasmid, FOPFLASH was included to control for changes in TK minimal promoter activity.

4.5 Results

4.5.1 Effect of GSK3 inhibitors on cell viability

4.5.1.1 SB415286

Incubation of SaOS-2 cells with up to 50 μ M SB415286 had no significant effect on culture biomass when compared to vehicle control at day 4 (Figure 4-1; Figure 4-2). When incubated with a concentration of 100 μ M, SaOS-2 culture biomass remained static over the course of the experiment (Figure 4-1). At 200 μ M, culture biomass was seen to drop to levels below that observed at time point 0 (Figure 4-1).

Concentrations of up to 12 μ M SB415286 had no effect on the culture biomass of NHU cells when compared to vehicle control at the same time point (Figure 4-3). Interestingly, a slight increase in cell biomass was seen with 5-10 μ M SB415286 when compared to vehicle control, but this was not statistically significant. Concentrations of 15 μ M or higher significantly reduced NHU culture biomass ($P < 0.01$; Figure 4-4).

4.5.1.2 LiCl

Up to 20mM LiCl did not affect the culture biomass of SaOS-2 cells compared to vehicle control at day 4 (Figure 4-7). 50mM and 100mM LiCl significantly reduced SaOS-2 culture biomass when compared to vehicle control ($P < 0.01$, Figure 4-8).

LiCl was not well tolerated by NHU cells (Figure 4-5). By day 4, concentrations of 10 μ M and above resulted in a significant reduction in NHU culture biomass compared to vehicle control ($P < 0.01$, Figure 4-6).

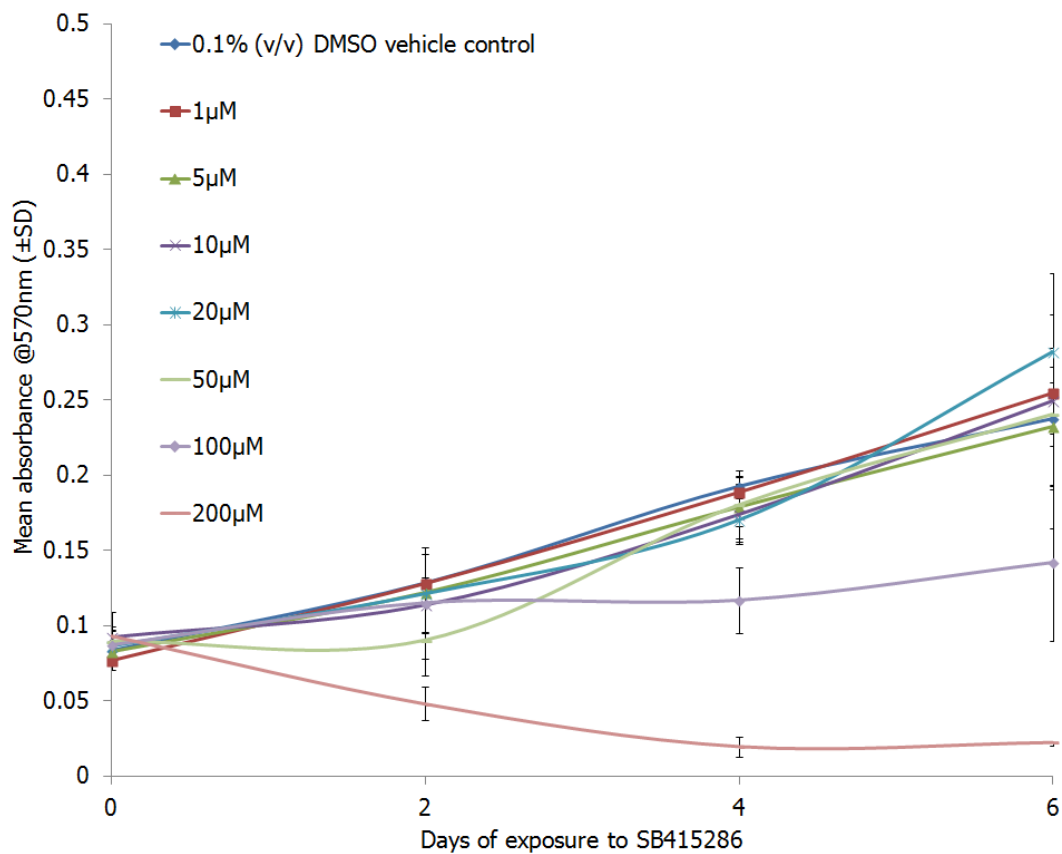


Figure 4-1 Effect of SB415286 on SaOS-2 cell viability

MTT assay from SaOS-2 cells cultured in McCoy's 5A + 15% (v/v) FBS + 0-200µM SB415286 for up to 6 days. 0.1% (v/v) DMSO was included in all cultures as the vehicle control. Medium and inhibitors were replenished on day 3. Data shows the mean absorbance at 570nm (±SD) of 6 technical replicates.

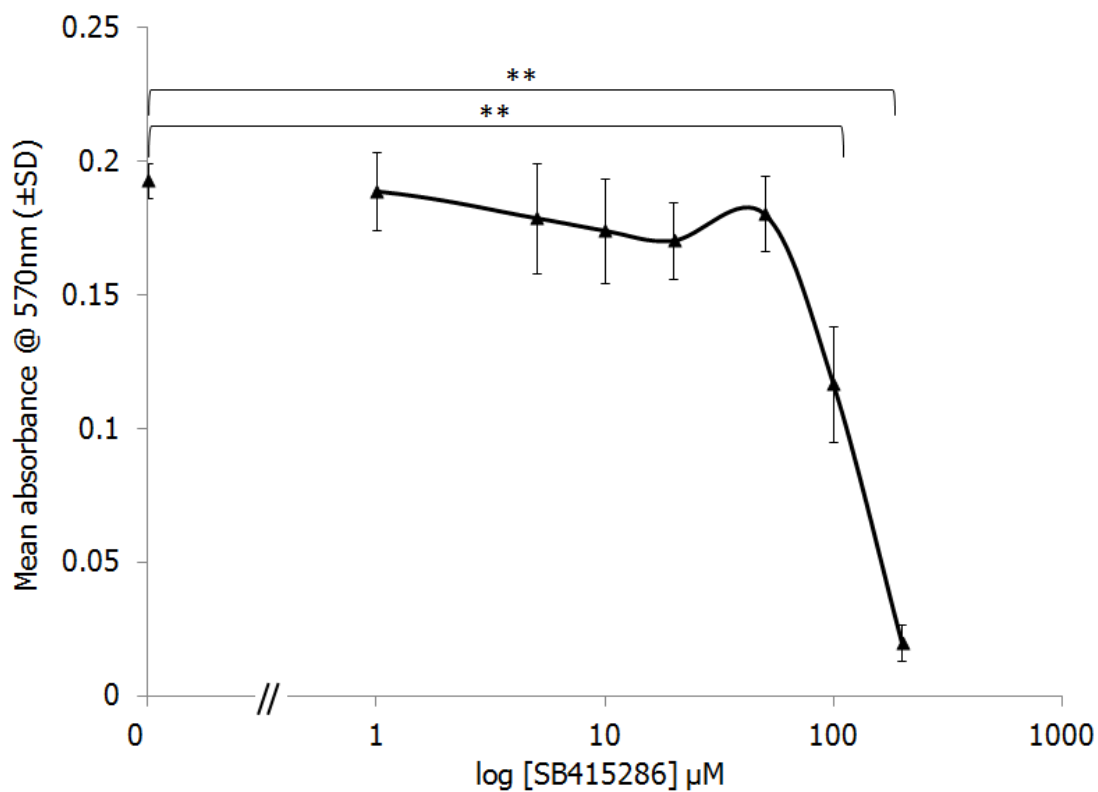


Figure 4-2 SaOS-2 dose response curve to SB415286

Mean absorbance from SaOS-2 cells after a 4-day incubation with 0-200μM SB415286 in 0.1% (v/v) DMSO. Data shows the mean absorbance at 570nm (±SD) of 6 technical replicates. ** p<0.01, one way ANOVA with Dunnett's post-test.

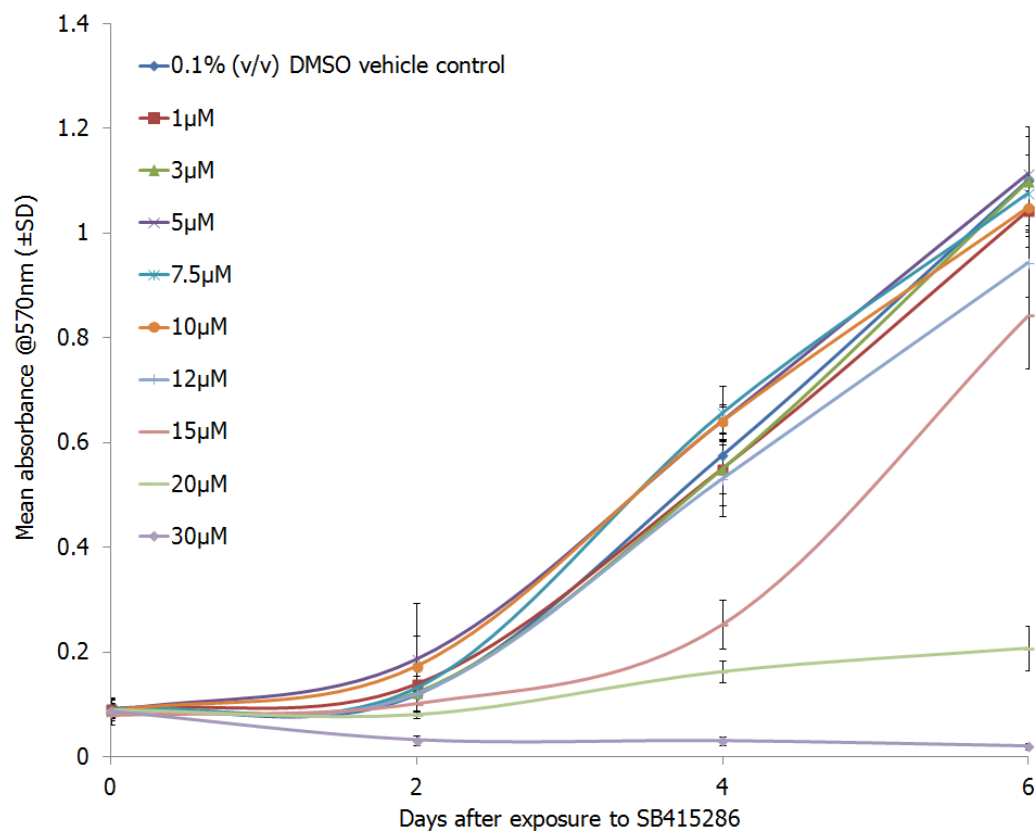


Figure 4-3 Effect of SB415286 on NHU cell viability

MTT assay from NHU cells (Y924 at P4) cultured in KSFMc + 0-30µM SB415286 for up to 6 days. 0.1% (v/v) DMSO was included in all cultures as the vehicle control. Medium and inhibitors were replenished on day 3. Data shows the mean absorbance at 570nm (±SD) of 6 technical replicates.

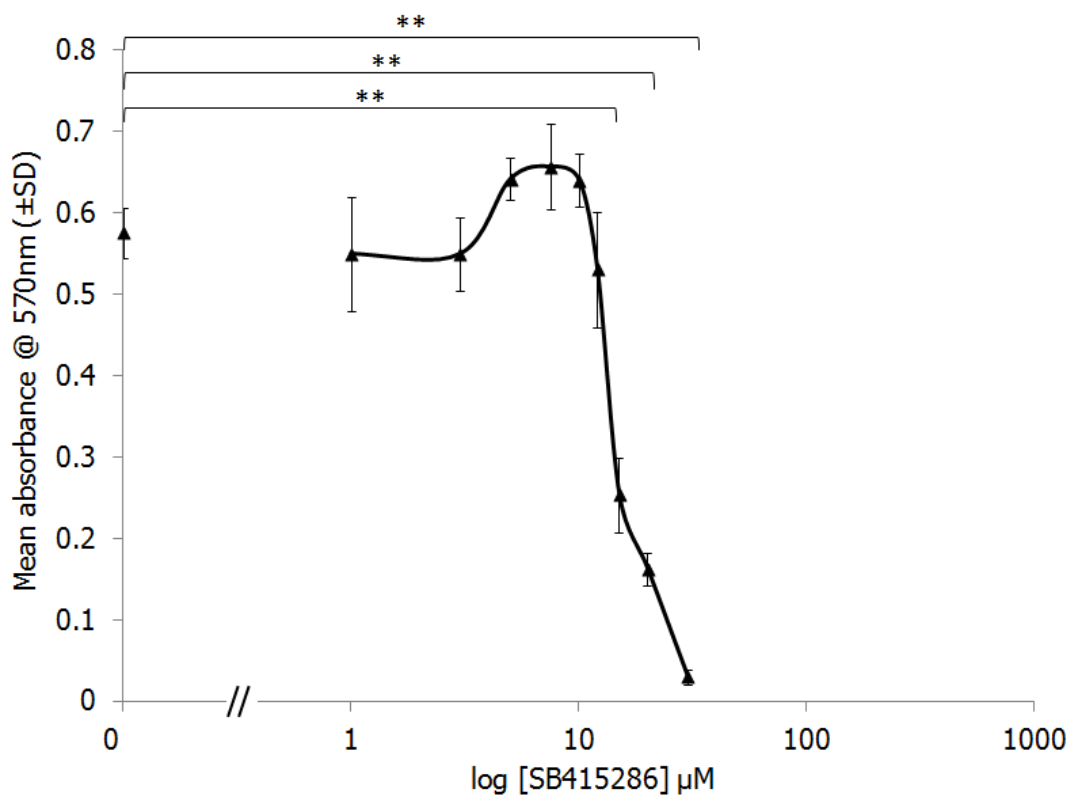


Figure 4-4 NHU dose response curve to SB415286

Mean absorbance from NHU cells after a 4-day incubation with 0-30μM SB415286 in 0.1% (v/v) DMSO. Data shows the mean absorbance at 570nm (±SD) of 6 technical replicates. ** p<0.01, one way ANOVA with Dunnett's post-test.

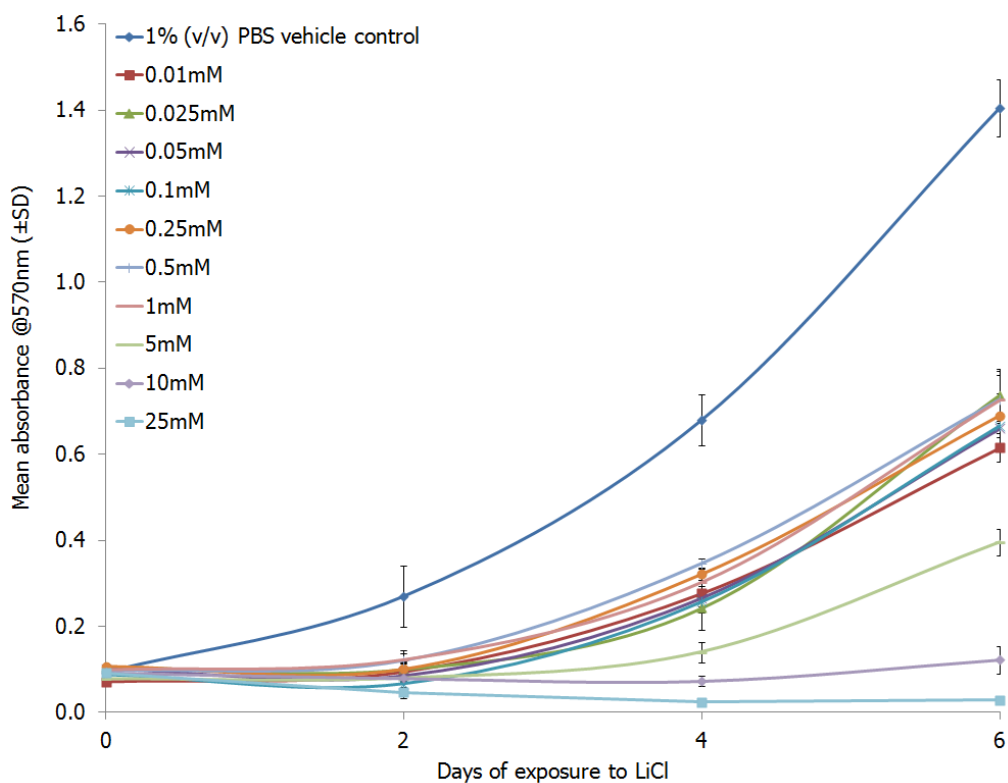


Figure 4-5 Effect of LiCl on NHU cell viability

MTT assay from NHU cells (Y924 at P4) cultured in KSFMc + 0-25mM LiCl for up to 6 days. 1% (v/v) PBS was included in all cultures as the vehicle control. Medium and inhibitors were replenished on day 3. Data shows the mean absorbance at 570nm (\pm SD) of 6 technical replicates.

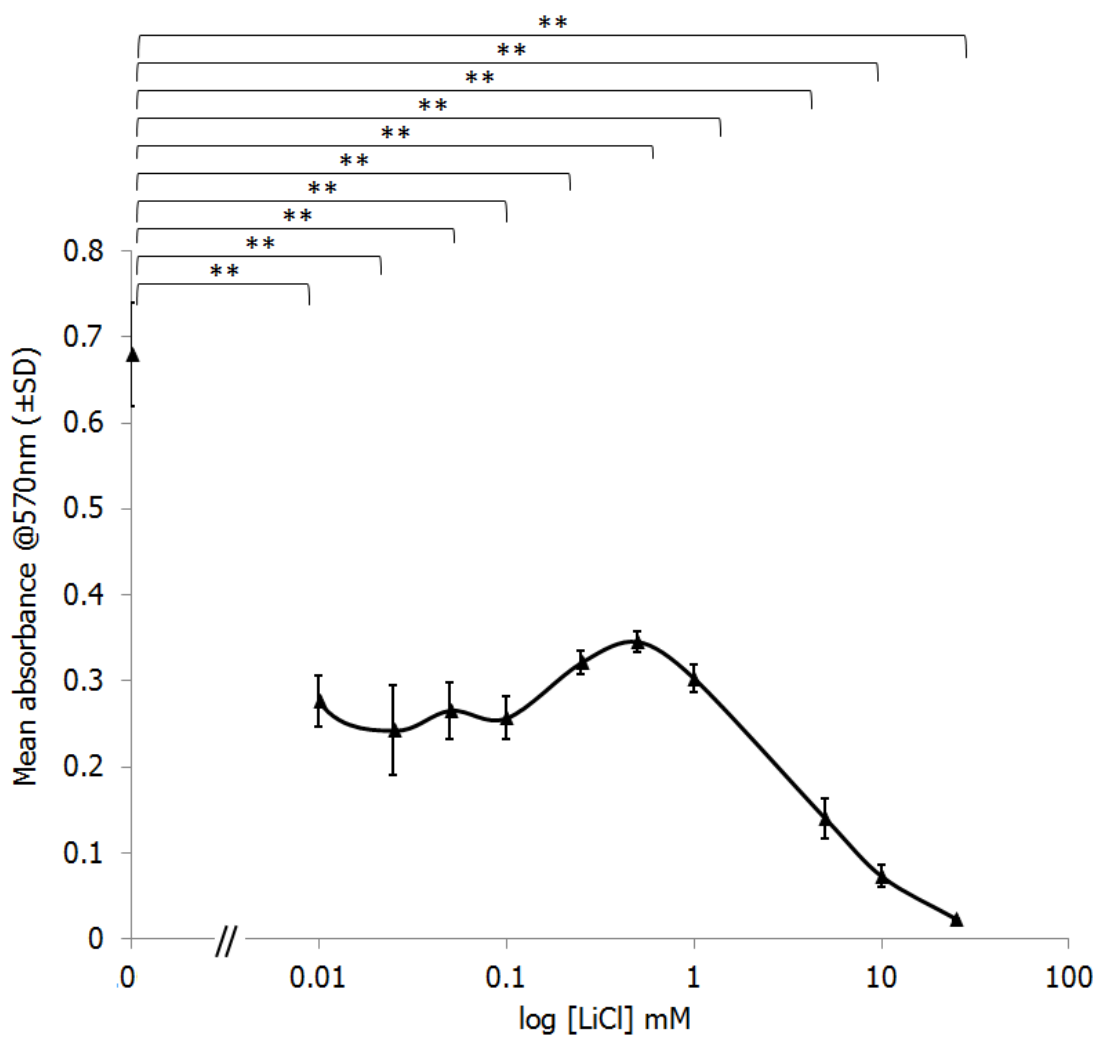


Figure 4-6 NHU dose response curve to LiCl

Mean absorbance from NHU cells after a 4-day incubation with 0-25mM LiCl in 1% (v/v) PBS. Data shows the mean absorbance at 570nm (\pm SD) of 6 technical replicates. ** $p < 0.01$, one way ANOVA with Dunnett's post-test.

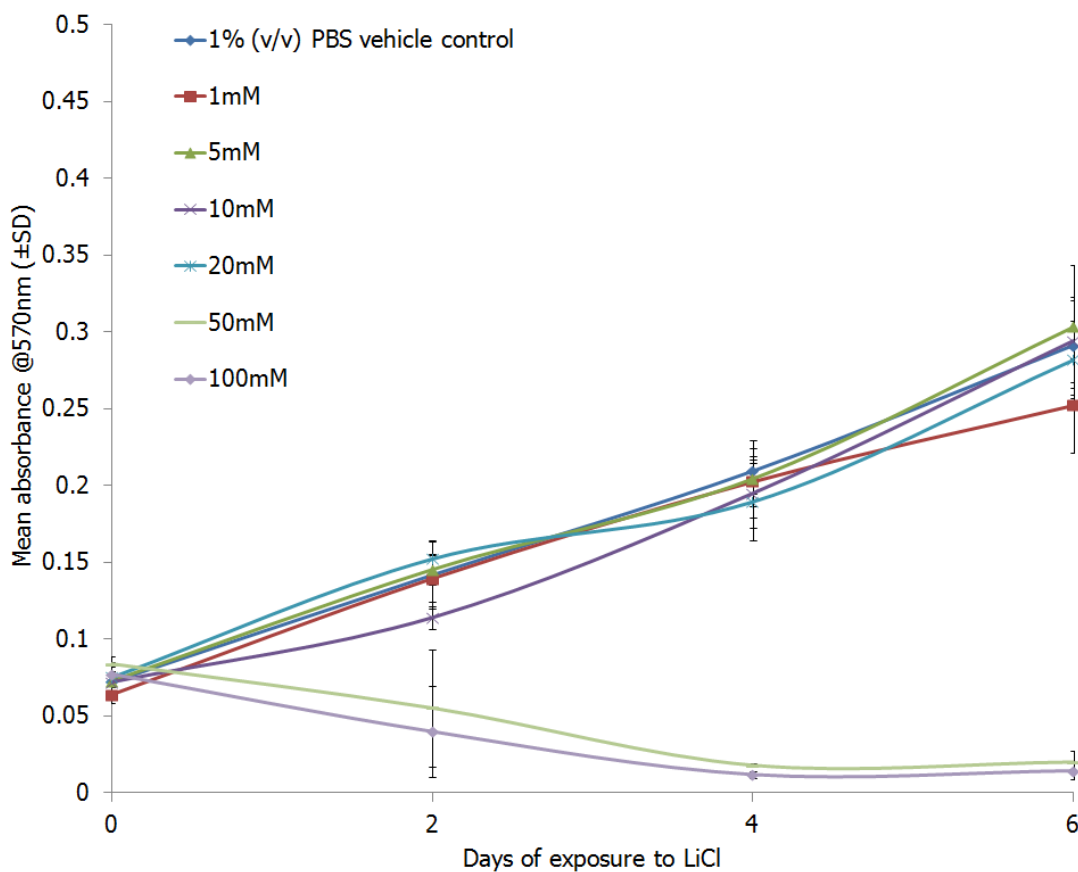


Figure 4-7 Effect of LiCl on SaOS-2 cell viability

MTT assay from SaOS-2 cells cultured in McCoy's 5A + 15% (v/v) FBS + 0-100mM LiCl for up to 6 days. 1% (v/v) PBS was included in all cultures as the vehicle control. Medium and inhibitors were replenished on day 3. Data shows the mean absorbance at 570nm (\pm SD) of 6 technical replicates.

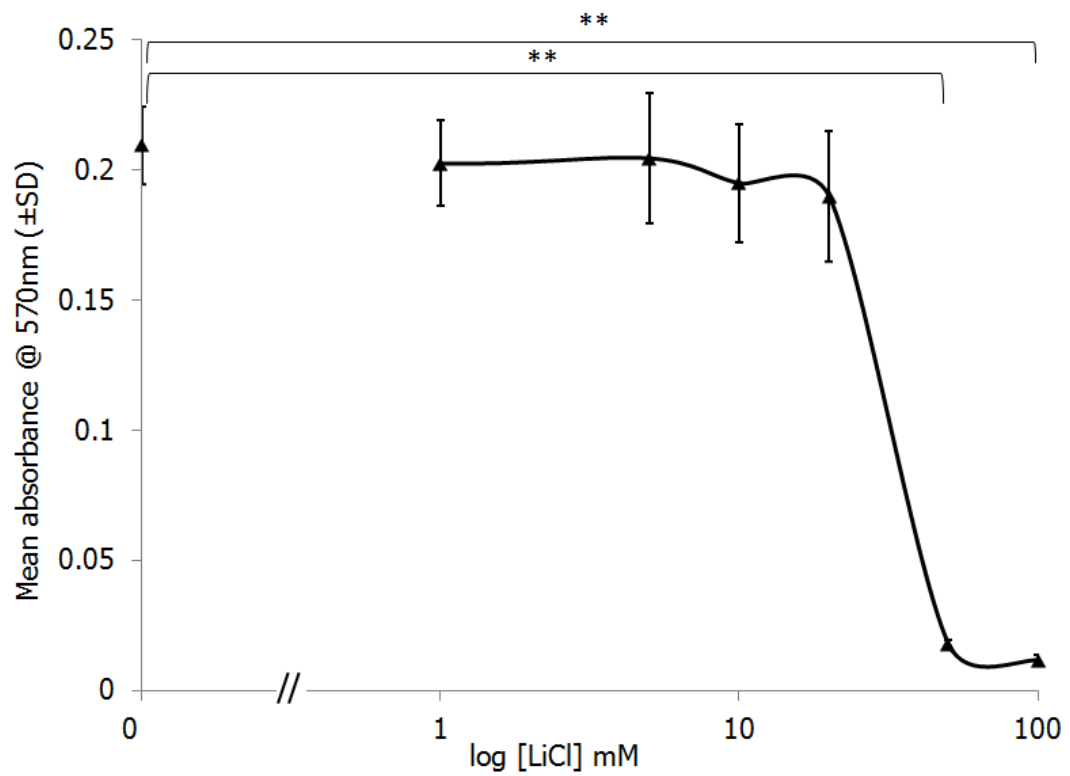


Figure 4-8 SaOS-2 dose response curve to LiCl

Mean absorbance from SaOS-2 cells after a 4-day incubation with 0-100mM LiCl in 1% (v/v) PBS. Data shows the mean absorbance at 570nm (\pm SD) of 6 technical replicates. ** $p < 0.01$, one way ANOVA with Dunnett's post-test.

4.5.2 Effect of GSK3 β inhibition on cell morphology

No morphological differences were observed between SaOS-2 cells incubated with 10-20 μ M SB415286 and vehicle control (Figure 4-9A, B and C). SaOS-2 cell cultures incubated in the presence of 20mM LiCl appeared to be slightly less densely populated than vehicle control cultures, but cells still appeared phase-bright (Figure 4-9D). NHU cells treated with between 5-10 μ M SB415286 lacked any morphological changes compared to vehicle control (Figure 4-9 E,F,G and H).

4.5.3 Effect of GSK3 β inhibition on β -catenin localisation

Labelling of SaOS-2 cells with anti- β -catenin antibody resulted in a diffuse cytoplasmic labelling pattern with no nuclear labelling visible (Figure 4-10 A). With 10-20 μ M SB415286 and 20mM LiCl, SaOS-2 cell nuclei were clearly labelled, signifying activation and translocation of β -catenin to the nucleus (Figure 4-10 A,B,C and D). Mean nuclear pixel intensity was 2.3-fold higher after treatment with 10 μ M SB415286, 2.7-fold higher with 20 μ M SB415286 and 2.9-fold higher with 20mM LiCl when compared to control (Figure 4-11). By contrast, NHU cells (Figure 4-10 E,F,G and H) exhibited a large proportion of nuclear β -catenin in the untreated control culture and only developed a modest increase in nuclear labelling after treatment with 5, 7.5 and 10 μ M SB415286 (1.1-fold, 1.2-fold and 1.4-fold vs. control, respectively; Figure 4-11). This data inferred that NHU cells already had a pool of active β -catenin which was present in the nucleus.

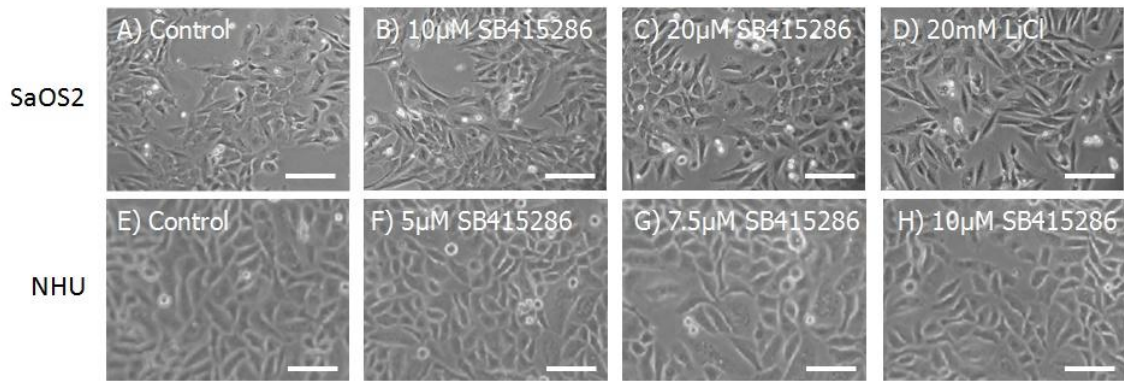


Figure 4-9 Effect of GSK3 inhibitors on cell morphology of SaOS-2 and NHU cells *in vitro*

Phase micrographs of SaOS-2 and NHU cells after a 24 hour incubation with GSK3 inhibitors. **(A-D)** SaOS-2 cells cultured in McCoy's 5A + 15% (v/v) FBS and treated with the following: **(A)** 0.1% (v/v) DMSO (solvent control); **(B)** 10µM SB415286; **(C)** 20µM SB415286; **(D)** 20mM LiCl. **(E-H)** Y924 P4 NHU cells cultured in KSFMc and treated with the following: **(E)** 0.1% (v/v)DMSO (solvent control); **(F)** 5µM SB415286; **(G)** 7.5µM SB415286; **(H)** 10µM SB415286. Scale bar: 50µm.

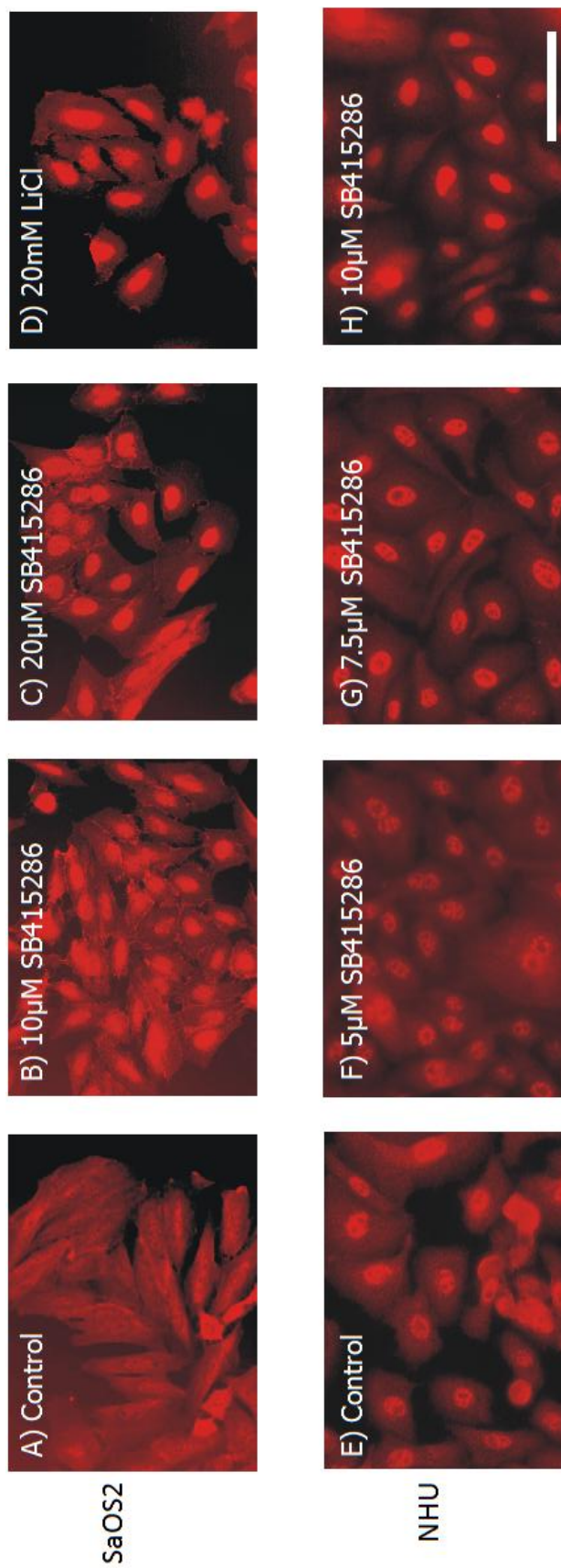


Figure 4-10 Expression and localisation of β -catenin after GSK3 β inhibition in SaOS-2 and NHU cells *in vitro*

β -catenin indirect immunofluorescence labelling of formalin-fixed SaOS-2 and Y924 NHU cells after a 24-hour treatment with GSK3 inhibitors. **(A-D)** SaOS-2 cells cultured in McCoy's 5A + 15% (v/v) FBS and treated with the following: **(A)** 0.1% (v/v) DMSO (solvent control); **(B)** 10 μ M SB415286; **(C)** 20 μ M SB415286; **(D)** 20mM LiCl. **(E-H)** Y924 P4 NHU cells cultured in KSMc and treated with the following: **(E)** 0.1% (v/v) DMSO (solvent control); **(F)** 5 μ M SB415286; **(G)** 7.5 μ M SB415286; **(H)** 10 μ M SB415286. Scale bar: 100 μ m.

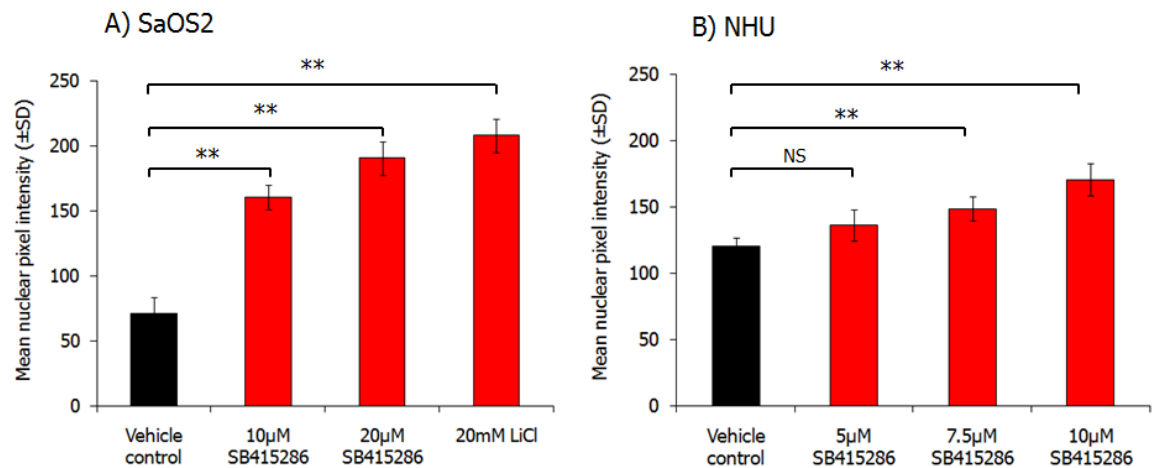


Figure 4-11 Nuclear translocation of β -catenin in SaOS-2 and NHU cells after GSK3 inhibition

Mean nuclear pixel intensities from photomicrographs of β -catenin labelled cells after a 24-hour incubation \pm GSK3 inhibitors (fig 4.10). **(A)** SaOS-2 cells cultured in McCoy's 5A + 15% (v/v) FBS; **(B)** Y924 NHU cells cultured in KSFMc. Vehicle control was 0.1% (v/v) DMSO in normal culture medium. (** P<0.01, NS non-significant, one-way ANOVA with Dunnett's post-test versus vehicle control). (Mean nuclear pixel intensity calculated as described in section 2.9.1.6).

4.5.4 Effect of GSK3 inhibitors on TCF transcription factor activity

As expected, the positive control cell line, SaOS-2, had significantly higher luciferase expression when treated with either SB415286 or LiCl compared to vehicle only control. Normalised TOPFLASH luciferase activity after SB415286 treatment was 7.5-fold higher than vehicle control ($P < 0.05$) and 12-fold higher after LiCl treatment ($P < 0.001$). This data verified that both compounds not only led to a nuclear translocation of β -catenin (Figure 4-12) but also activated TCF transcription factors and thus mimicked active Wnt signalling. No significant change was observed in the FOPFLASH TCF-mutant control when SaOS-2 cells were incubated with GSK3 inhibitors.

By contrast to the response seen in the SaOS-2 cells, no change in TOPFLASH luciferase activity was observed in the NHU cells after SB415286 treatment (Figure 4-13). Interestingly, TOPFLASH and FOPFLASH luciferase activity was much higher in the NHU cells than in the SaOS-2 cells. Basal luciferase activity from the TOPFLASH plasmid was 143-fold higher in the NHU cells compared to the SaOS-2 cells. NHU FOPFLASH activity was 63-fold higher in the NHU cells compared to the SaOS-2 cells, and was most likely caused by differences in TK minimal promoter activity between the two cell lines. Surprisingly, in NHU cells, normalised FOPFLASH luciferase activity was higher than TOPFLASH under all conditions, suggesting luciferase gene transcription was being driven via the mutant site in FOPFLASH. To investigate the cause of this background transcription, both the TCF-binding promoter insert within TOPFLASH and the mutant non-TCF binding promoter insert within FOPFLASH (appendix VIII) were interrogated for potential transcription factor binding sites using MATInspector (Genomatix).

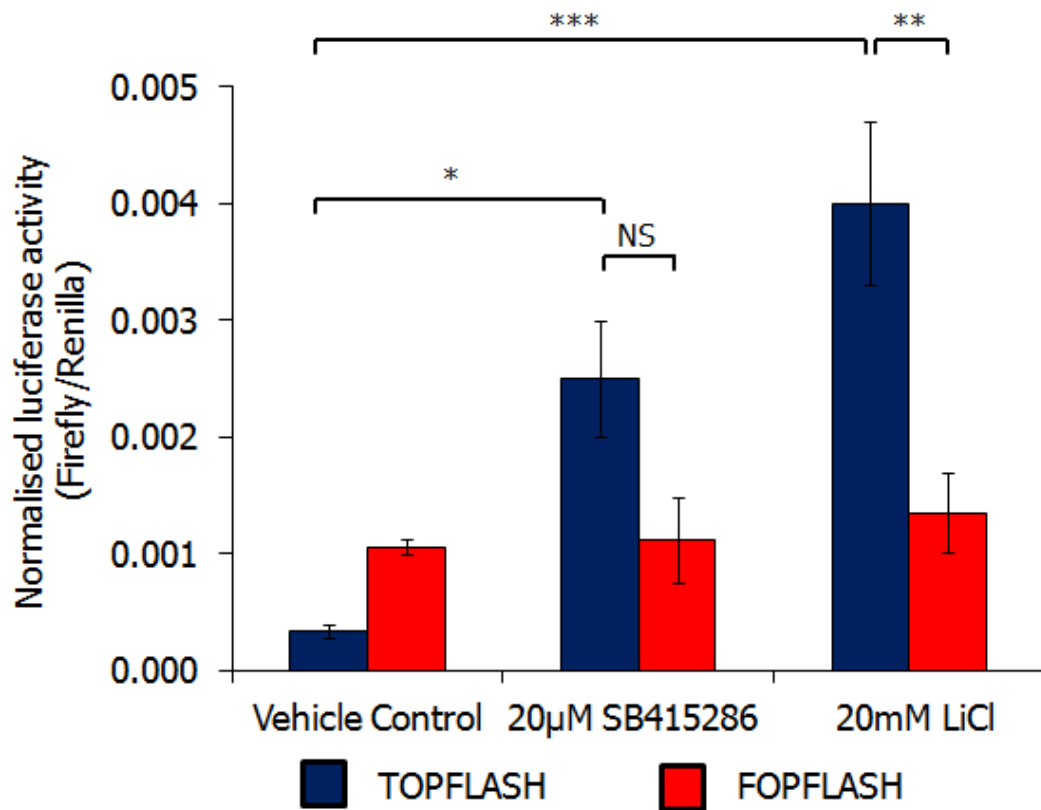


Figure 4-12 TCF transcription factor activity in SaOS-2 cells after GSK3 inhibition

SAOS-2 cells were transfected 24-hours after seeding with either 0.5µg of TOPFLASH or FOPFLASH (negative control) plasmid along with 0.01µg pRL-CMV (loading control). 24 hours after transfection, SaOS-2 cells were treated with 20µM SB415286, 20mM LiCl or vehicle control for 24 hours. A dual luciferase assay was performed on 3 biological replicates and data represents the mean luciferase activity after normalisation to loading control (\pm SD). (***) $P < 0.001$, ** $P < 0.01$, * $P < 0.05$, NS non significant using a one-way ANOVA with Dunnett's multiple comparison post-test).

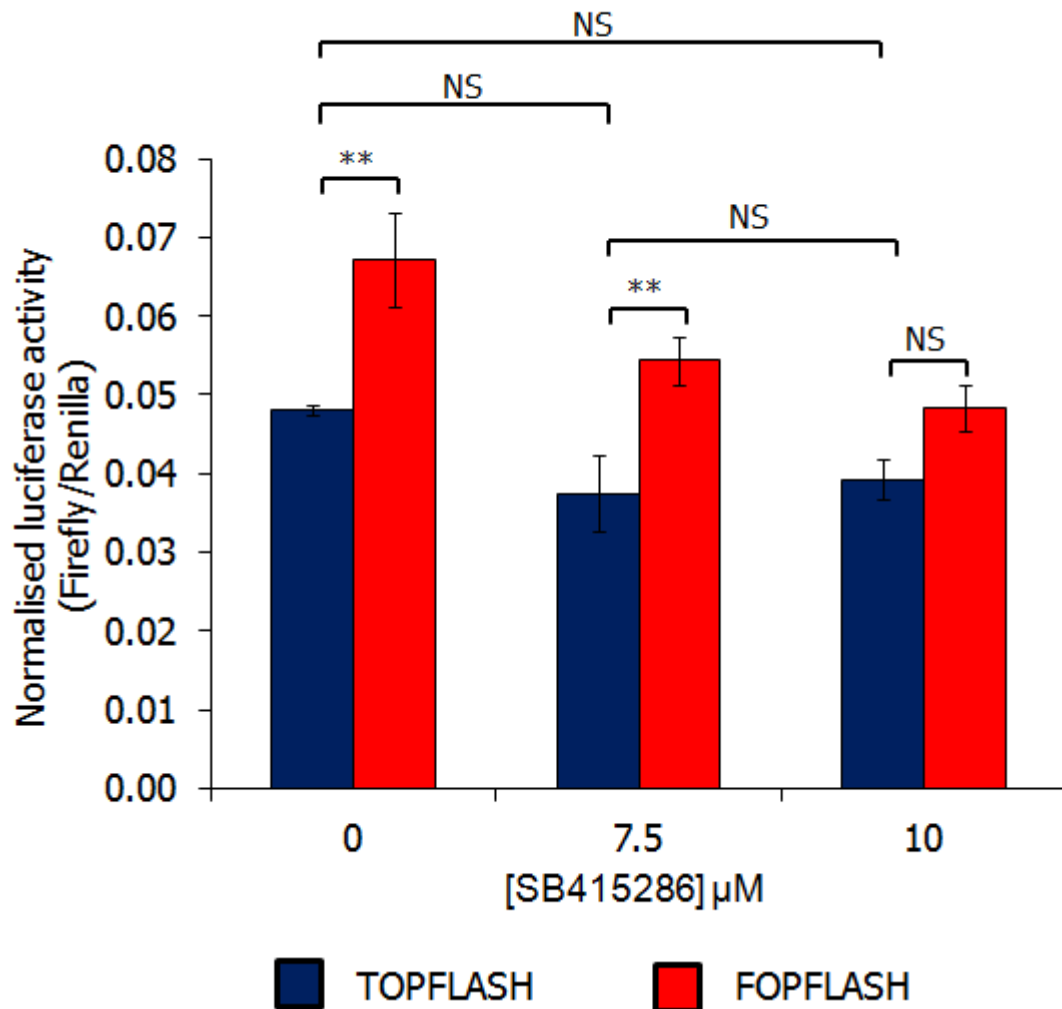


Figure 4-13 TCF transcription factor activity in NHU cells after GSK3 inhibition

Y924 NHU cells (at P3) were seeded into a 24-well Primaria® plate at 4×10^4 cells/well and transfected 24-hours after seeding with either; 0.5 μg TOPFLASH or FOPFLASH (negative control) plasmid along with 0.01 μg loading control, pRL-CMV. 24 hours post-transfection, NHU cells were medium changed to KSMc + 0.1% (v/v) DMSO with 0-10 μM SB415286 for 24 hours. A dual luciferase assay was performed on 3 technical replicates and data represents the mean luciferase activity after normalisation to loading control (\pm SD). (***) $P < 0.001$, ** $P < 0.01$, * $P < 0.05$, NS non significant using a one-way ANOVA with Bonferroni multiple comparison post-test). Please note differences in the Y-axis scale bar between fig 4-12 and fig 4.13.

4.5.4.1 TOPFLASH promoter analysis

Analysis of the TOPFLASH plasmid clearly showed four LEF1/TCF binding sites along with several other potential transcription factor binding sites, such as nuclear receptor sub-family 2 factors and GATA binding sites (Table 4-1). Unexpectedly, two of the four LEF1/TCF binding sites were present on the negative strand leaving only two on the template strand.

Analysis of the mutant TCF binding site within the FOPFLASH vector exposed a plethora of potential binding sites. Of notable interest were potential PPAR γ binding sites, with 3 present on the template strand (Table 4-2).

NAME	FROM	TO	ANCHOR	STRAND	CORE SIMILARITY	MATRIX SIMILARITY	SEQUENCE
Chorion-specific transcription factors with a GCM DNA binding domain	4	18	11	(-)	1	0.832	cttacCCCCtttgat
Pleomorphic adenoma gene	8	30	19	(+)	1	1	aaGGGGgtaagatcaaagggggt
Krueppel like transcription factors	11	27	19	(+)	1	0.87	ggggtaagatcaaAGGG
Nuclear receptor subfamily 2 factors	11	35	23	(+)	1	0.823	ggggtaagatCAAagggggtaaaat
RXR heterodimer binding sites	11	35	23	(+)	0.821	0.819	ggggtaaGATCaaagggggtaaaat
GATA binding factors	14	26	20	(+)	1	0.926	gtaAGATcaaagg
LEF1/TCF	14	30	22	(+)	1	0.987	gtaagaTCAAagggggt
Krueppel like transcription factors	15	31	23	(+)	1	1	taagatCAAAGggggt
GLI zinc finger family	19	33	26	(-)	1	0.862	tttaCCCCtttgat
Pleomorphic adenoma gene	23	45	34	(+)	1	1	aaGGGGgtaaaatcaaaggggggc
Krueppel like transcription factors	26	42	34	(+)	1	0.894	ggggtaaaatcaaAGGG
LEF1/TCF	29	45	37	(+)	1	0.956	gtaaaatCAAAGgggggc
Pleomorphic adenoma gene	29	51	40	(-)	1	1	aaGGGGgccccctttgatattac
Growth factor independence transcriptional repressor	30	44	37	(+)	1	0.928	taaAATCaaaggggg
Krueppel like transcription factors	30	46	38	(+)	1	1	taaaatCAAAGggggcc
Pleomorphic adenoma gene	38	60	49	(+)	1	1	aaGGGGgccccctttgatcttac
Nuclear receptor subfamily 2 factors	39	63	51	(-)	1	0.824	ggggtaagatCAAagggggccccct
Krueppel like transcription factors	43	59	51	(-)	1	1	taagatCAAAGggggcc
LEF1/TCF	44	60	52	(-)	1	0.987	gtaagaTCAAagggggc
Pleomorphic adenoma gene	44	66	55	(-)	1	1	aaGGGGgtaagatcaaaggggggc
Krueppel like transcription factors	47	63	55	(-)	1	0.87	ggggtaagatcaaAGGG
GATA binding factors	48	60	54	(-)	1	0.926	gtaAGATcaaagg
Nuclear receptor subfamily 2 factors	54	78	66	(-)	1	0.823	ggggtaagatCAAagggggtaaagat
RXR heterodimer binding sites	54	78	66	(-)	0.821	0.829	ggggtaaGATCaaagggggtaaagat
Chorion-specific transcription factors with a GCM DNA binding domain	56	70	63	(+)	1	0.832	cttacCCCCtttgat
Krueppel like transcription factors	58	74	66	(-)	1	1	taagatCAAAGggggt
LEF1/TCF	59	75	67	(-)	1	0.987	gtaagaTCAAagggggt
Pleomorphic adenoma gene	59	81	70	(-)	1	1	aaGGGGgtaagatcaaagggggt
Krueppel like transcription factors	62	78	70	(-)	1	0.87	ggggtaagatcaaAGGG
GATA binding factors	63	75	69	(-)	1	0.926	gtaAGATcaaagg
Chorion-specific transcription factors with a GCM DNA binding domain	71	85	78	(+)	1	0.832	cttacCCCCtttgat
Krueppel like transcription factors	73	89	81	(-)	1	1	taagatCAAAGggggt

Table 4-1 Potential transcription factor binding sites within the TCF promoter of TOPFLASH

Transcription factor binding sites within the TCF-specific promoter of the TOPFLASH plasmid (Millipore) were analysed using MATInspector (Genomatix) and default parameters. Matrix similarity score >0.8 are classed as potential binding sites. Note the four LEF1/TCF binding sites, two of which are on the negative (-) strand.

NAME	FROM	TO	ANCHOR	STRAND	CORE SIMILARITY	MATRIX SIMILARITY	SEQUENCE
GLI zinc finger family	1	15	8	(-)	1	0.862	tttaCCCCtttggc
C2H2 zinc finger protein PLZF	9	23	16	(+)	0.958	0.866	gggTAAAGgccaag
Peroxisome proliferator-activated receptor gamma	1	23	12	(+)	1	0.92	gccaaggggtAAAGgccaag
NGFI-B response elements, nuclear subfamily of nuclear receptors	10	24	17	(+)	1	0.877	ggtaAAGGccaag
Nuclear receptor subfamily 2 factors	2	26	14	(+)	0.75	0.854	ccaaaggggTAAAGgccaagggg
Pleomorphic adenoma gene	5	27	16	(+)	1	1	aaGGGGgtaagccaaggggg
Peroxisome proliferator-activated receptor gamma	8	30	19	(+)	1	0.902	gggtaagggccAAAGggggtaa
Chorion-specific transcription factors with a GCM DNA binding domain	17	31	24	(-)	1	0.832	cttacCCCCtttggc
Nuclear receptor subfamily 2 factors	9	33	21	(+)	1	0.87	gggtaagggcCAAAGggggtaaaggc
Pleomorphic adenoma gene	21	43	32	(+)	1	1	aaGGGGgtaagccaagggggc
Peroxisome proliferator-activated receptor gamma	23	45	34	(+)	1	0.902	ggggtaagggccAAAGggggccc
Nuclear receptor subfamily 2 factors	24	48	36	(+)	1	0.871	gggtaagggcCAAAGggggcccctt
Pleomorphic adenoma gene	27	49	38	(-)	1	1	aaGGGGgccccctttggccttac
CTCF and BORIS gene family, transcriptional regulators with 11 highly conserved zinc finger domains	24	50	37	(+)	1	0.817	gggtaagggccaagggGGGCCCCttt
Pleomorphic adenoma gene	36	58	47	(+)	1	1	aaGGGGgccccctttggccttac
Nuclear receptor subfamily 2 factors	37	61	49	(-)	1	0.871	gggtaagggcCAAAGggggcccctt
CTCF and BORIS gene family, transcriptional regulators with 11 highly conserved zinc finger domains	35	61	48	(-)	1	0.817	gggtaagggccaagggGGGCCCCttt
Peroxisome proliferator-activated receptor gamma	40	62	51	(-)	1	0.902	ggggtaagggccAAAGggggccc
Pleomorphic adenoma gene	42	64	53	(-)	1	1	aaGGGGgtaagccaagggggc
Chorion-specific transcription factors with a GCM DNA binding domain	54	68	61	(+)	1	0.832	cttacCCCCtttggc
Nuclear receptor subfamily 2 factors	52	76	64	(-)	1	0.87	gggtaagggcCAAAGggggtaaaggc
Peroxisome proliferator-activated receptor gamma	55	77	66	(-)	1	0.902	ggggtaagggccAAAGggggtaa
Pleomorphic adenoma gene	57	79	68	(-)	1	1	aaGGGGgtaagccaagggggt
Chorion-specific transcription factors with a GCM DNA binding domain	69	83	76	(+)	1	0.832	cttacCCCCtttggc

Table 4-2 Potential transcription factor binding sites within the mutant TCF promoter of FOPFLASH

Transcription factor binding sites within the mutant TCF promoter of the FOPFLASH plasmid (Millipore) were analysed using MATInspector (Genomatix) and default parameters. Matrix similarity score >0.8 are classed as potential binding sites. Note the five PPAR γ binding sites, three of which are on the template (+) strand.

4.6 Discussion

The aim of this study was to utilise pharmacological antagonists of GSK3 to inactivate the destruction complex and mimic canonical Wnt signalling in NHU cells.

Two GSK3 inhibitors were used in this study: LiCl, a seminal GSK3 inhibitor which has a long history within the Wnt literature, and a relatively new drug, SB415286, a maleimide derivative developed by SmithKline Beecham (148). LiCl is an alkali metal chloride which inhibits the activity of GSK3 via two mechanisms: firstly, it acts as a competitive inhibitor of Mg^{2+} , required for substrate phosphorylation (145, 149) and secondly, by inhibition of protein phosphatase 1, the enzyme which dephosphorylates and re-activates GSK3 β at serine 9 (150). LiCl is however not a specific GSK3 inhibitor; it has been shown to affect other kinases including casein kinase 2 (CK2 IC_{50} 44mM), mitogen-activated protein kinase-activated protein kinase 5 (PRAK IC_{50} 56mM) and mitogen-activated protein kinase-activated protein kinase 2 (MAPKAPK2 IC_{50} 21mM)(151) and therefore data must be interpreted with caution. SB415286 inhibits GSK3 in an ATP competitive manner and has so far not been shown to significantly inhibit any other protein kinases when used at a concentration of 10 μ M (tested against a panel of 24-protein kinases) (144, 148, 152). Another maleimide derivative, SB216763 was not used in this study because of reported precipitation issues when incubated for periods greater than 90 minutes in aqueous solution (144).

4.6.1 Toxicity of GSK3 inhibitors

Up to 10 μ M SB415286 had no effect on NHU morphology or cell viability in culture. LiCl on the other hand, was not well tolerated by NHU cells. The reasons for this were not fully investigated in this study but could be linked to its effect not only on GSK3 but also on a variety of other protein kinases, included at least two involved in the p38 stress response pathway (151).

Ideally the effect of two structurally unrelated inhibitors of GSK3 β would have been used throughout this study, but as LiCl was not suitable for use with NHU cells the remainder of this investigation was completed with SB415286 alone.

4.6.2 β -catenin nuclear translocation

Indirect immunofluorescence from SaOS-2 cells treated with LiCl or SB415286 showed clear nuclear translocation of β -catenin and verified the efficacy of both inhibitors. Surprisingly, when NHU cells incubated with vehicle alone were immunolabelled with anti- β -catenin antibodies, most of the cells already had a significant pool of nuclear β -catenin. This suggested one of two things, either NHU cells were autocrine Wnt signalling; or the destruction complex was repressed in NHU cells, allowing non-phosphorylated β -catenin to accumulate and translocate to the nucleus.

Treatment of NHU cells with GSK3 inhibitor resulted in a visual increase in nuclear β -catenin above that observed in vehicle control cultures. This suggested that in control cultures there was still a pool of β -catenin that was being inactivated via GSK3 and implied that the destruction complex was present in NHU cells but was probably repressed either via signalling from Wnt, or by phosphorylation of GSK3 from another protein kinase.

Previous data from chapter 3 indicated that proliferating NHU cells produced transcript for four Wnt ligands which suggests they may have the potential for autocrine Wnt signalling. The production of functional Wnt ligand is known to involve several tiers of post-translational modification. Once translated, Wnt protein is targeted to the endoplasmic reticulum (ER) where it undergoes glycosylation and palmitoylation (96, 97, 153). Both modifications are fundamentally important and are reviewed in detail in chapter 6. In brief, glycosylation is thought to be important in the secretory pathway and transfer from the ER to the trans Golgi network (TGN) (154-157), whereas palmitoylation is thought to be important for Wnt bioactivity (157, 158). For

production and secretion of active Wnt ligand *in vitro*, Willert and colleagues have shown that serum is required and have postulated this to be because of the need for palmitic acid (96). NHU cells are cultured in a serum-free medium (KSFMc) with no palmitic acid present in the medium (Invitrogen; personal communication), therefore it is unlikely that the pool of nuclear β -catenin seen in proliferating NHU cells is the result of autocrine Wnt signalling. The role of palmitic acid in Wnt secretion and autocrine signalling of NHU cells could be of significance during urothelial regeneration and is explored further in chapter 6.

As mentioned above, there are several cell-specific mechanisms that can regulate the activity and subsequent nuclear translocation of β -catenin. Growth factors such as epidermal growth factor (EGF), hepatocyte growth factor (HGF) and insulin-like growth factor-1 (IGF-1) have all been shown to regulate the activity of β -catenin (159, 160). This type of intersection between mitogen-activated pathways is termed pathway crosstalk and potentially could be an important regulator of β -catenin/TCF signalling in NHU cells and is explored in chapter 5.

4.6.3 TCF activity

Results from the SaOS-2 cell line verified both the integrity of the GSK3 inhibitors and the DLA assay. No significant increase in luciferase activity was seen in NHU cells after treatment with SB415286. This lack of a response could mean one of two things: either NHU cells already have active TCF-transcription factor, or the action of β -catenin on TCF is blocked via an antagonist such as CBY, ICAT or NLK, all of which are expressed at the mRNA level in proliferating NHU cells.

Both TOPFLASH and FOPFLASH are manufactured from the same vector backbone; the only difference is the presence of TCF-binding sites within TOPFLASH and mutated sites in FOPFLASH. It was therefore surprising to find a higher basal level of luciferase activity in NHU cells transfected with

FOPFLASH compared to TOPFLASH. A published report by Da Costa and colleagues has also shown similar findings in other epithelial cell lines. Unfortunately, no explanation of the cause of this TCF-independent activity was reported by the investigator (161). FOPFLASH contains a mutated TCF binding site and is used to control for changes in minimal promoter (TK) activity. Closer inspection of the mutant TCF binding domain revealed several potential binding sites for other transcription factors including PPAR γ , which has been shown to be active in proliferating NHU cells (personal communication; P. Rubenwolf). This questions the usefulness of the FOPFLASH plasmid as a negative control.

4.6.4 Conclusions

NHU cells have a high level of endogenous active β -catenin that is nuclear in location. The action of this endogenous nuclear β -catenin in proliferating NHU cells remains unclear. Background activity with the FOPFLASH plasmid suggest that it is not a good negative control in this cell system and thus the results from the TCF reporter assay are inconclusive. Data from chapter 3 showed proliferating NHU cells expressing transcript from several Wnt target genes and thus suggests TCF transcription factors are active when NHU cells are proliferating in culture.

5 The interrelationships of different signalling mechanisms and cell:cell contact in modulating urothelial tissue homeostasis

5.1 Rationale

The dynamics between growth factor signalling and cell:cell contact play an important role in regulating self-renewal mechanisms, but to date, it remains unclear how this is properly coordinated. Research has focused on proteins that localise to both sites of cell contact and to the nucleus in the hope of finding the key mediators of this process. Proliferating NHU cells contain nuclear as well as cytoplasmic and membrane bound pools of β -catenin (chapter 4). These data would suggest that β -catenin is important in both NHU cell signalling and cell contact and therefore could be an important player in the proliferative/quiescent switch seen during urothelial regeneration.

In culture, NHU proliferation is driven via autocrine/juxtacrine activation of the EGFR family of receptors. This chapter aims to address whether EGFR cell signalling and cell:cell adhesion (adherens junction formation) modulate the activity of β -catenin and whether the dynamics between them is important in maintaining NHU tissue homeostasis.

To fully address this aim and for ease of reading this chapter is divided into 3 sections:

Section 1: EGFR signalling and its effect on β -catenin localisation and activity; the potential role of signalling crosstalk in Wnt-independent β -catenin activation.

Section 2: The effect of culture confluence and cell:cell contacts on β -catenin localisation; the role of contact inhibition.

Section 3: The role of β -catenin in NHU cell proliferation.

Each section contains its own short introduction, aims, objectives, experimental design and results section. A comprehensive discussion of all the data can be found at the end of the chapter.

5.2 Wnt-independent β -catenin activation: The role of pathway crosstalk

5.2.1 Signalling Crosstalk

At any one time, a cell may be bombarded with many extracellular cues and must take into account all of them to elicit the appropriate cellular response. Many such signals may be contradictory, while others intersect and override one another. Intersection between pathways is known as signalling crosstalk and is thought to add robustness and adaptability to the system, allowing a cell to respond quickly and effectively to important cues for such things as repair and cell cycle arrest, where lack of tight regulation could result in failure to repair or unwarranted proliferation.

5.2.2 Crosstalk with the Wnt pathway

Crosstalk between the Wnt pathway and other signalling pathways is well documented and can be characterised as either GSK-dependent or GSK-independent.

5.2.3 GSK-dependent crosstalk mechanisms

GSK proteins are unlike most protein kinases in that they are constitutively active and are regulated primarily through phospho-inhibition of their activity (serine 21 in GSK3 α or serine 9 in GSK3 β (162, 163)). Several serine/threonine kinases have been suggested as effectors of this, including: p38 MAPK, P90RSK and P70 S6 (effectors of MAPK and ERK signalling) as well as AKT/PKB (PI3K signalling) (162-166). A plethora of research articles linking mitogen-activated protein kinases and Wnt pathway activation have been published and have demonstrated crosstalk at the level of GSK3 via such growth factors as IGF-1, insulin (159, 167), IGF-II (167) EGF via ERK/MAPK (168-171), EGF via PI3K/PKB (172) but disputed by (173), HGF (170), TGF β (174) and FGF (175). The impact of the above crosstalk mechanisms could be substantial and if

correct would suggest that the Wnt cascade is not as exclusive as was originally thought. One paper has however shed doubt on the importance of GSK3 phospho-inhibition in Wnt-driven β -catenin activation. McManus and colleagues have shown in the transgenic mouse that conversion of GSK3 β serine 9 to an alanine had no effect on the release of β -catenin from the destruction complex upon Wnt3a stimulation and thus implied that destruction complex inhibition did not mediate β -catenin release (176).

5.2.4 GSK-independent crosstalk mechanisms

GSK-independent crosstalk is mainly composed of mechanisms that release sequestered β -catenin from the adherens junction and is reviewed and addressed in section 5.3.2.

5.2.5 Rationale

Cell signalling pathways were once viewed as distinct and independent transduction cascades. Evidence however now suggests many points of convergence may exist between cascades and therefore cell signalling studies should not focus solely on one particular pathway but should be investigated as a single global network (177). This sub-chapter will address the role of pathway crosstalk in modulating the sub-cellular location and activity of β -catenin and will investigate the mechanism(s) regulating the expression of Wnt-independent nuclear β -catenin seen in cultured NHU cells.

5.2.6 Hypothesis

In NHU cells, β -catenin activity is modulated via EGFR signalling crosstalk.

5.2.7 Aim

The aim of this sub-chapter was to ascertain if signalling crosstalk between the downstream EGFR pathways and β -catenin was present in NHU cells.

5.2.8 Objectives

Specific objectives of this sub-chapter were:

- To use EGFR, PI3K and MAPK antagonists to block all or part of the EGFR signalling cascade and assess whether this affects the phosphorylation status and location of β -catenin as well as expression of β -catenin transcriptionally regulated gene targets (Objective 1).
- To determine if NHU cells respond to pharmacological GSK3 β inhibition when EGFR signalling was blocked and to assess the importance of active β -catenin alone in driving NHU cell proliferation (Objective 2).

5.2.9 Experimental Design (Objective 1)

NHU cells were cultured for up to 72 hours in KSFMc containing 1 μ M PD153035 (EGFR tyrosine kinase inhibitor), 5 μ M U0126 (MEK1/MEK2 inhibitor) or 5 μ M LY294002 (PI3K inhibitor). DMSO was kept at a concentration of 0.1%(v/v) in all cultures and controls. At 24 intervals, parallel cultures were treated as follows (Figure 5-1

- Formalin-fixed on 12-well Teflon[®]-coated multi-spot slides to allow indirect- immunofluorescence photomicroscopy to be performed. Changes in the amount and sub-cellular location of β -catenin was visualised using the anti β -catenin antibody (clone C2206) and anti-active β -catenin antibody (ABC; clone 8E7). Nuclear and cytoplasmic signal intensities for active β -catenin were quantified from photomicrographs all taken at the same exposure, as previously described (section 2.9.1.6).
- Lysed *in situ* using 2x SDS lysis buffer to produce whole cell lysates. Western blot was employed to verify that the applied antagonists had been effective. Changes in the relative expression of active β -catenin, as

well as the phosphorylation status of GSK3 β over the 72 hour time course were investigated.

- Scraped *in situ* into TRIzol[®] reagent. The effect of EGFR, MAPK and PI3K inhibition on mRNA expression of three downstream targets of β -catenin/TCF mediated transcription (Axin2 c-MYC and Lef1), as well as one negatively regulated target (CDH1) were quantified using SYBR[®] Green I qPCR.

NHU cells were also cultured in KSFM with BPE and cholera toxin but minus exogenous rhEGF to assess the effect of autocrine EGFR signalling on β -catenin activation.

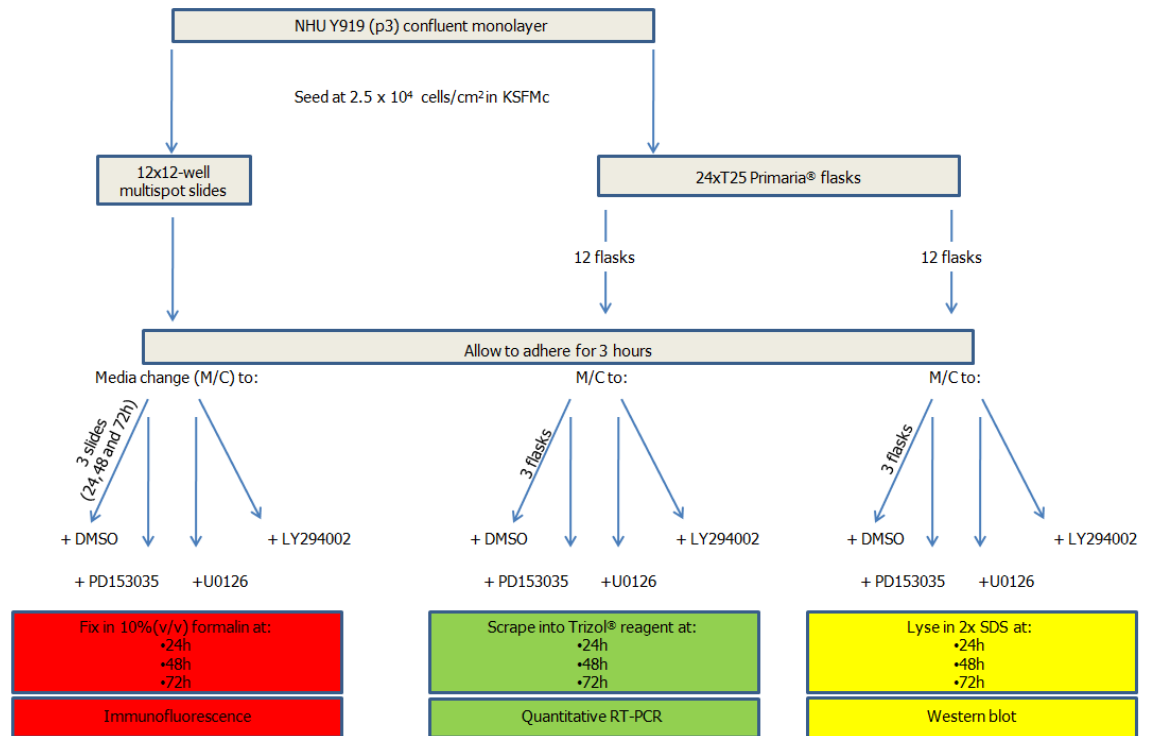


Figure 5-1 Experimental design used to assess potential EGFR and β -catenin crosstalk

One ureteric NHU cell line (Y919) was seeded onto 12-well multispot slides and T25 Primaria flasks at a cell density of 2.5×10^4 cells/cm². Cells were allowed to adhere and then cultured with inhibitors or 0.1% (v/v) DMSO vehicle control. At 24, 48 and 72 hours, cells were harvested and the effect of EGF inhibition on β -catenin nuclear translocation and β -catenin/TCF driven transcription was assessed.

5.2.10 Results (Objective 1)

5.2.10.1 Manipulation of the EGFR signalling cascades and its effect on active β -catenin expression and sub-cellular location

The amount of active β -catenin contained within the nucleus of NHU cells cultured without inhibitors was seen to fluctuate over the 72 hour time course. Nuclear labelling for active β -catenin was most intense 48 hours post seeding, after which it was seen to reduce (Figure 5-2A-C). This change in nuclear β -catenin labelling was also seen with the anti-total β -catenin antibody (C2206; Figure 5-2G-I). Photoshop quantification of the nuclear fluorescent signal affirmed the visual change across the course of the experiment (Figure 5-4). Cytoplasmic labelling for active β -catenin remained constant over the 72 hour time-course. Parallel cultures grown without exogenous rhEGF also had high levels of nuclear-active β -catenin at 48 hours post-seeding and like the cultures grown in KSFMc, they exhibited a reduction in nuclear labelling 72 hours post seeding (Figure 5-3). Results thus implied that the fluctuation of nuclear-active β -catenin was not caused by the addition and subsequent exhaustion of exogenous rhEGF in the medium, but was more likely due to alternative factors, such as the density of the culture.

Western blot data from parallel cultures corroborated the immunofluorescence findings (Figure 5-5). Densitometry confirmed peak expression of active β -catenin to be 48 hours post-seeding. Relative active β -catenin expression (active/total) was calculated as being 0.61, 1.55 and 1.22 at 24, 48 and 72 hours, respectively. Interestingly, relative phospho-ERK expression was also seen to peak 48 hours post-seeding (Figure 5-5B/D). To investigate whether this increase in active β -catenin expression was due to a change in the activity of the destruction complex, an antibody targeted to the inactive (phospho serine 9) form of GSK3 β was used. Results revealed that the increase in relative active β -catenin expression seen at 48 hours post-seeding was accompanied by an increase in phospho-GSK3 β (Figure 5-5F). These data thus

indicated that β -catenin activity was being modulated via a Wnt-independent GSK3 β -dependent mechanism.

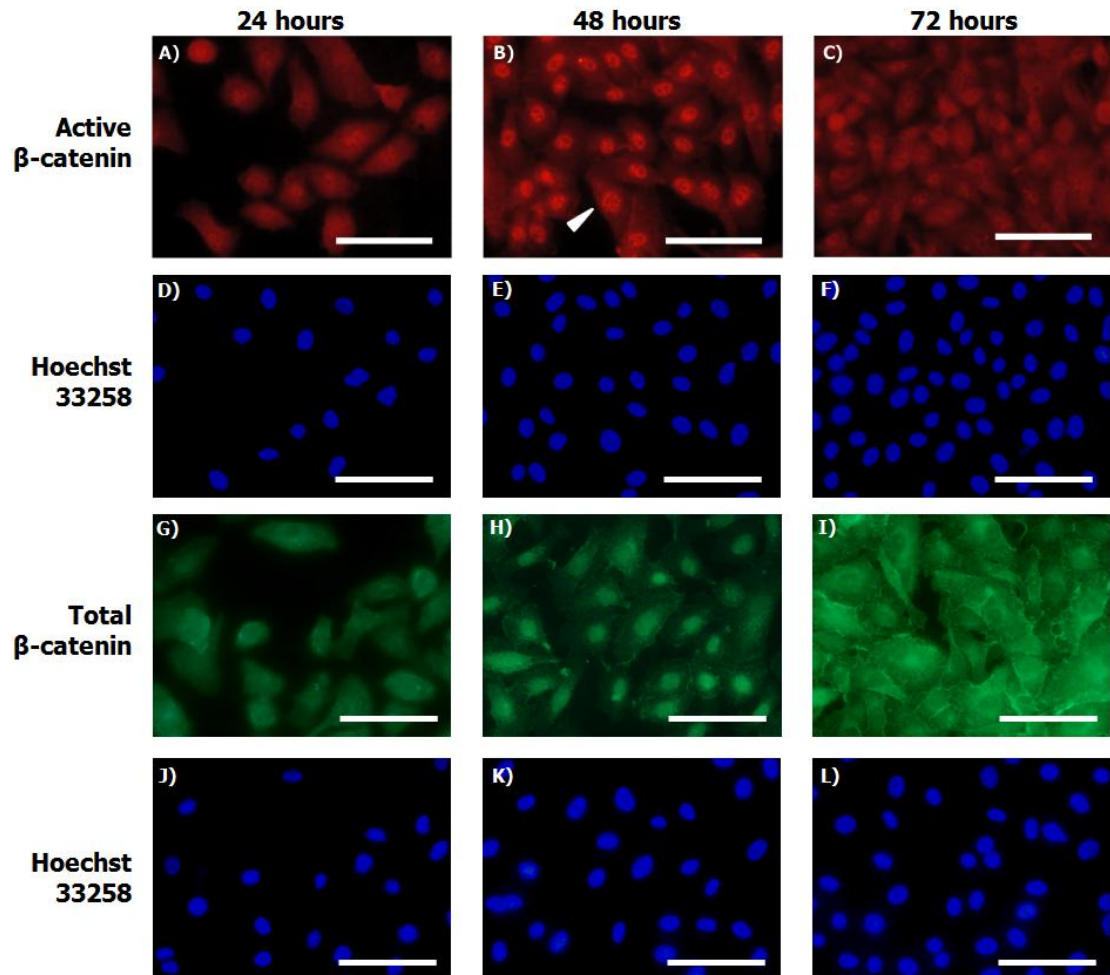


Figure 5-2 Expression and localisation of β -catenin in NHU cells

NHU cells (Y919) at P4 were cultured for 24 hours, 48 hours and 72 hours in KSFMc + 0.1%(v/v) DMSO. Slides were formalin-fixed and immunolabelled with active β -catenin antibody (8E7) and rabbit anti-mouse IgG-Alexa 594 secondary antibody or total β -catenin (C2206) and goat anti-rabbit IgG Alexa 488 secondary antibody. All slides were stained with Hoechst 33258 to delineate the nucleus and labelling was visualised under epi-fluorescent illumination. Scale bar: 100 μ M. Micrographs are representative of two technical replicates (N=2). Arrow denotes strong punctate nuclear active β -catenin labelling at 48 hours post-seeding and indicates activation of the Wnt pathway changes over time.

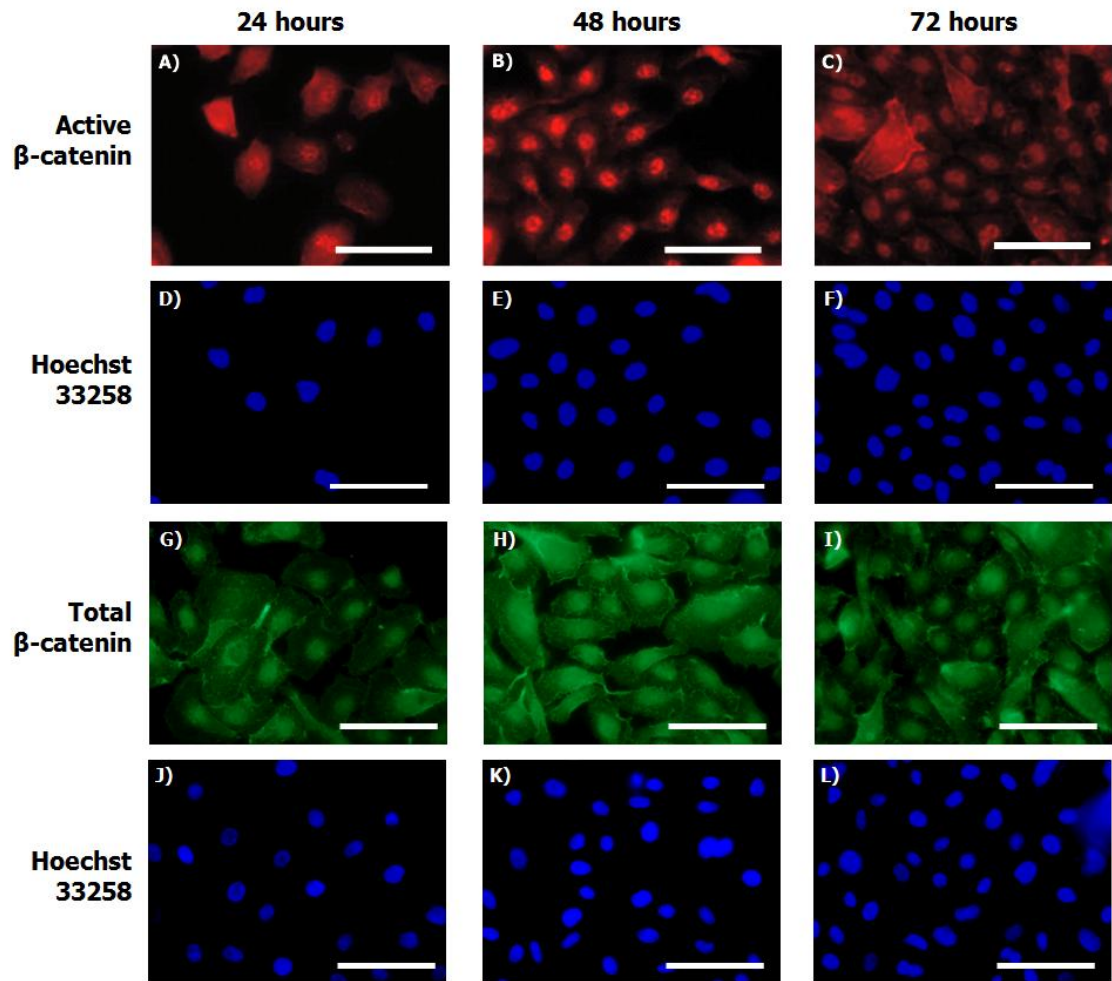


Figure 5-3 Expression and localisation of β -catenin when NHU cells were cultured without exogenous rhEGF

NHU cells (Y919) at P4 were cultured for 24 hours, 48 hours and 72 hours in KSFM + BPE + Cholera toxin + 0.1% (v/v) DMSO (KSFM-rhEGF). Slides were formalin-fixed and immunolabelled with active β -catenin antibody (8E7) and rabbit anti-mouse IgG-Alexa 594 secondary antibody or total β -catenin (C2206) and goat anti-rabbit IgG Alexa 488 secondary antibody. All slides were stained with Hoechst 33258 to delineate the nucleus and labelling was visualised under epi-fluorescent illumination. Scale bar: 100 μ M. N=1. Data implies the fluctuation in nuclear active β -catenin seen over the course of 72 hours is not caused by exogenous EGF depletion but more likely due to culture confluence.

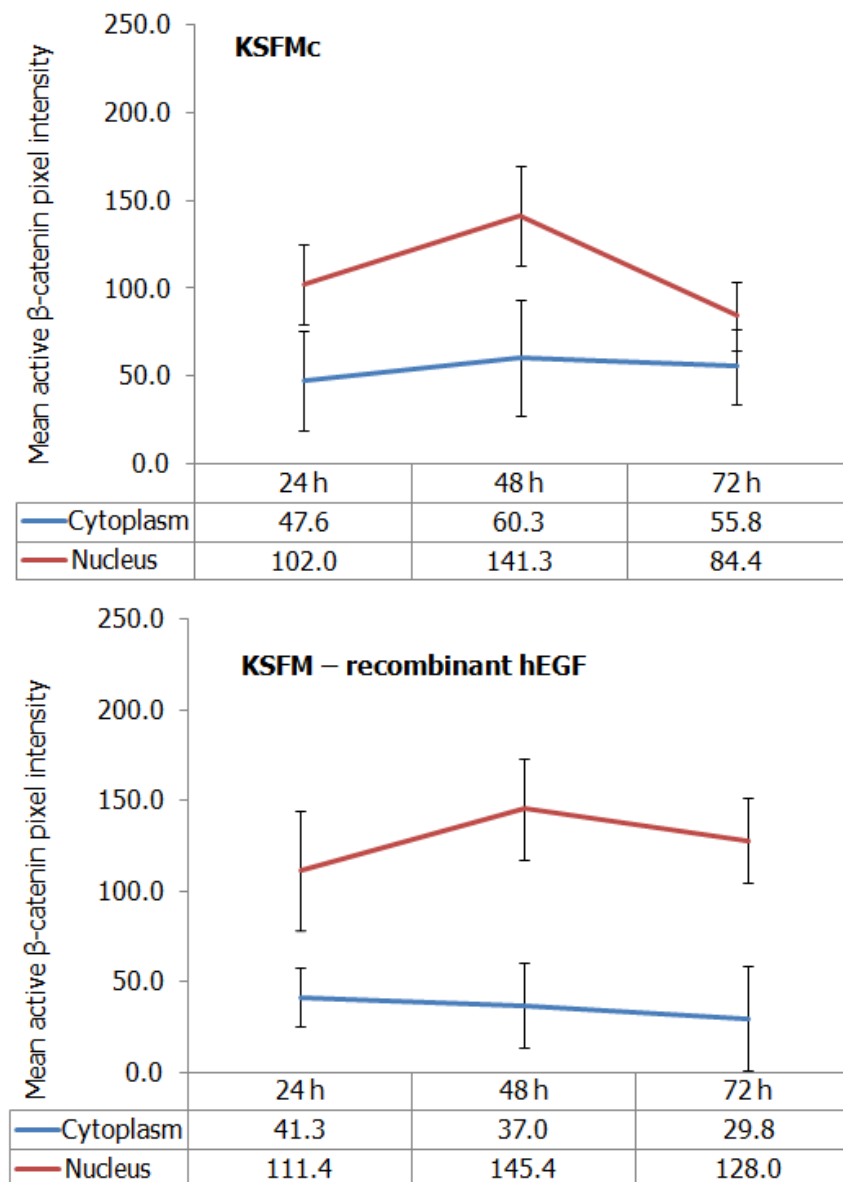


Figure 5-4 Quantification of nuclear and cytoplasmic active β -catenin over 72 hours in normal growth medium (KSFMc) and without exogenous rhEGF

Line graph represents nuclear and cytoplasmic active β -catenin pixel intensities and standard deviations as quantified from each micrograph (fig 5-2 A-C and fig 5.3 A-C) using Adobe Photoshop[®] software.

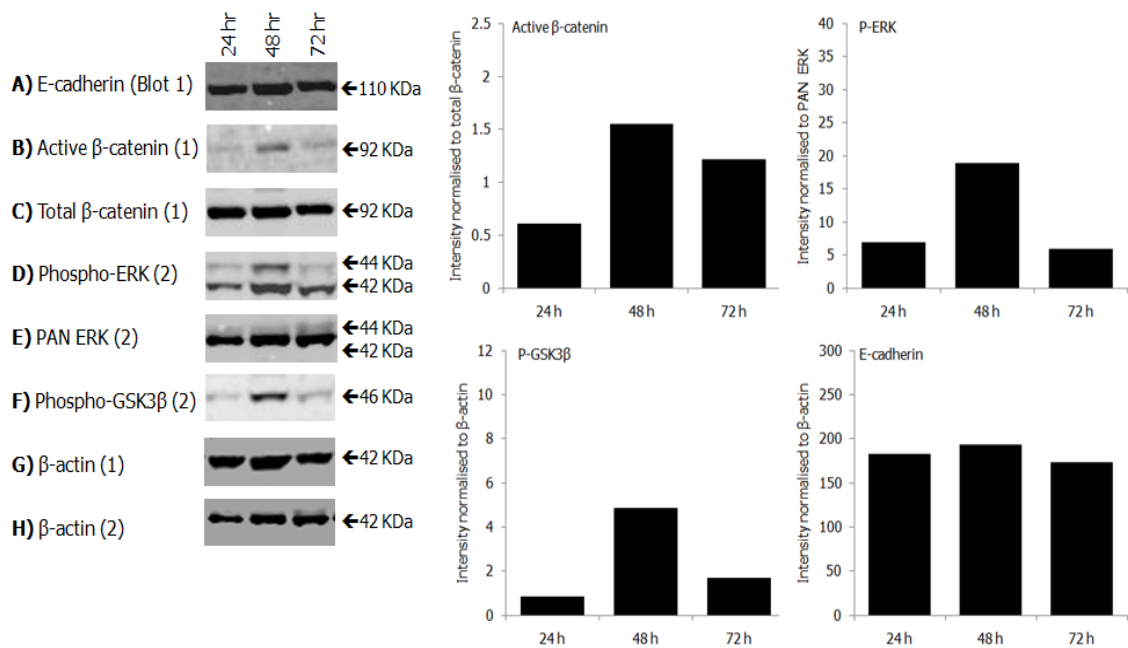


Figure 5-5 Wnt-independent expression of β -catenin via inhibition of GSK3 β

NHU cells (Y919) at P4 were cultured for 24 hours, 48 hours and 72 hours in KSMc + 0.1% (v/v) DMSO prior to lysis in 2X SDS-lysis buffer. 20 μ g of each protein lysate was subjected to SDS-PAGE within a 4-12% (w/v) Bis-Tris gel under denaturing conditions and immunoblotted onto PVDF membrane. The PVDF membranes were blocked and then probed for 16 hours with antibodies raised against E-cadherin (A), active β -catenin (B), total β -catenin (C), phospho-ERK (D), total ERK (E), phospho-GSK3 β (serine 9) (F) and β -actin to control for equal lysate loading (G, H). Membranes were incubated for 1 hour with either goat anti-mouse IgG Alexa 680 or goat anti-rabbit IgG Alexa 800 depending on the antigen and primary antibody used. Antibody binding was visualised by scanning at 700 and 800nm. Densitometry results were represented graphically relative to the appropriate loading control. N=1. Note how the pattern for active β -catenin, phospho-ERK and phospho-GSK3 β expression is all similar. Whole blots for each antibody can be found in appendix IX.

Parallel cultures incubated in the presence of PD153035 and labelled with active β -catenin antibody (8E7) demonstrated weak nuclear and cytoplasmic signal over the time course of the experiment, with very little nuclear labelling visible by 72 hours (Figure 5-6). Quantification estimated there to be a 43.6% reduction in signal intensity between the 24 and 72 hour culture (Figure 5-7). Cytoplasmic active β -catenin labelling was also seen to reduce over the 72 hour time course (37.4% reduction; Figure 5-7).

Densitometry analysis of western blots from parallel cultures showed no significant change in expression of active β -catenin over the course of the experiment (Figure 5-8B/C). Expression of P-ERK was also low confirming the efficacy of the EGFR tyrosine kinase inhibitor (Figure 5-8D/E). Expression of inactive-GSK3 β (phosphorylated on serine 9) was low throughout the 72-hour time course suggestive of an active destruction complex.

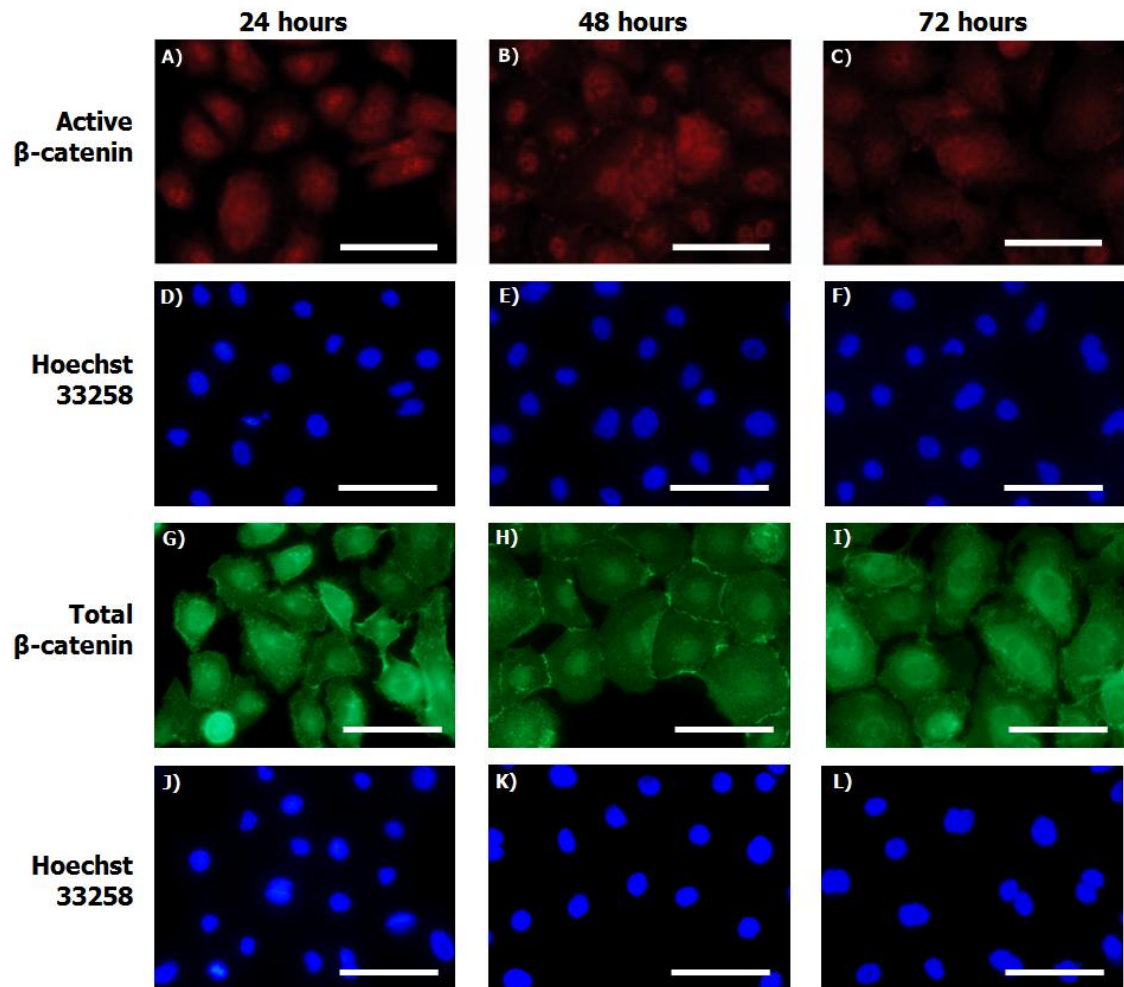


Figure 5-6 Expression and localisation of active β -catenin in NHU cells after EGFR tyrosine kinase inhibition

NHU cells (Y919) at P4 were cultured for 24 hours, 48 hours and 72 hours in KSFMc + 1 μ M PD153035. Slides were fixed and immunolabelled with active β -catenin antibody (8E7) and rabbit anti-mouse IgG-Alexa 594 secondary antibody or total β -catenin (C2206) and goat anti-rabbit IgG Alexa 488 secondary antibody. All slides were stained with Hoechst 33258 to delineate the nucleus and labelling was visualised under epi-fluorescent illumination. Scale bar: 100 μ M. Micrographs are representative of two technical replicates (N=2). Note the low nuclear labelling with both the active and total β -catenin antibodies over the 72 hour time course.

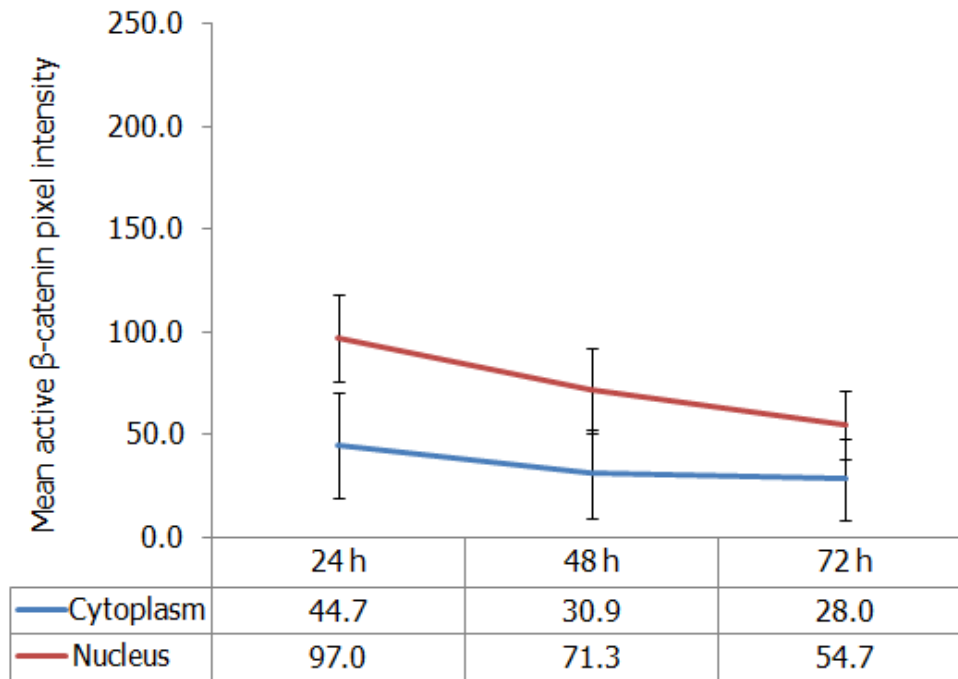


Figure 5-7 Quantification of nuclear and cytoplasmic active β -catenin in NHU cells when cultured with EGFR tyrosine kinase inhibitor

Line graph represents nuclear and cytoplasmic active β -catenin pixel intensities and standard deviations as quantified from each micrograph (fig 5-.6 A-C) using Adobe Photoshop® software.

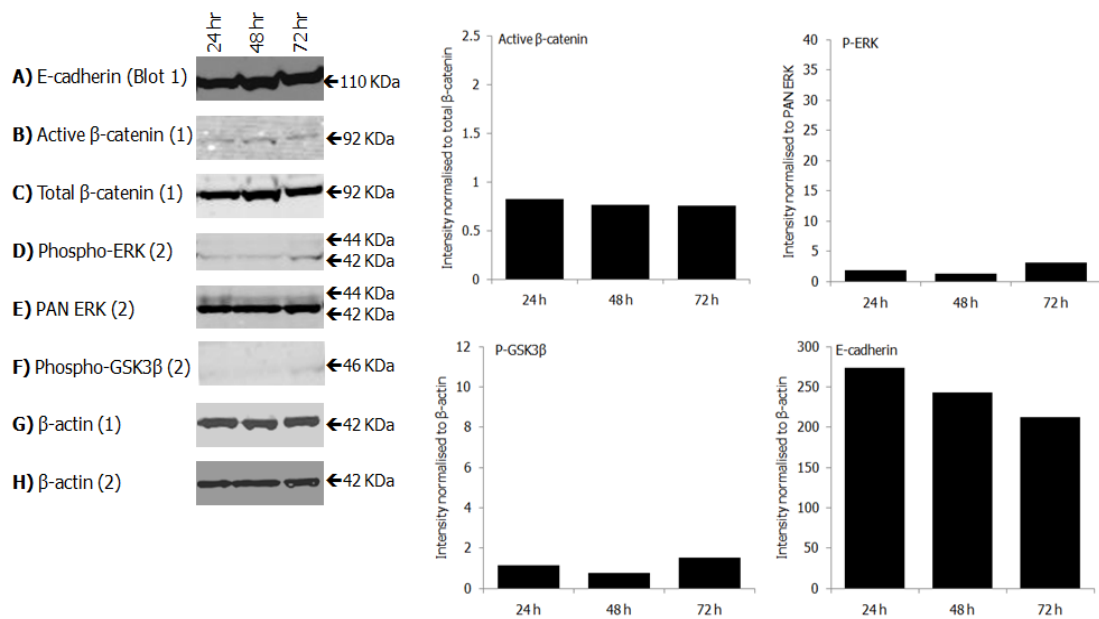


Figure 5-8 Effect of EGFR tyrosine kinase inhibition on expression of Wnt signalling components

NHU cells (Y919) at P4 were cultured for 24 hours, 48 hours and 72 hours in KSFMc + 1 μ M PD153035 prior to lysis in 2X SDS-lysis buffer. 20 μ g of each protein lysate was subjected to SDS-PAGE within a 4-12% (w/v) Bis-Tris gel under denaturing conditions and immunoblotted onto PVDF membrane. The PVDF membranes were blocked and probed with antibodies raised against E-cadherin (A), active β -catenin (B), total β -catenin (C), phospho-ERK (D), total ERK (E), phospho-GSK3 β (serine 9) (F) and β -actin antibodies to control for equal lysate loading (G, H). Membranes were incubated for 1 hour with either goat anti-mouse IgG Alexa 680 or goat anti-rabbit IgG Alexa 800 depending on the antigen and primary antibody used. Antibody binding was visualised by scanning at 700 and 800nm. Densitometry results were represented graphically relative to the appropriate loading control. N=1. Note the low expression of active β -catenin, phospho-ERK and phospho-GSK3 β in comparison to fig 5-5. Whole blots for each antibody can be found in appendix IX.

Inhibition of MEK1/MEK2 with U0126 resulted in a reduced nuclear active β -catenin expression compared to the solvent balanced control culture at both the 24 hour and 48 hour time points (Figure 5-2 vs. Figure 5-9). Signal intensity for both nuclear and cytoplasmic active β -catenin was reduced, but was not as striking as with PD153035 treatment (Figure 5-6). Western blot using an antibody targeted to P-ERK (p42/44) verified the efficacy of the MEK1/MEK2 inhibitor (Figure 5-10). Densitometry revealed no change in the relative expression of active β -catenin over the time course of the experiment (Figure 5-10). Expression of P-GSK3 β was low over the entire course of the experiment (Figure 5-10).

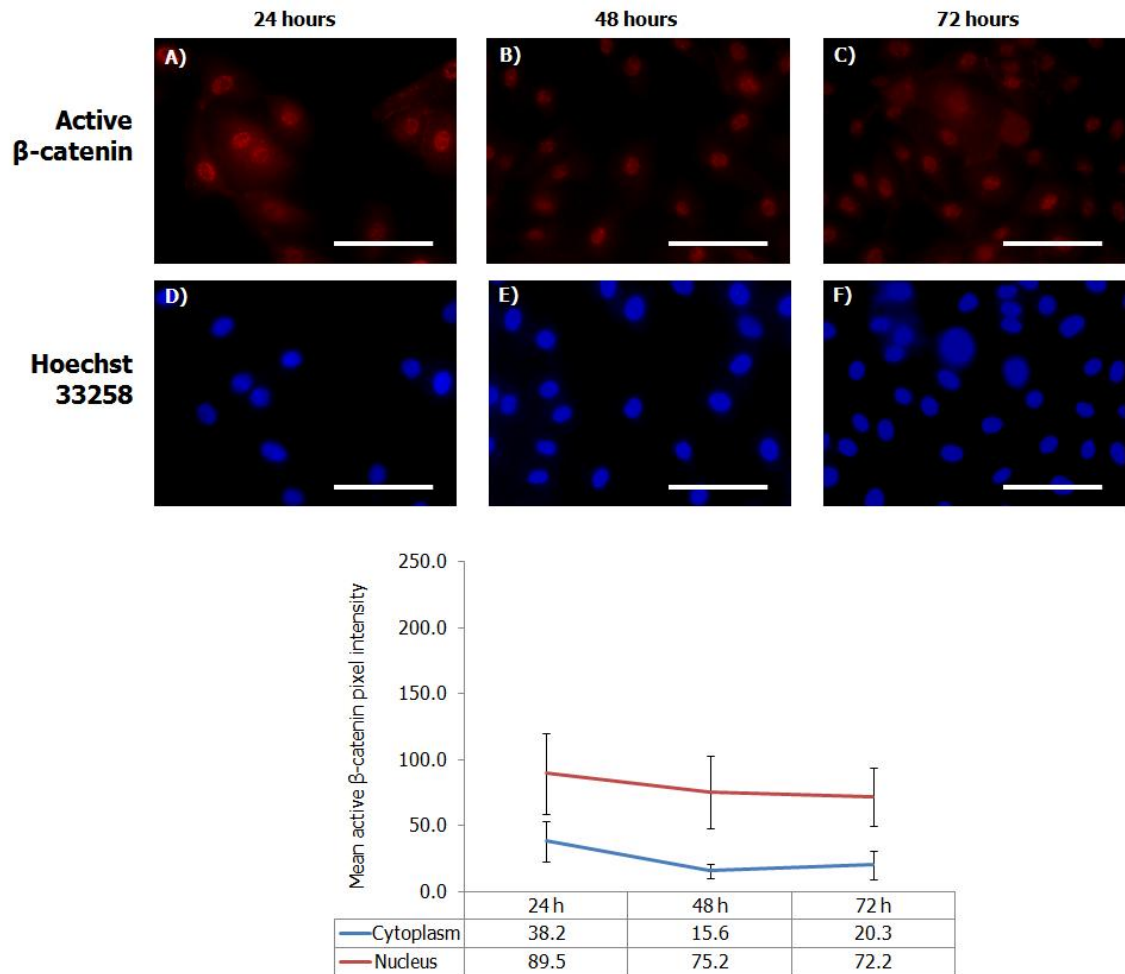


Figure 5-9 Expression and sub-cellular location of active β -catenin after MEK1/MEK2 inhibition

NHU cells (Y919) at P4 were cultured for 24 hours, 48 hours and 72 hours in KSFMc + 5 μ M U0126. Slides were fixed and immunolabelled with active β -catenin antibody (clone ABC; 8E7) and rabbit anti-mouse IgG-Alexa 594 and stained with Hoechst 33258. Antibody binding was visualised under epi-fluorescent illumination. Scale bar: 100 μ M. Micrographs are representative of duplicate experiments (N=2). Line graph represents nuclear and cytoplasmic active β -catenin pixel intensities and standard deviations as quantified from each micrograph using Adobe Photoshop[®] software. Note the low expression of active β -catenin over the course of the experiment.

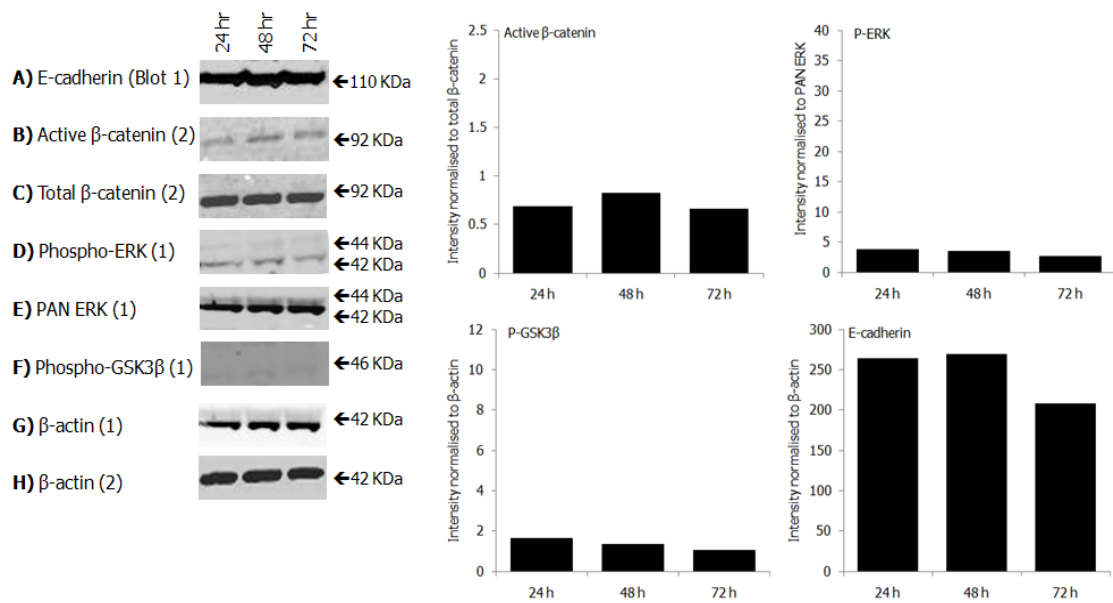


Figure 5-10 Effect of MEK1/MEK2 inhibition on components of the Wnt signalling pathway

NHU cells (Y919) at P4 were cultured for 24 hours, 48 hours and 72 hours in KSFMc + 5 μ M U0126 prior to lysis in 2X SDS-lysis buffer. 20 μ g of each protein lysate was subjected to SDS-PAGE within a 4-12% (w/v) Bis-Tris gel under denaturing conditions and immunoblotted onto PVDF membrane. The PVDF membranes were blocked and then probed for 16-hours with antibodies raised against E-cadherin (A), active β -catenin (B), total β -catenin (C), phospho-ERK (D), total ERK (E), phospho-GSK3 β (serine 9) (F) and anti β -actin antibodies to control for equal lysate loading (G, H). Membranes were incubated for 1-hour with either goat anti-mouse IgG Alexa 680 or goat anti-rabbit IgG Alexa 800 depending on the antigen and primary antibody used. Antibody binding was then visualised by scanning at 700 and 800nm. Densitometry results were represented graphically relative to the appropriate loading control. N=1. Active β -catenin expression as well as phospho-GSK3 β and phospho-ERK remained low over the 72 hour time course. Whole blots for each antibody can be found in appendix IX.

NHU cell cultures treated with 5 μ M LY294002 and labelled with active β -catenin antibody (8E7) showed strong nuclear labelling which peaked at 48 hours post-seeding (Figure 5-11). This coincided with a reduction in the intensity of cytoplasmic labelling at the same time point (Figure 5-11). Interestingly, some cells had membrane localised labelling, which was not evident in the solvent balanced control cultures (Figure 5-11 white arrow heads vs. Figure 5-2). At 72 hours post-seeding, nuclear labelling for active β -catenin was variable with some cells showing intense nuclear labelling and others with very little (Figure 5-11). The efficacy of the PI3K inhibitor, LY294002 was verified by western blot from parallel cultures using an anti phospho-AKT antibody (S473; D9E; Figure 5-12). Densitometry results showed an increase in relative active β -catenin expression over the course of the experiment with the highest expression observed at 72 hours post-seeding (Figure 5-12). P-GSK3 β labelling was intense at both the 24 hour and 48 hour time points but surprisingly had disappeared completely by 72 hours (Figure 5-12).

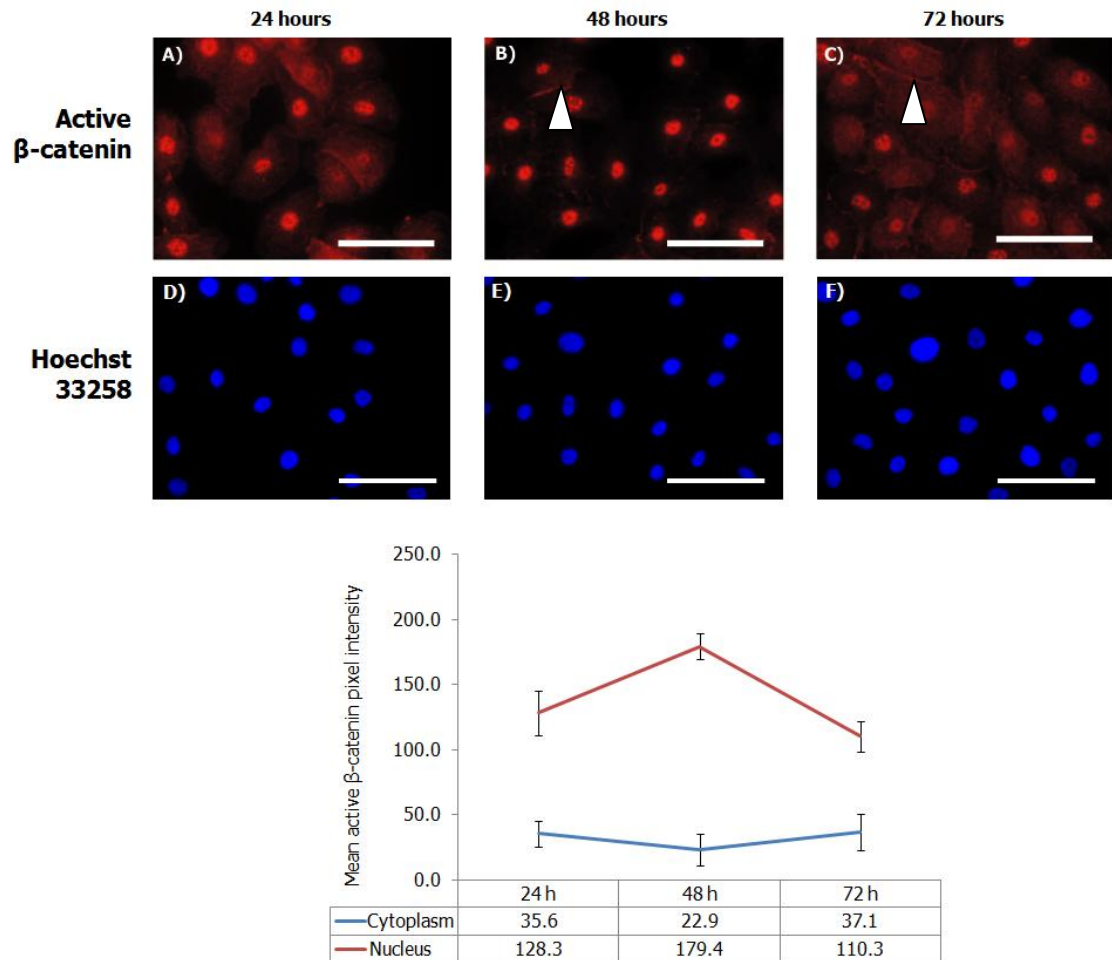


Figure 5-11 Expression and localisation of active β -catenin in NHU after treatment with LY294002

NHU cells (Y919) at P4 were cultured for 24 hours, 48 hours and 72 hours in KSFMc + $5\mu\text{M}$ LY294002. Slides were fixed and immunolabelled with active β -catenin antibody (clone ABC; 8E7) and rabbit anti-mouse IgG-Alexa 594 and stained with Hoechst 33258. Antibody binding was visualised under epi-fluorescent illumination. Scale bar: $100\mu\text{M}$. $N=1$. Arrow heads indicate membrane labelling. Line graph represents nuclear and cytoplasmic active β -catenin pixel intensities and standard deviations as quantified from each micrograph using Adobe Photoshop[®] software.

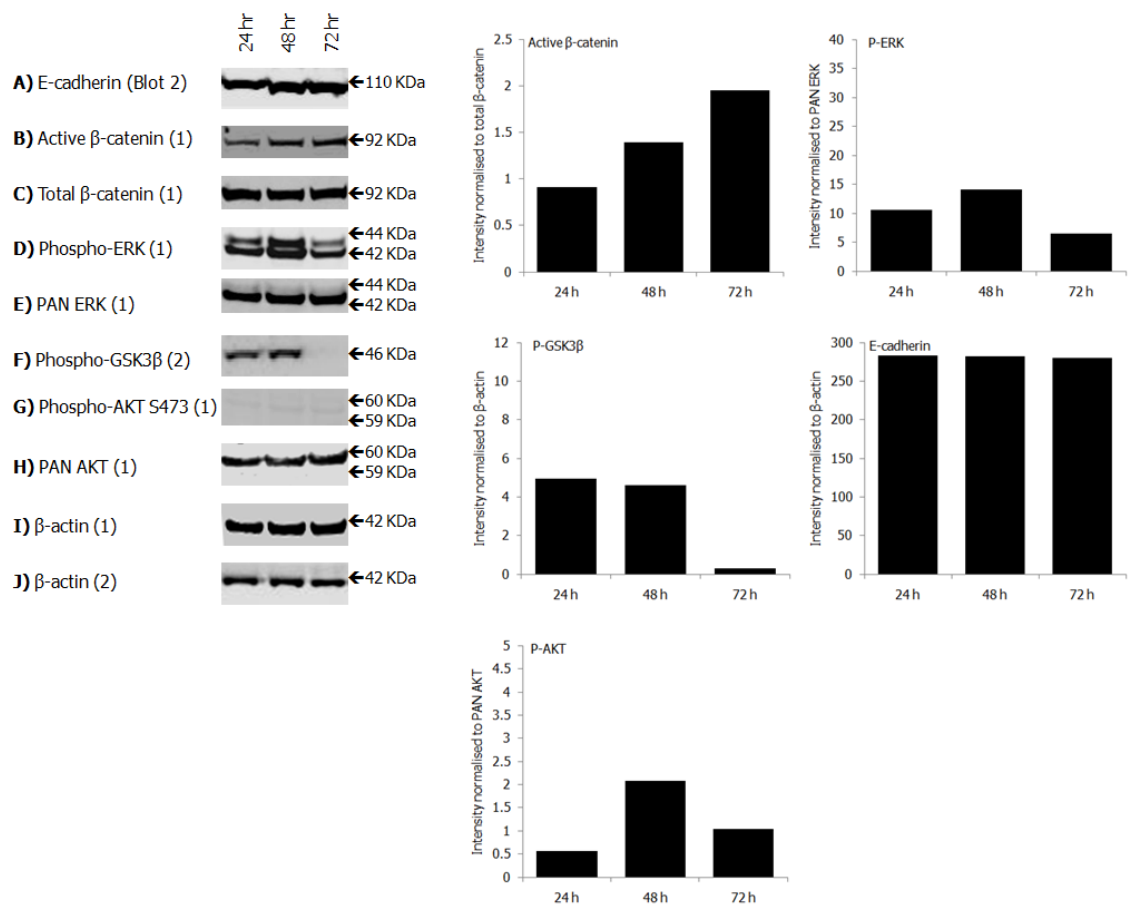


Figure 5-12 Effect of PI3K inhibition on components of the Wnt signalling pathway

NHU cells (Y919) at P4 were cultured for 24 hours, 48 hours and 72 hours in KSFMc + 5 μ M LY294002 prior to lysis in 2X SDS-lysis buffer. 20 μ g of each protein lysate was subjected to SDS-PAGE within a 4-12% (w/v) Bis-Tris gel under denaturing conditions and immunoblotted onto PVDF membrane. The PVDF membranes were blocked and then probed for 16 hours with antibodies raised against E-cadherin (A), active β -catenin (B), total β -catenin (C), phospho-ERK (D), total ERK (E), phospho-GSK3 β (serine 9) (F), phospho-AKT (S473) (G), total AKT (H) and anti β -actin antibodies to control for equal lysate loading (I, J). Membranes were incubated for 1 hour with either goat anti-mouse IgG Alexa 680 or goat anti-rabbit IgG Alexa 800 depending on the antigen and primary antibody used. Antibody binding was visualised by epi-fluorescence illumination at 700 and 800nm. N=1. Densitometry results are graphically represented relative to the appropriate loading control. Whole blots for each antibody can be found in appendix IX.

5.2.10.2 Effect of EGF signalling inhibition on β -catenin/TCF mediated transcription

Expression of three direct targets of β -catenin/TCF transcription (Axin2, c-MYC and LEF1), as well as one negatively-regulated target (CDH1) were quantified after incubation with EGFR signalling inhibitors. Expression of Axin2 was significantly down-regulated (> 2 -fold) after 24, 48 and 72 hours in culture with 1 μ M PD153035 and implies inhibition of EGFR signalling reduces TCF-mediated transcription (Figure 5-13). Treatment with U0126 also reduced the expression of Axin2 by more than 2-fold at both the 24 and 48 time point but not at the 72 hour timepoint (Figure 5-13). LY294002 did not significantly alter the transcription of Axin2 (Figure 5-13). Expression of c-MYC was significantly down regulated when NHU cells were incubated with PD153035 or U0126 at the 48 hour timepoint only. Quantification of LEF1 expression was hampered by low expression and resulted in high standard deviation. CDH1 mRNA expression was significantly higher in the PD153035-treated culture at 48 and 72 hours post-seeding when compared to the solvent balanced control at the same time point (Figure 5-13). Neither U0126, nor LY294002 treatment affected the mRNA expression of CDH1 (Figure 5-13).

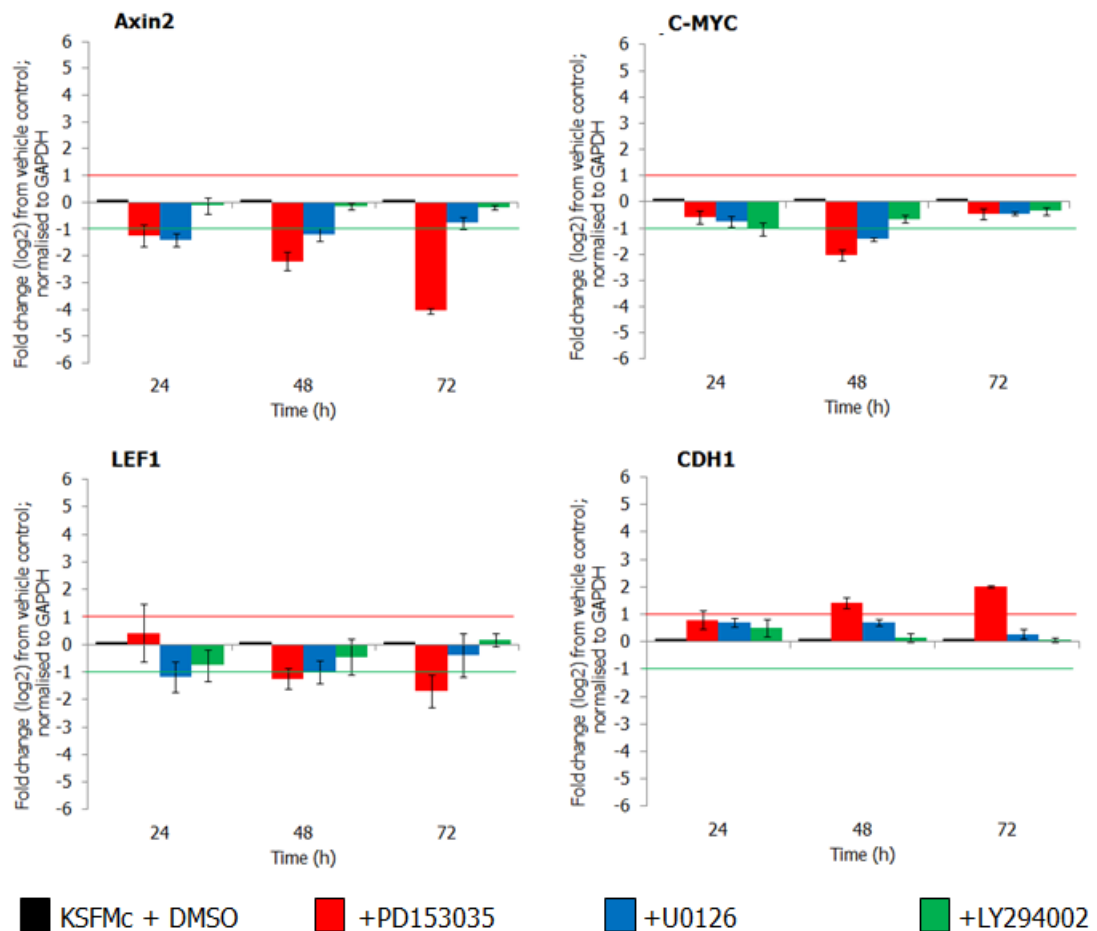


Figure 5-13 Effect of EGF signalling on β -catenin/TCF mediated transcription

NHU cells (Y919) at P4 were cultured for 24, 48 and 72 hours in KSFMc with 0.1% (v/v) DMSO, 1 μ M PD153035, 5 μ M U0126 or 5 μ M LY294002. Cells were solubilised *in situ* with Trizol[®] reagent and the total RNA content from the culture was extracted. All samples were subjected to *DNase I* digestion to remove residual gDNA prior to first-strand cDNA synthesis using 1 μ g of template mRNA and random hexamers. Quantitative RT-PCR was performed for three direct downstream β -catenin/TCF targets: Axin2, c-Myc and LEF1. The repression of E-cadherin mRNA expression was also quantified. Data was normalised to GAPDH and expressed relative to solvent balanced control. Data represents the log₂ mean expression of three-technical replicates with the corresponding standard deviation. Red and green lines represent 2-fold up/down regulation.

5.2.11 Summary

- Labelling intensity for nuclear active β -catenin was not constant over time in culture. Nuclear labelling using two different antibodies raised against active and total β -catenin both labelled much more intensely 48 hours post-seeding than at any other time point. After 72 hours in culture, nuclear labelling had reduced, indicating a possible link between β -catenin release and culture confluence/contact inhibition. Nuclear accumulation of β -catenin was not affected by the omission of exogenous rhEGF but was reduced by the addition of PD153035 to the growth medium.
- Western blot from parallel cultures revealed a correlation between active β -catenin expression, high phospho-ERK and inhibition of GSK3 β by phosphorylation at serine 9. Inhibition of the EGFR pathways with PD153035 reduced the amount of active β -catenin and also led to a reduction in phospho-GSK3 β indicating a link between the pathways downstream of EGFR and β -catenin.
- Treatment of NHU cells with MEK1/MEK2 inhibitor reduced the nuclear labelling intensity for active β -catenin but not to the extent seen with PD153035. Western blot data corroborated this reduction in active β -catenin expression after MEK1/MEK2 inhibition and indicated that the MAPK pathway may be important in the regulation of β -catenin.
- Treatment with the PI3K inhibitor, LY294002, increased the nuclear labelling intensity seen with the active β -catenin antibody (8E7). Western blot data verified this increase in active β -catenin. Phospho-GSK3 β (serine 9) expression was high with LY294002 treatment but disappeared completely by the 72 hour time-point.

- Quantitative RT-PCR revealed a significant decrease in Axin2 expression when NHU cells were cultured in the presence of PD153035 compared to solvent balanced control cultures at the same time-point and implies a reduction in TCF-mediated transcription.

5.2.12 Experimental design (Objective 2)

NHU cells were pre-treated for 24 hours in KSMc containing 0.1% (w/v) DMSO (vehicle control), 1 μ M PD153035, 5 μ M U0126 or 5 μ M LY294002 to block all, or specific parts of the EGF signalling cascade. After pretreatment, NHU cells were cultured in KSMc \pm 5-10 μ M SB415286 GSK3 β inhibitor in the continued presence of fresh EGF signalling inhibitors for up to 5 days to determine whether NHU cells respond to pharmacological inhibitors when EGFR signalling was blocked. The following experiments were undertaken to assess the effects on β -catenin sub-cellular location, TCF-mediated transcription and NHU cell growth (Figure 5-14):

- Morphology: NHU cells were visualised by phase contrast microscopy and representative photomicrographs were taken to allow comparison.
- Indirect immunofluorescence microscopy: NHU cells were formalin-fixed 24 hours after the addition of SB415286 and immunolabelled with active β -catenin antibody (ABC; clone 8E7). The nuclear signal intensity for active β -catenin was quantified from photomicrographs taken at the same exposure using Hoechst 33258 to delineate the nucleus.
- Cell viability assays: viable cell biomass was measured using MTT assays over a 5 day time course to assess proliferation rate.
- TOPFLASH dual luciferase assay: NHU cells were lysed 24 hours after treatment with SB415286. TCF activity was assessed in triplicate wells using the TOPFLASH dual luciferase reporter assay. Results were normalised to constitutively active Renilla luciferase and compared to those obtained with the negative control plasmid, FOPFLASH.

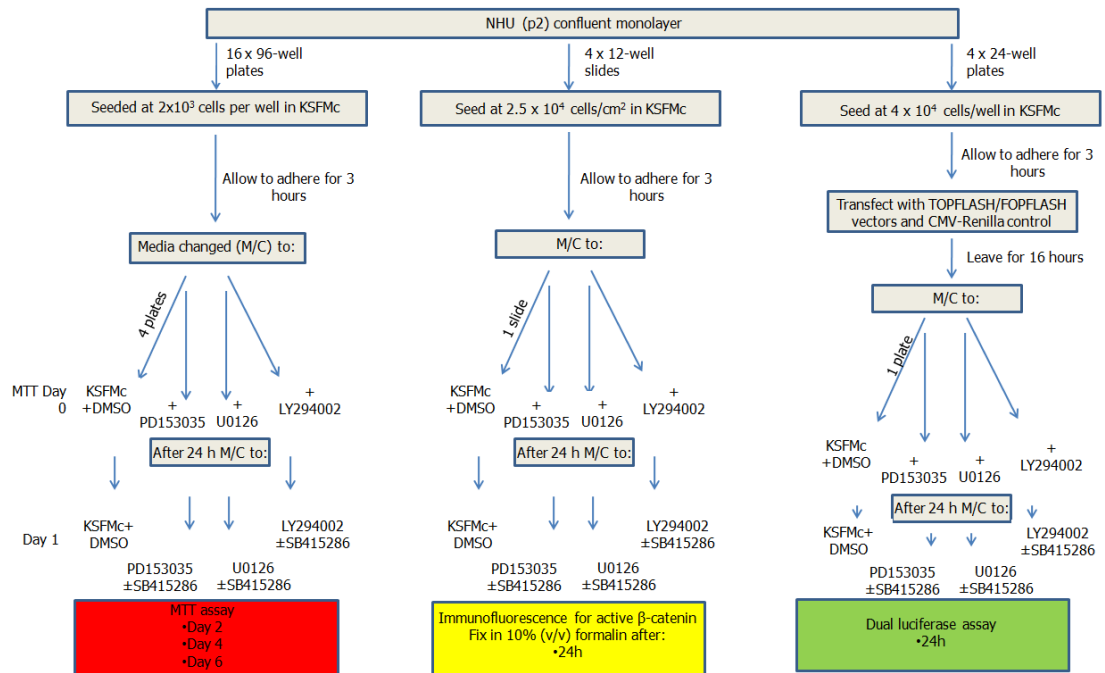


Figure 5-14 Experimental design to assess the effect of combined EGF and GSK3 inhibition on β -catenin signalling

Ureteric NHU cell line (Y924) was cultured in KSMc with 0.1% (v/v) DMSO (vehicle control), 1 μ M PD153035, 5 μ M U0126 or 5 μ M LY294002 to inhibit all or specific parts of the EGFR signalling cascade (day 0). After 24 hours, the medium and EGF signalling inhibitors were replenished and cultures were incubated with 0-10 μ M SB415286 (day 1). DMSO was kept constant at 0.1% (v/v) in all experiments and controls. To assess the effect of EGF and GSK3 inhibition on cell proliferation, MTT assays were performed on days 2, 4 and 6 with medium and inhibitors replenished on day 3. Cell morphology, TCF activation and β -catenin nuclear translocation were assessed at day 2 (24 hours post SB415286).

5.2.13 Results

5.2.13.1 The effect of combined EGFR pathway and GSK3 inhibition on NHU morphology

When cultured in normal growth medium + 0.1% (v/v) DMSO, NHU cells were small in size ($\sim 20\mu\text{m}$ in diameter) with phase-bright cell borders (Figure 5-15). Cells formed a non-stratified monolayer with typical epithelioid pavement morphology (Figure 5-15).

In the presence of $1\mu\text{M}$ PD153035, NHU cells were seen to adopt an enlarged and flatter appearance (Figure 5-15; white arrow). Cell borders were not phase-bright. $10\mu\text{M}$ SB415286 in combination with PD153035 had little effect on cell morphology compared to PD153035 alone (Figure 5-15). Both cultures appeared to be quiescent, with no mitotic figures apparent.

When applied alone, $5\mu\text{M}$ U0126 reduced the culture density and individual cell size compared to solvent balanced control (Figure 5-15). A proportion of highly elongated cells were evident throughout the culture (Figure 5-15 black arrows). Co-treatment with $10\mu\text{M}$ SB415286 and $5\mu\text{M}$ U0126 reduced the cell density further, while cell morphology remained the same (Figure 5-15).

Treatment with $5\mu\text{M}$ LY294002 had little effect on cell morphology or culture density when compared to solvent balanced control (Figure 5-15). Co-treatment with SB415286 and LY294002 had no visible effect on cell morphology compared to LY294002 alone (Figure 5-15).

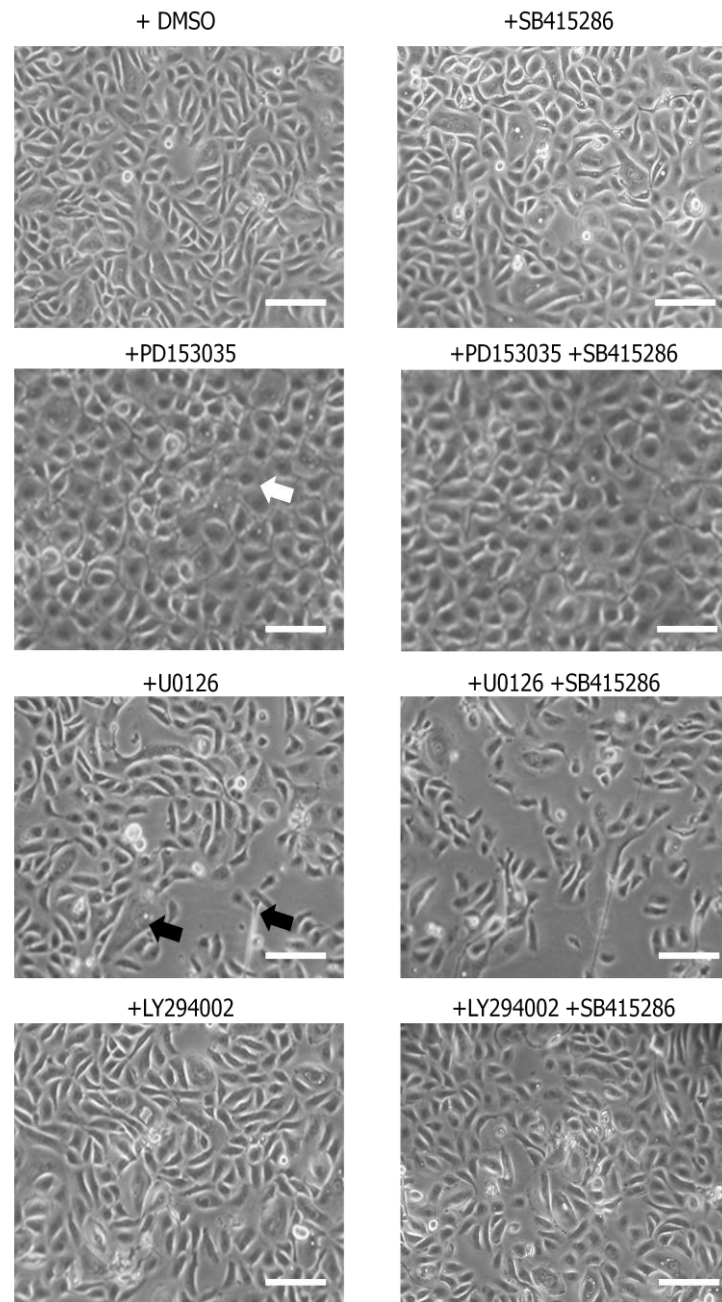


Figure 5-15 Effect of combined EGFR and GSK3 inhibition on morphology

Phase contrast micrographs of Y924 (P3) NHU cells after a 24-hour incubation with EGFR signalling inhibitors and a further 24 hour incubation with EGFR inhibitors $\pm 10 \mu\text{M}$ SB415286. White arrow denotes flat and enlarged cells. Black arrows highlight elongated cells. Scale bar: 100 μm .

5.2.13.2 The effect of combined EGFR pathway and GSK3 inhibition on active β -catenin expression and localisation

Nuclear labelling intensity for active β -catenin was dramatically reduced in the PD153035-treated culture compared to vehicle control (Figure 5-16). Co-treatment with SB415286 and PD153035 resulted in a more intense and punctate/granular nuclear labelling than with PD153035 alone and was possible the result of aggregate formation. Hoechst 33258 staining revealed nuclei to also be enlarged (Figure 5-16). NHU cells co-treated with PD153035 and SB415286 also showed cytoskeletal distribution of β -catenin (Figure 5-16; white arrow). A comparison of the mean nuclear pixel intensities obtained from PD153035-treated cells (110.8 ± 11.7 SD) and PD153035 plus SB415286 treated cells (143 ± 25.0 SD) revealed a statistically significant difference between the two cultures ($P < 0.01$; Figure 5-17).

With U0126 treatment alone, active β -catenin expression was seen to be more diffuse with both nuclear and cytoplasmic labelling visible. Nuclear labelling appeared less intense than in the vehicle control. In a large proportion of cells, active β -catenin labelling was also evident at the cell membrane (Figure 5-16; grey arrow). No profound change in the expression or localisation of active β -catenin was noticeable when U0126 pre-treated NHU cells were cultured in medium containing both U0126 and SB415286 (Figure 5-16).

Treatment with LY294002 did not affect the expression or localisation of active β -catenin. No difference was observed in expression or localisation of β -catenin when cells were co-treated with SB415286 and LY294002 (Figure 5-16).

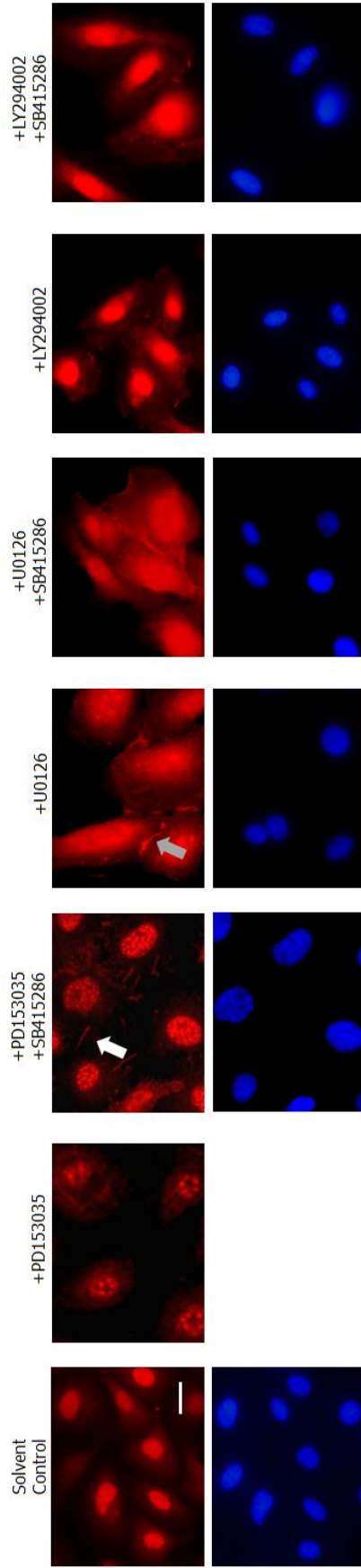


Figure 5-16 The effect of combined GSK3 and EGFR pathway inhibition on active β -catenin localisation

NHU cells (Y924) at P3 were cultured for 24 hours in KSMc supplemented with EGF signalling inhibitors or 0.1% (v/v) DMSO (solvent control). Medium with respective inhibitors was replenished and the effect of GSK3 β inhibition on β -catenin expression and localisation was tested by supplementing the growth medium with 0-10 μ M SB515286 for a further 24 hours. Slides were formalin-fixed and immunolabelled with active β -catenin (8E7) and rabbit anti-mouse IgG-Alexa 594 secondary antibody. All slides were then stained with Hoechst 33258 to delineate the nucleus and labelling was visualised under epi-fluorescent illumination. White arrow denoted unusual labelling in PD153035 and SB415286 treated cells. Grey arrow indicates membrane labelling. Scale bar: 20 μ M. N=1. Note granular labelling and nuclear size difference between solvent control and cells treated with PD153035 + SB415286.

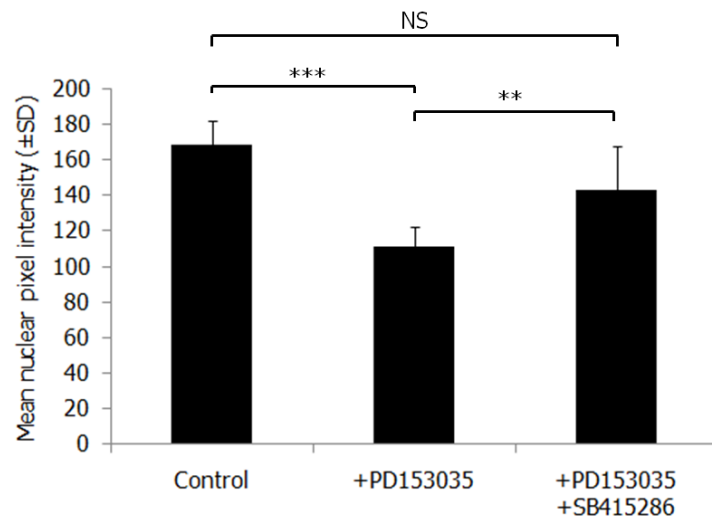


Figure 5-17 Quantification of nuclear active β -catenin in NHU cells treated with combined EGFR signalling and GSK3 inhibitors

Bar chart represents nuclear active β -catenin as assessed from the pixel intensities of each micrograph in fig 5-16 using Adobe Photoshop® software. Error bars represent standard deviations obtained from 20 randomly picked cells selected from the Hoechst 33258 image. (** $p < 0.001$, ** $p < 0.01$, NS not significant, Tukey-Kramer multiple comparisons test).

5.2.13.3 Cell viability assays

PD153035-treated cultures were severely growth retarded when compared to vehicle control cultures at the same timepoint (Figure 5-18A). Cultures treated with 1 μ M PD153035 and 5 μ M SB415286 showed no statistically significant difference in growth rate compared to cultures treated with PD153035 alone. On the other hand, cultures co-treated with 7.5-10 μ M SB41528 and PD153035 had a statistically significant higher proliferation rate when compared to PD153035 alone (Figure 5-18B; $P < 0.05$). This indicated that treatment with SB415286 was able to alleviate the proliferative block seen with PD153035 alone and implied that β -catenin was able to drive NHU cell proliferation alone.

NHU cells incubated with U0126 also had a reduced proliferation rate compared to control cultures at the same timepoint (Figure 5-19A). However, addition of 5-10 μ M SB415286 did not significantly alter the proliferation rate of U0126 treated cells (Figure 5-19B).

Cultures incubated in 5 μ M LY294002 had a reduced growth rate compared to control cultures, but not to the extent observed with 1 μ M PD153035 or 5 μ M U0126 (Figure 5-20A). Addition of 5-10 μ M SB415286 had no effect on the growth rate of LY294002 treated NHU cells (Figure 5-20B).

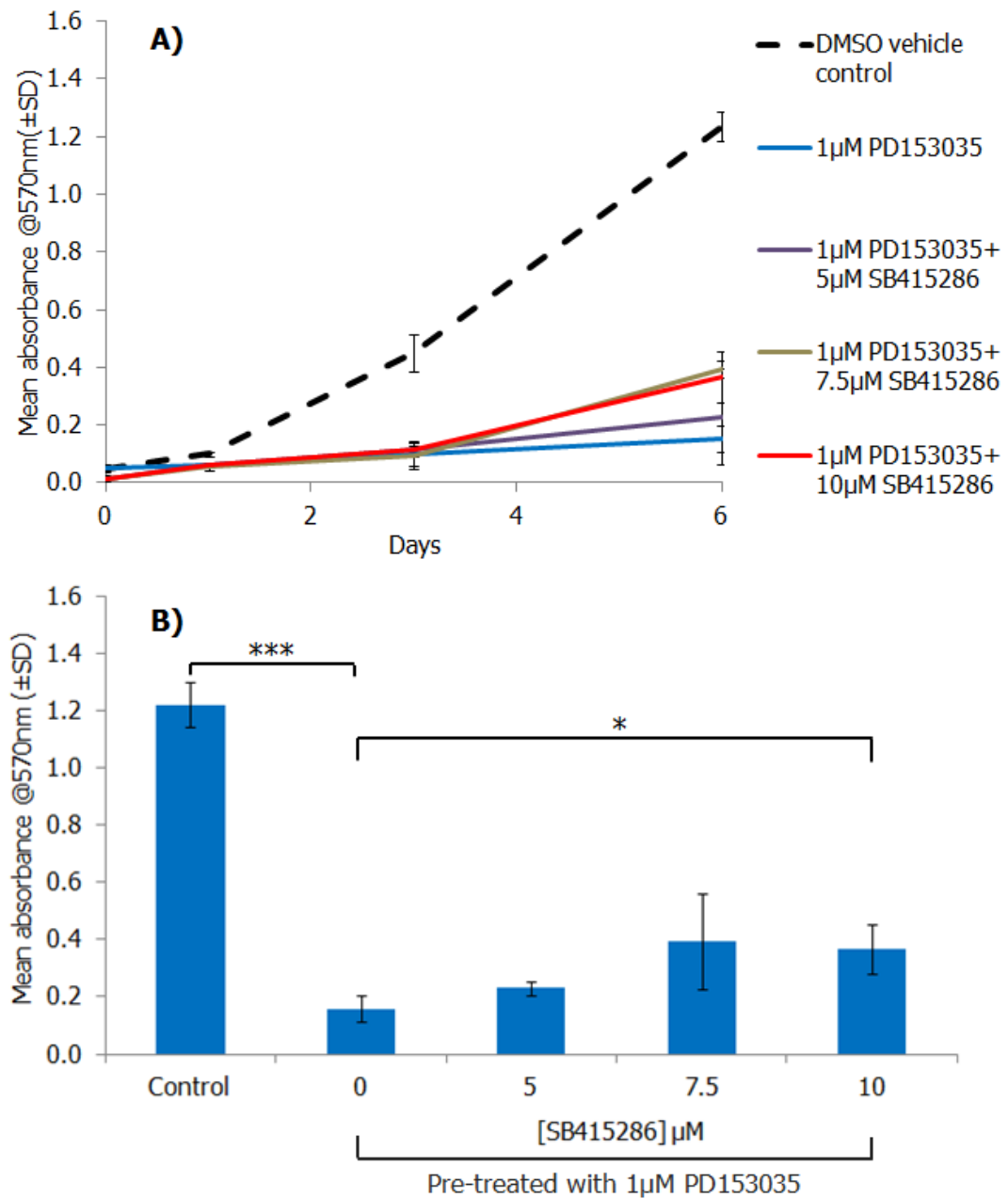


Figure 5-18 Effect of combined EGFR and GSK3 inhibition on NHU cell viability

MTT assays were performed on NHU cells (Y911) at P3 on days 0, 1, 3 and 6. On day 0, cells were cultured in KSMc ± 1μM PD153035. On day one, PD153035 was replenished and the medium was supplemented with 0-10μM SB415286 where indicated. **A)** Data shows the mean absorbance at 570nm (±SD) of 3 technical replicates. **B)** Bar graph and statistical analysis from day 6 only. Each data point is the average of 3 technical replicates ± SD. (***) $p < 0.001$, * $p < 0.05$, one way ANOVA with multiple comparisons post-test).

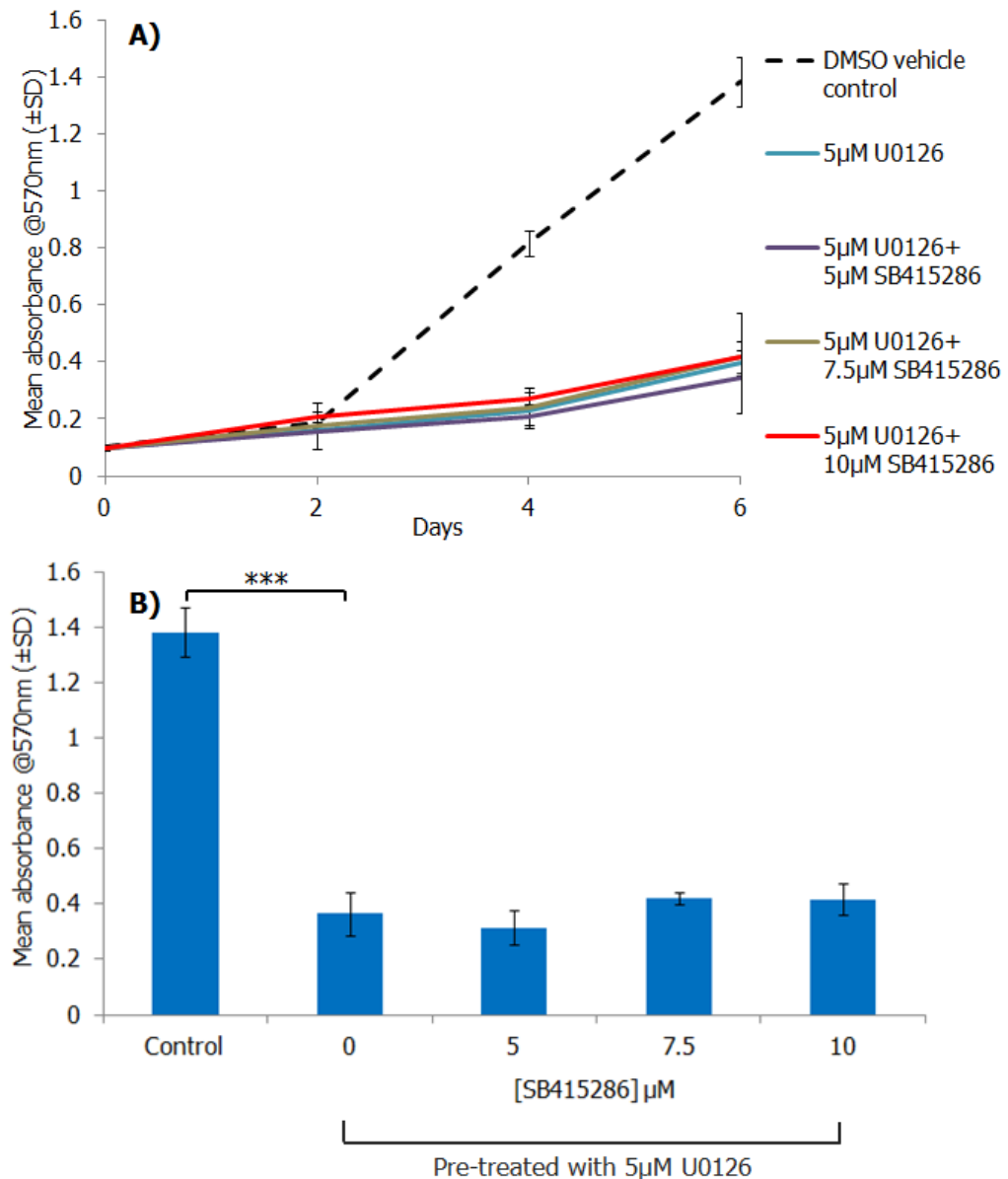


Figure 5-19 Effect of combined MEK1/MEK2 and GSK3 inhibition on NHU cell viability

MTT assays were performed on NHU cells (Y911) at P3 on days 0, 2, 4 and 6. On day 0, cells were cultured in KSMc \pm 5 μ M U0126. On day one, U0126 was replenished and the medium was supplemented with 0-10 μ M SB415286 where indicated. **A)** Data shows the mean absorbance at 570nm (\pm SD) of 3 technical replicates. **B)** Bar graph and statistical analysis from day 6 only. Each data point is the average of 3 technical replicates \pm SD. (***) $p < 0.001$, * $p < 0.05$, one way ANOVA with multiple comparisons post-test).

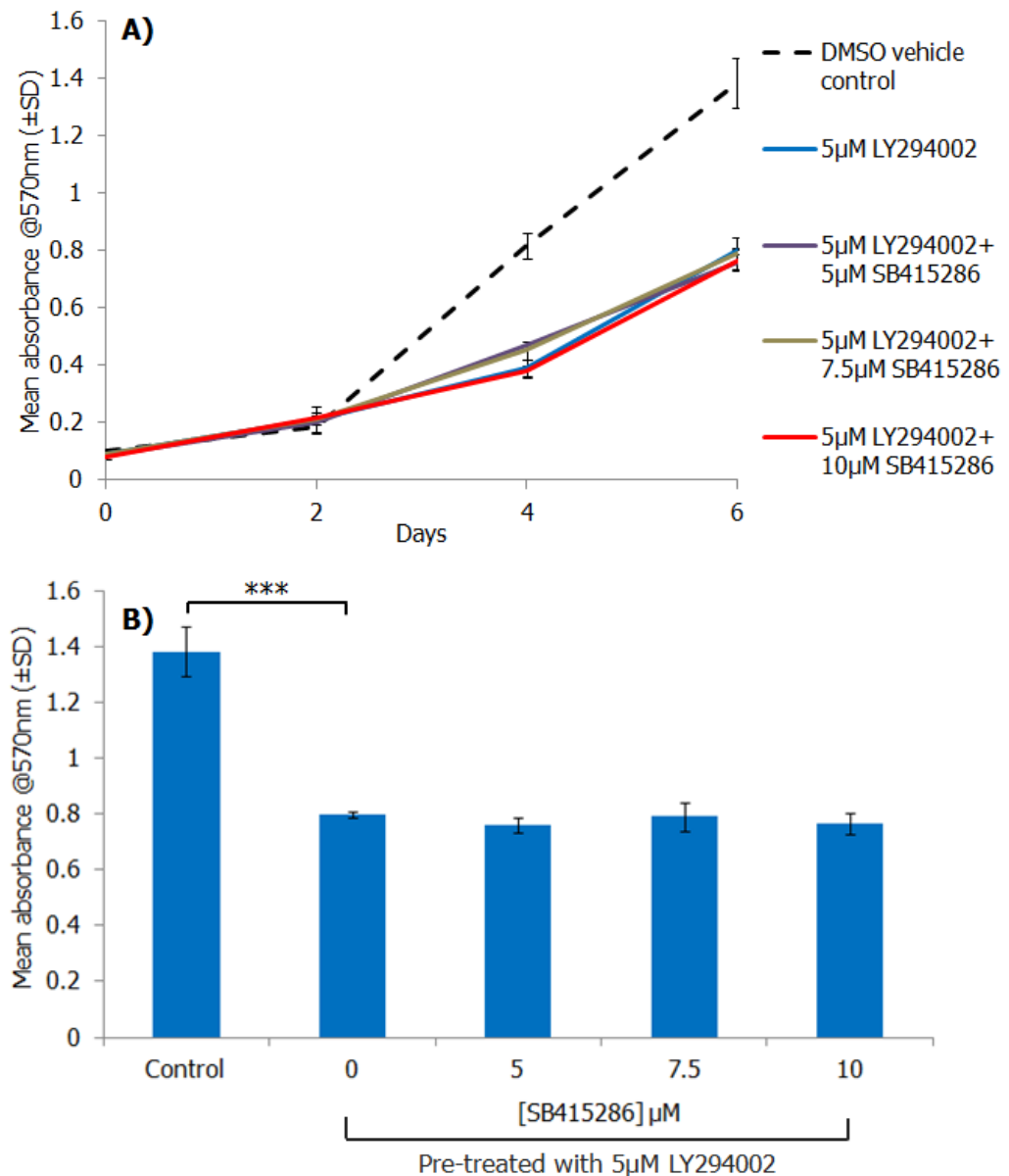


Figure 5-20 Effect of combined PI3K and GSK3 inhibition on NHU cell viability

MTT assays were performed on NHU cells (Y911) at P3 on days 0, 2, 4 and 6. On day 0, cells were cultured in KSFMc \pm 5 μ M LY294002. On day one, LY294002 was replenished and the medium was supplemented with 0-10 μ M SB415286 where indicated. **A)** Data shows the mean absorbance at 570nm (\pm SD) of 3 technical replicates. **B)** Bar graph and statistical analysis from day 6 only. Each data point is the average of 3 technical replicates \pm SD. (***) $p < 0.001$, one way ANOVA with multiple comparisons post-test).

5.2.13.4 Assessing the effect of EGFR signalling and GSK3 inhibition on TCF activity

NHU cell cultures treated for 24 hours with 0-10 μ M SB415286 did not show any change in TCF activity (Figure 5-21). Normalised luciferase activity (Firefly/Renilla) in the TOPFLASH assay was in fact less than in the negative FOPFLASH control assay (Figure 5-21A). Treatment with 1 μ M PD153035 reduced the luciferase activity in both the TOPFLASH and FOPFLASH assay, indicating a possible reduction in the activity of the TK minimal promoter (Figure 5-21B). When 10 μ M SB415286 was added to PD153035 pre-treated cultures, TOPFLASH normalised luciferase activity significantly increased, but FOPFLASH activity did not, indicate any increase in TCF mediated transcription ($P < 0.01$; Figure 5-21B).

Addition of 7.5-10 μ M SB415286 to NHU cultures pretreated for 24 hours with 5 μ M U0126 slightly elevated the mean TOPFLASH luciferase activity above that obtained with the FOPFLASH negative control but this was not statistically significant (Figure 5-21C).

Pre-treatment of NHU cultures for 24 hours with 1 μ M LY294002 prior to the addition of 7.5-10 μ M SB415286 had no effect on TCF activity (Figure 5-21D).

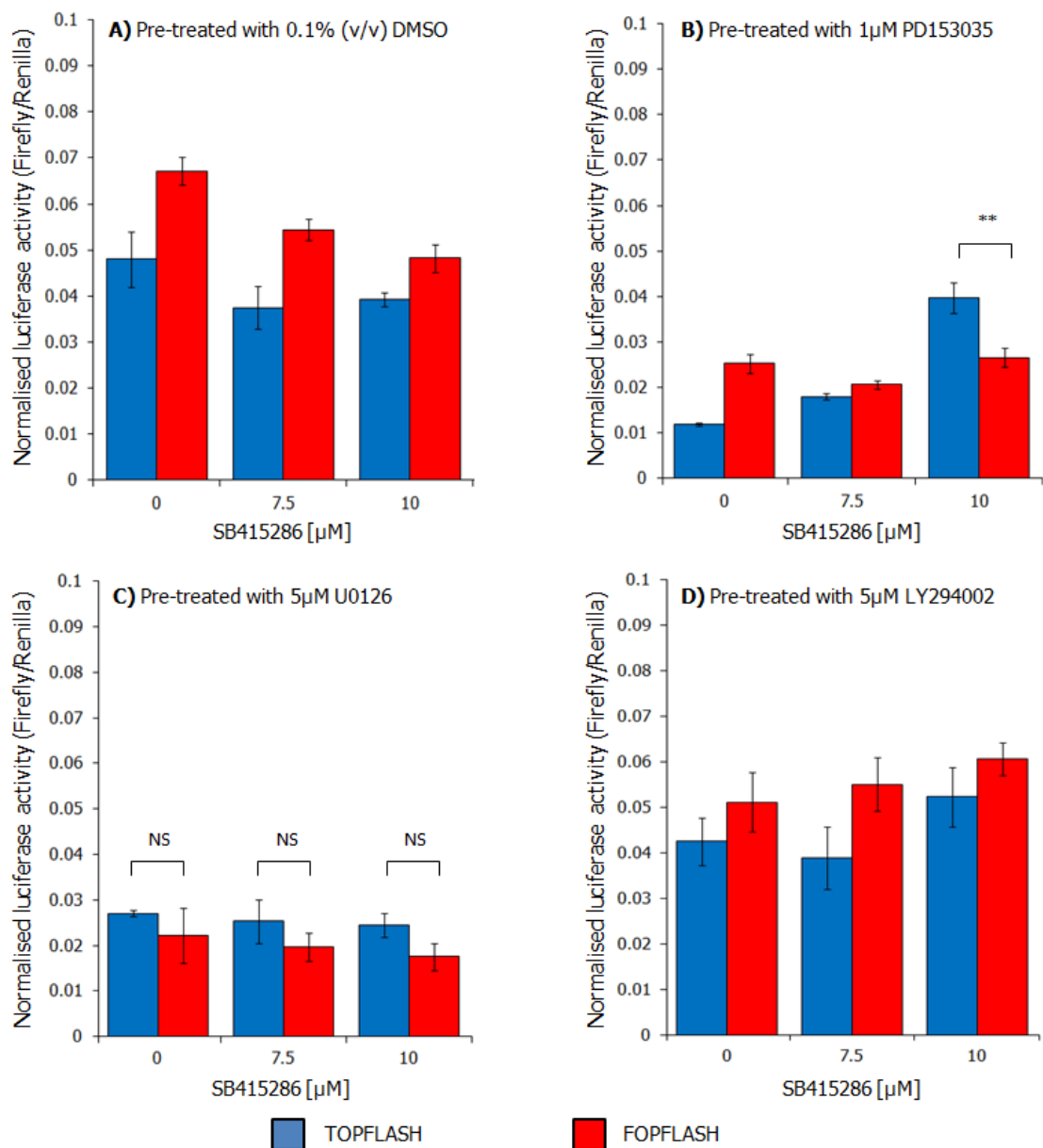


Figure 5-21 TCF transcription factor activity after co-treatment with EGFR signalling and GSK3 inhibitors

NHU cells (Y924) were seeded into a 24-well Primaria[®] plate at 4×10^4 cells/well and transfected with either 5 μ g of TOPFLASH or FOPFLASH plasmid along with 0.01 μ g of pRL-CMV (loading control). 16 hours after transfection, NHU cells were pre-treated with 0.1% (v/v) DMSO (**A**), 1 μ M PD153035 (**B**), 5 μ M U0126 (**C**) or 5 μ M LY294002 (**D**) in KSMc for 24 hours and then incubated for a further 24 hours with 0-10 μ M SB415286 in the continued presence of EGFR signalling inhibitors. A dual luciferase assay was performed on 3 technical replicates and data represents the mean luciferase activity after normalisation to loading control \pm SD. (** $p < 0.01$, NS not significant, one-way ANOVA with Bonferroni multiple comparisons post test).

5.2.14 Summary

- Addition of 1 μ M PD153035 to the culture medium of NHU cells significantly reduced the nuclear labelling intensity of active β -catenin indicating active β -catenin is regulated by signalling downstream of EGFR. This reduction in nuclear active β -catenin could be partially restored by the addition of 10 μ M SB415286 .
- Incubation with either EGFR (1 μ M PD153035) or MAPK inhibitor (5 μ M U0126) severely retarded the proliferation rate of NHU cells. Addition of 10 μ M SB415286 to PD153035 treated cells increased the viable cell biomass of the culture indicative of an increase in cell proliferation and suggests active β -catenin can drive proliferation in NHU cells. SB415286 had no effect on the proliferation rates of NHU cells treated with MEK1/MEK2 or PI3K inhibitors.
- Incubation with 10 μ M SB415286 led to an increase in TCF transcription factor activity but only when all downstream signalling via the EGFR was blocked.

5.3 The role of cell:cell contacts in modulating β -catenin activity

5.3.1 Cell:cell interactions

Intercellular or cell:cell junctions are classified into three main types: the tight junction, which has an important role in barrier function, the communication or gap junction and the anchoring junctions, which are composed of adherens junctions and desmosomes (Figure 5-22).

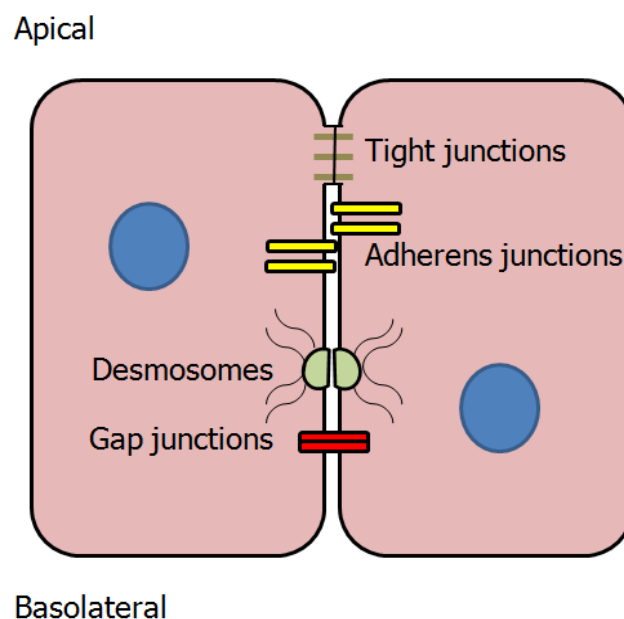


Figure 5-22 Cell:cell junctions

Schematic illustrating the four types of cell:cell junctions found between epithelial cells: tight junctions, adherens junctions, desmosomes and gap junctions.

5.3.1.1 Tight junctions

Tight junctions (TJ) can be found between the lateral membranes of two adjacent cells and limit para-cellular diffusion of water and solutes by bringing together the cell membranes of adjacent cells and sealing the paracellular space (reviewed by (20)). TJ are multi-protein junctions composed of up to 40 different proteins that show tissue-specific distributions. Three main groups of proteins are recognised:

- Integral TJ proteins that bridge the intercellular space and include the occludins (178), claudins (179) and junctional adherens molecule (JAM-1)(180).
- Adaptor proteins which cluster and anchor the integral TJ proteins to the cytoskeleton and include zonular occludens (ZO-1, -2, -3), member of the membrane-associated guanylate kinases (MAGUK), which bind to claudins via their PDZ domain (181).
- A miscellaneous group which are composed of cytosolic proteins. Tight junctional complexes not only regulate polarity and barrier function but have been shown to be involved in cell proliferation and tumour suppression by recruiting such molecules as pTEN (182) and transcription factors such as cold shock domain protein A (CSDA alias Zonab (183)).

5.3.1.2 Communication junctions

Gap junctions are channels directly connecting the cytoplasm of two adjacent cells and allow intracellular communication via the passage of small molecules up to 1KDa in size such as K⁺ ions, Ca²⁺ ions, ATP and glucose (reviewed by (184)). Each channel is composed of two end-to-end hemi-channels which are themselves composed of a hexamer (connexon) of transmembrane proteins called connexins (Cxs). Gap junctions can be homotypic (composed of the same

connexon unit) or heterotypic (composed of 2 differing connexon units) which affects the selectivity and functional properties of the channel. In humans there are 24 connexin genes, but to date, the expression profile in human urothelium is unknown.

5.3.1.3 Anchoring junctions

In epithelia, adherens junctions (AJ) are the principal form of intercellular adhesion and are important in the organisation and stratification of the tissue. Adherens junctions form between adjacent cells via calcium-dependent, homophilic engagement of E-cadherin molecules (Figure 5-23)(69). The amino (N)-terminal extracellular domain of E-cadherin is composed of five domains (EC1-EC5), four of which bind Ca^{2+} ions and are necessary for adherens junctions to form (185-187). The intracellular cytoplasmic tail of E-cadherin complexes directly with two members of the catenin family, β -catenin and P120 and forms a stabilising bridge with α -catenin and vinculin to the actin cytoskeleton (Figure 5-23) (186, 188-190).

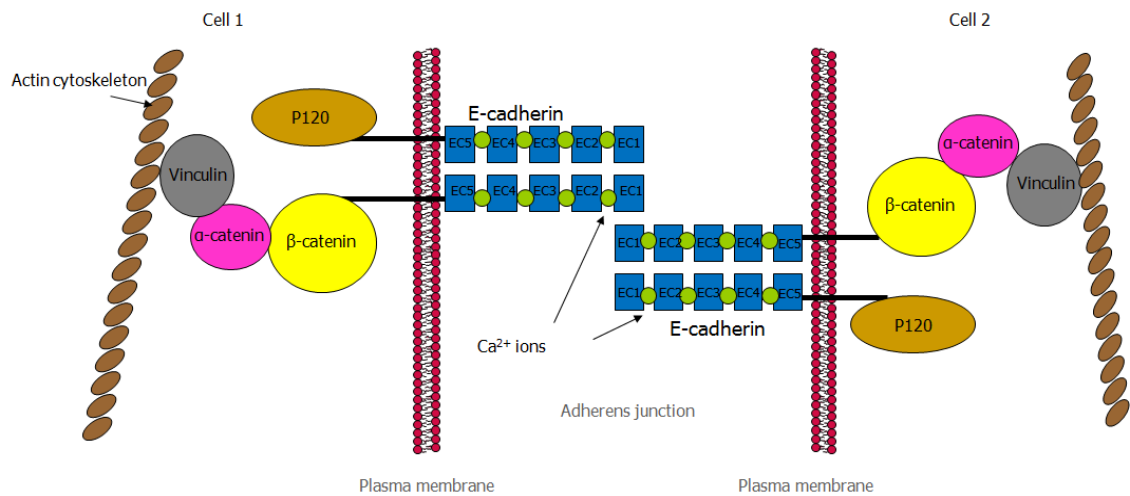


Figure 5-23 Schematic representation of an adherens junction between two adjacent cells

The adherens junction (AJ) is a calcium-dependent cell:cell adhesion junction composed of a complex of cadherins (E-cadherin) and catenins (P120, β -catenin and α -catenin) which form a bridge via vinculin to the actin cytoskeleton.

5.3.2 β -catenin sequestration at the adherens junction

When bound as an intracellular component of the adherens junction, β -catenin is spatially separated from the soluble cytoplasmic pool and is unable to translocate to the nucleus. In sub-confluent cultures, β -catenin is found to be tyrosine phosphorylated at its C-terminal domain and does not interact with the components of the adherens junction (191-193). Examples of tyrosine (tyr) phosphorylation events which disrupt the adherens junction include phosphorylation of β -catenin at tyr-654 by Src or EGFR (disrupting the cadherin/ β -catenin complex) and tyr-142 phosphorylation by Fer or Fyn (abrogating β -catenin interacting with α -catenin) (193-198). In contrast to this, confluent cultures have been shown to mainly express non-tyrosine phosphorylated, serine/threonine phosphorylated β -catenin which localises at the

membrane as an intrinsic component of the adherens junction (191-193). Tyrosine phosphatase (PTPase) which stabilise the adherens junction complex and thus increase cell:cell adhesion include, PTP1B and PTPmu (199-201).

Other mechanisms that may affect the formation of the adherens junction independently of β -catenin include: threonine phosphorylation of E-cadherin by CKII (202), E-cadherin endocytosis (108) and E-cadherin transcriptional repression by Snail (203).

In certain situations, modulation of the membrane-bound pool of β -catenin has been reported to result in increased TCF transcription activity. For example, in one study, short-term exposure of A431 human epidermoid cancer cells, A549 human small cell lung carcinoma cells and DU145 prostate cancer cells to exogenous EGF was shown to induce caveolae-mediated E-cadherin endocytosis and subsequent release of β -catenin. Most importantly, this study also showed that long-term EGF exposure increased E-cadherin repression by β -catenin/TCF-mediated expression of the transcriptional repressors, Snail and Twist, suggesting a positive feedback mechanism between the two pathways (168, 203). Other mitogen-activated pathways which have been implicated in the same positive feedback loop include: FGFR1(204) and TGF β 1 (205).

5.3.3 Rationale

Active β -catenin can be sequestered at adherens junctions resulting in a coordinated reduction in β -catenin-regulated gene expression and increased cell:cell adhesion. This sequestration of β -catenin may be antagonised by a number of growth factor signalling mechanisms which either disrupt the adherens junction or down-regulate E-cadherin expression and lead to a reduction in cell:cell contact coupled with an increase in TCF-mediated gene transcription. The literature suggests that β -catenin may be a key mediator in overseeing the close coordination of growth factor-induced proliferation with cell:cell adhesion. This chapter will explore the dynamics between adherens junctions and β -catenin/TCF-mediated gene transcription as a potential mechanism controlling NHU cell proliferation.

5.3.4 Hypothesis

Cell:cell contact and the sequestration of β -catenin at the adherens junction is an important means of curtailing β -catenin/TCF-mediated transcription and cell proliferation.

5.3.5 Aim

To ascertain whether increased cell adhesion reduces the availability of active β -catenin, in order to test the hypothesis that cell:cell contact and β -catenin signalling act cooperatively in switching urothelial cells between a proliferative and quiescent state.

5.3.6 Objectives

- To assess the effect of culture confluence on the translocation of β -catenin to the nucleus.
- To employ a calcium switch approach (sub- to near-physiological Ca^{2+} concentrations) to prohibit or permit the formation of adherens junctions

respectively, in order to assess whether their formation modulated β -catenin activity and TCF-mediated transcription.

5.3.7 Experimental design

The effect of culture confluence on active β -catenin expression and localisation was assessed in NHU cells (Y919) at P4. Cells were plated at low (1.25×10^4 cells/cm²) and high (5×10^4 cells/cm²) seeding densities and then formalin-fixed and detergent-permeabilised at 24, 48, 72 and 144 hours post-seeding. Cultures were immunolabelled for active and total β -catenin. The proportion of nuclear to cytoplasmic β -catenin was visualised by immunofluorescence photo-microscopy and quantified from photo-micrographs captured at constant exposure.

The regulation of β -catenin activity by sequestration at adherens junctions was investigated by modulating the extracellular calcium concentration. NHU cells were cultured in either low calcium conditions (0.09mM CaCl₂) which restricted the formation of adherens junctions, or with 2mM CaCl₂ for up to 72 hours. At 24 hour intervals, parallel cultures were: formalin-fixed and immunolabelled for active β -catenin, total β -catenin and E-cadherin; used to generate whole cell lysates in 2x SDS lysis buffer or; lysed in Trizol[®] reagent for subsequent extraction of mRNA. The sub-cellular location of β -catenin and E-cadherin was determined by immunofluorescence photo-microscopy and the relative expression of active and total β -catenin was assessed by western blot. Downstream targets of β -catenin signalling were quantified by SYBR[®] Green I RT-qPCR.

5.3.8 Results

5.3.8.1 The effect of cell density

Seeding NHU cells at a low density (1.25×10^4 cells/cm²) prolonged the length of time β -catenin was present in the nucleus (Figure 5-24 vs. Figure 5-2 for comparison). Strong β -catenin nuclear labelling was present for at least 72 hours when NHU cells were seeded at 1.25×10^4 cells/cm² (Figure 5-24A-C and I-K). A reduction in the nuclear β -catenin pool was seen 144 hours post seeding (Figure 5-24). Coincidentally, quantification of the cytoplasmic signal displayed the opposite effect, with weak labelling seen up to 72 hours and then a sharp increase 144 hours post-seeding (Figure 5-25).

Seeding NHU cells at a higher plating density of 5×10^4 cells/cm² did not completely ablate the nuclear translocation of active β -catenin but did reduce the labelling intensity (Figure 5-26 vs. fig Figure 5-2). Quantification of the nuclear localised active β -catenin signal was verified as being lower in the higher density culture compared to the lower density culture (111 vs. 171 arbitrary units; Figure 5-27 vs. Figure 5-25).

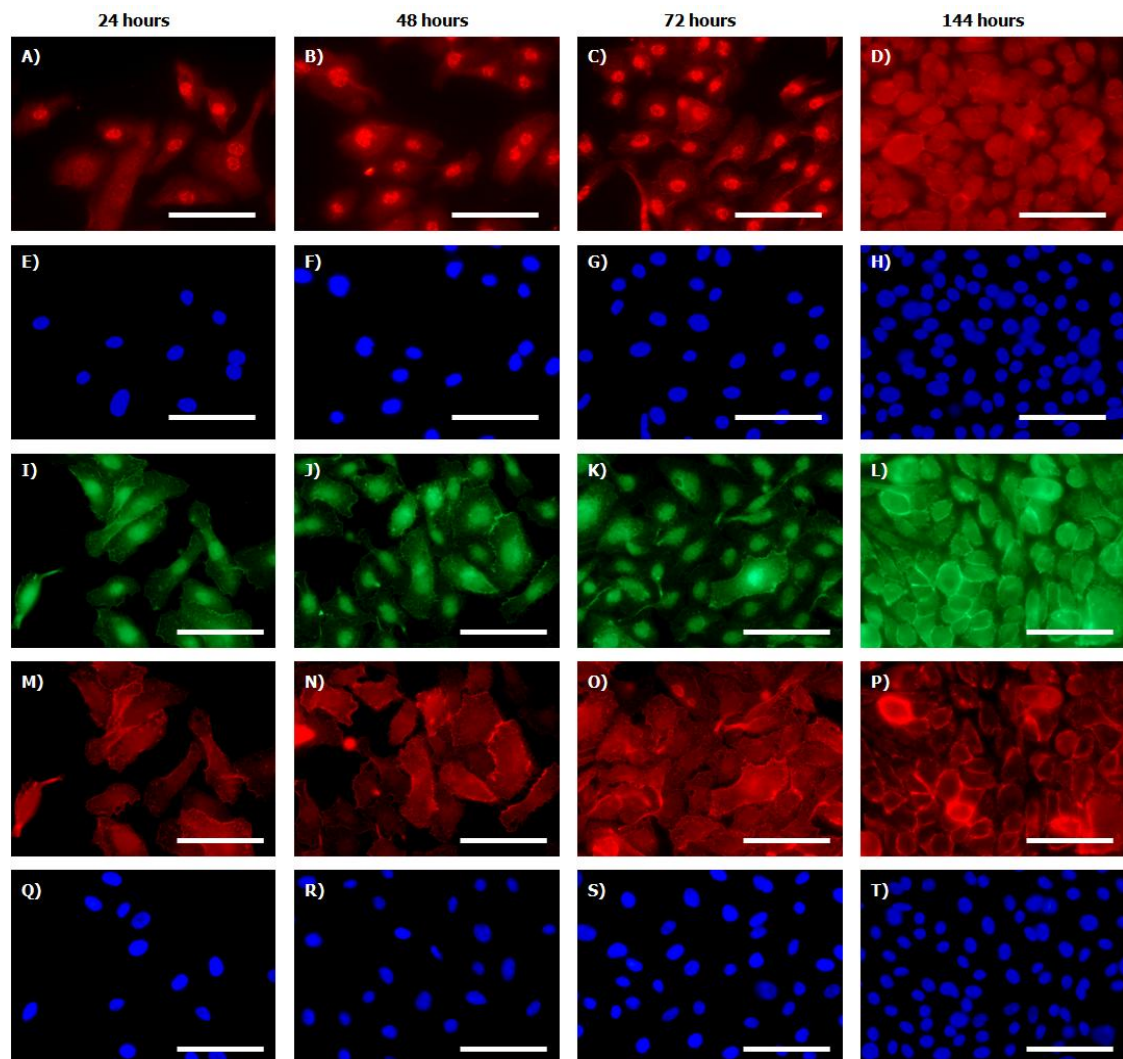


Figure 5-24 Expression and localisation of β -catenin in NHU cells over time when seeded at low plating density

NHU cells (Y919) at P4 were seeded at 1.25×10^4 cells/cm² and cultured for 24 hours, 48 hours, 72 hours and 144 hours in KFSMc. Medium was replaced every 3 days to replenish growth factors. Slides were fixed and immunolabelled with active β -catenin antibody (8E7), total β -catenin (C2206) or E-cadherin antibody (HECD1). All slides were stained with Hoechst 33258 to delineate the nucleus and labelling was visualised under epi-fluorescent illumination. Photo-micrographs are of NHU cells labelled with anti-active β -catenin (A-D), total β -catenin (I-L) and E-cadherin (M-P) with matched Hoechst 33258 staining underneath. Scale bar:100 μ M. N=1. β -catenin was present in the nucleus of NHU cells for longer when seeded at a lower plating density.

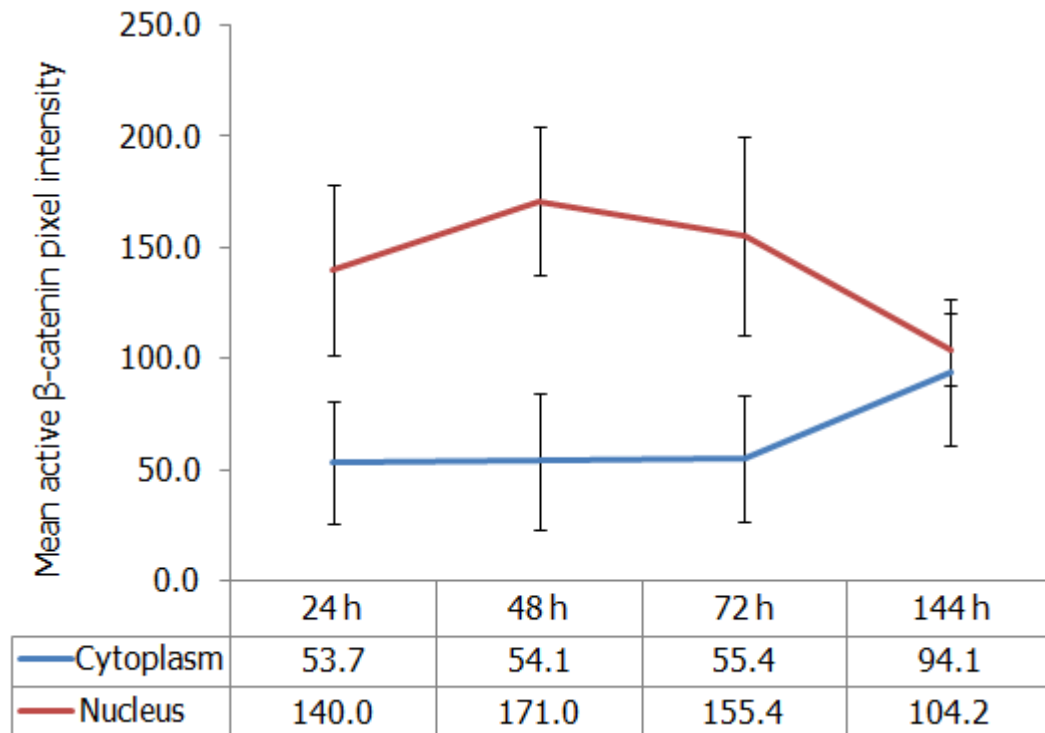


Figure 5-25 Quantification of nuclear and cytoplasmic active β -catenin in NHU cells over time when seeded at low density

Line graph represents nuclear and cytoplasmic active β -catenin pixel intensities and standard deviations as quantified from each micrograph (fig 5-24A-D) using Adobe Photoshop[®] software. Note inverse relationship between nuclear and cytoplasmically localised β -catenin.

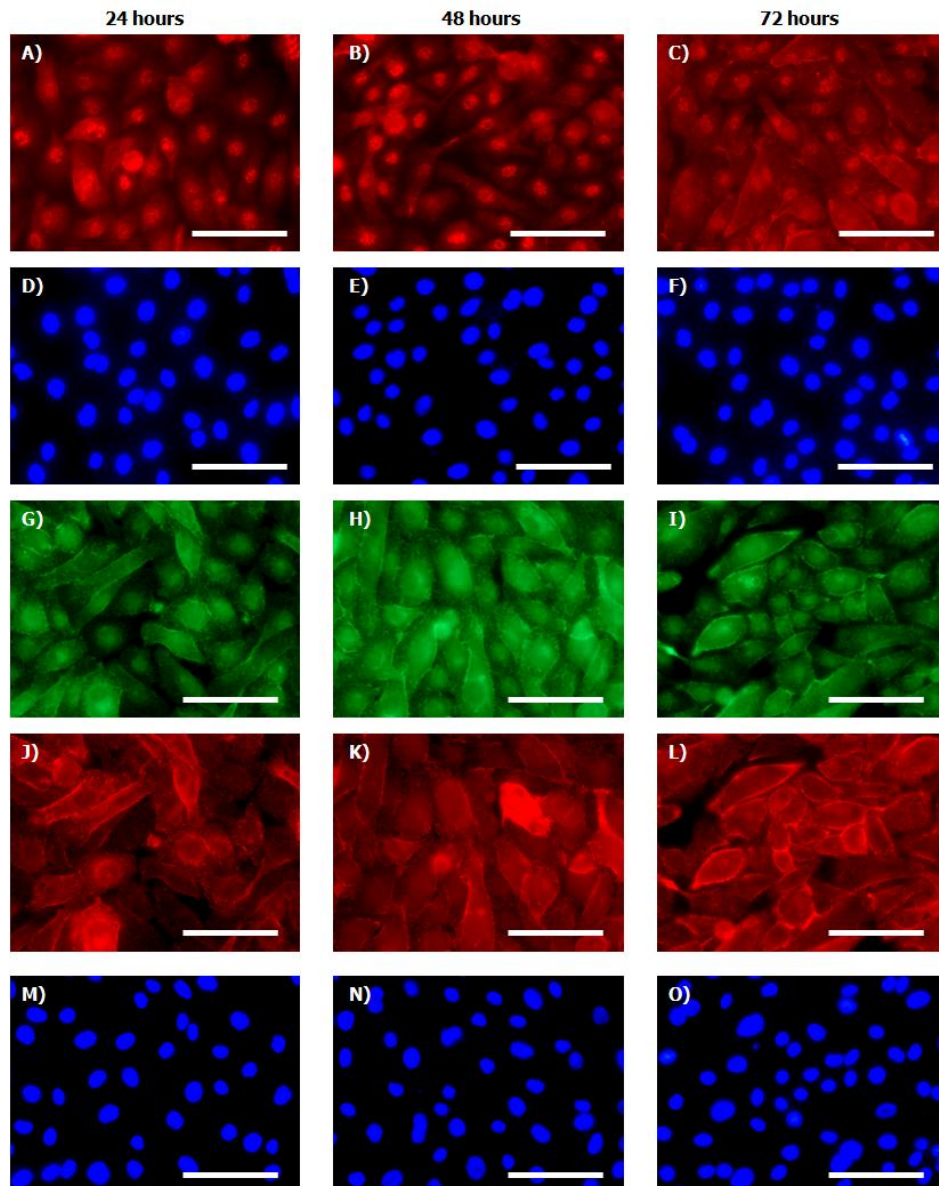


Figure 5-26 Expression and localisation of β -catenin in NHU cells over time when seeded at high plating density

NHU cells (Y919) at P4 were seeded at 5×10^4 cells/cm² and cultured for 24 hours, 48 hours and 72 hours. Slides were fixed and immunolabelled with active β -catenin antibody (8E7), total β -catenin (C2206) or E-cadherin antibody (HECD1). All slides were stained with Hoechst 33258 to delineate the nucleus and labelling was visualised under epi-fluorescent illumination. Photomicrographs are of NHU cells labelled with anti-active β -catenin (A-C), total β -catenin (G-I) and E-cadherin (J-L) with matched Hoechst 33258 staining underneath. Scale bar: 100 μ M. N=1.

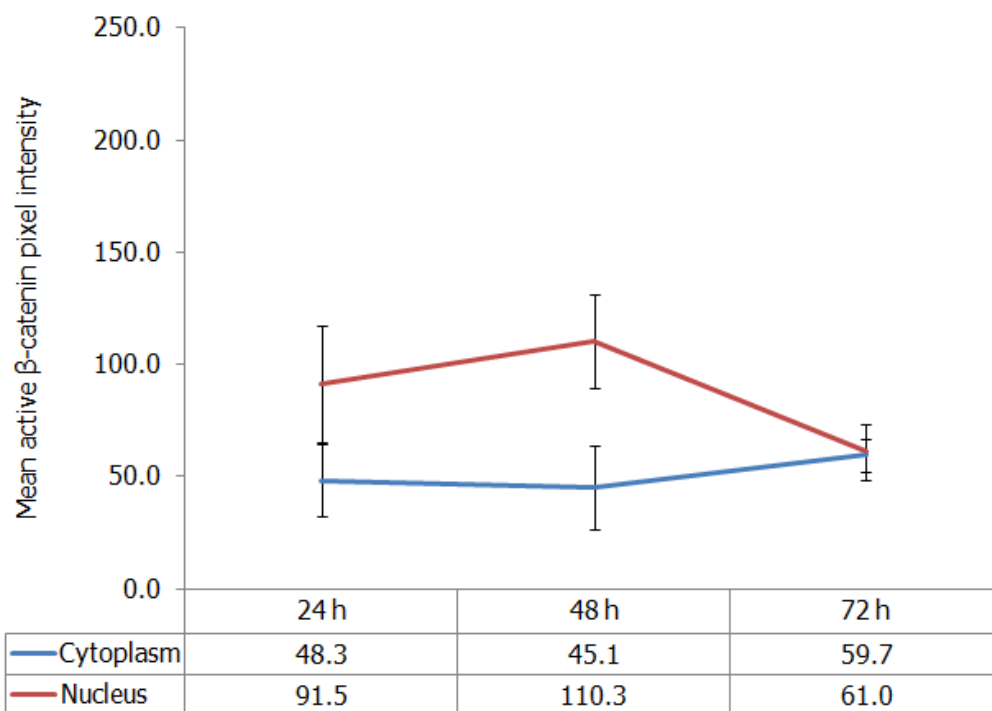


Figure 5-27 Quantification of nuclear and cytoplasmic active β -catenin in NHU cells over time when seeded at high plating density

Line graph represents nuclear and cytoplasmic active β -catenin pixel intensities and standard deviations as quantified from each micrograph (fig 5.26 A-C) using Adobe Photoshop® software.

5.3.8.2 The impact of adherens junction formation on sequestration of active β -catenin from the nucleus

The addition of physiological calcium concentrations to the growth medium of NHU cells stimulated the formation of adherens junctions. By 48 hours, E-cadherin and β -catenin could clearly be seen at the membrane (Figure 5-28A-C and J-L). β -catenin was seen to enter the nuclear compartment 48 hours post seeding and was cytoplasmically localised by 72 hours; the same pattern of expression seen with NHU cells cultured in low calcium (Figure 5-2). Quantification verified the observed increase in nuclear-localised active β -catenin at 48 hours post seeding. The nuclear-active β -catenin signal was seen to increase from a pixel intensity of $87.8 \pm 20.9SD$ (arbitrary units) at 24 hours post seeding to $150.6 \pm 34.6SD$ at 48 hours (Figure 5-29) and was thus similar to that observed in low calcium conditions. Sequestration of β -catenin at points of cell:cell contact via inclusion into calcium-dependent adherens junctions was not seen to inhibit the translocation of β -catenin to the nucleus.

Western blot data from parallel cultures revealed a 2.5 fold increase in active β -catenin (Figure 5-30) between the 24 hour and 48 hour time points and was thus similar to that observed in low calcium conditions. This increase in active β -catenin coincided with when P-ERK signalling was at its most active (Figure 5-30) and was accompanied by an 11-fold increase in P-GSK3 (serine 9) at the same time point (Figure 5-30).

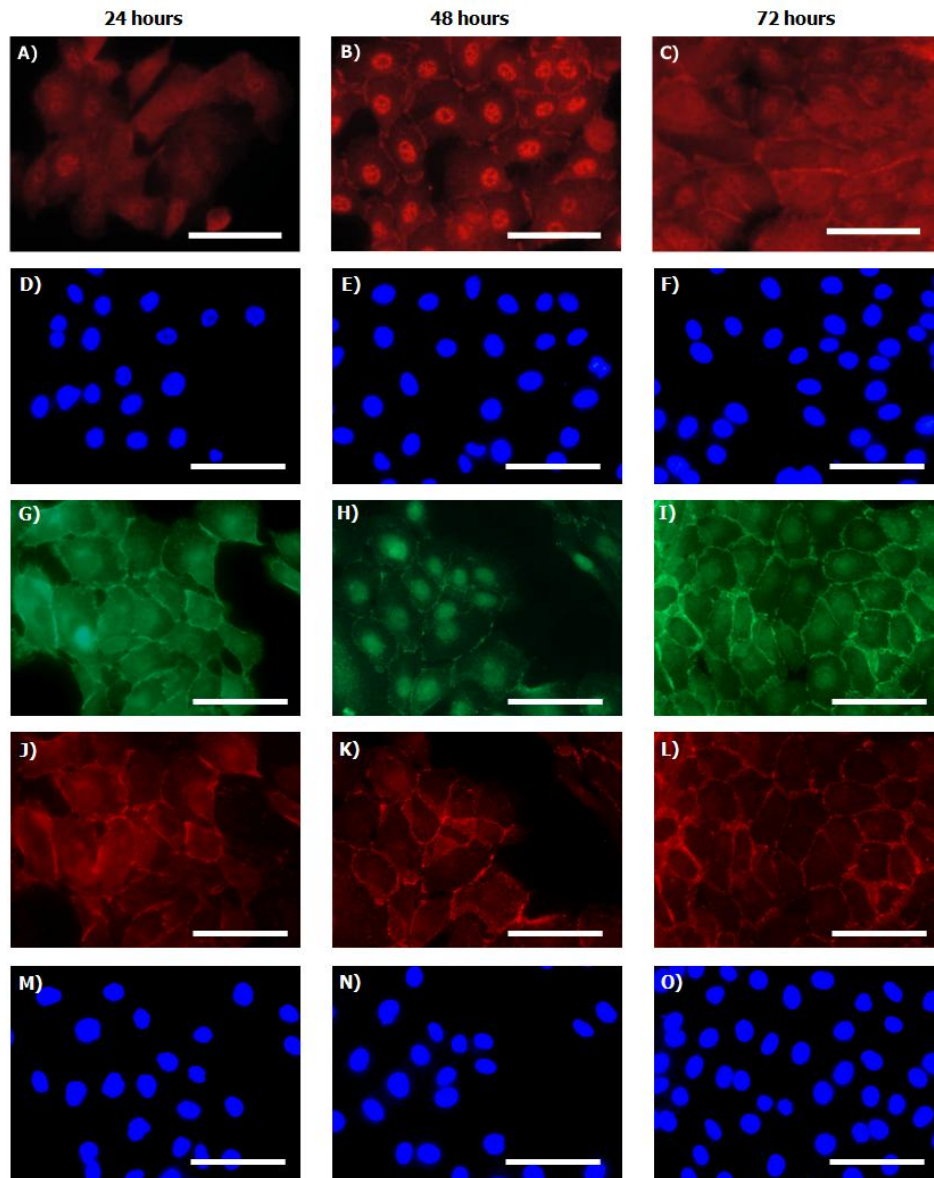


Figure 5-28 Expression and localisation of β -catenin in NHU cells over a 72 hour time course in KSFMc supplemented with physiological calcium

NHU cells (Y919) at P4 were cultured for 24 hours, 48 hours and 72 hours in KSFMc+2mM CaCl_2 . Slides were fixed and immunolabelled with active β -catenin antibody (8E7), total β -catenin (C2206) or E-cadherin antibody (HECD1). All slides were stained with Hoechst 33258 to delineate the nucleus and labelling was visualised under epi-fluorescent illumination. Photomicrographs are of NHU cells labelled with anti-active β -catenin (A-C), total β -catenin (G-I) and E-cadherin (J-L) with matched Hoechst 33258 staining underneath. Scale bar: 100 μM . N=1.

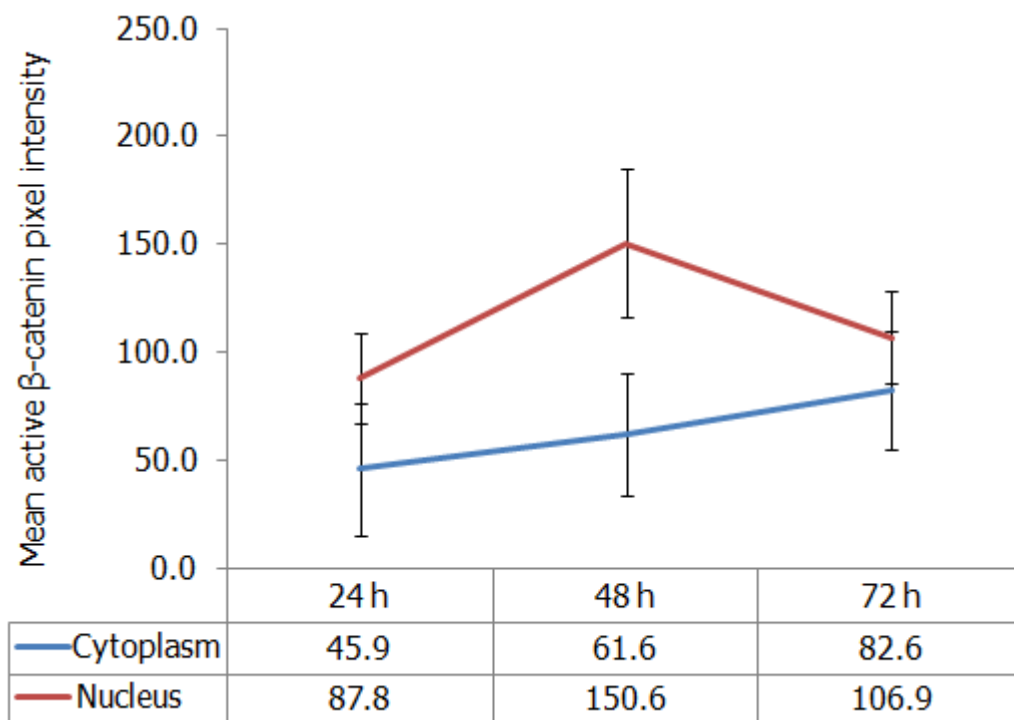


Figure 5-29 Quantification of nuclear and cytoplasmic active β -catenin in NHU cells over time when cultured in KSFMc supplemented with physiological calcium concentrations

Line graph represents nuclear and cytoplasmic active β -catenin assessed from the pixel intensities. Error bars represent standard deviations as quantified from each micrograph (fig 5-28 A-C) using Adobe Photoshop[®] software.

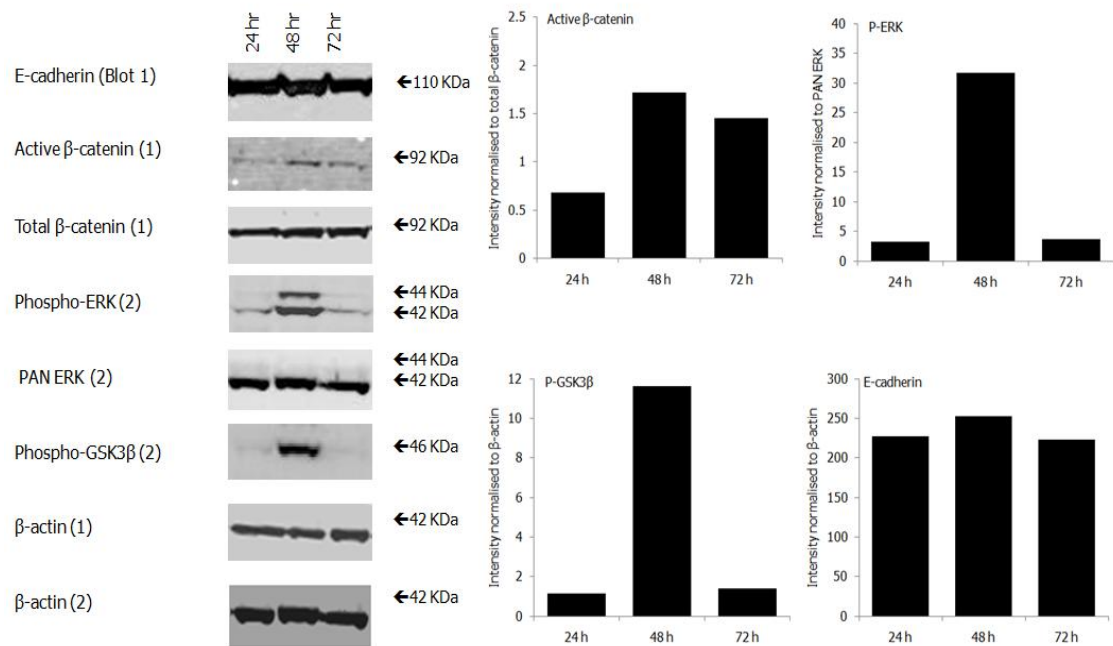


Figure 5-30 Effect of calcium on components of the Wnt signalling pathway

NHU cells (Y919) at P4 were cultured for 24 hours, 48 hours and 72 hours in KSMc+2mM CaCl₂ prior to lysis in 2X SDS-lysis buffer. 20μg of each protein lysate was separated by SDS-PAGE onto 2 duplicate 4-12% (w/v) Bis-Tris gels under denaturing conditions and immunoblotted onto PVDF membranes. PVDF membranes were probed for 16 hours with antibodies raised against E-cadherin, active β-catenin, total β-catenin, phospho-ERK, total ERK, phospho-GSK3β and β-actin to control for equal lysate loading. Membranes were incubated for 1 hour with either; goat anti-mouse IgG Alexa 680 or; goat anti-rabbit IgG Alexa 800 depending on the antigen and primary antibody used. Antibody binding was visualised by epi-fluorescent illumination at 700 and 800nm. Densitometry results are represented graphically normalised to the appropriate loading control.

5.3.8.3 Assessing the effect of adherens junction formation on sequestration of β -catenin and subsequent TCF activity

Expression of Axin2 was less in high calcium (2mM CaCl_2) compared to low calcium (0.09mM CaCl_2) at both the 48 and 72 hour time points but the observed down-regulation did not meet the 2-fold change threshold and was therefore deemed insignificant (Figure 5-31). E-cadherin and c-MYC expression did not change (Figure 5-31). LEF1 mRNA expression was the only β -catenin/TCF-mediated downstream target to alter when compared to control (low calcium; 0.09mM). However, expression of LEF1 mRNA was low in both conditions and thus standard deviations were seen to be high (Figure 5-31). Addition of 2mM CaCl_2 to the growth medium of NHU cells was deemed to not affect β -catenin/TCF-mediated transcription.

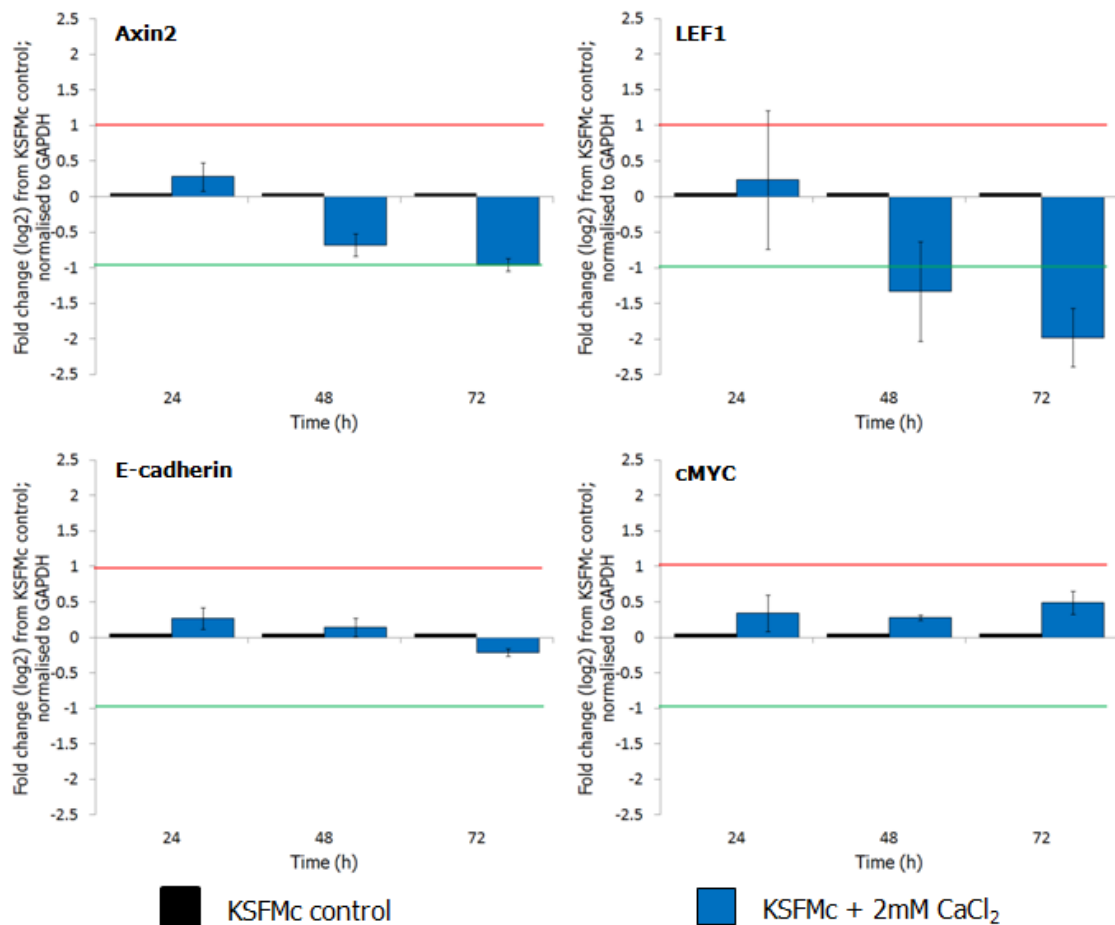


Figure 5-31 Effect of adherens junction formation on β -catenin/TCF-mediated transcription

NHU cells (Y919) at P4 were cultured for 24, 48 and 72 hours in KSFMc or KSFMc+ 2mM CaCl₂. Cells were solubilised *in situ* with TRIzol[®] reagent and the total RNA content from the culture was extracted. All samples were subjected to *DNAse I* digestion to remove residual gDNA prior to first-strand cDNA synthesis using 1 μ g of template mRNA and random hexamers. Quantitative RT-PCR was performed for three direct downstream β -catenin/TCF targets (Axin2, LEF1 and c-Myc) using SYBR-green I. The repression of E-cadherin transcription (assumed to be via Twist) was also quantified. Data was normalised to GAPDH and expression was quantified relative to KSFMc (low calcium; 0.09mM CaCl₂) at the same time point. Data represents the log₂ mean expression of three-technical replicates with the corresponding standard deviation. Red and green lines represent significant 2-fold change in expression. Addition of 2mM CaCl₂ to the growth medium of NHU cells was seen to not affect β -catenin/TCF-mediated transcription.

5.3.9 Summary

- Seeding NHU cells at a lower plating density prolonged the length of time active β -catenin was visible in the nucleus of NHU cells by at least 24 hours.

Seeding NHU cells at a higher than normal plating density did not completely ablate nuclear translocation of β -catenin but did reduce it by $\sim 35\%$. Data thus suggests that cell density regulates β -catenin activity.

- In the presence of near physiological calcium concentrations that promoted formation of adherens junctions, β -catenin was still seen to translocate to the nucleus with strong nuclear labelling visible at 48 hours post seeding. This coincided with high MAPK activity and high P-GSK3 β at the same time point. At 72 hours post seeding, β -catenin was lost from the nucleus and relocalised to the membrane. Data thus suggests that cell:cell contacts may act to sequester β -catenin away from the nucleus.

5.4 The role of β -catenin signalling in NHU cell proliferation

5.4.1 Rationale

Data from section 5.2 showed that signalling downstream of EGFR could regulate the localisation and activity of β -catenin and lead to Wnt ligand-independent TCF-mediated transcription. To determine if this crosstalk was important in inducing/maintaining the proliferative phenotype of NHU cells, EGFR and β -catenin signal transduction cascades would need to be disentangled.

5.4.2 Aim

To determine if β -catenin signalling via pathway crosstalk was important in human urothelial proliferation.

5.4.3 Objectives

- To generate and validate a stable urothelial cell line expressing either an shRNA targeted to β -catenin (termed β CATKD cells) or a scrambled shRNA control.
- To investigate the consequential changes of β -catenin knock-down on urothelial cell morphology and proliferation *in vitro*.
- To investigate if there were any consequential changes to the MAPK and PI3K signalling when β -catenin signalling was reduced.

5.4.4 Experimental design

A validated and published β -catenin siRNA (206) was modified to produce an shRNA hairpin and ligated into the retroviral vector, pSIREN-RetroQ via the *EcoRI* and *BamHI* restriction sites (Appendix X). The resulting plasmid was transformed into *E.coli* and insertion of the shRNA sequence was confirmed by *MluI* digestion (Appendix XI). PT67TM packaging cells were transfected with plasmid containing either the β -catenin shRNA (β CATKD) or with a scrambled shRNA control (developed by Clontech) and selected for stable expression using 4 μ g/ml puromycin. NHU cells (Y970) at low passage (P1) were transduced with retrovirus containing either the β -catenin KD shRNA or scrambled control shRNA and subjected to antibiotic selection (2 μ g/ml puromycin) prior to use in the following experiments:

- Both sub-lines were cultured in complete growth medium and visualised using phase-contrast microscopy. Representative photomicrographs were taken to allow morphological comparison between β CATKD and control cells.
- Cells were cultured in KSFMc \pm 2mM CaCl₂ and lysed *in situ* in 2x SDS (electrophoresis sample buffer) during exponential growth phase. Western blotting studies were performed to verify β -catenin knock-down. Changes in the relative expression of active β -catenin, total β -catenin and E-cadherin were quantified alongside phospho-ERK and phospho-AKT. β -actin was used as a loading control in all experiments.
- Cells were seeded onto 12-well multispot slides and incubated for 24 hours in KSFMc \pm 2mM CaCl₂. Slides were fixed in the appropriate fixative for the antigen of interest and immunolabelled with the following: active β -catenin antibody and total β -catenin to assess β -catenin expression and sub-cellular location, P-ERK and P-AKT to assess MAPK and PI3K signalling status. Hoechst 33258 staining was included to allow delineation of the nuclear compartment.

- Sub-lines were seeded into 96-well plates and cultured in KSFMc \pm 2mM CaCl₂. The viable cell biomass of the culture was determined over a 6-day time course to assess the effect of β -catenin knock-down on proliferation.
- Transduced sub-lines were seeded into 96-well plates and cultured in KSFMc \pm 2mM CaCl₂ with 1 μ M PD153035, 5 μ M U0126 or 5 μ M LY294002 for 6 days. The viable biomass of the culture was measured on days 1, 4 and 6 to determine the sensitivity of each sub-line to EGFR, MAPK and PI3K inhibition.

5.4.5 Results

5.4.5.1 Morphology

Following retroviral transduction, stable sub-lines expressing either β -catenin (β CATKD) or scrambled shRNA were established by antibiotic selection with 2 μ g/ml puromycin. A non-transduced isogenic control culture selected at the same time and with the same concentration of antibiotic had perished by 48 hours and thus clearly demonstrated the toxicity of the antibiotic when NHU cells did not possess the resistance gene (Figure 5-32C). At 48 hours post selection, both the scrambled control and β CATKD cultures still contained viable cells which were resistant to the effects of puromycin (Figure 5-32A/B). Percentage survival was estimated to be slightly higher in the scrambled control culture compared to the β CATKD culture at the same time point. At 96 hours post selection, both the scrambled control and β CATKD cultures had successfully recovered from antibiotic selection and grew as a monolayer culture with typical epithelioid pavement morphology (Figure 5-32D/E). The majority of cells in both cultures had phase-bright intracellular borders. A small proportion of rounded (possibly mitotic) cells were evident (Figure 5-32D/E; black arrow heads). Both cultures reached confluence and were passaged successfully without significant cell loss.

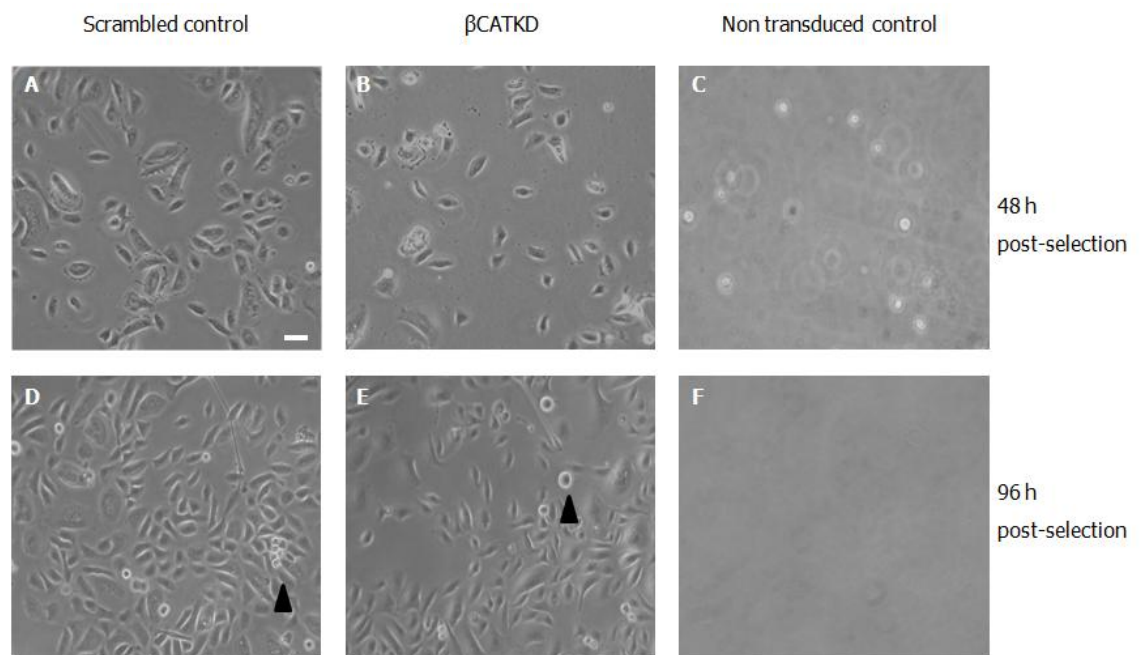


Figure 5-32 Morphological characteristics of β -catenin knock-down cells after antibiotic selection

NHU (Y970) at P1 were transduced with retrovirus containing β -catenin-targeted shRNA (β CATKD) or scrambled control. 48 hours post transduction, cultures were trypsinised, split 1:3 and allowed to attached to the tissue culture flask prior to addition of 2mg/ml puromycin. A 100% stably transduced cell population was assumed when all cells in the nontransduced control flask had perished. Phase contrast images were taken at 48 hours and 96 hours post selection. **(A-C)** 48 hours post-selection, **(D-F)** 96 hours post-selection. Note the lack of cells in both **(C)** and **(F)** verifying a successful selection with puromycin. Black arrow heads denote rounded (possibly mitotic) cells seen after antibiotic selection.

5.4.5.2 Validating β -catenin knock-down in urothelial cells

Whole cell lysates from β CATKD and scrambled control sub-lines were probed for expression of active and total β -catenin (Figure 5-33A). Normalised densitometry results demonstrated a substantial decrease in active β -catenin as well as total β -catenin expression in the β CATKD culture compared to control (Figure 5-33B). Transformation of the normalised densitometry data revealed a 66% reduction in active β -catenin protein expression and a 58% reduction in total β -catenin expression in the β CATKD culture compared to control (Figure 5-33D).

Formalin-fixed cultures of β CATKD and scrambled control sub-lines were probed for active and total β -catenin expression. Signal intensities for active and total β -catenin were clearly reduced in the β CATKD cultures compared to control when photomicrographs were taken at the same exposure (Figure 5-33C). Both nuclear and cytoplasmic labelling was visibly reduced in the β CATKD culture.

5.4.5.3 Effect of β -catenin knock-down on urothelial cell viability

Human urothelial cell biomass was determined by MTT assay after 1, 4 and 6 days in culture with KSFMc \pm 2mM CaCl₂. In KSFMc alone, both cultures entered a lag phase for the first 24 hours, after which, cell biomass was seen to increase at an exponential rate until the end of the time course. By day six, the biomass of the control culture was seen to be significantly greater than the biomass of the β CATKD culture (Figure 5-34; $p < 0.001$). When cultured in the presence of 2mM calcium, both sub-lines proliferated at a greater rate than their KSFMc only counterpart (Figure 5-34). Scrambled control cultures were once again seen to obtain a greater biomass at day six compared to the β CATKD culture indicating a potential growth disadvantage with knock-down of β -catenin (Figure 5-34, $p < 0.001$).

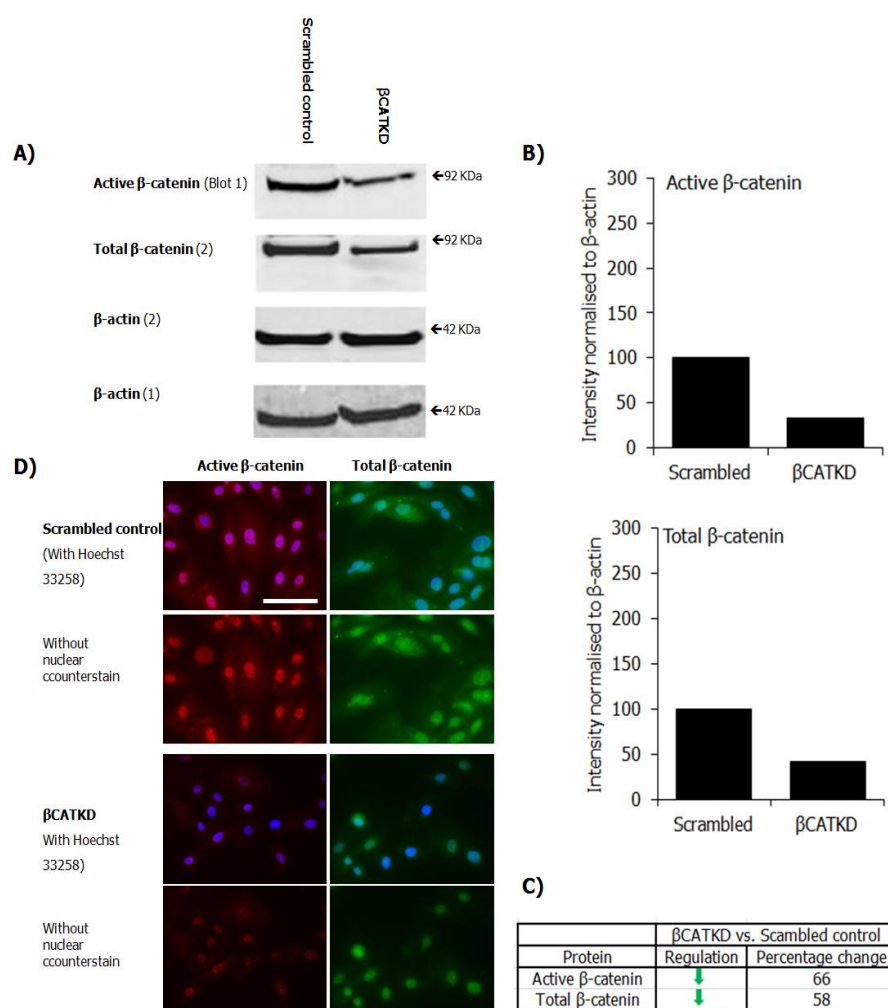


Figure 5-33 Effect of β -catenin shRNA on β -catenin protein expression and localisation in HU cells

(A) Y970 NHU cells expressing either β -catenin shRNA (β CATKD) or scrambled control shRNA were lysed and 20 μ g of each protein lysate was subjected to SDS-PAGE within a 4-12% (w/v) Bis-Tris gel followed by immunoblotting onto PVDF membrane. Membranes were probed for active β -catenin (8E7), total β -catenin (C2206), and β -actin (to control for equal lysate loading) along with the appropriate secondary antibody. **(B)** Signal intensities were normalised relative to β -actin control and represented graphically as bar charts. **(C)** Data was transformed and expressed as percentage change vs. scrambled control. **(D)** β CATKD and control sub-lines were labelled with active β -catenin (8E7) and total β -catenin (C2206) antibodies. All slides were stained with Hoechst 33258 to delineate the nucleus and visualised under epi-fluorescent illumination. Photo-micrographs were taken at identical exposures for comparison. Micrographs and western blots are representative of duplicate experiments. Note the reduction in active β -catenin in the β CATKD cells compared to the control.

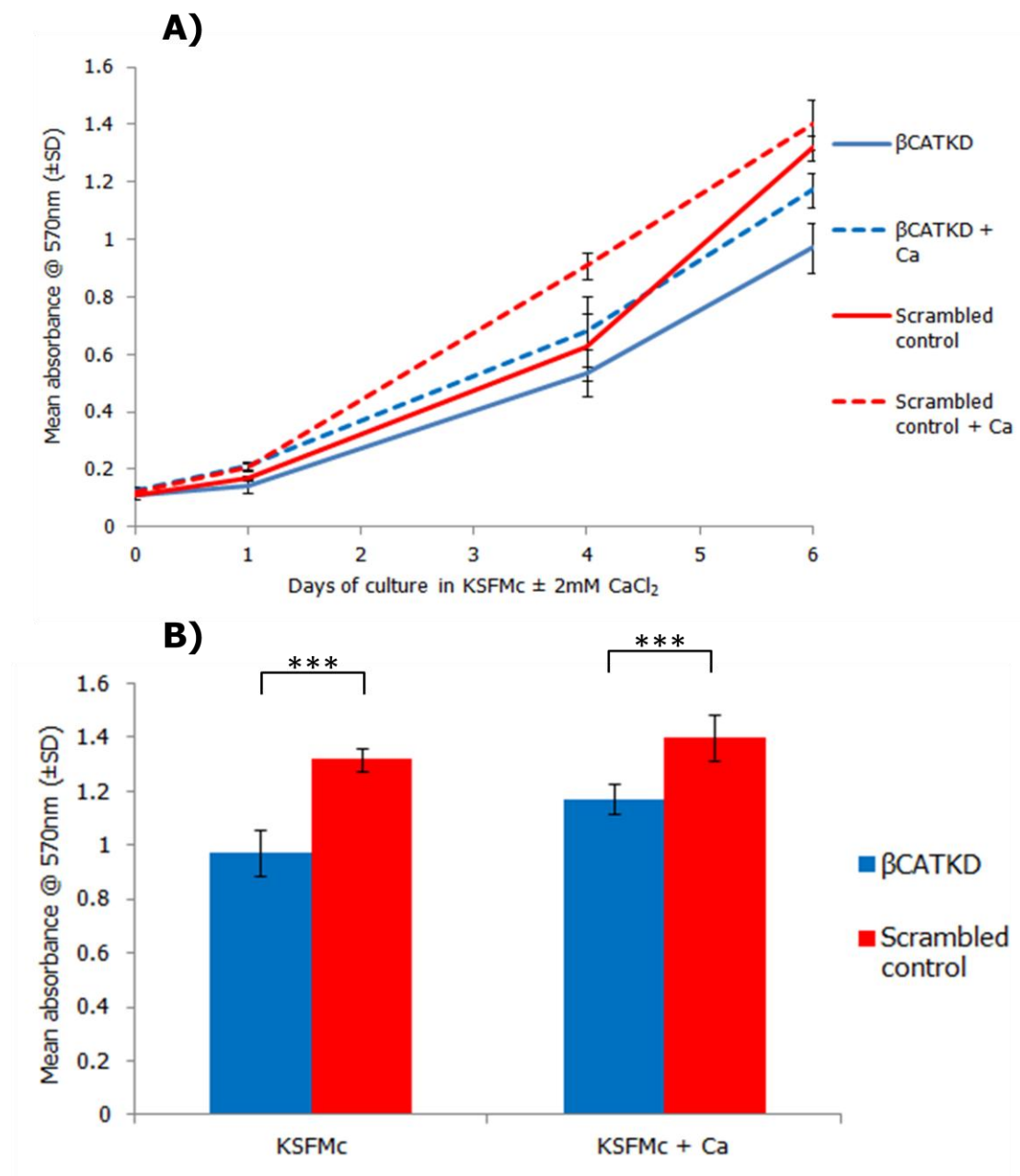


Figure 5-34 Effect of β -catenin knock –down on NHU cell viability

β -catenin knock-down cells (β CATKD) and scrambled control from the NHU cell line Y970 were seeded at 2×10^3 cells/well into a 96-well plate and grown for up to 6 days in complete growth medium \pm 2mM CaCl_2 . **(A)** MTT assays were performed on days 0, 1, 4 and 6 with KSFMc and CaCl_2 replenished on day 3. Each data point is the average of 6 biological replicates \pm SD. **(B)** Transformed data from day six (***) $p < 0.001$, unpaired t-test.). Note the reduced absorbance obtained from the β CATKD sub-line compared to control at the same time point.

5.4.5.4 Assessing the effect of β -catenin knock-down on EGFR signalling

When β CATKD and scrambled control were cultured in normal growth medium (KSFMc; 0.09mM CaCl_2) both sub-lines appeared morphologically normal but the β CATKD culture appeared to have a reduced proliferation rate (Figure 5-34). Immunofluorescence labelling of both sub-lines with the proliferation marker MKi67 revealed a lower proportion of cells in the β CATKD culture (66%) were in the cell cycle compared to control (84%; Figure 5-35). To investigate the effects of β -catenin knock-down on pathways downstream of EGFR signalling, immunofluorescence microscopy and immunoblotting were utilised. Immunofluorescent labelling of the two sub-lines highlighted an increased expression of phospho-AKT in the β CATKD cells (Figure 5-35). Immunoblotting from parallel cultures quantified this change in P-AKT expression as being a 2.16 fold increase over the scrambled control, implying that knock-down of β -catenin increased activity of the PI3K pathway (Figure 5-36). By contrast, expression of P-ERK was seen to be reduced by 80% in the β CATKD culture (Figure 5-36). E-cadherin expression was increased by 2.7 fold in the β CATKD culture.

When cultured in the presence of 2mM CaCl_2 , both sub-lines appeared to form calcium-dependent E-cadherin-mediated adherens junctions at the cell membrane (Figure 5-37). Nuclear expression of MKi67 was similar to that observed in the KSFMc cultures, with 54% of cells in the β CATKD culture expressing the proliferation marker and 75% in the scrambled control (Figure 5-37). When cultured in physiological calcium, shRNA-mediated knock-down of β -catenin resulted in a significant reduction in both P-AKT and P-ERK expression relative to scrambled control (Figure 5-37). Scrambled control cultures clearly showed nuclear expression of both P-ERK and P-AKT, whereas β CATKD cultures showed weak perinuclear localisation of both P-ERK and P-AKT (Figure 5-37).

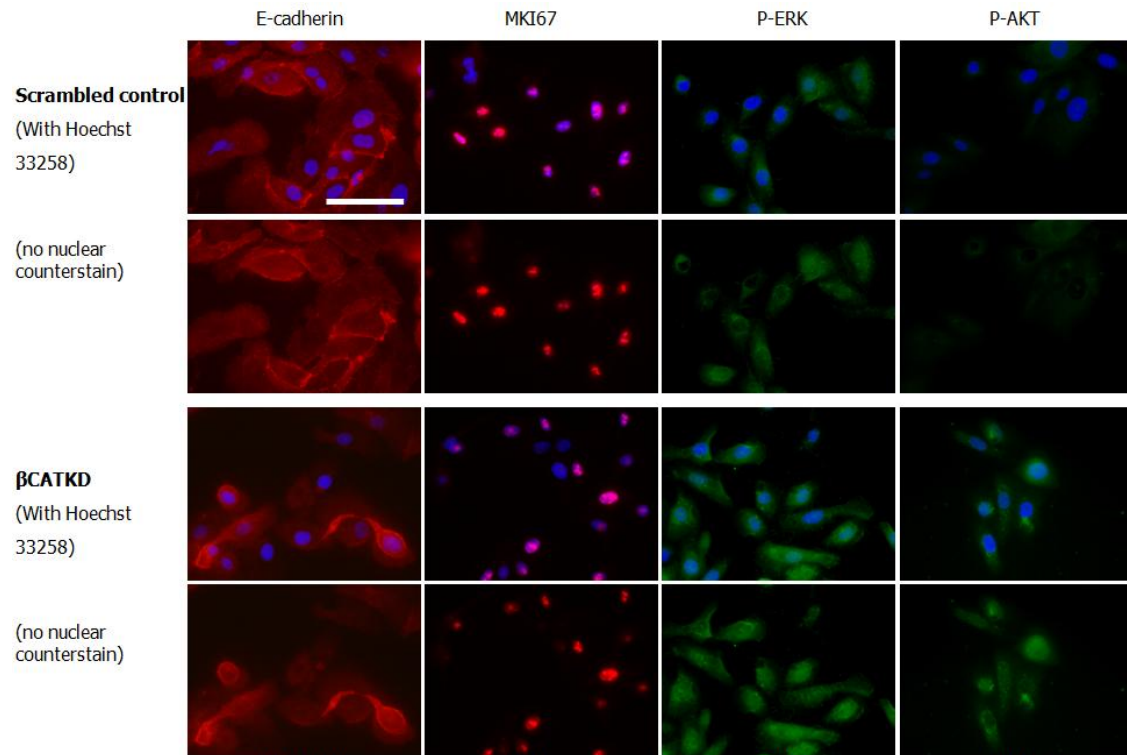


Figure 5-35 Effect of β -catenin knock-down on the localisation of P-ERK and P-AKT in human urothelial cells

NHU cells (Y970) expressing either β -catenin shRNA (β CATKD) or a scrambled control shRNA were methanol:acetone (50:50) fixed and labelled with the following primary antibodies: E-cadherin antibody (HECD1), MKi67 (MM1), P-ERK (D13.14.4E) and P-AKT (D9E). Slides were stained with Hoechst 33258 to delineate the nucleus and visualised under epi-fluorescent illumination. Photomicrographs are representative of duplicate experiments (N=2). All photomicrographs with the same primary antibody were taken at the same exposure. Note the increase in P-AKT expression in the β CATKD cells vs. the scrambled control.

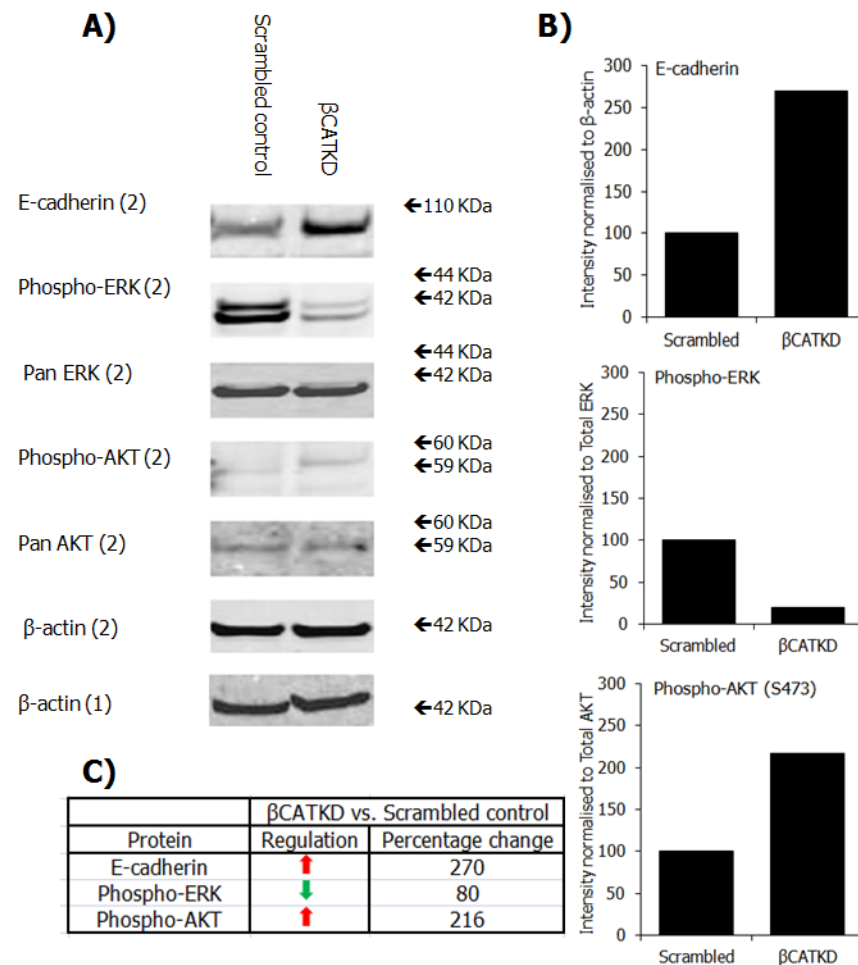


Figure 5-36 Effect of β -catenin knock-down on the expression of P-ERK, P-AKT and E-cadherin in human urothelial cells

NHU cells (Y970) expressing either β -catenin shRNA or scrambled control were lysed and 20 μ g of each was subjected to SDS-PAGE within a 4-12% (w/v) Bis-Tris gel under denaturing conditions. **(A)** PVDF membranes were probed for E-cadherin, phospho-ERK, total ERK, phospho-AKT, total AKT and β -actin (to control for equal lysate loading). Membranes were incubated for 1 hour with either goat anti-mouse IgG Alexa 680 or goat anti-rabbit IgG Alexa 800 and visualised by epi-fluorescent illumination at 700 and 800nm. **(B)** Densitometry results were represented graphically as bar charts. Signal intensities were normalised relative to the appropriate loading control. **(C)** Transformed densitometry data expressed as percentage change vs. scrambled control. Note the decrease in P-ERK and increase in P-AKT and E-cadherin expression in the β CATKD cells compared to control. Representative micrographs from duplicate experiments shown.

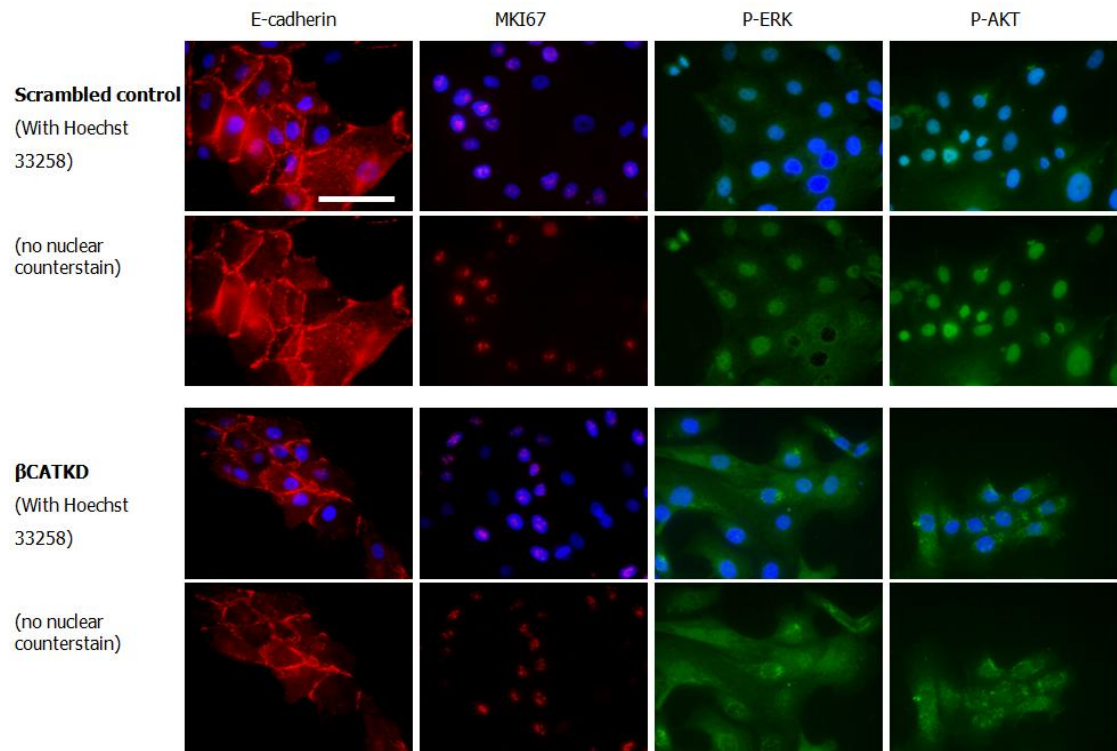


Figure 5-37 Effect of β -catenin knock-down on the localisation of P-ERK and P-AKT in human urothelial cells when cultured in 2mM CaCl_2

NHU cells (Y970) expressing either β -catenin shRNA (β CATKD) or a scrambled control shRNA were incubated for 24 hours in KSFMc + 2mM CaCl_2 prior to Methanol:acetone (50:50) fixation and labelling with the following primary antibodies: E-cadherin antibody (HECD1), Ki67 (MM1), P-ERK (D13.14.4E) and P-AKT (D9E). All slides were stained with Hoechst 33258 to delineate the nucleus and labelling was visualised under epi-fluorescent illumination. Representative photo-micrographs were taken at the same exposure for each antibody. N=1. Note the reduced expression of nuclear P-ERK and P-AKT in the β CATKD cell culture.

5.4.5.5 Cell viability in the presence of EGFR signalling inhibitors

To ascertain whether P-AKT was important in maintaining the proliferative phenotype of the β CATKD sub-line, both cultures were incubated in the presence of EGFR, PI3K and MAPK -specific signalling inhibitors.

When cultured in KSFMc + 0.1%(v/v) DMSO, the β CATKD culture was seen to contain a significantly smaller viable biomass compared to scrambled control by day 6 (Figure 5-38, $p < 0.001$). In the presence of 1 μ M PD153035, proliferation was severely attenuated in both cultures, no significant difference in culture biomass was observed between the two sub-lines (Figure 5-38). In the presence of 5 μ M U0126, the viable cell biomass of the β CATKD cell culture was seen to reduce over the 6 day time course, indicating a possible increase in cell death (Figure 5-39). This was seen regardless of whether the culture had been incubated in 0.09mM or 2mM CaCl₂. Viable biomass of the scrambled control culture remained constant over the course of the experiment, indicating either growth arrest or an increase in cell death (Figure 5-39). When β CATKD cultures were grown in the presence of the PI3K inhibitor, LY294002, viable biomass was significantly reduced compared to scrambled control ($p < 0.001$; Figure 5-40, Figure 5-41) and implied PI3K signalling was driving proliferation in the β CATKD cell culture but not in the scrambled control.

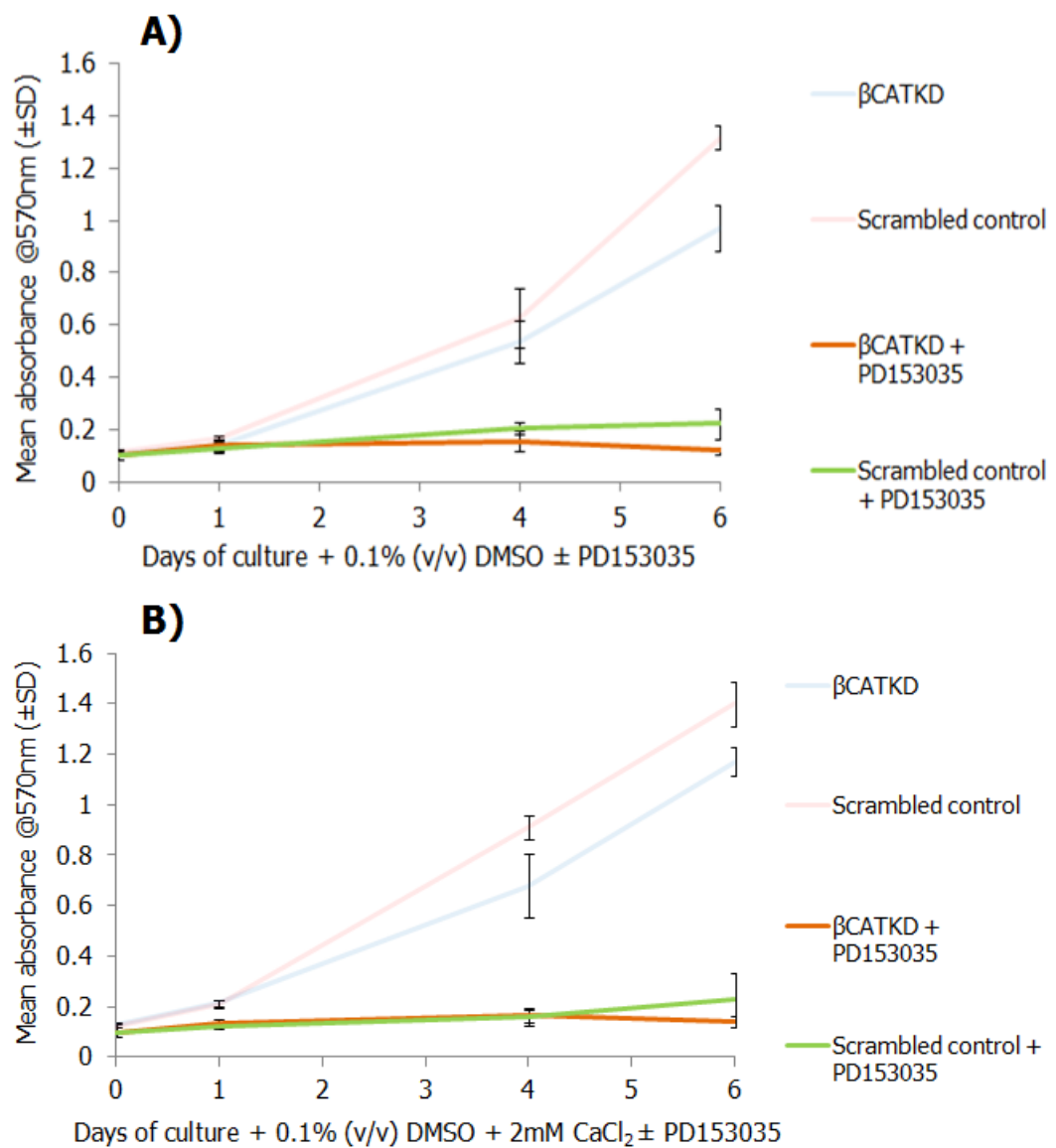


Figure 5-38 Effect of EGFR tyrosine kinase inhibition on the viability of human urothelial with reduced β -catenin expression

β -catenin knock-down cells (β CATKD) and scrambled control cells were seeded at a density of 2×10^3 cells/well into a 96-well plate and grown for up to 6 days in either **A)** KSFMc $\pm 1 \mu$ M PD153035 or **B)** KSFMc + 2mM CaCl₂ $\pm 1 \mu$ M PD153035. MTT assays were performed on days 0, 1, 4 and 6 with growth medium and inhibitor replenished on day 3. Each data point is the average of 6 biological replicates \pm SD.

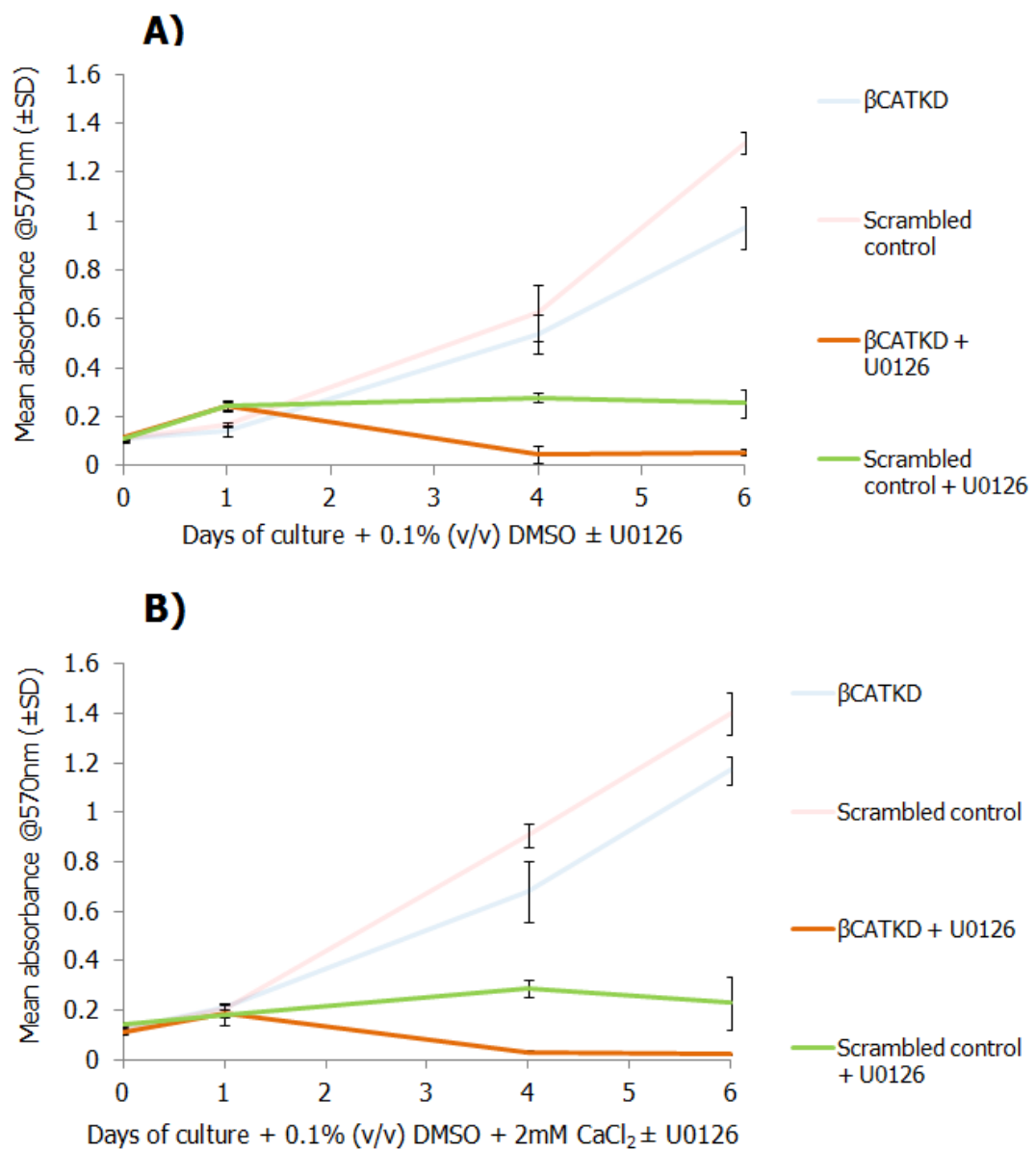


Figure 5-39 Effect of MEK1/MEK2 inhibition on the viability of human urothelial cells with reduced β -catenin expression

β -catenin knock-down (β CATKD) cells and scrambled control cells were seeded at a density of 2×10^3 cells/well into a 96-well plate and grown for up to 6 days in either **A)** KSFMc \pm $5 \mu\text{M}$ U0126 or **B)** KSFMc + 2mM CaCl₂ \pm $5 \mu\text{M}$ U0126. MTT assays were performed on days 0, 1, 4 and 6 with growth medium and inhibitor replenished on day 3. Each data point is the average of 6 biological replicates \pm SD.

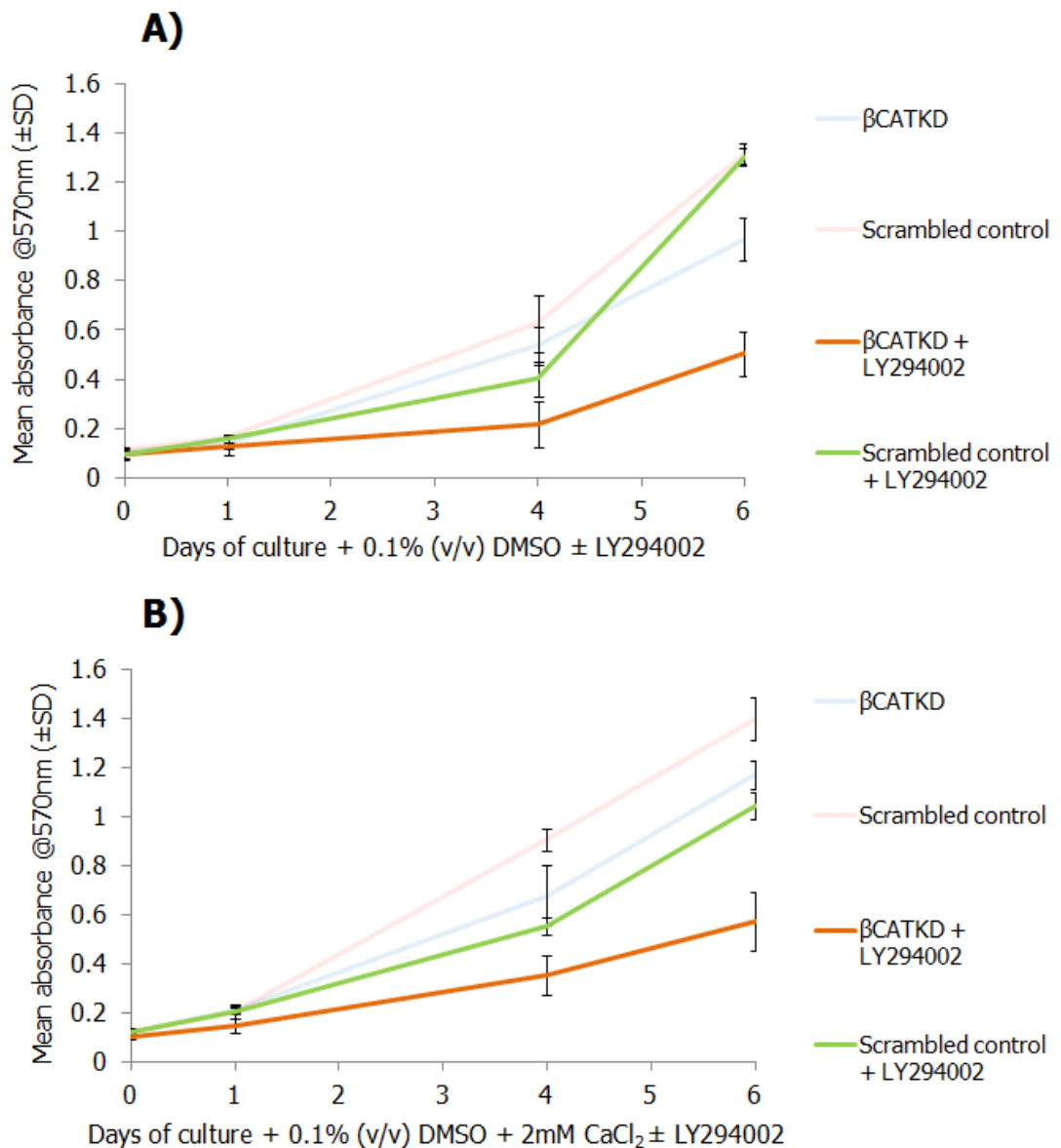


Figure 5-40 Effect of PI3K inhibition on the viability of human urothelial cells with reduced β -catenin expression

β -catenin knock-down cells (β CATKD) and scrambled control cells were seeded at a density of 2×10^3 cells/well into a 96-well plate and grown for up to 6 days in either **A)** KSMc \pm 5 μ M LY294002 or **B)** KSMc + 2mM CaCl₂ \pm 5 μ M LY294002. MTT assays were performed on days 0, 1, 4 and 6 with growth medium and inhibitor replenished on day 3. Each data point is the average of 6 biological replicates \pm SD. Note the recovery of scrambled control cells in the presence of LY294002 as previously seen in (207).

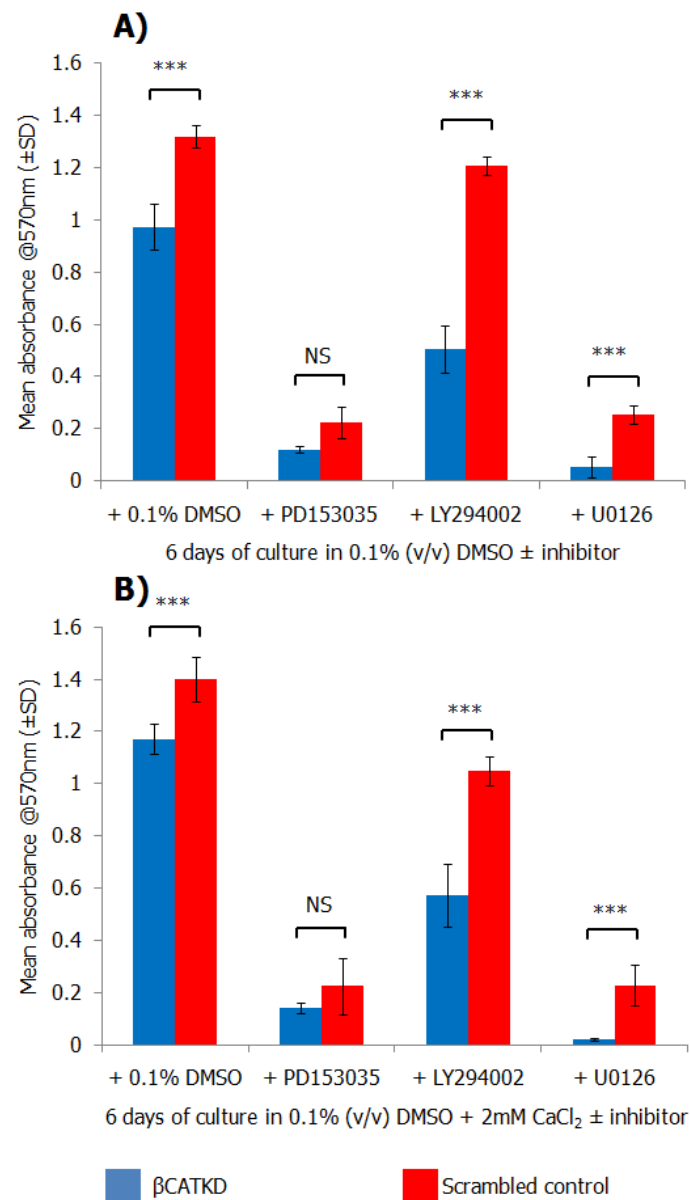


Figure 5-41 Effect of EGFR, MAPK and PI3K inhibitors on the viable biomass of β CATKD cells

Mean absorbance from β -catenin knock-down (β CATKD) cells and scrambled control cells after 6 days in culture with **(A)** KSFMc supplemented with 0.1% (v/v) DMSO, 1 μ M PD153035, 5 μ M U0126 or 5 μ M LY294002. **(B)** KSFMc + 2mM CaCl₂ supplemented with 0.1% (v/v) DMSO, 1 μ M PD153035, 5 μ M U0126 or 5 μ M LY294002. Each data point is the average of 6 biological replicates \pm SD. (***) $p < 0.001$, * $p < 0.05$, one way ANOVA with multiple comparisons post-test). Note the significant difference in biomass between β CATKD and scrambled control cells when cultured in LY294002 or U0126 but not in PD153035. Data is derived from fig 5.38-40).

5.5 Discussion

5.5.1 Wnt-independent β -catenin activation via signalling crosstalk

Under normal growth conditions, NHU cell cultures demonstrated confluence-associated changes in their expression of nuclear β -catenin, whereas cytoplasmic expression remained constant. Cross-reactivity with an unknown nuclear antigen has previously been reported with the active β -catenin antibody (8E7) used in this study (208). Nuclear expression was however also evident with an independent β -catenin antibody (C2206; raised against amino acids 768-781) and therefore expression was assumed to be genuine. The fact that the cytoplasmic pool of β -catenin did not change implied an increase in active β -catenin expression rather than cytoplasmic translocation. Western blotting for active β -catenin supported this theory; with the expression of active β -catenin increasing 3-fold between the 24 and 48 hour time points. For active β -catenin to increase, mechanisms that regulate its degradation or transcription/translation would have to change. Western blotting revealed a correlation between active β -catenin expression, ERK activity (phospho 42/44) and the serine 9 phosphorylated (inactive) form of GSK3. Both EGFR and MAPK blockades reduced active β -catenin expression/nuclear translocation, ablated expression of phosphorylated GSK3 and impaired expression of the TCF-transcriptional target, Axin2. From these results it can be inferred that in the absence of Wnt ligand, TCF-gene targets such as Axin2 were still being transcribed via β -catenin-dependent crosstalk with the EGFR MAPK signalling cascade. The exact mechanism of crosstalk was not fully explored in this study, but evidence in the literature suggests β -catenin-dependent crosstalk with the MAPK pathway can be driven via ERK activation of P70 S6/P90 RSK and subsequent phosphorylation of the destruction complex component GSK3 β (Figure 5-42) (166, 169). Work by McManus and colleagues has shown that mutating GSK β at serine 9 does not impact on β -catenin release via the classical

Wnt ligand pathway and implies another form of destruction complex inhibition is utilised during canonical signalling (176). Further studies such as immunoprecipitation of GSK3 would be a useful experiment to ascertain whether P70 S6/P90 RSK does in fact phosphorylate GSK3 β . Over-expression of a mutant form of GSK3 (at serine 9) could also be employed and would establish the definitive role of GSK3 β phospho-inhibition in β -catenin release from the destruction complex.

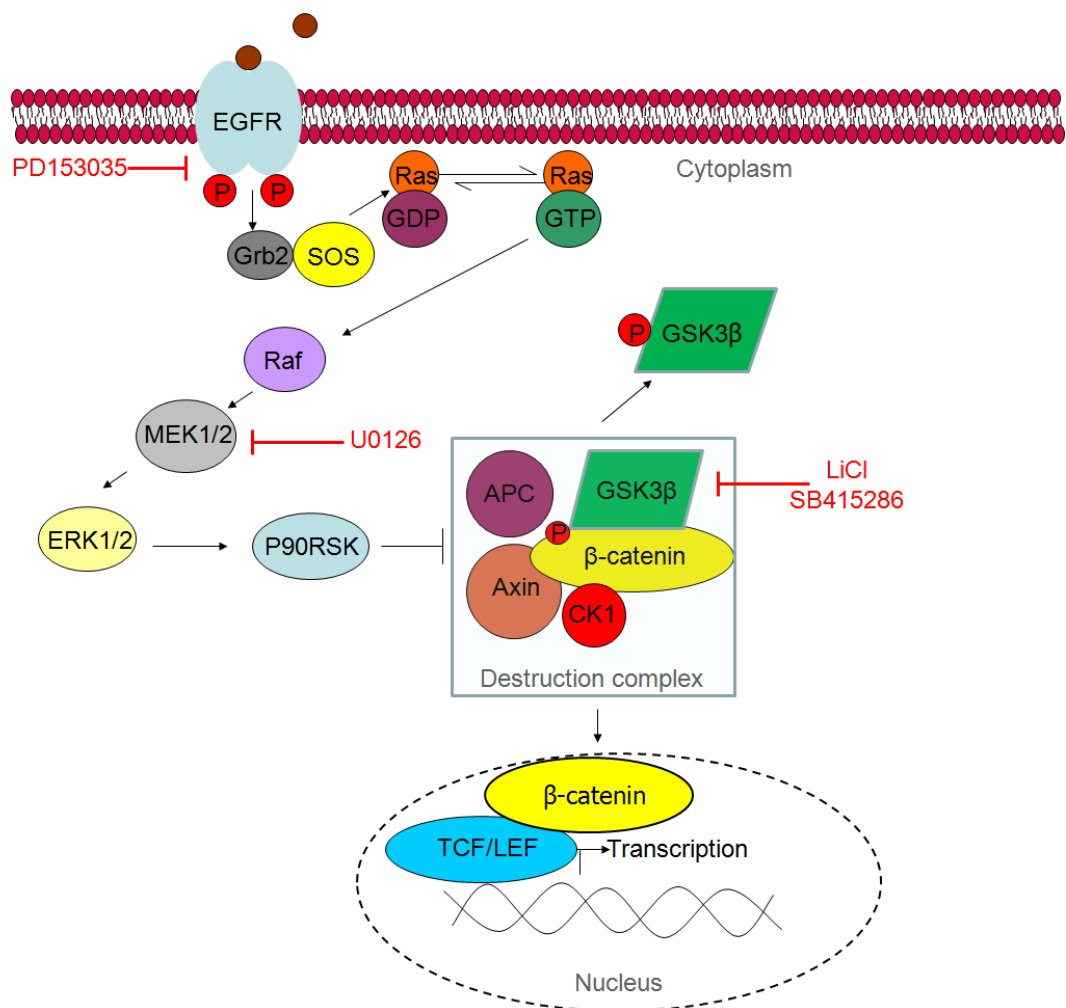


Figure 5-42 β -catenin and EGFR/MAPK crosstalk

Illustration of β -catenin-dependent crosstalk with the EGFR/MAPK pathway. ERK/P90RSK associates with GSK3 β and primes its inactivation resulting in up regulation of active β -catenin and cell proliferation via TCF-mediated transcription of target genes. Pharmacological inhibitors are shown in red. Adapted from (169).

Previous experiments with the GSK3 β inhibitor, SB415286 failed to elicit a significant response in NHU cells. Pre-treatment with the EGFR tyrosine kinase inhibitor, PD153035 and sequential co-treatment with SB415286 and PD153035 resulted in an increase in β -catenin nuclear translocation, viable cell biomass and TCF-mediated transcription, compared to cells treated with PD153035 alone. These results suggest that no response was seen with SB415286 alone because of masking via signalling crosstalk and demonstrate for the first time that β -catenin activation and TCF-mediated transcription of target genes can drive NHU cell proliferation in the absence of EGFR signalling. No increase in nuclear β -catenin, proliferation rate or TCF-activity was evident when NHU cells were pre-treated with either U0126 or LY294002. The fact that all signalling downstream from the EGFR must be blocked to observe any response with SB415286 implies phospho-inhibition of GSK3 via MAPK/ERK may not be the only point of crosstalk between the EGFR and β -catenin signalling cascade. NHU cells immunolabelled with active β -catenin antibody (8E7) revealed a residual nuclear β -catenin pool remained after treatment with U0126 and implied a second convergence point between EGFR and β -catenin may exist. One such convergent point could be at the EGFR tyrosine kinase itself. EGFR TK activity has previously been shown to phosphorylate β -catenin at tyr-654, destabilising the E-cadherin/ β -catenin complex and releasing β -catenin for translocation to the nucleus (193, 195, 198).

5.5.2 The role of cell:cell contact

Seeding NHU cells at a low density resulted in prolonged nuclear expression of β -catenin, whereas high seeding densities resulted in weak nuclear expression. The most obvious explanation for this apparent confluence-related effect on β -catenin activity is the previously published data showing EGFR down-regulation in confluent NHU cell cultures (33). Data corroborates these published findings, as a reduction in P-ERK expression was seen as cell cultures became more densely populated. Adherens junction formation has been shown

to modulate the availability of β -catenin for nuclear translocation by sequestration at the cell membrane (209) and could potentially be an important link in modulating the proliferative/quiescent switch seen in NHU cells. In low calcium growth medium such as KSFMc, calcium-dependent cell:cell engagement is weak and β -catenin expression at the cell membrane is low. Permitting adherens junction engagement by increasing extracellular calcium did not reduce nuclear β -catenin or TCF activity. These results suggest that once released from the destruction complex, β -catenin preferentially translocates to the nucleus. How this is regulated remains unclear, but evidence from the literature suggests activated EGFR can phosphorylate β -catenin at tyr-654, negating its ability to complex with E-cadherin at the adherens junction (195, 198). Data in appendix XII supports this theory, as treatment with an EGFR tyrosine kinase inhibitor (PD153035) not only reduced nuclear localised β -catenin but also increased β -catenin at the membrane.

5.5.3 The role of β -catenin in NHU proliferation

In NHU cells, β -catenin protein expression was successfully reduced by ~58% using RNA interference. Over a six day time course, MTT assays revealed a significantly reduced biomass in the β CATKD cell culture compared to isogenic control. In sub-confluent culture, fewer β CATKD cells appeared to be actively dividing (as measured by MKi67 expression) and thus a decrease in proliferation, rather than an increase in apoptosis was deemed to be the cause. Western blotting on β CATKD whole cell lysates revealed a significant reduction in phospho-ERK expression compared to control. Interestingly, phospho-AKT expression showed the opposite effect and was up-regulated in comparison to control. These results implied β CATKD urothelial cells had switched from a mainly ERK-driven mode of proliferation, to one utilising the PI3K pathway. Normally, NHU cells treated with PI3K inhibitor suffer only a short-lived inhibition of proliferation which they rapidly overcome (207). Growth assays performed in the presence of LY294002 revealed β CATKD urothelial cells to be

more reliant on the PI3K/AKT pathway. Data thus implied that phospho-AKT activity was being used as an alternate pathway to drive proliferation when MAPK/ERK signalling was impaired (70). The cause of this reduced ERK activity was not fully revealed during this study, but evidence from the literature would suggest there may be several points of convergence between β -catenin and the pathways downstream of EGFR. In the mouse liver, constitutive β -catenin signalling was shown to lead to an increase in EGFR transcription and might account for the observed changes in phospho-ERK activity in β CATKD cells (210). Another mechanism by which β -catenin/TCF-mediated transcription might influence ERK/AKT signalling was postulated by Yun and colleagues in 2005 (211). In their NIH-3T3 mouse fibroblast cell model, TCF-mediated transcription of an as yet unidentified molecule resulted in an increase in Raf-1 and subsequent MAPK/ERK activity (211, 212).

By collating all the published data on Wnt/ERK crosstalk, Kim and colleagues have postulated that a positive feedback loop between Wnt and ERK signalling may exist (Figure 5-43(213)). In their computational model, EGFR and/or Wnt signalling, stabilises the activity of both pathways and could be a potentially important mechanism during urothelial tissue homeostasis. One should note, however, that many of the studies claiming crosstalk with β -catenin have been undertaken in transformed cell lines and thus their relevance to normal cell systems remains to be proven.

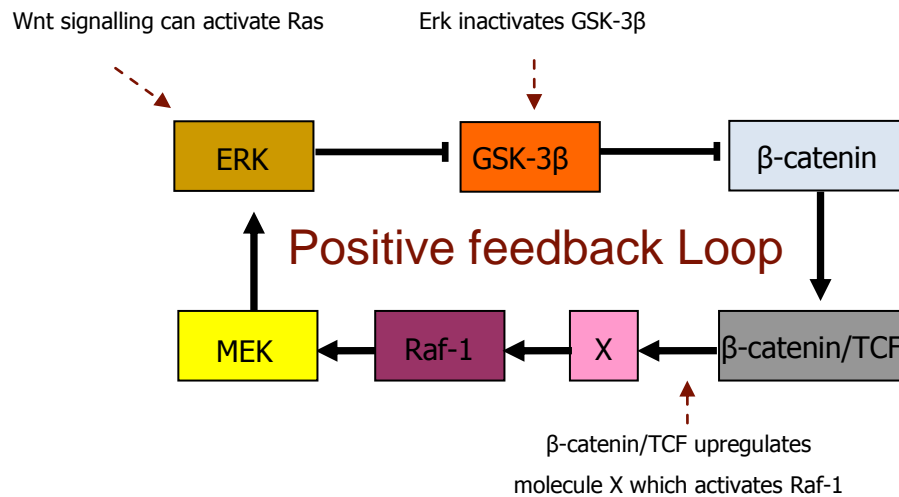


Figure 5-43 A schematic diagram summarising the proposed positive feedback loop between Wnt and ERK signalling

1)Activation of Ras by Wnt signalling (211) leads to the phosphorylation of ERK, 2)Phospho-ERK phosphorylates GSK3 β inactivating the destruction complex (169, 214), 3) β -catenin is released from the destruction complex and translocates to the nucleus where it mediates the transcription of an unknown molecule (molecule X), 4)Molecule X activates Raf-1 which activates the MAPK/ERK pathway (211, 212). Adapted from (213).

In summary, data presented in this chapter has demonstrated the following:

1. Crosstalk between the pathways downstream of EGFR and β -catenin.
2. A role for cell:cell contact in the reduction of β -catenin/TCF-mediated transcription.
3. A positive feedback mechanism between β -catenin and ERK which potential could lead to the stabilisation of both pathways.

Data present in this chapter provided preliminary evidence for a communication network between EGFR signalling, β -catenin signalling and cell:cell contact and is outlined in figure 5-44.

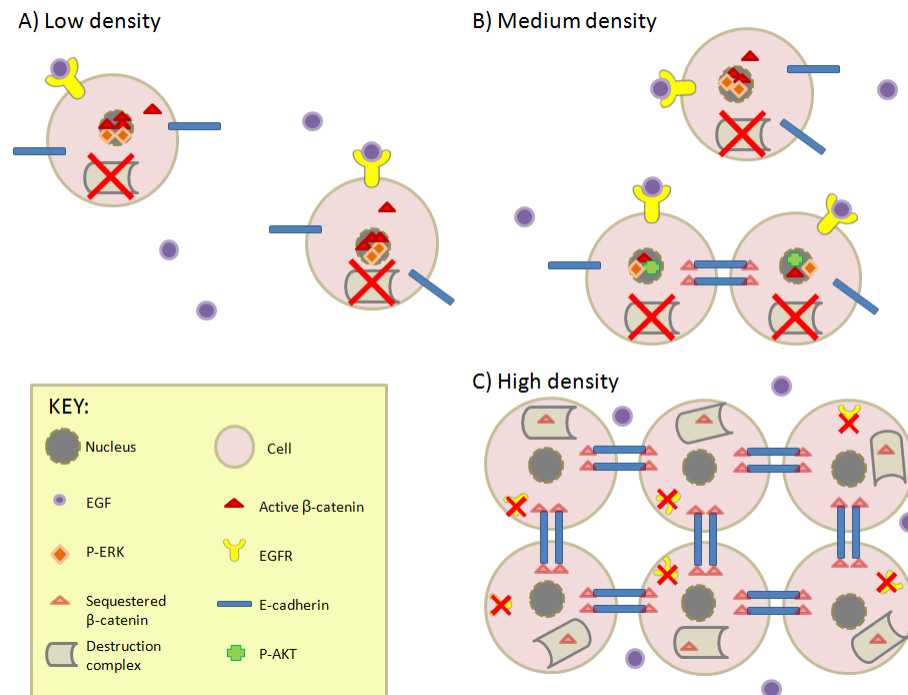


Figure 5-44 Schematic illustrating the potential role of signalling crosstalk and cell:cell contact in modulating NHU cell proliferation

(A) At low density, the receptor tyrosine kinase (RTK) EGFR is present on the cell surface and binds EGF ligand. Activation of the RTK leads to phosphorylation of ERK, translocation to the nucleus and cell proliferation. P-ERK inactivates the destruction complex allowing β -catenin to accumulate and enter the nucleus. (B) Crosstalk between β -catenin and AKT/ERK leads to a positive feedback loop and highly proliferative phenotype. Proliferation leads to an increase in cell number. (C) Confluency-induced reduction in the expression of EGFR (or up-regulation in ERBB2/3) leads to a decline in EGFR signalling and reduction in phospho-inhibition of GSK3 β . Activity of the destruction complex is reinstated. Cytosolic β -catenin binds to the cytoplasmic tail of E-cadherin and adherens junctions form. Once a critical number of cell:cell contacts have been made, excess β -catenin is targeted for degradation via the destruction complex. P-ERK is low, active β -catenin is low and the cells enter G₁ growth arrest.

6 Wnt ligand activation of the canonical Wnt cascade in NHU cells

6.1 Introduction

6.1.1 Wnt ligand

The Wnt family of growth factors comprises a large group of highly conserved, secreted glycoproteins which are named after their two founding members, Int-1 in the mouse (215) and Wingless in the Fruit fly (216). In humans, 19 Wnt genes have been identified and have demonstrated important tissue-specific effects in a variety of areas, including development, tissue homeostasis and disease (Table 6-1). Even though they have very diverse roles, every member of the Wnt family has several characteristics in common: all are approximately 350-400 amino acids in length and 40KDa in weight; all contain a cysteine-rich amino acid sequence making them highly-charged (153). Despite this charged state, Wnts are hydrophobic in nature due to the many essential lipid modifications that occur during the maturation process. This lipid modification makes Wnt proteins highly insoluble and once secreted they are found mainly bound to either cell membranes or the extracellular matrix (ECM) (217).

6.1.2 Processing of Wnt ligand

Post-translational modification of Wnt occurs in the endoplasmic reticulum (ER) and begins with the addition of a hydrophobic palmitate moiety, a process known as palmitoylation which occurs on the first, absolutely conserved cysteine residue (Cys77 in Wnt 3a and Cys104 in Wnt 5a)(96, 218). Mutations at this conserved cysteine result in secretion of non-biologically active protein and indicate that this modification is essential for activity, but not secretion (96, 158). Over the last five years, other lipid modifications have also been discovered. Takada and colleagues have shown that Wnt 3a is acylated with a mono-unsaturated palmitoleic acid group at serine 209, a modification which was shown to be necessary for exit from the ER (219). It thus appears from

the data that these two acylation sites serve different functions: Serine 209 for secretion and cysteine 77 for activity. The enzyme(s) that catalyse this process are still debated but evidence suggests porcupine in *Drosophila melanogaster* (220)/PORCN in human (221), a multipass, transmembrane O-acetyltransferase, may be important, as loss of function mutants of porcupine fail to secrete Wnt ligand (222).

Once palmitoylated, Wnt undergoes N-linked glycosylation at several asparagine residues (in Wnt 3a; Asn83 and Asn298), a process thought to be undertaken via the oligosaccharyl transferase complex (OST)(153, 220). The role of these glycans is still not fully understood, but two reports have shown that mutation at these sites results in reduced ligand secretion and retention of Wnt in the ER (157, 158).

6.1.3 Secretion of Wnt ligand

Secretion (exocytosis) of Wnt is not fully understood. Once post-translational modification is complete, Wnt is thought to associate with its chaperone, Bip before being transferred to the trans-Golgi network (TGN)(154, 223). Once in the TGN, Wnt interacts with Wntless (WLS; synonym Evi and Sprinter), a transmembrane protein first identified in *Drosophila melanogaster* which transports Wnt from the TGN to the plasma membrane (155, 156, 224). Loss of WLS results in detainment in the Golgi and Wnt never exiting the secretory pathway (156, 225, 226). WLS is then recycled back to the TGN in clathryn-coated endosomes through a retromer cargo-recognition complex composed of Vps26a, Vps29 and Vps35 proteins (227).

6.1.4 Receptor binding and activation

Wnt signalling is not intrinsically mediated by the presence of Wnt protein but by receptor availability (228). Fzd receptors are seven-pass transmembrane G-protein coupled receptors (GPCR) which were first shown to transduce Wnt

signalling by Bhanot and colleagues approximately 15 years ago (112). At present there are 10 human Fzd genes, all of which result in a protein of approximately 650-700 amino acids in length. Structurally, all Fzd receptors contain the following: an N-terminal extracellular region containing a conserved cysteine rich domain (CRD) which binds to Wnt protein; a seven-pass transmembrane region which binds Dsh and a Ser/Thr-X(any amino acid)-Val motif (SXV) at the C-terminus (Figure 6-1) (229, 230).

Interestingly, the CRD domain of Fzd is also found in two other receptors: smoothed (SMOH in humans) and receptor tyrosine kinase-like orphan receptors (ROR). SMOH, although structurally similar to Fzd, does not bind Wnt ligand at the CRD (231). ROR2, however, has been shown to interact with Wnt 5a ligand and can act as an inhibitor of canonical signalling by blocking TCF-mediated gene transcription (Figure 6-2) (123).

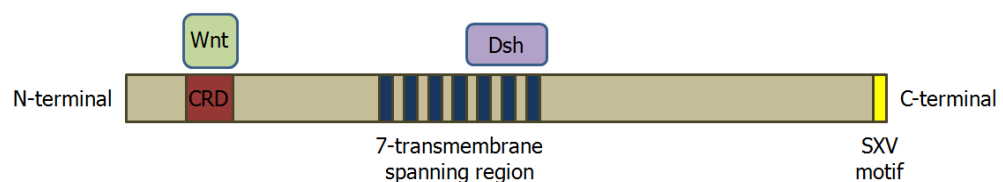


Figure 6-1 The three domains of Fzd and the approximate binding sites for Wnt and Dsh

Schematic depicting the three main domains of Frizzled (Fzd): a cysteine rich domain (CRD), a 7-pass transmembrane region and a Ser/Thr-X-Val motif. Adapted from (232).

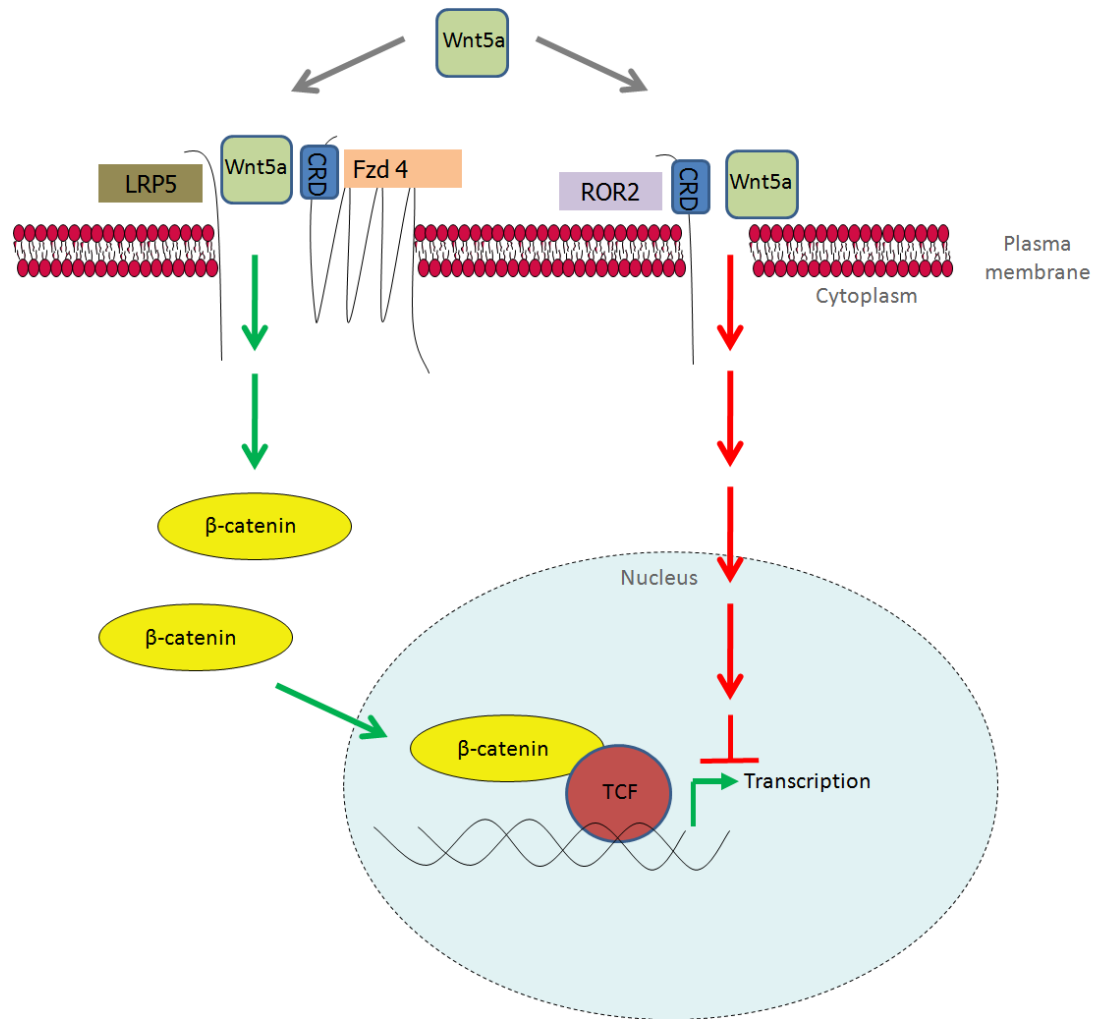


Figure 6-2 Activation and inhibition of the canonical Wnt pathway by Wnt 5a

In the presence of Fzd4 and LRP5, Wnt5a activates the canonical Wnt signalling pathway. However, when ROR2 is expressed, Wnt5a inhibits canonical Wnt signalling at the level of TCF-mediated transcription. Adapted from (123).

Name	Classification	Receptor(s)	Role in development	Associated with disease	Other info
Wnt1	Canonical	Fzd1 (233), Fzd2, Fzd8 (234).			
Wnt2		Fzd1			
Wnt3	Canonical	Fzd7 (120, 235), Fzd1 (233).		Homozygous mutations cause Tetro-Amelia (236). Cancer of breast, rectal, lung and gastric.	84% homology to Wnt3a.
Wnt3a	Canonical/non canonical	Fzd1 (233), Fzd2/ROR2 (128), Fzd6 (237), Fzd8 (238)			
Wnt4		Fzd6 (239).		Loss of function causes SERKAL syndrome (236).	
Wnt5a	Canonical/non canonical	Fzd1(233), Fzd4, Fzd2/ROR2 (123).	Promotes adipocyte differentiation (240)	Silenced in oesophageal cell carcinoma (130)	Can bind Fzd2 inhibiting Wnt3a
Wnt5b	non canonical		Promotes adipogenesis in 3T3-L1 preadipocytes (241)	Associated with type 2 diabetes (242)	80% homology to Wnt5a.
Wnt7a	Canonical/non canonical	Fzd5 (122)		sFzd4 blocks Wnt7a in ovarian cancer(121) Down-	
Wnt7b	Canonical	Fzd1,Fzd2, Fzd4, Fzd10 (244)	Important in kidney and lung development (245, 246)	Up-regulated in superficial but not invasive bladder cancer (247)	77.1% homology to Wnt7a.
Wnt8b	Unknown			Up-regulated in human gastric cancer (248)	
Wnt9a	Unknown			Up-regulated in human gastric/pancreatic and breast cancer cell lines (249)	
Wnt9b	non canonical		Plays central role in MET during organogenesis of urogenital system (250)		
Wnt10a	Canonical			Co-expressed with Wnt6 in colon cancer(251)Odonto-onycho-dermal dysplasia (252)	
Wnt10b	Canonical		Inhibits development of white and brown adipose tissue (253)	Split hand/foot malformation (254)	
Wnt11	non canonical		Important in ureteric branching (255)		Represses Wnt1,3 and 3a activation of β -catenin in NIH3T3 cells (256)
Wnt16	Unknown				Highly expressed in adult kidney (257)

Table 6-1 Human Wnt genes

Information compiled from the Wnt homepage (232), GeneCards[®] Human Gene database (258) and from Ingenuity[®] Pathway Analysis. No data available for Wnt2b, Wnt6 and Wnt8a.

6.2 Rationale

Wnt has been shown to play a major role not only in development but also during normal tissue homeostasis. Recent evidence from the mouse suggests a sub-population of basal urothelial cells respond in a paracrine manner to Wnt ligand stimulation (42). It is as yet unknown whether human urothelial cells respond in the same way. Data from chapter 3 has indicated that proliferating NHU cells transcribe mRNA from several Wnt as well as Fzd genes, hinting at a possible autocrine Wnt signalling loop in human urothelium. *In vitro*, production and secretion of bioactive Wnt is achieved only when fetal bovine serum (FBS) is present in the growth medium (96, 97). The exact component(s) necessary have not yet been characterised, but the literature would suggest albumin-bound palmitic acid (a requirement for post-translational modification of Wnt) could be a candidate (96, 97). NHU cells are routinely cultured in serum-free KSFMc which does not contain palmitic acid (proprietary ingredients; personal communication from Invitrogen), one can therefore deduce that under normal growth conditions, NHU cells are unlikely to produce bioactive Wnt ligand.

6.3 Aims

- To assess whether exogenous Wnt ligand can activate the canonical Wnt signalling pathway in NHU cells and thus provide evidence for its role as a potential growth factor in urothelial regeneration.
- To determine if supplementation of low-serum/ no serum growth medium with palmitic acid results in the production of bioactive Wnt ligand.
- To determine whether NHU cells have the potential to process and secrete functional Wnt ligand and whether this can be used to drive paracrine (in other cell types) and/or autocrine (in same cell type) canonical Wnt signalling.

6.4 Experimental Plan

6.4.1 Wnt ligand choice

Like many signalling pathways, the canonical Wnt pathway contains a lot of degeneracy between ligand-and receptor (Table 6-1). Two Wnt ligands were tested on NHU cells for the following reasons:

- Wnt3a was chosen as a candidate exogenous ligand because it was previously shown to interact with several Fzd receptors (Table 6-1) including Fzd2 and 6 which were expressed at the mRNA level in proliferating NHU cultures. Also, Wnt3a was readily available in the form of a secreted protein from the L Wnt-3a cell line, a genetically engineered L cell line which secretes high levels of soluble Wnt3a into the medium (96, 97, 197).
- Wnt5a was tested as Affymetrix™ mRNA analysis revealed high Wnt5a mRNA expression in proliferating NHU cultures and as with the Wnt3a ligand, it was available as an active ligand secreted by L Wnt-5a cells (96, 97). Wnt5a has been shown to act as both an inhibitor and activator of the canonical Wnt pathway depending on receptor availability. If Fzd4 is present, Wnt5a can activate canonical signalling, however, if the tyrosine kinase ROR2 is present, Wnt5a inhibits the canonical Wnt cascade (Figure 6-2) (123). Affymetrix analysis suggested ROR2 was absent but Fzd4 mRNA was present in proliferating NHU cell cultures and therefore in these circumstances canonical signalling should prevail.

6.4.2 Verification of Wnt secreting L-cell lines

Parental, Wnt-3a and Wnt-5a secreting L cells (originally developed by the Nusse laboratory as stable cell clones (96)) were obtained from Dr. P.Genever (University of York). Cross contamination of L-cell lines was ruled out by RT-

PCR using primers designed against Wnt3a and Wnt5a transcript (Appendix V). Genomic DNA was used as a positive control in all PCR experiments along with a reverse transcriptase negative test for each RNA sample. Integrity of the cDNA was verified using primers targeted to the house-keeping gene, GAPDH. Conditioned medium (CM) from each cell line was harvested in DMEM supplemented with 4mM L-glutamine, 4.5g/L glucose and 10% (v/v) FBS (96, 97) and tested on the Wnt responding osteoblast cell line, SaOS-2 at the recommended dilution of 1:10 in complete growth medium for 24 hours (259). β -catenin nuclear translocation and the TOPFLASH DLA assay were used to assess canonical Wnt pathway activity. 20mM LiCl was used as a positive control for inducing β -catenin activity in both immunofluorescence and TOPFLASH DLA experiments.

6.4.3 Assessing the effect of exogenous Wnt ligand on NHU cells

The effect of exogenous Wnt3a and Wnt5a ligand was assessed on both proliferating and EGFR-blocked NHU cells (pre-treated for 24 hours and maintained in 1 μ M PD153035 throughout the experiment). NHU cell morphology, β -catenin localisation and TOPFLASH DLA activity were assessed. 10 μ M SB415286 was included as a positive control and NHU cell cultures in non-conditioned medium or in CM from the parental L cell line were used as negative controls.

6.4.4 Assessing the impact of low serum concentrations on the production of active Wnt ligand

Over a period of four passages, all three L-cell lines were adapted to grow in low serum conditions (1% (v/v) FBS) and were renamed L Wnt 3a 1%, L Wnt 5a 1% and L-cells 1%, respectively. The effect of reduced serum on Wnt secretion and function was then assessed using the Wnt-responsive

SaOS-2 cell line. β -catenin nuclear translocation and TOPFLASH DLA were used to evaluate the activity of the canonical Wnt pathway after a 24 hour incubation in normal growth medium containing a 1:10 dilution of CM.

6.4.5 Assessing the effect of palmitic acid on the production of active Wnt ligand

20-80 μ M Palmitic acid (solubilised in Ab. EtOH) was added to pre-warmed DMEM supplemented with 4mM L-glutamine, 4.5g/L glucose and 1% (v/v) FBS. L Wnt 3a 1%, L Wnt 5a 1% and L-cells 1% were then incubated in this medium for 3 days. Whole cell lysates were probed with antibodies against Wnt 3a (3A6) and Wnt 5a (C-16) by western blot. CM was tested for its ability to activate the canonical Wnt pathway in SaOS-2 cells as assessed using both immunofluorescence and the TOPFLASH TCF dual luciferase assay (DLA). 20mM LiCl was used as a positive control in all experiments. L-cell only CM was used as a negative control, as well as a solvent-only control (DMEM supplemented with 4mM L-glutamine, 4.5g/L glucose, 1% (v/v) FBS and 0.1% (v/v) EtOH).

6.4.6 Assessing the production of Wnt ligand in NHU cells

AffymetrixTM Genechip data from proliferating, quiescent and differentiated NHU cell cultures was mined for components necessary for Wnt ligand post-translational modification and secretion. MAS5 normalised data obtained from proliferating NHU cell cultures was used to generate a present, absent or marginal "calls" database. Changes in expression were expressed as log₂ fold change relative to the proliferating NHU culture.

NHU cells express mRNA from the following Wnt genes: Wnt3, Wnt5a, Wnt6, and Wnt7a. Of the most interest was Wnt3, as it is a known canonical ligand that signals via Fzd1/7(120, 233). To permit palmitoylation of any potential Wnt proteins, palmitic acid (PA) was added to the growth medium of NHU cells

in two forms: pure palmitic acid (40-80 μ M) solubilised in 0.1%(v/v) EtOH or albumin-bound as a component of FBS. CM was harvested at day 3, filtered and diluted 1:10 into SaOS-2 normal growth medium. SaOS-2 cells were utilised as a responding cell line as they had previously been shown to express, at the mRNA level, a number of Fzd receptors (Fzd 1, 2, 3, 4, 5, 6, 7, 8 and 9) as well as the necessary co-receptors; LRP5 and LRP6 (259-261). Most importantly, the protein expression of Fzd1 receptor (required for Wnt3 signalling) had previously been established via western blot in these cells (262). After a 24 hour incubation with CM, β -catenin nuclear translocation and TOPFLASH DLA assay were used to assess activation of the Wnt pathway. 20mM LiCl was used as a positive control.

6.4.7 Assessing NHU autocrine response to Wnt ligand

NHU cells (Y1056) were pre-treated with 1 μ M PD153035 for 24 hours to inhibit crosstalk via the EGFR. Cultures were then maintained in PD153035 for a further 24 hours with CM from NHU cells grown in the presence of 40-80 μ M PA. β -catenin nuclear translocation was used as a hallmark of canonical Wnt signalling. 10 μ M SB415286 was used as a positive control for β -catenin nuclear translocation.

6.5 Results

6.5.1 Verification of Wnt secreting L-cells

6.5.1.1 RT-PCR

Both Wnt secreting L-cell lines (L Wnt-3a and L Wnt-5a) as well as the L-cell parental control cell line were as described, with no cross contamination (Figure 6-3).

6.5.2 Testing CM from L Wnt-3a and L Wnt 5a cells on SaOS-2 cells

6.5.2.1 Morphology

Photo-micrographs from Wnt-responsive SaOS-2 cells treated with L Wnt-3a, L Wnt-5a or L-cell CM for 24 hours showed no obvious change in morphology (Figure 6-4). A slightly higher number of rounded and detached cells were evident in the SaOS-2 cultures treated with CM compared to the no treatment control but the majority of cells still appeared phase-bright and were firmly attached to the tissue culture flask (Figure 6-4 A-C vs. E).

6.5.2.2 Active β -catenin expression and localisation

In the non-treated SaOS-2 cell cultures, β -catenin localised cytoplasmically (Figure 6-5 E and J), whereas cultures treated with 20mM LiCl (positive control) showed strong nuclear labelling for β -catenin, (Figure 6-5 D and I). Addition of CM from L Wnt-3a cells led to a strong nuclear expression similar in intensity to cultures treated with 20mM LiCl (white arrow heads; Figure 6-5 B and G vs. D and I). Incubation with CM from L Wnt-5a or L-cells showed no translocation of β -catenin to the nucleus (Figure 6-5 C and H; L-Wnt 5a cells, A and F; L-cells).

6.5.2.3 TCF transcription factor activity

Treatment with 20mM LiCl resulted in a significantly higher luciferase activity from TOPFLASH in comparison to FOPFLASH (8-fold increase in activity TOPFLASH vs. FOPFLASH; Figure 6-6, $P < 0.001$) and verified the integrity of the assay. Normalised TCF DLA data revealed a significant higher TOPFLASH luciferase activity compared to FOPFLASH when SaOS-2 cultures were incubated with L Wnt-3a CM (TOPFLASH activity was 16-fold higher than in the FOPFLASH control; Figure 6-6 $P < 0.001$). Cultures incubated with L Wnt-5a CM and L cell control CM did not evoke any significant TCF activity in SaOS-2 cells (Figure 6-5). These data verified that Wnt 3a ligand secreted from L Wnt-3a was active and able to elicit a response in cells expressing the appropriate Fzd receptor.

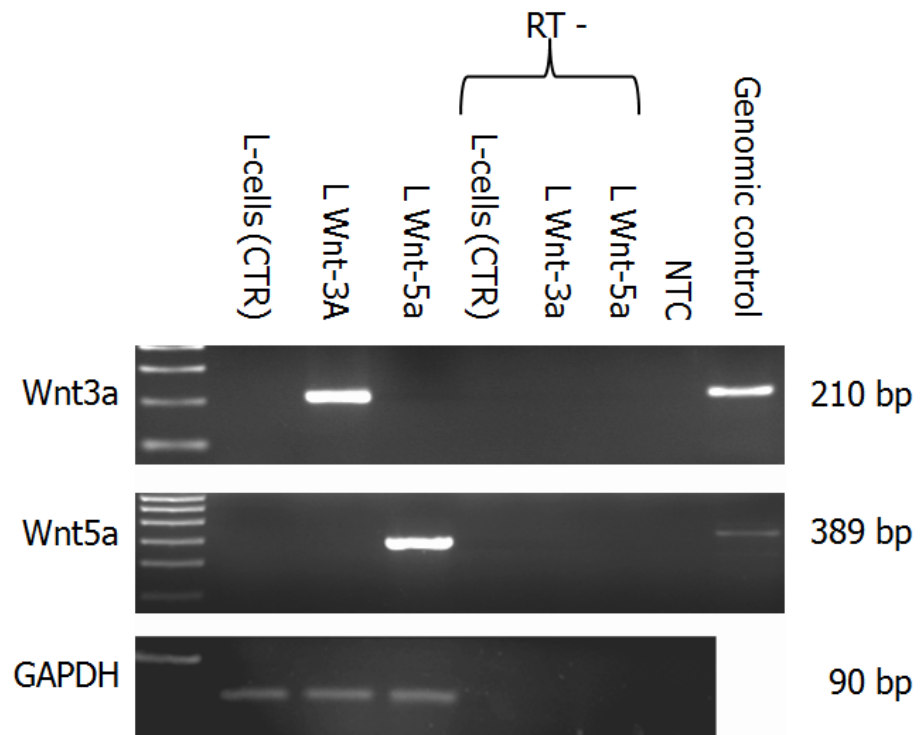


Figure 6-3 Cross contamination analysis of Wnt secreting L-cells using RT-PCR

Wnt secreting L-cells (L Wnt-3a and L Wnt-5a) as well as the parental control L-cell line were tested for cross-contamination via RT-PCR. RNA was extracted using TRIzol™ reagent and converted to cDNA using the Superscript first-strand cDNA synthesis kit. PCR was performed using primers designed to mouse Wnt3a and Wnt5a using Surestart Taq polymerase and PCR products were run on a 1% (w/v) agarose gel and visualised using UV trans-illumination. PCR for Wnt3a and Wnt5a confirmed that none of the cell lines were cross contaminated. Genomic DNA was used as a template control. Water only was used as the no template control (NTC). GAPDH was used as a positive control to verify intact cDNA. RT negatives were included to certify that there was no gDNA contamination in the cDNA. N=1.

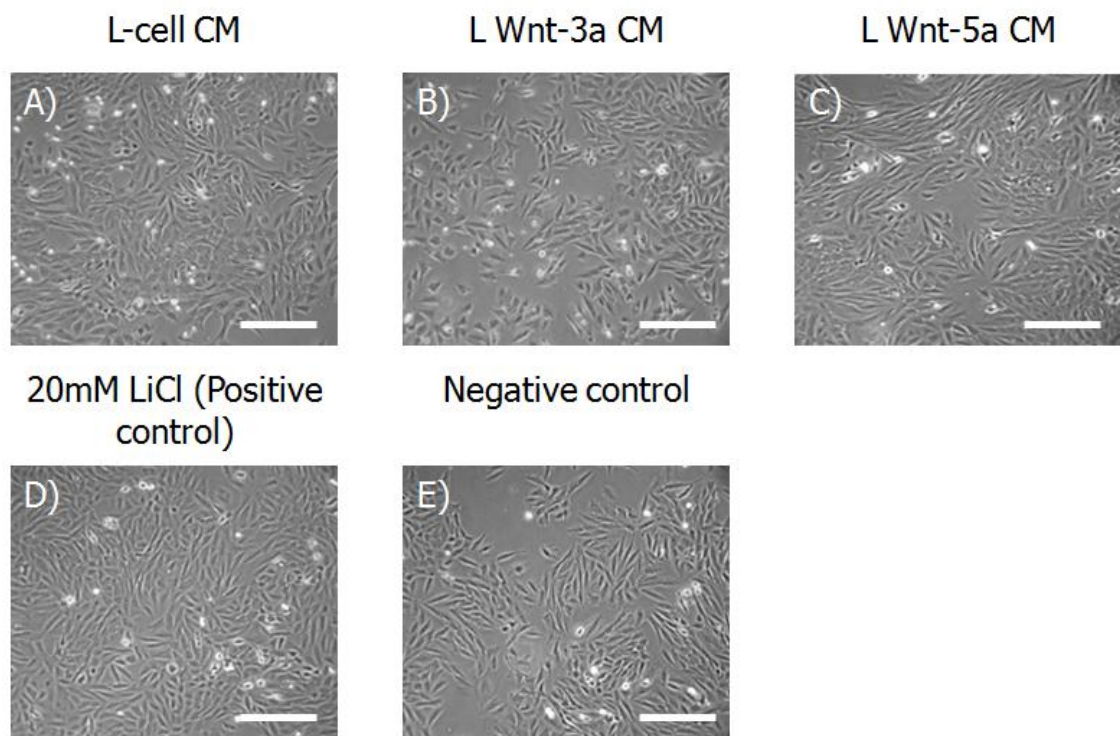


Figure 6-4 Effect of L Wnt-3a and L Wnt-5a CM on SaOS-2 cell morphology

Phase contrast micrographs of SaOS-2 cells after a 24 hour incubation with CM from L cells, L Wnt-3a or L Wnt-5a diluted 1:10 with normal growth medium (McCoys 5A + 15% (v/v) FBS) **(A)** L-cell CM (parental control); **(B)** L Wnt-3a CM; **(C)** L Wnt-5a CM; **(D)** 20mM LiCl (destruction complex inhibitor; positive control), **(E)** Negative control (no treatment). Scale bar: 200 μ m.

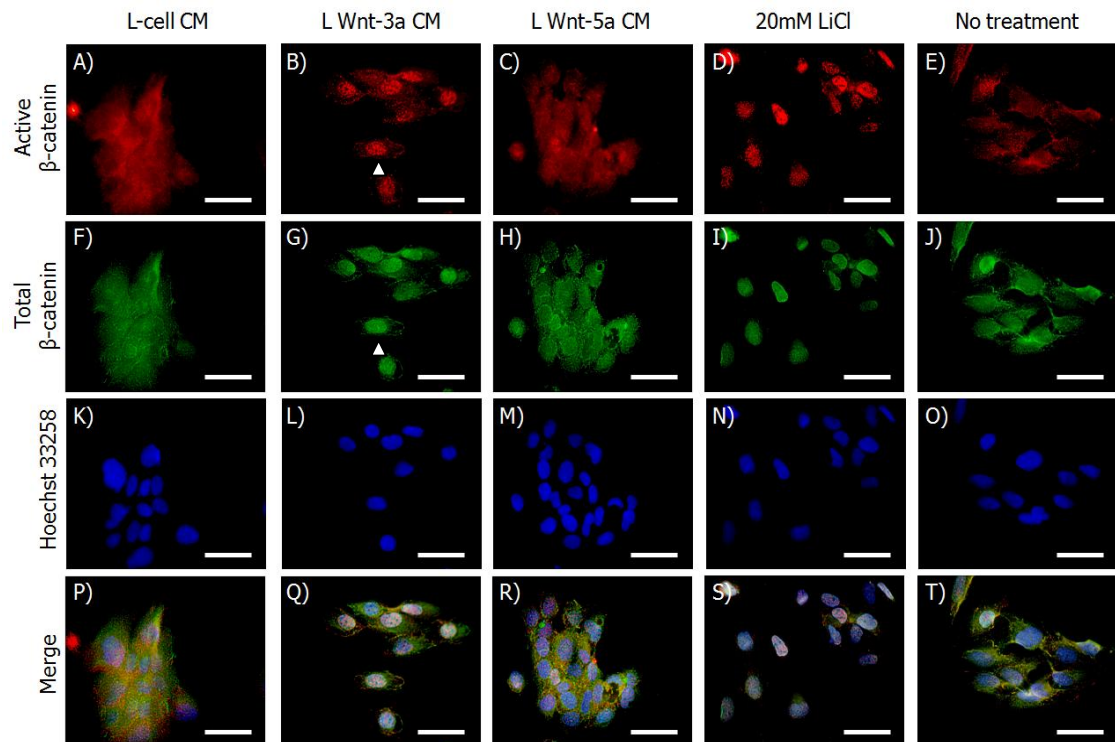


Figure 6-5 Effect of L Wnt-3a and L Wnt-5a CM on β -catenin expression and localisation in SaOS-2 cells

Indirect immunofluorescent labelling of SaOS-2 cells for β -catenin after a 24-hour incubation with L Wnt-3a, L Wnt-5a or L-cell (parental control) CM diluted 1:10 in normal growth medium (McCoy's 5A + 15% (v/v) FBS). Slides were formalin-fixed and immunolabelled with active β -catenin antibody (8E7) and rabbit anti-mouse IgG-Alexa 594 secondary antibody or total β -catenin (C2206) and goat anti-rabbit IgG Alexa 488 secondary antibody. All slides were stained with Hoechst 33258 to delineate the nucleus and labelling was visualised under epifluorescent illumination. **(A-E)** Labelling with active β -catenin antibody (8E7); **(F-J)** Labelling with total β -catenin antibody (C2206); **(K-O)** Hoechst 33258 staining of the nucleus; **(P-T)** Merged active, total and Hoechst 33258 stain. 20mM LiCl treatment was used as a positive control for β -catenin nuclear labelling. Negative controls were L-cell (parental control) CM and non-treated SaOS-2 cells. Scale bar: 50 μ m. N=1. White arrow heads denote strong nuclear labelling after treatment with L Wnt-3a CM.

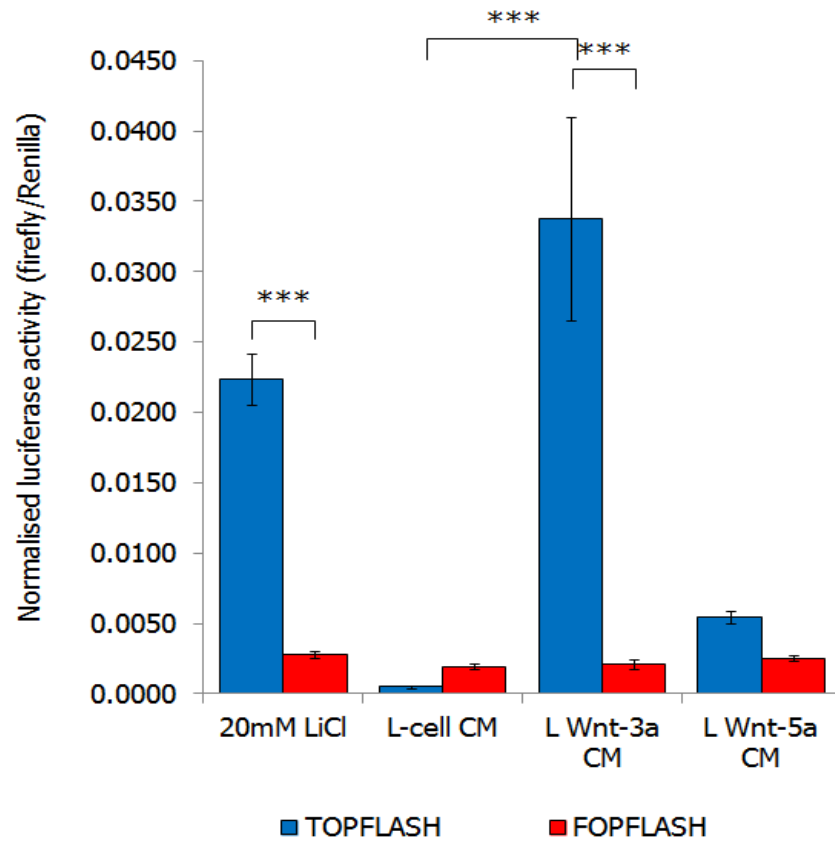


Figure 6-6 TCF activity in SaOS-2 cells after treatment with L Wnt 3a or L Wnt-5a CM

SaOS-2 cells were seeded into a 24-well plate at 4×10^4 cells per well and were transfected 24-hours after seeding with either 0.5 μ g of TOPFLASH or FOPFLASH (negative control) plasmid along with 0.01 μ g of loading control, pRL-CMV. 24 hours after transfection, SaOS-2 cells were incubated with a 1:10 dilution of L Wnt-3a, L Wnt-5a or L-cell CM mixed with normal growth medium (McCoys 5A + 15% (v/v) FBS). After 24 hours, cells were lysed and a dual luciferase assay was performed on 3 biological replicates. Positive control was 20mM LiCl. Negative control was CM from L-cell parental control cell line. Data represents the mean luciferase activity after normalisation to loading control (\pm SD).*** P<0.001, using a one-way ANOVA with Bonferroni multiple post-test comparison.

6.5.3 Effect of adding exogenous Wnt 3a and Wnt 5a ligand to NHU cells

6.5.3.1 Morphology

When NHU cells were incubated with a 1:10 dilution of CM from L Wnt-3a, L Wnt-5a or parental control, cultures were seen to adopt a more differentiated morphology similar in appearance to cultures treated with 5% (v/v) ABS/2mM CaCl₂. This change in morphology was attributed to the fact that serum was present in the CM (Figure 6-7).

6.5.3.2 Active β -catenin expression and localisation

A 24-hour incubation of sub-confluent NHU cells with a 1:10 dilution of CM from either L Wnt-3a, L Wnt-5a or parental control did not increase the amount of nuclear active β -catenin compared to no-treatment control (Figure 6-8). Addition of CM from all three L-cell lines did however lead to an increase in β -catenin expression at the cell membrane (Figure 6-8; white arrow heads). This was indicative of adherens junction engagement probably driven by the increase in calcium ions present in the CM (1.8mM in undiluted DMEM). Nuclear expression of active β -catenin was evident in all samples, including the no treatment control (Figure 6-8). Expression and localisation of active β -catenin was very different when cultures were pre-treated and maintained in 1 μ M PD153035 throughout the experiment. NHU which were not exposed to CM had very low levels of nuclear active- β -catenin with only diffuse cytoplasmic labelling visible (Figure 6-8; white arrow). Some cells labelled for active β -catenin at the membrane as previously seen with PD153035 treatment. Cells appeared enlarged and flattened as has previously been described after EGFR blockade (207). Incubation with CM from either L Wnt-3a or L Wnt-5a resulted in strong nuclear as well as membrane labelling for active β -catenin which was as intense as the positive control (10 μ M SB415286) (Figure 6-8; grey arrow

heads). Treatment with L-cell CM had no effect on nuclear or membrane labelling for active β -catenin when compared to the no treatment control (Figure 6-8;white arrow).

6.5.3.3 TCF activity

TCF DLA revealed no statistically significant increase in TCF activity when sub-confluent NHU cells were incubated for 24 hours with a 1:10 dilution of L Wnt-3a, L Wnt-5a or L-cell control CM in KSFMc (Figure 6-9). TCF activity did however increase significantly when cells were pre-treated and maintained in PD153035 NHU and incubated with either L Wnt-3a, or L Wnt-5a (Figure 6-9; $P < 0.001$ compared to L-cell parental control CM).

These results implied that NHU cells responded canonically to both Wnt3a and Wnt5a ligand but only when crosstalk from the EGFR signalling cascade was blocked.

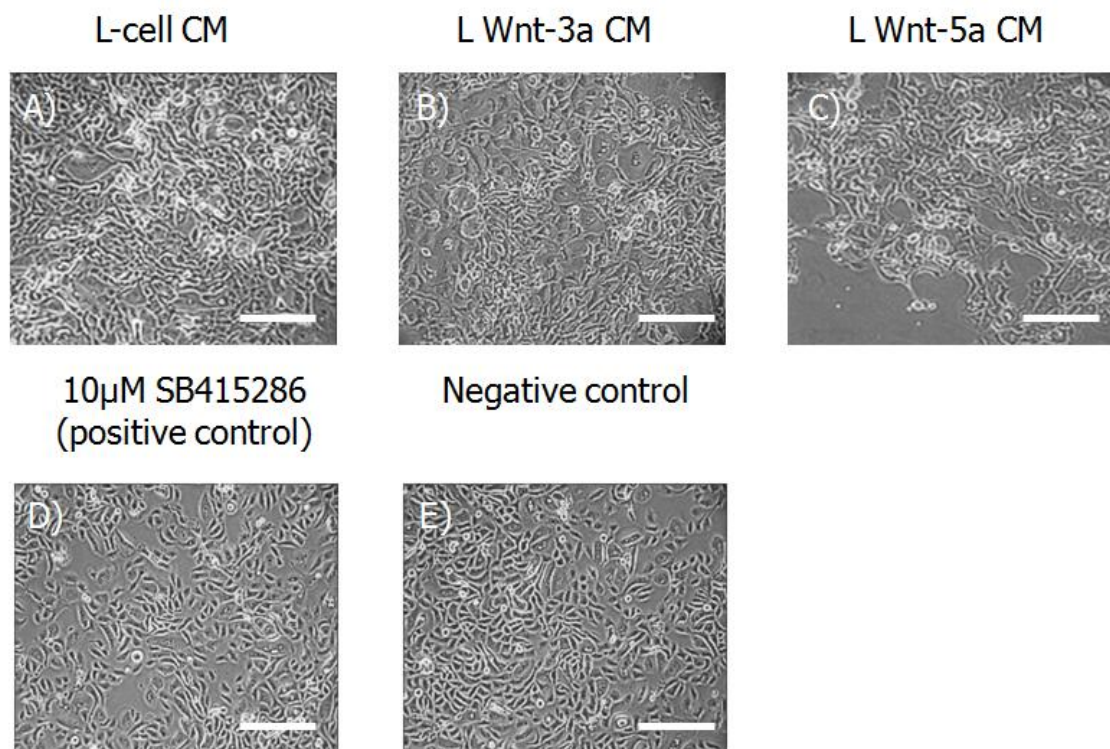


Figure 6-7 Effect of Wnt 3a and Wnt5a CM on NHU cell morphology

Phase contrast micrographs of NHU cells (Y1056) after a 24-hour incubation with CM from Wnt3a and Wnt5 secreting L-cells diluted 1:10 with normal growth medium (KSFMc) **(A)** L-cell CM; **(B)** L Wnt-3a CM; **(C)** L Wnt-5a CM; **(D)** 10µM SB415286 (destruction complex inhibitor; positive control), **(E)** Negative control (no treatment). A 24 hour incubation with CM from Wnt-secreting L-cells caused NHU cells to adopt a differentiated appearance. Scale bar: 200µm.

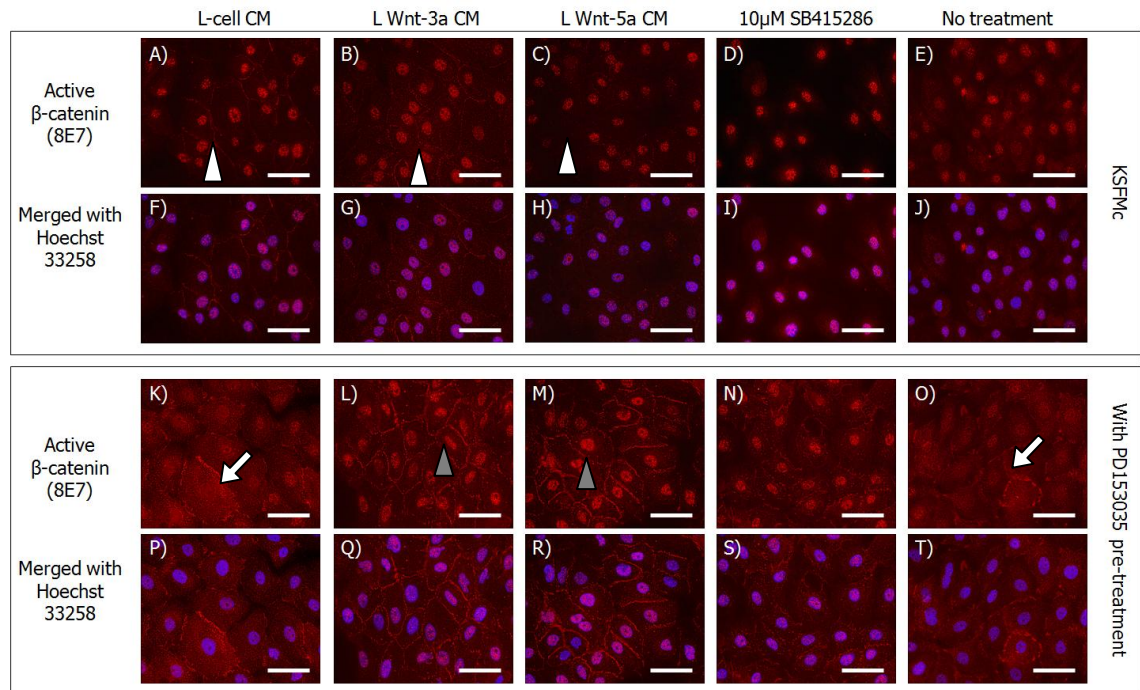


Figure 6-8 Effect of Wnt 3a and Wnt5a CM on β -catenin expression and localisation in EGF responsive and EGFR blocked NHU cells

β -catenin indirect immunofluorescent labelling of NHU cells (Y1056) after a 24-hour pre-treatment with $\pm 1\mu\text{M}$ PD153035 followed by a 24-hour incubation $\pm 1\mu\text{M}$ PD153035 with L Wnt-3a, L Wnt-5a or L-cell CM diluted 1:10 in normal growth medium (KSFMc). Slides were formalin-fixed and immunolabelled with active β -catenin antibody (8E7) and rabbit anti-mouse IgG-Alexa 594 secondary antibody. All slides were stained with Hoechst 33258 to delineate the nucleus and labelling was visualised under epi-fluorescent illumination. **(A-E)** Active β -catenin antibody (8E7) labelling in non-PD153035 pre-treated NHU cells; **(F-J)** Active β -catenin labelling merged with Hoechst 33258 staining **(K-O)** Active β -catenin labelling (8E7) in $1\mu\text{M}$ PD153035 pre-treated and maintained NHU cells; **(P-T)** Active β -catenin labelling merged with Hoechst 33258 staining. $10\mu\text{M}$ SB410286 treatment was used as a positive control for β -catenin nuclear translocation. Negative controls were L-cell CM and non-treated (no CM) NHU cells. White arrow heads denote membrane labelling due to the increase in exogenous calcium concentrations and adherens junction formation. Scale bar: $50\mu\text{m}$. $N=1$. Grey arrow heads denote strong nuclear labelling after incubation with L Wnt-3a or L Wnt-5a CM. White arrows denote weak nuclear labelling in PD153035 pre-treated cultures and after incubation with PD153035 and L-cell CM.

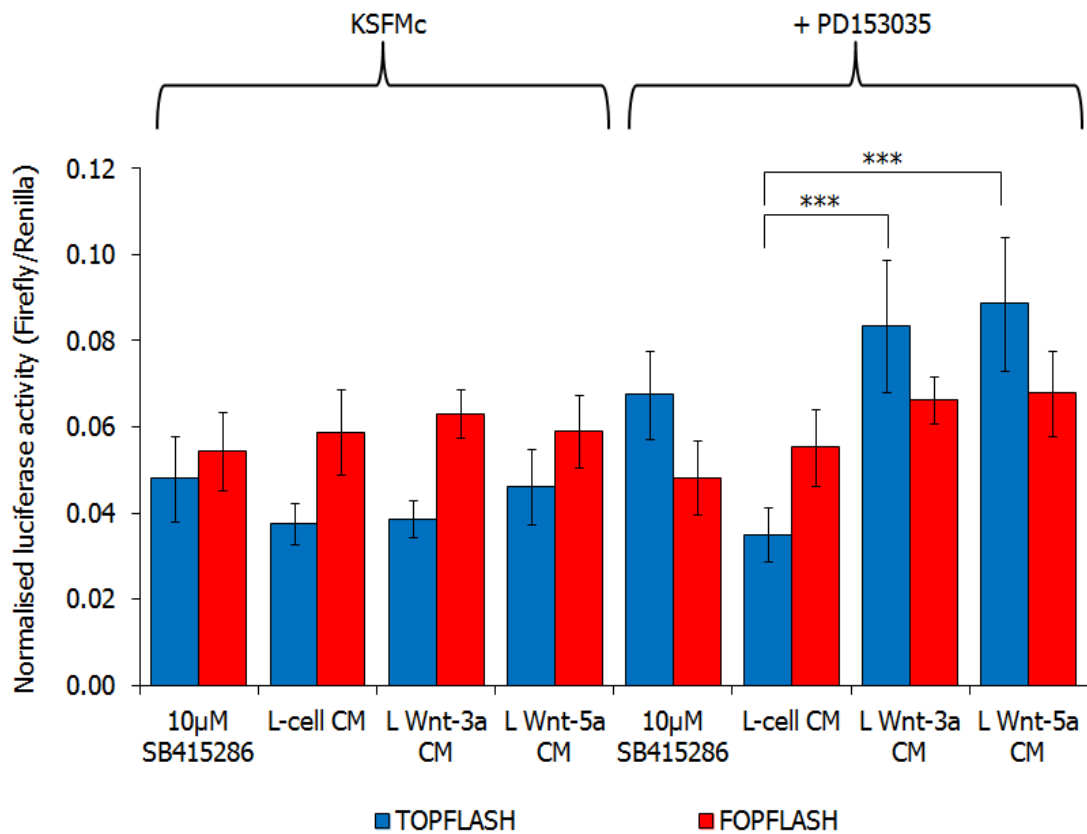


Figure 6-9 TCF activity in EGF responsive and EGFR blocked NHU cells after treatment with L Wnt 3a and L Wnt-5a CM

NHU cells (Y1056) were seeded into a 24-well Primaria® plate at 4×10^4 cells per well and were transfected 24-hours after seeding with either 0.5µg of TOPFLASH or FOPFLASH (negative control) plasmid along with 0.01µg of loading control, pRL-CMV. 6 hours after transfection, cells were medium changed to KSFMc \pm 1µM PD153035 for 24 hours (pre-treatment) and then incubated with a 1:10 dilution of either L Wnt-3a, L Wnt-5a or L-cell CM mixed with normal growth medium (KSFMc) \pm 1µM PD153035. After 24 hours, cells were lysed and a dual luciferase assay was performed on 3 biological replicates. Positive control was 10µM SB415286. Data represents the mean luciferase activity after normalisation to loading control (\pm SD). (***) $P < 0.001$, using a one-way ANOVA with Bonferroni multiple post-test comparison). Results revealed a significant increase in TCF activity when NHU cells were treated with L Wnt-3a and L Wnt-5a but only when EGFR signalling was blocked with PD153035.

6.5.4 The effect of reduced serum on the production and secretion of Wnt ligand

6.5.4.1 Expression and localisation of β -catenin in Wnt responding SaOS-2 cells

When harvested in 10% FBS, L Wnt-3a CM clearly resulted in nuclear translocation of β -catenin in SaOS-2 cells. (Figure 6-5). This however was not the case when L Wnt-3a cells were adapted to grow in low serum 1% (v/v) FBS (L Wnt-3a 1%). A 24 hour treatment of SaOS-2 cells with a 1:10 dilution of CM from L Wnt-3a 1% resulted in only cytoplasmic expression of β -catenin and no visible nuclear translocation suggesting bioactive Wnt 3a was not being secreted (Figure 6-10; white arrow heads).

6.5.4.2 Effect on TCF activity in SaOS-2 cells

A 24 hour incubation with a 1:10 dilution of CM from L Wnt-3a 1% did not elicit any TCF activity in SaOS-2 cells (Figure 6-11). TOPFLASH luciferase activity was less than that observed from the FOPFLASH mutant TCF luciferase plasmid, FOPFLASH (Figure 6-11). Data thus implied that either Wnt 3a ligand was not being processed or secreted properly by the low serum-adapted L Wnt-3a 1% cell line.

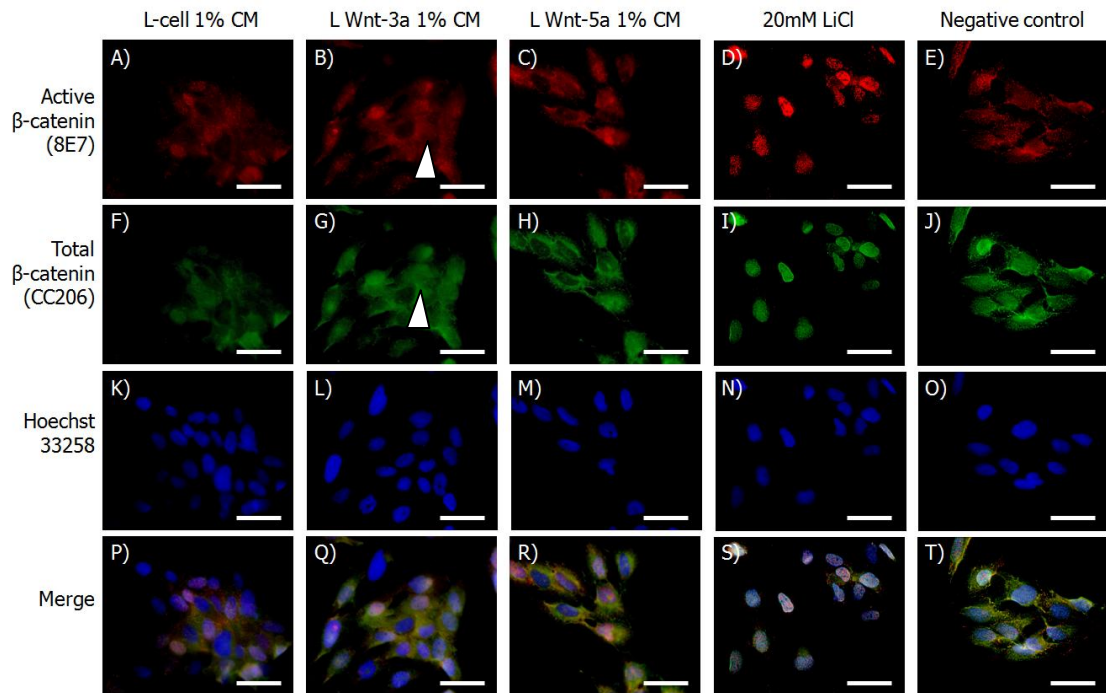


Figure 6-10 Effect of culturing Wnt secreting L-cells in low serum

β -catenin indirect immunofluorescent labelling of SaOS-2 cells after a 24-hour incubation with L Wnt-3a 1%, L Wnt-5a 1% or L-cell 1% CM diluted 1:10 in normal SaOS-2 growth medium (McCoy's 5A + 15% (v/v) FBS). Slides were formalin-fixed and immunolabelled with active β -catenin antibody (8E7) and rabbit anti-mouse IgG-Alexa 594 secondary antibody or total β -catenin (C2206) and goat anti-rabbit IgG Alexa 488 secondary antibody. All slides were stained with Hoechst 33258 to delineate the nucleus and labelling was visualised under epifluorescent illumination. **(A-E)** Labelling with active β -catenin antibody (8E7); **(F-J)** Labelling with total β -catenin antibody (C2206); **(K-O)** Hoechst 33258 staining of the nucleus; **(P-T)** Merged active, total and Hoechst 33258 stain. 20mM LiCl treatment was used as a positive control for β -catenin nuclear labelling. Negative controls were L-cell 1% CM and non-treated SaOS-2 cells. Scale bar: 50 μ m. N=1. White arrow heads denote lack of nuclear labelling after treatment with L Wnt-3a 1% CM.

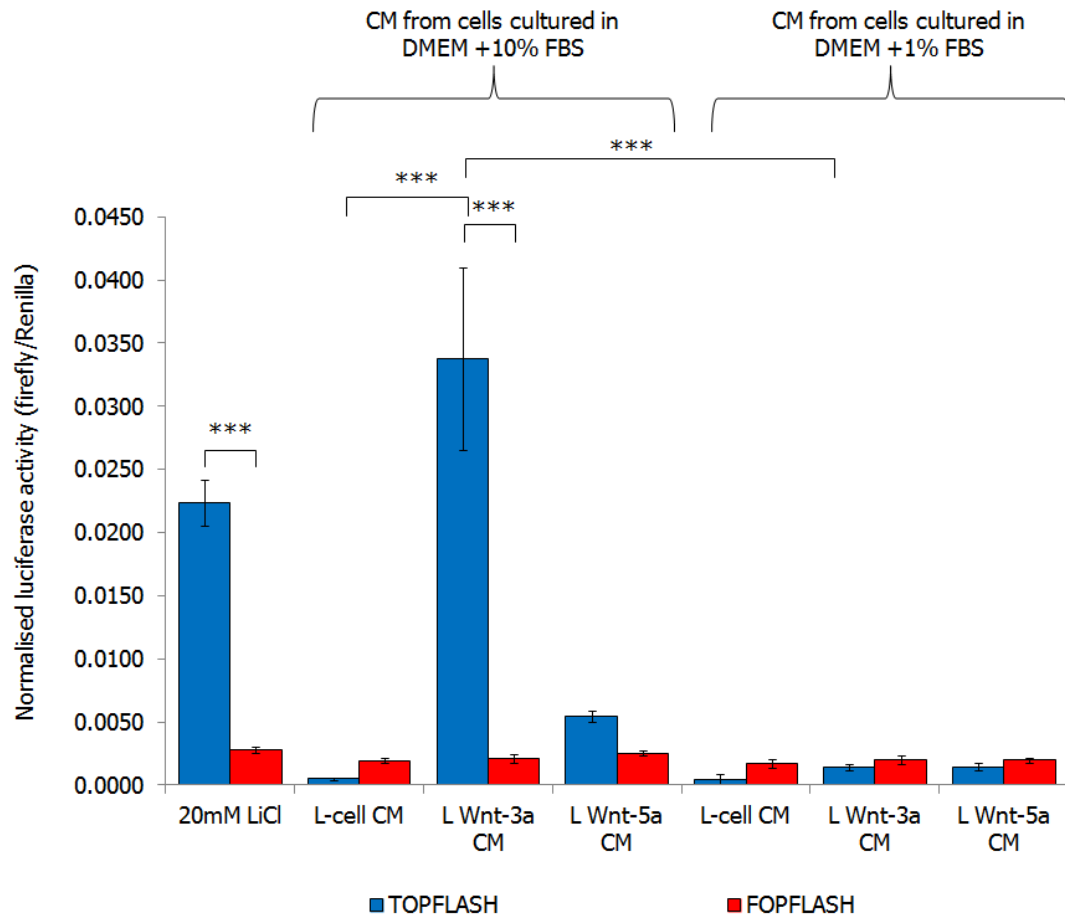


Figure 6-11 TCF assay from SaOS-2 cells after treatment with CM from L-cells grown in low serum

SaOS-2 cells were seeded into a 24-well Primaria® plate at 4×10^4 cells per well and were transfected 24-hours after seeding with either 0.5 μ g of TOPFLASH or FOPFLASH (negative control) plasmid along with 0.01 μ g of loading control, pRL-CMV. 24 hours after transfection, SaOS-2 cells were incubated with a 1:10 dilution of CM from Wnt secreting L-cells cultured in high serum (10%(v/v) FBS) or low serum (1%(v/v) FBS). After 24 hours, cells were lysed and a dual luciferase assay was performed on 3 biological replicates. Positive control was 20mM LiCl. Data represents the mean luciferase activity after normalisation to loading control (\pm SD). (***) $P < 0.001$, using a one-way ANOVA with Bonferroni multiple post-test comparison). Adaptation of Wnt secreting L-cells to low serum resulted in no functional Wnt ligand being secreted.

6.5.5 The role of palmitic acid in the production and secretion of Wnt Ligand

6.5.5.1 Expression of Wnt protein in L Wnt-3a and L Wnt-5a cell lines

Whole cell lysates were generated and analysed for Wnt protein by western blot. L Wnt-3a 1% cell line supplemented with 40 μ M PA, 80 μ M PA or 10% (v/v) FBS labelled weakly with the anti-Wnt3a antibody (3A6) at the expected molecular weight of 39KDa (Figure 6-12). This band was not evident in the parental L-cell line or the L Wnt-5a cell line suggesting that it was specific for Wnt3a. Multiple bands were visualised with the anti-Wnt5a antibody (C16) and was therefore deemed non-specific (Figure 6-12). Normalised densitometry results for Wnt 3a revealed a >3.4-fold increase in band intensity when L Wnt-3a cells were incubated in 80 μ M palmitic acid compared to solvent balanced control (Figure 6-13) and was only slightly less than that observed with 10% (v/v) FBS (3.7-fold; Figure 6-13).

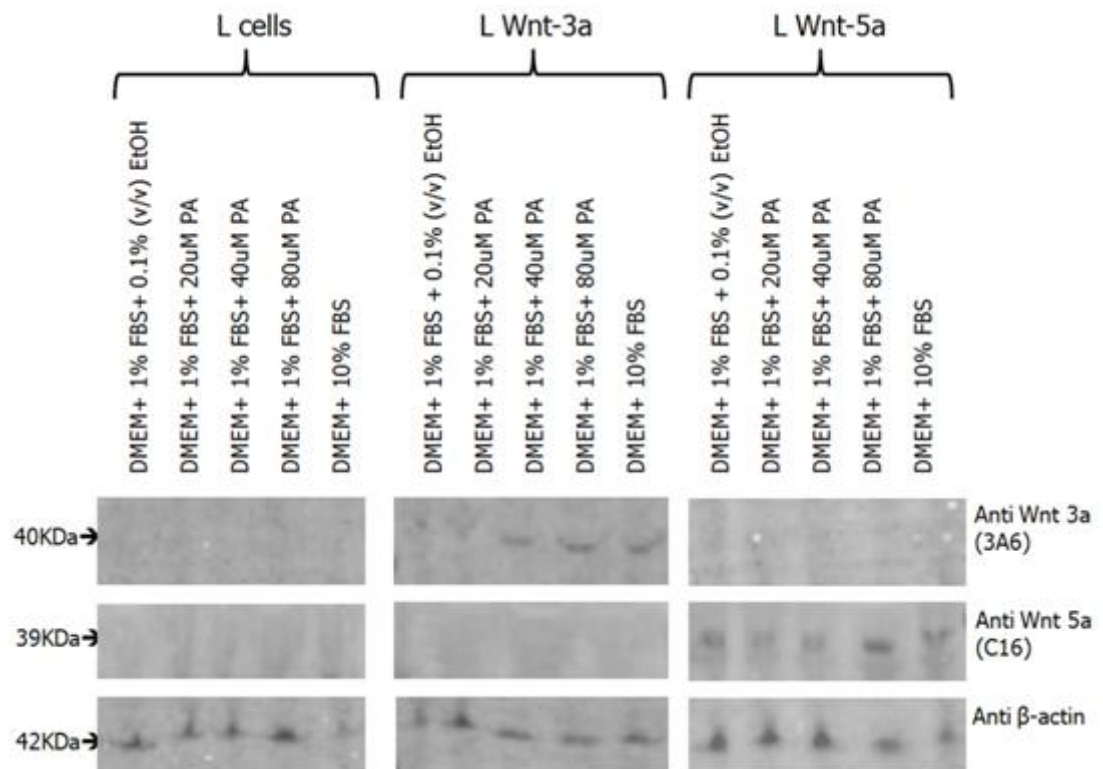


Figure 6-12 Assessing the effect of palmitic acid on Wnt ligand production

Whole cell lysates were taken from L Wnt-3a 1%, L Wnt-5a 1% and L-cell 1% lines after a 3-day treatment with 20-80 μ M palmitic acid in DMEM, 4mM L-glutamine, 4.5g/L glucose + 1% (v/v) FBS. Positive and negative controls were 10% (v/v) FBS and 0.1%(v/v) EtOH (solvent only), respectively. 20 μ g of each protein lysate was subjected to SDS-PAGE within a 4-12% (w/v) Bis-Tris gel under denaturing conditions and immunoblotted onto PVDF membrane. Western blots were probed with anti-Wnt 3a (3A6), anti-Wnt 5a (C16) and β -actin (AC-15; to control for equal lysate loading). Membranes were then incubated for 1 hour with either; goat anti-mouse IgG Alexa 680 for Wnt 3a and β -actin or donkey anti-goat IgG Alexa 680 for Wnt-5a. Antibody binding was visualised by epi-fluorescence illumination at 700nm. N=1.

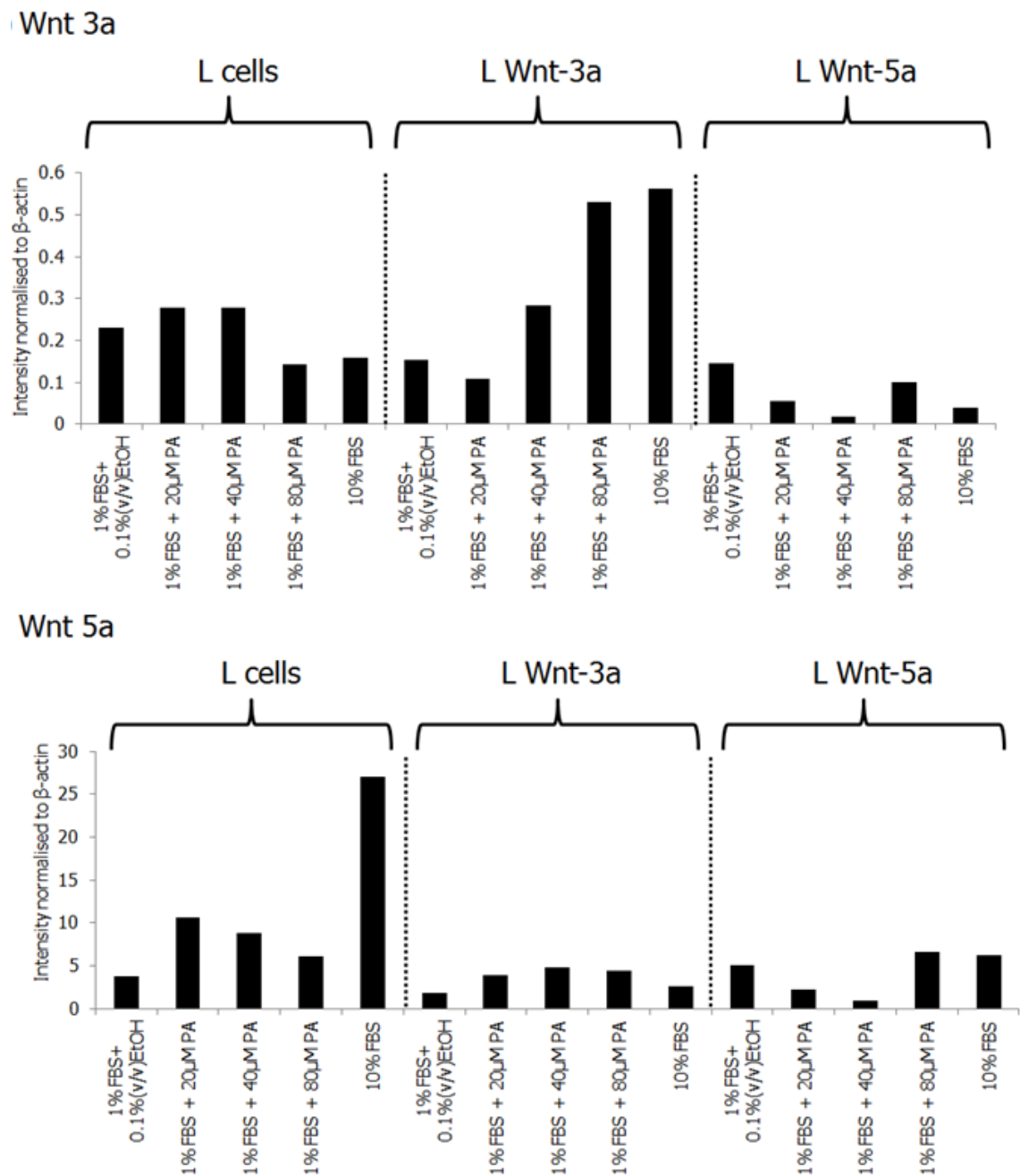


Figure 6-13 Normalised densitometry from western blots assessing the effect of palmitic acid on Wnt ligand production

Normalised Densitometry results from Figure 6-12 represented graphically as bar charts.

6.5.5.2 Active β -catenin expression and localisation in SaOS-2 cells

Indirect-immunofluorescence with active and total β -catenin antibodies was undertaken on SaOS-2 cells after a 24 hour incubation with a 1:10 dilution of CM from L Wnt-3a 1% or L-cell 1% cell lines which were cultured in the presence of 20-80 μ M palmitic acid. As expected, CM from L-cells did not evoke a response in SaOS-2 cells regardless of the harvesting conditions (Figure 6-14). Both active and total β -catenin antibodies labelled the nuclear compartment of SaOS-2 cells when incubated with L Wnt-3a CM harvested in the presence of 40 or 80 μ M palmitic acid (Figure 6-15). No nuclear labelling was visible in the solvent balanced control (Figure 6-15).

6.5.5.3 TCF activity in SaOS-2 after treatment with CM from L Wnt-3a 1% cells cultured in medium supplemented with palmitic acid

Addition of 40 μ M or 80 μ M PA to the growth medium of L Wnt-3a 1% resulted in a significant higher TOPFLASH luciferase activity in SaOS-2 cells than that observed in the solvent balanced control culture (L Wnt-3a 1% + 0.1% (v/v) EtOH, $P > 0.001$; Figure 6-16). Normalised TOPFLASH luciferase activity from CM containing 40-80 μ M PA was ~1.8-2.0- fold higher than that obtained from L-Wnt-3a 1% cultures grown without additional PA (Figure 6-16). Activity was however not as strong as that observed from L Wnt-3a cultures incubated with 10 (v/v) FBS (normalised activity was 0.030, 0.027 from CM harvested in 40 and 80 μ M PA, respectively and 0.042 from CM harvested in 10%(v/v) FBS; Figure 6-16). This data along with the immunofluorescence results substantiated the role of palmitic acid in the proper processing and secretion of Wnt ligand *in vitro* and suggested that high serum concentrations (10% (v/v)FBS) could in part be substituted for by palmitic acid alone.

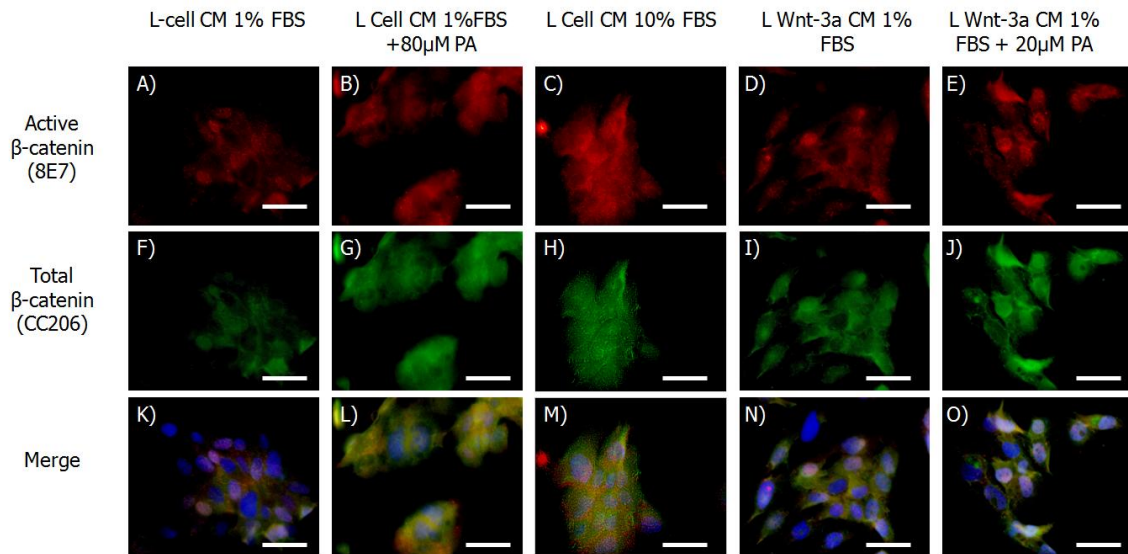


Figure 6-14 Assessing activation of the canonical Wnt pathway in SaOS-2 cells after treatment with CM from L Wnt 3a 1% cells cultured in the presence of palmitic acid

β -catenin indirect immunofluorescent labelling of SaOS-2 cells after a 24-hour incubation with a 1:10 dilution of CM from L Wnt-3a 1% or L-cell 1% cell lines cultured with 20-80 μ M Palmitic acid. Slides were formalin-fixed and immunolabelled with active β -catenin antibody (8E7) and rabbit anti-mouse IgG-Alexa 594 secondary antibody or total β -catenin (C2206) and goat anti-rabbit IgG Alexa 488 secondary antibody. All slides were stained with Hoechst 33258 to delineate the nucleus and labelling was visualised under epi-fluorescent illumination. 20mM LiCl treatment was used as a positive control (fig 6-15). Negative control was non-treated SaOS-2 cells (fig 6-15). Scale bar: 50 μ m. N=1.

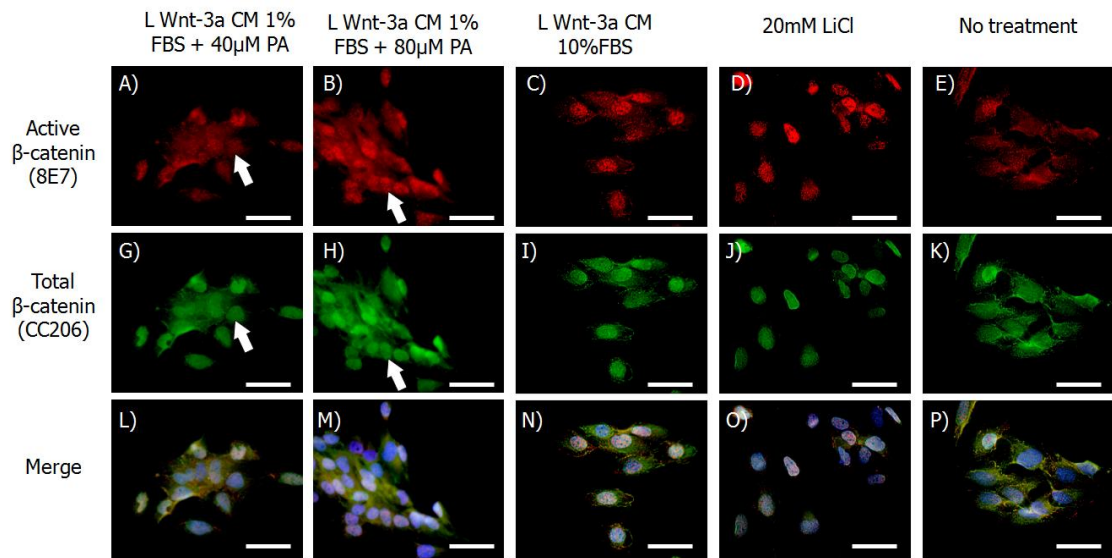


Figure 6-15 Assessing activation of the canonical Wnt pathway in SaOS-2 cells after treatment with CM from L Wnt 3a 1% cells cultured in the presence of palmitic acid

β -catenin indirect immunofluorescent labelling of SaOS-2 cells after a 24-hour incubation with a 1:10 dilution of CM from L Wnt-3a 1% or L-cell 1% cell lines cultured with 20-80 μ M Palmitic acid. Slides were formalin-fixed and immunolabelled with active β -catenin antibody (8E7) and rabbit anti-mouse IgG-Alexa 594 secondary antibody or total β -catenin (C2206) and goat anti-rabbit IgG Alexa 488 secondary antibody. All slides were stained with Hoechst 33258 to delineate the nucleus and labelling was visualised under epi-fluorescent illumination. 20mM LiCl treatment was used as a positive control. Negative control was non-treated SaOS-2 cells. Scale bar: 50 μ m. N=1. White arrows denote strong nuclear labelling when cells were treated with CM from L Wnt-3a 1% + 40 μ M PA and from L Wnt-3a 1% + 80 μ M PA.

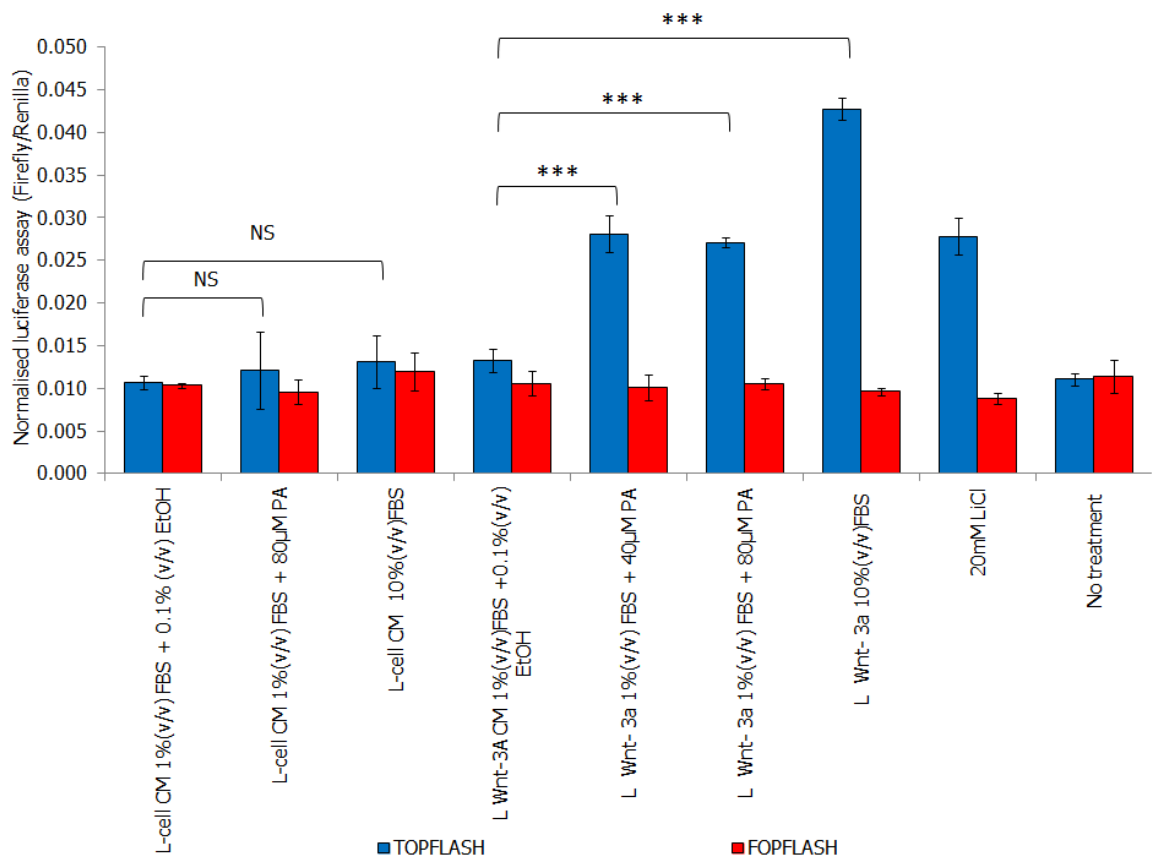


Figure 6-16 Assessing TCF activity in SaOS-2 cells after treatment with CM from L Wnt 3a 1% cells cultured in the presence of palmitic acid

SaOS-2 cells were incubated with a 1:10 dilution of CM from Wnt secreting L-cells cultured in: high serum (10% FBS): low serum (1% FBS) or low serum + 40-80µM PA. After 24 hours, cells were lysed and a dual luciferase assay was performed on 3 biological replicates. Positive control was 20mM LiCl. Negative controls were solvent balanced CM containing 0.1% (v/v) EtOH and no treatment control. Data represents the mean luciferase activity after normalisation to loading control (\pm SD). (***) $P < 0.001$, NS non-significant using a one-way ANOVA with Bonferroni multiple comparison post-test). Low serum in the growth medium of L-Wnt-3a cell cultures resulted in poor Wnt ligand secretion into the medium but this could be improved by the addition of PA.

6.5.6 Assessing the production of Wnt ligand in NHU cells

6.5.6.1 Gene Microarray analysis

Previously validated and ranked Affymetrix™ data (chapter 3) was mined for components of the Wnt post-translation and secretory pathway. In the proliferative NHU culture, PORCN was classified as present by the MAS5 generated calls database, as well as WLS and all three components of the retromer cargo-recognition complex (Vps26a, Vps29 and Vps35; Table 6-2). The data set was then mined for changes in the Wnt ligand processing and secretory pathway after differentiation or quiescence. No striking differences were observed in expression. Only WLS mRNA expression significant changed (>2-fold) in the TZ/PD culture and was not mirrored in the ABS/Ca model (Table 6-2).


Gene	Function	MAS5 call in proliferative culture (Absent, Present, Marginal)	Fold change vs. Proliferative culture (log2)		
			Quiescent	TZ/PD	ABS/Ca
PORCN	Required for acylation	Present	0.16	-0.33	-0.54
WLS	Required for transport to membrane	Present	0.04	-1.12 	-0.94
Vps35	Recycling of WLS	Present	-0.10	-0.50	0.05
Vps26a		Present	-0.15	-0.28	-0.26
Vps29		Present	-0.44	-0.06	-0.04

Table 6-2 Genes necessary for production of functional Wnt ligand

MAS5 normalised Affymetrix™ mRNA microarray analysis of components of the Wnt ligand post-translational processing and secretory pathway in cultures of proliferating, quiescent and differentiated (TZ/PD and ABS/Ca) NHU cells (Y676). Genes with at least a 2-fold change in expression compared to the proliferative culture are highlighted with either a red (up-regulated) or green arrow (down-regulated). Actual changes in mRNA expression are detailed within the table and are expressed as signal log ratios (log base 2).

6.5.6.2 Morphology of NHU cells after PA treatment

NHU cells cultured for 3 days with palmitic acid appeared morphologically similar to the solvent-balanced control and to the no-treatment control (Figure 6-17). A slightly higher proportion of rounded and detached cells were evident in the culture treated with 80 μ M PA. All cultures appeared to be at a similar density (Figure 6-17).

6.5.6.3 Active β -catenin expression and localisation in SaOS-2 cells after treatment with CM from NHU cells

SaOS-2 cells were incubated for 24 hours with a 1:10 dilution of CM from NHU cultured in KSFMc \pm 40-80 μ M palmitic acid; 10% (v/v) FBS or solvent only control (0.1% (v/v) EtOH). When labelled with the active β -catenin antibody (8E7) it was evident that CM from NHU cells incubated in the presence of 10% (v/v) FBS or 80 μ M PA did evoke clear nuclear translocation of β -catenin (White arrows; Figure 6-18 B and G). Labelling was however not as intense as that seen with 20mM LiCl treatment (Figure 6-18). CM from NHU cells which had been harvested in the presence of 40 μ M PA showed some nuclear labelling but the majority of cells labelled only cytoplasmically (white arrow heads; Figure 6-18C). CM from solvent balanced NHU cell cultures did not evoke any nuclear translocation of β -catenin in SaOS-2 cells (Figure 6-18 panel A).

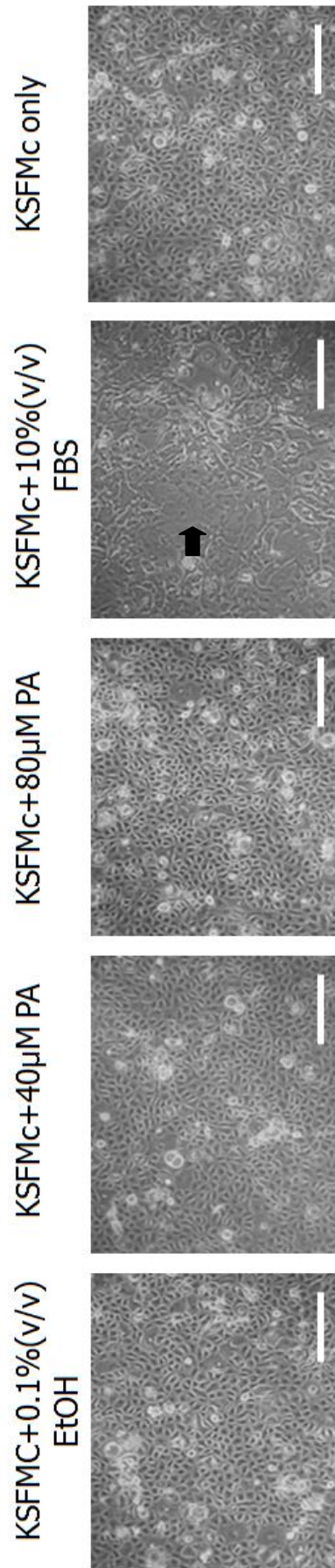


Figure 6-17 Morphology of NHU cells after a 3-day incubation in KSFMC supplemented with palmitic acid

Phase contrast micrographs of NHU cells (Y1056) after a 3-day incubation with KSFMC \pm 20-80 μ M PA in 0.1% (v/v) EtOH or 10% (v/v) FBS. 72-hour incubation with PA appeared to have little effect on cell morphology whereas addition of FBS at a final concentration of 10% (v/v) resulted in NHU cells adopting a more differentiated phenotype with loss of bright cell borders and an increase in stratification (black arrow). Scale bar: 200 μ m.

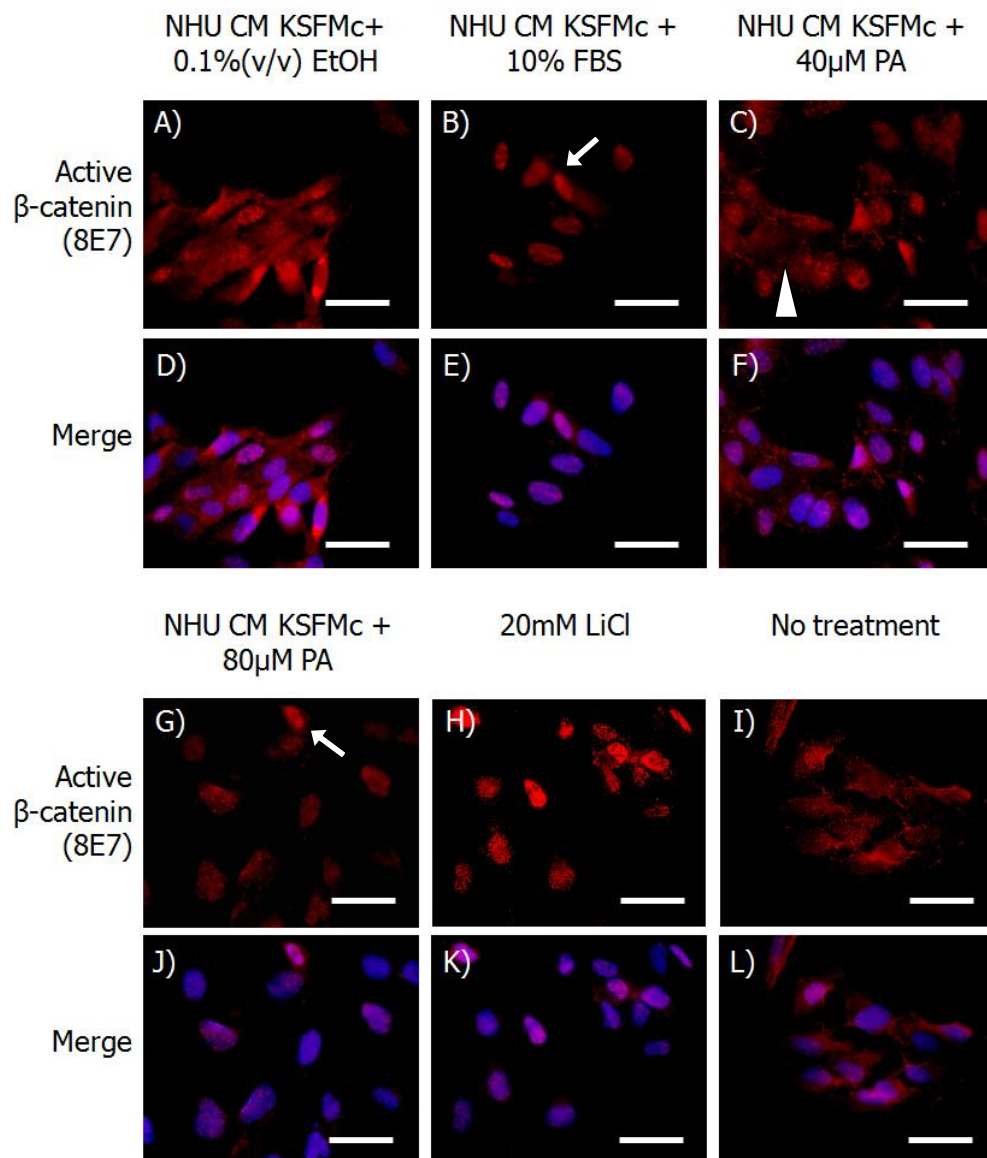


Figure 6-18 Assessing the production of Wnt ligand in NHU cells

SaOS-2 cells after a 24-hour incubation with CM from NHU cells (Y1056) cultured in KSFMc + 10% (v/v) FBS or 40-80 μ M PA. Slides were formalin-fixed and immunolabelled with active β -catenin antibody (8E7) and rabbit anti-mouse IgG-Alexa 594 secondary antibody. All slides were stained with Hoechst 33258 to delineate the nucleus and labelling was visualised under epi-fluorescent illumination. 20mM LiCl treatment was used as a positive control. Negative controls were CM from NHU cells harvested in KSFMc + 0.1% (v/v) EtOH (solvent balanced control) as well as non-treated SaOS-2 cells. Scale bar: 50 μ m. N=1. White arrows denote strong nuclear labelling when cells were treated with CM from NHU cells cultured in the presence of 10%(v/v)FBS or 80 μ M PA. White arrow head denotes cytoplasmic labelling in SaOS-2 cells treated with CM from NHU cells cultured in 40 μ M PA.

6.5.6.4 TCF activity in SaOS-2 cells after incubation with NHU CM

Treatment with 20mM LiCl resulted in a strong TCF-driven luciferase activity from TOPFLASH and no significant luciferase activity from the FOPFLASH negative control, thus verifying the integrity of the experiment (Figure 6-19). Incubation with a 1:10 dilution of NHU CM did not elicit any significant increase in TOPFLASH TCF-driven luciferase activity, regardless of harvesting conditions (Figure 6-19).

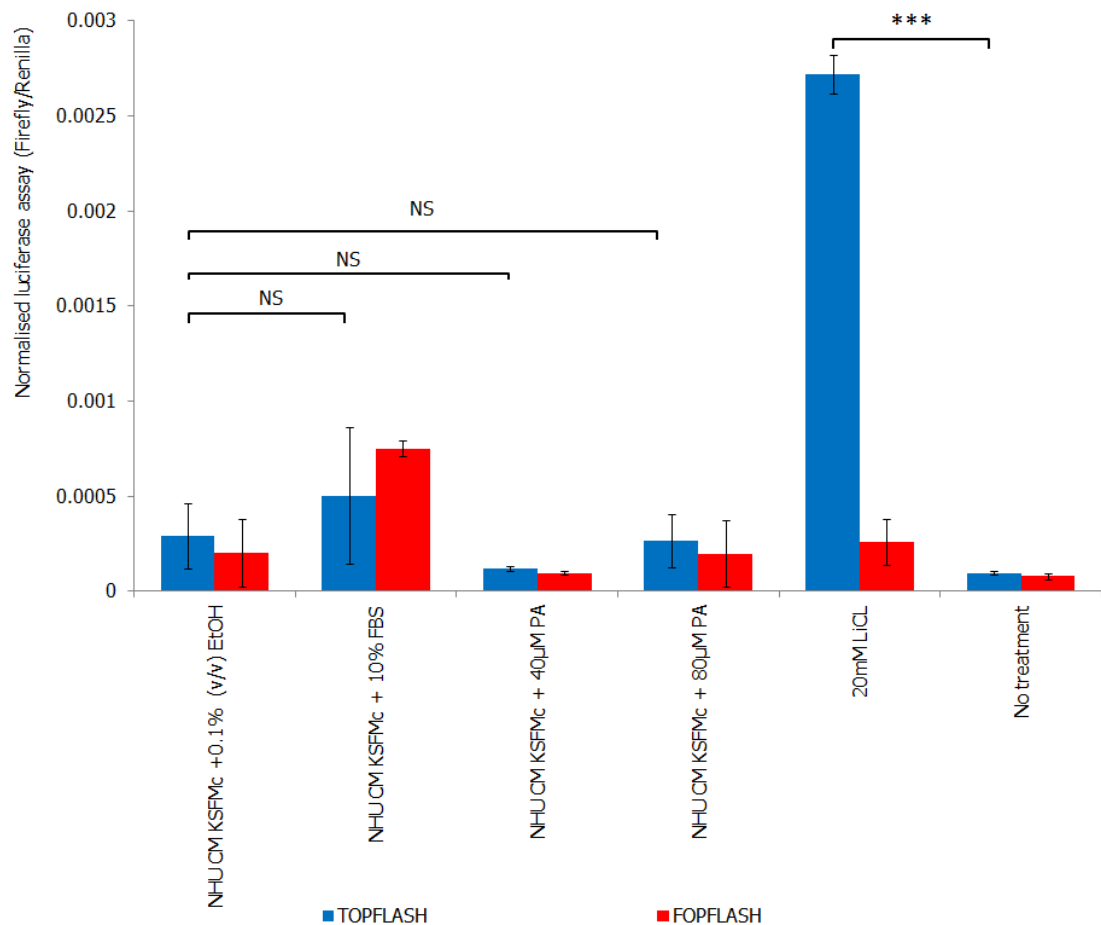


Figure 6-19 Assessing Wnt ligand production in NHU cells

SaOS-2 cells were incubated for 24 hours with a 1:10 dilution of CM from NHU cells (Y1056) cultured in KSMc + 10% (v/v) FBS or 40-80µM PA. Cells were then lysed and a DLA was performed on 3 biological replicates. Positive control was 20mM LiCl. Negative controls were solvent balanced CM (0.1% (v/v) EtOH) and a no treatment control. Data represents the mean luciferase activity after normalisation to loading control (\pm SD). (***) $P < 0.001$, NS non-significant using a one-way ANOVA with Bonferroni multiple comparison post-test). CM from NHU cells did not elicit any significant increase in TOPFLASH TCF-driven luciferase activity in SaOS-2 cells.

6.5.7 Autocrine Wnt signalling

6.5.7.1 Active β -catenin expression in EGFR-blocked NHU cells after treatment with NHU CM containing palmitic acid

Upon first inspection, EGFR-blocked NHU cells incubated with CM from PA treated NHU cells appeared not to have any nuclear active β -catenin (Figure 6-20). However, on closer inspection, approximately 5% of cells did show some nuclear labelling. In the culture treated with CM + 40 μ M PA and CM + 80 μ M PA, approx 5% of cells labelled strongly for nuclear β -catenin (White arrowheads; Figure 6-20B). NHU cells treated with the positive control (10 μ M SB415286) had strong nuclear labelling verifying the integrity of the experiment (Figure 6-20).

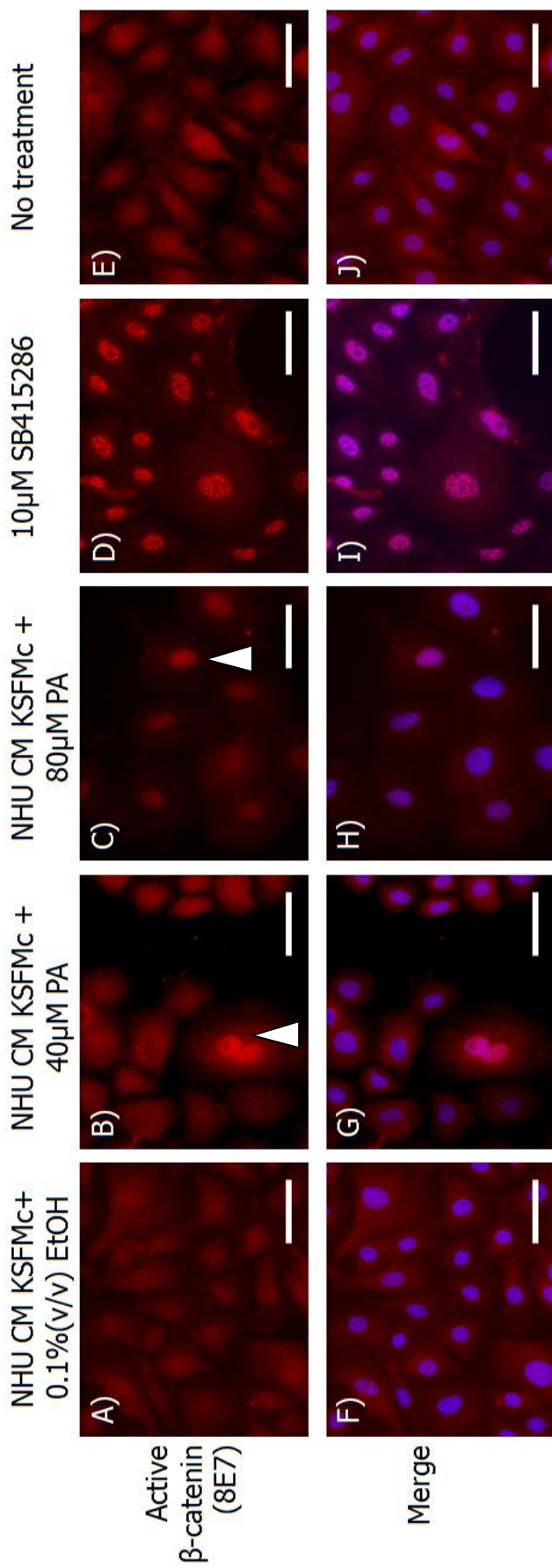


Figure 6-20 Assessing autocrine Wnt signalling in NHU cells

EGFR-blocked NHU (Y1056) cells after a 24-hour incubation with CM from palmitic acid treated NHU cells. Slides were formalin-fixed and immunolabelled with active β-catenin antibody (8E7) and rabbit anti-mouse IgG-Alexa 594 secondary antibody. All slides were stained with Hoechst 33258 to delineate the nucleus and labelling was visualised under epi-fluorescent illumination. 10µM SB415286 treatment was used as a positive control (fig ** panel D). Negative controls were CM from NHU cells harvested in KSFMc + 0.1% (v/v) EtOH (solvent balanced control) as well as non-treated NHU cells (EGFR blocked but no CM). Scale bar: 50µm. N=1. White arrowhead denotes strong nuclear labelling in a subset of cells treated with NHU CM + 40µM PA and 80µM PA.

6.6 Discussion

6.6.1 Response to exogenous Wnt ligand

Incubation of NHU cells with exogenous Wnt3a ligand induced nuclear translocation of β -catenin and TCF activation, two hallmarks of canonical Wnt signalling. Activity of the Wnt pathway was however masked by EGFR signalling and was only visible when EGFR signalling was blocked. By mining data generated from the AffymetrixTM mRNA analysis (chapter 3) it could be inferred that NHU cells were probably signalling via Fzd2 or Fzd6, as both these receptors are known to dock with Wnt3a and were expressed as transcripts in proliferating NHU cells. NHU cells also appeared to signal canonically via Wnt5a, a dual acting Wnt known to activate but also block canonical Wnt signalling, depending on receptor availability (123). When ROR2 receptor is expressed on the cell surface, Wnt5a inhibits the canonical Wnt pathway, whereas when Fzd4 is expressed, a canonical Wnt signal is transduced. Interestingly, both RT-PCR and Q-PCR analysis of ABS/Ca²⁺ treated NHU cells vs. proliferating NHU cell cultures showed a significant down-regulation in Fzd4 expression upon differentiation suggesting that a canonical response to Wnt5a may be reduced upon differentiation.

6.6.2 The role of serum in the processing and secretion of Wnt ligand

NHU cells are routinely cultured under serum-free conditions, where they adopt a “wound-healing” response and lose markers of terminal differentiation such as the uroplakins and tight junctional markers. Addition of serum and physiological calcium to the growth medium of NHU cells results in mitotic quiescence and expression of markers of terminal differentiation. To date, research into the production of bioactive Wnt ligand has always recommended the inclusion of 10% (v/v) FBS when harvesting CM, as serum contains albumin-bound palmitic

acid, the fatty acid required for Wnt post-translational palmitoylation (232). This posed a real difficulty to assessing whether NHU cells secreted their own Wnt ligand, as addition of serum would inevitably result in phenotypic changes and the induction of differentiation.

CM from serum-reduced Wnt secreting L cell lines did not produce significant amounts of bioactive Wnt ligand and thus supported previous publications (96, 97). To try and overcome this, palmitic acid was added to the growth medium of L Wnt-3a cells instead of 10% (v/v) FBS. The concentration of palmitic acid found in bovine serum has previously been quantified as $\sim 1.1\text{mM}$ (or $110\mu\text{M}$ in DMEM+10%(v/v)FBS; as assessed by gas-liquid chromatography) (263). Because of issues with the solubility and precipitation of PA in aqueous medium it was not possible to obtain a concentration of $110\mu\text{M}$. A maximum concentration of $80\mu\text{M}$ PA was obtained. Addition of PA at a concentration of 40 or $80\mu\text{M}$ was seen to restore Wnt ligand secretion and activity to $\sim 50\%$ of that seen with 10% (v/v) FBS, thus confirming that palmitic acid was required for the production of bioactive Wnt ligand. This provides the first conclusive evidence that serum can be reduced when harvesting bioactive Wnt ligand, but only if the growth medium is supplemented with palmitic acid.

6.6.3 Secretion of Wnt ligand from urothelial cells

Analysis of Affymetrix[®] mRNA expression data revealed all components necessary for post-translational modification and secretion of Wnt ligand were present at the mRNA level in proliferating NHU cultures. CM from NHU cells cultured in PA resulted in an increase in nuclear β -catenin in SaOS-2 cells but did not elicit a significant TCF response via the TOPFLASH DLA. The most likely cause for this may be assay sensitivity or may possibly be the result of some form of nuclear inhibition, such as CBY or NLK activation in SaOS-2 cells after treatment with NHU CM. One could potentially test this by adding L Wnt-3a in conjunction with CM from NHU cells.

6.6.4 Autocrine Wnt signalling in NHU cells

EGFR-blocked NHU cells which had been incubated with CM from isogenic PA-treated NHU cell cultures showed limited evidence of Wnt pathway activation. Nuclear β -catenin expression was however evident in a small proportion of cells (<5%) treated with NHU CM harvested in the presence of 40 μ M PA. At present the basis for this heterogeneity and its implications are unclear, however data would imply that there may be a subset of cells capable of driving self-renewal in response to their own Wnt ligand.

6.6.5 Further work

Ideally one would perform an ELISA on CM to test for secreted proteins but unfortunately no suitable antibodies against Wnt3, 5a, 6 or 7a were available at the time of this study. Production of reliable antibodies to vertebrate Wnt proteins has been difficult to manufacture and those that have been made can usually only detect over-expressed Wnt protein and not endogenous levels (232). In the last six months, several new Wnt antibodies have come to market and would be worth testing on CM from NHU cells.

7 Thesis overview and conclusions

This thesis has investigated Wnt signalling in normal human urothelial cells and has made the following novel observations:

1. All components necessary for a functional Wnt cascade are present at the mRNA level in proliferating NHU cell cultures.
2. Several components of the canonical Wnt pathway are differentially expressed between quiescent, differentiated and proliferative NHU cell cultures.
3. Proliferating NHU cells display a high level of endogenous active β -catenin that is driven via EGFR-mediated phosphorylation of GSK3 β .
4. Pharmacological activation of the Wnt pathway can drive NHU proliferation in the absence of EGFR signalling.
5. Culture density affects β -catenin activity but not via sequestration at the adherens junction.
6. β -catenin regulates the activity of ERK and AKT and forms a bi-directional feedback loop with EGFR signalling.
7. All NHU cells can respond to exogenous Wnt3a and Wnt5a but only a subset can respond to an autocrine Wnt signal.

These points are discussed in more detail and in the context of other knowledge below:

All components necessary for a functional Wnt cascade are present at the mRNA level in proliferating NHU cell cultures.

The interrogation of previously generated arrays provided a powerful screening tool to assess the presence of an intact Wnt signalling pathway and to identify key regulators as a starting point for further analysis. MicroarrayTM chip files generated from non-differentiated cultures over time were ranked according to their expression of a core set of proliferation-associated markers called the

“proliferation signature” (115). Analysis of the most proliferative culture implied all components for a functional Wnt cascade were present at the mRNA level. Seven Fzd receptors were expressed suggesting proliferating NHU cells may respond to several Wnt ligands. In fact, proliferating NHU cells also expressed mRNA transcribed from 4 Wnt genes (Wnt3, Wnt5a, Wnt6 and Wnt7a) indicating that they may possess an autocrine Wnt signalling mechanism. Interestingly, RT-PCR on freshly isolated (quiescent) urothelium expressed no Wnt3 or Wnt7a mRNA implying that their expression was either culture-induced or activated in response to perceived “injury”. No mRNA transcript was found for either Wif1 or sFrp1; two secreted Wnt antagonists whose expression is down-regulated by promoter hypermethylation in UC (79-81). Negative regulation of the Wnt pathway by secreted antagonists has been postulated as an important mechanism to curtail Wnt-driven proliferation in the urothelium and therefore the lack of Wif1 expression in proliferating NHU cell cultures was promising evidence for pathway activity (79-81).

The expression of Axin2, a hallmark of canonical Wnt signalling (131, 264) was evident in proliferative NHU cell culture along with several other downstream gene targets, indicating that the pathway was active.

Several components of the canonical Wnt pathway are differentially expressed between quiescent, differentiated and proliferative NHU cell cultures

The microarray interrogation approach adopted to identify components of Wnt signalling also revealed several Wnt signalling components as well as downstream targets were differentially expressed when compared to the proliferating NHU cell culture. Noteworthy changes included: the down regulation of two Fzd receptors (Fzd2 and Fzd4) and up-regulation of Fzd1 using both differentiation protocols, the induction of Wif1 expression in quiescent NHU cells and the down-regulation of four Wnt signalling

transcriptional targets, including Axin2, in both differentiated cultures as well as quiescence. The regulation of Fzd receptor has been described as one of the major mechanisms used to modulate Wnt signalling activity and may represent an important mode of Wnt pathway control in human urothelium (123). This is supported by the findings indicating a reduction in transcript for four Wnt gene targets.

No expression of Wif1 was evident in freshly isolated urothelium and therefore contradicts the hypothesis present by Urakami and colleagues, implying Wif1 suppression via promoter hypermethylation is an important factor in the onset of UC (79).

The aims of this analysis were to determine if fundamental components of the canonical Wnt signalling pathway were present at the mRNA level in NHU cells and to investigate the hypothesis that Wnt signalling was involved in the development and maintenance of the proliferative phenotype. Based on the presented evidence, one can conclude that at the transcript level, all components for a functional canonical Wnt cascade were present in NHU cells and evidence was found for potential repression of the pathway when cells were displaying a non-proliferative phenotype.

Proliferating NHU cells display a high level of endogenous active β -catenin that is driven via EGFR-mediated phosphorylation of GSK3 β

Proliferating NHU cells were shown to contain a significant nuclear-localised pool of β -catenin (indicative of an active cascade). A review of published literature implied Wnt ligand would not be active in serum-free tissue culture system and therefore pathway activity was assumed to be via another mechanism other than ligand-receptor engagement (96, 97). Intersection between signalling pathways had previously been shown to regulate β -catenin activity in other cell types and was therefore investigated as a potential means

of pathway activation in our normal urothelial cell system (159, 167-175). Endogenous β -catenin activity was demonstrated to be the result of pathway crosstalk via EGFR-mediated phosphorylation of GSK3 β and inhibition of the β -catenin destruction complex. Both EGFR and MEK1/2 blockades impaired active β -catenin nuclear labelling, ablated the phospho-inhibition of GSK3 and reduced Axin2 transcription, thereby advocating MAPK/ERK signalling as the point of convergence. The exact mechanism of crosstalk was not fully explored in this study, but the literature suggests GSK-dependent crosstalk with the MAPK pathway can be driven via ERK activation of P70 S6/P90 RSK (166, 169).

Pharmacological activation of the Wnt pathway can drive NHU proliferation in the absence of EGFR signalling

Results demonstrated for the first time that β -catenin activation and TCF-mediated transcription of target genes could promote NHU cell proliferation *in vitro* and highlighted β -catenin as a potentially important player in the regulation of urothelial tissue homeostasis.

Culture density affects β -catenin activity but not via sequestration at the adherens junction

When cultured in low calcium containing medium, culture density was shown to affect the expression of β -catenin within the nucleus of NHU cells. In high density cultures, β -catenin was mainly cytoplasmic, whereas cells seeded at a low initial plating density displayed strong nuclear labelling with the anti-active β -catenin antibody. In the literature, cell:cell contact had previously been highlighted as a means of modulating the activity of the canonical Wnt pathway by sequestration of β -catenin into the adherens junction complex (reviewed by (209)). To test this potentially important link between cell:cell contact and β -catenin/TCF-mediated gene expression, the extracellular calcium concentration was altered to permit or prohibit the formation of adherens junctions. In low

calcium containing growth medium, such as KSMc (0.09mM CaCl₂), calcium-dependent adherens junction formation was weak. This resulted in low β -catenin expression at the membrane and strong nuclear localisation. Increasing the extracellular calcium concentration to near physiological levels (2mM CaCl₂) led to strong β -catenin expression at the membrane and strong nuclear expression. EGFR tyrosine kinase activity has previously been shown to phosphorylate β -catenin at tyr-654, inhibiting its ability to complex with E-cadherin at the membrane (195, 198). This would potentially lead to a reduction in cell:cell contact in the presence of EGF growth factor stimulation and is likely to be an important means of uncoupling cell:cell adhesion in preparation for proliferation. Data in appendix XII supports this theory, as treatment with an EGFR tyrosine kinase inhibitor (PD153035) not only reduced nuclear-localised β -catenin but also increased membrane labelling, thus confirming a role for EGFR tyrosine kinase activity in the regulation of β -catenin.

β -catenin regulates the activity of ERK and AKT and forms a bi-directional feedback loop with EGFR signalling

β -catenin protein expression was modulated to investigate its potential role in urothelial self-renewal. By utilising shRNA, β -catenin expression was successfully reduced by ~58%. NHU cells with reduced β -catenin expression appeared morphologically normal but MTT assays revealed a reduced proliferation rate which was attributed to both a reduction in β -catenin and a lower than normal level of MAPK/ERK activity. Proliferation in the β -catenin knock-down cells was shown to be more reliant on the PI3K/AKT pathway than isogenic control. The mechanism(s) controlling this switch from MAPK/ERK to PI3K/AKT driven proliferation was not fully elucidated in this study but previous published data has implied β -catenin can indirectly (ie via transcription) affect the activity of the MAPK/ERK and PI3K/AKT signalling cascades. For example, in the mouse liver, EGFR has been demonstrated to be a transcriptional target

of the β -catenin and could alter MAPK/ERK activity by modulating EGFR availability at the membrane (210). This mechanism would however not support the observed increase in phospho-AKT as all signalling downstream from the EGFR would potentially be impaired. A better explanation for the modulation in MAPK/ERK signalling may be the observed crosstalk between Raf-1 and an as yet, unidentified product of β -catenin/TCF-mediated transcription (211).

Knock-down of β -catenin also led to a significant increase in the expression of the adherens junction protein, E-cadherin, which was presumed to be via a reduction in the β -catenin/TCF-mediated transcriptional target, Twist, a known transcriptional repressor of E-cadherin (135).

All NHU cells can respond to exogenous Wnt3a and Wnt5a but only a subset can respond to an autocrine Wnt signal

The aim of this work was to determine whether cultured NHU cells had the potential to autocrine Wnt signal. Initial experiments from NHU cells treated with pre-validated conditioned medium containing either Wnt3a or Wnt5a demonstrated that all NHU cells within a culture were able to mount a full, paracrine-induced canonical Wnt cascade. Evidence in the literature implied that under normal growth conditions (without palmitic acid), NHU cells would not produce functional Wnt ligand (96, 97). To remedy this, palmitic acid was added to the growth medium of NHU cells. Interestingly, a small proportion of NHU cells displayed a high level of nuclear-localised β -catenin after incubation in NHU conditioned medium harvested in the presence of palmitic acid. This data, although not conclusive, may highlight a sub-population of cells with the ability to initiate their own programme of self-renewal, such as a stem cell.

7.1 Concluding Remarks

The purpose of this thesis was to investigate how the dynamics between growth factor-mediated gene transcription and cell:cell contacts regulate urothelial self-renewal. In this thesis, the canonical Wnt signalling cascade was examined as a potential key pathway due to the pivotal role of β -catenin in both Wnt-mediated gene transcription and intercellular adherens junctions. Before this work was undertaken, little was known about the role of Wnt signalling in the bladder urothelium. Research into UC had hinted at the possible involvement of β -catenin in urothelial transformation, but no conclusive evidence for a role in either normal or transformed cell growth had been demonstrated (73-81). Work by Thievessen and colleagues concluded that there was no active β -catenin signalling in normal human urothelium using the TOPFLASH/FOPFLASH TCF-reporter assay (72), but work presented here indicates that FOPFLASH is unsuitable for use in urothelial cells because of the high level of background it generates. In fact, evidence presented in this thesis establishes β -catenin as an important component of a bi-directional feedback loop, linking EGFR and β -catenin-mediated proliferation with cell:cell contact. As proposed in figure 7-1, β -catenin plays a central role in the regulation of this network and therefore catapults it into the limelight as a prominent figure in the maintenance of urothelial tissue homeostasis, as well as a potential target for deregulation in the transition from normal to malignant cell growth.

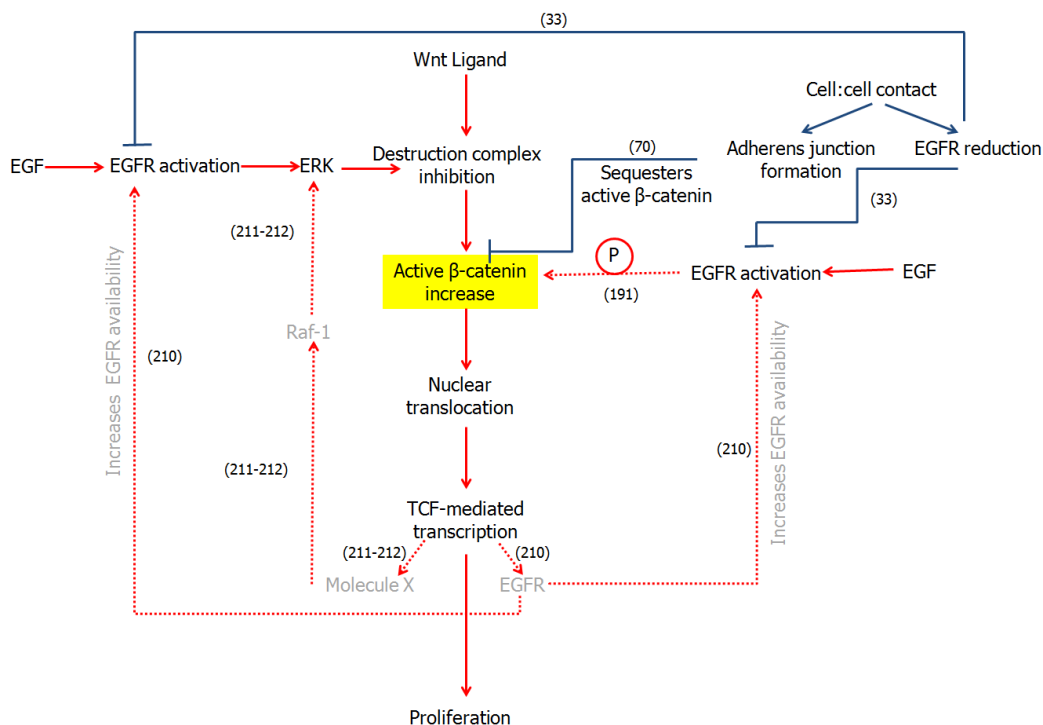


Figure 7-1 The role of β -catenin in NHU proliferation

Schematic illustrating the available data on the role of β -catenin in NHU proliferation. Sections in bold and with solid lines have either been demonstrated in this thesis or previously shown in human urothelium. Sections in grey with dotted lines are possible links seen in other cell types (references shown in brackets). Red lines indicate a positive effect on proliferation. Blue lines indicate a negative effect on cell proliferation.

Appendix I

List of Suppliers

Supplier	Webpage/Address
Adobe Systems Inc	www.adobe.com
Affymetrix UK Ltd	www.affymetrix.com
Agilent Technologies UK Ltd	www.agilent.co.uk
Ambion Europe Ltd	Supplied by Invitrogen
American Type Culture Collection	Supplied by LGC
Amersham Biosciences UK Ltd	www.gelifesciences.com
Applied Biosystems (ABI)	www.abi.org.uk
Autogen Bioclear UK Ltd	Holly Ditch Farm, Mile Elm, Calne, Wiltshire SN11
Axygen Inc	Supplied by Fisher Scientific
Beckman Coulter Inc	www.beckmancoulter.com
BD Biosciences	www.bdbiosciences.com/eu
BDH	Supplied by VWR
Bioline Reagents Ltd	www.bioline.com/h_uk.asp
Bio-Rad Laboratories Ltd	www.bio-rad.com
BOC UK	www.boconline.co.uk
C A Hendley Essex Ltd	Oakwood House, 12 Oakwood Hill Industrial
Calbiochem	Supplied by Merck
Clontech (Takara Bio Inc)	www.clontech.com
Cogenics (Beckman Coulter)	www.cogenics.com
ELGA (Veolia Water Solutions UK Ltd)	www.elgalabwater.com
Ensembl Genome Browser	www.ensembl.org
Envair Ltd	www.envair.co.uk
Eppendorf UK Ltd	www.eppendorf.co.uk
Eurofins MWG Operon	www.eurofinsdna.com
European Bioinformatics Institute	www.ebi.ac.uk
Falcon	Supplied by VWR
Fisher Scientific UK Ltd	www.fisher.co.uk
Genomatix Software GmbH	www.genomatix.de
Gentaur Ltd	www.gentaur.com
Graphpad Software Inc	www.graphpad.com
Greiner Bio-one Ltd	www.greinerbioone.com/en/england/start/
Harlan Sera-Lab Ltd	www.harlanseralab.co.uk
Hettich Centrifuges (DJB Labcare Ltd)	www.hettichcentrifuge.co.uk
Hybaid Ltd	Supplied by Thermo Scientific
Ingenuity Systems Inc	www.ingenuity.com
Insight Biotechnology Ltd	www.insightbio.com
Invitrogen Ltd	www.invitrogen.com
Jencons-PLS	Supplied by VWR International

Supplier	Webpage/Address
Leica Microsystems (UK) Ltd	www.leica-microsystems.com
LGC standards	www.lgcstandards.com
Li-Cor Biosciences UK Ltd	www.licor.com
Media Cybernetics Inc	www.mediacy.com
Merck KgaA	www.merck.co.uk
Microsoft Corporation	www.microsoft.com
Molecular Probes	Supplied by Invitrogen
Nalgene Europe Ltd	Supplied by Fisher Scientific
National Centre for Biotechnology	www.ncbi.nlm.nih.gov
National Diagnostics	www.nationaldiagnostics.com
New England Biolabs (UK) Ltd	www.neb.uk.com
Novacastra Laboratories Ltd	www.novacastra.co.uk/
Olympus Optical Company Ltd	www.microscopy.olympus.eu/microscopes/
Pall Life Sciences	Supplied by VWR
Parke Davis (Pfizer Ltd)	www.pfizer.co.uk
PerkinElmer Inc	www.perkinelmer.com
Pierce	Supplied by Thermo Scientific
Promega UK Ltd	www.promega.com
Qiagen Ltd	www.qiagen.com
R A Lamb Ltd	www.ralamb.co.uk
Roche Diagnostics Ltd	www.roche.co.uk/portal/uk/diagnostics
Santa Cruz Biotechnology	Supplied by Insight Biotechnology Ltd
Sartorius Ltd	www.sartorius.co.uk
Scientific Laboratory Supplies (SLS)	www.flowgen.net
Sigma-Aldrich Company Ltd	www.sigmaaldrich.com
Solent Scientific Ltd	www.solentsci.com
Sorvall Centrifuges (DJB Labcare)	www.sorvallcentrifuge.co.uk
Starlab (UK) Ltd	www.starlab.co.uk
Starstedt Ltd	www.sarstedt.com
Sterilin Ltd	Supplied by SLS
Statebourne Cryogenics Ltd	www.statebourne.com
Syngene (Synoptics Ltd)	www.syngene.com
Takara Bio Inc	www.takara-bio.com
ThermoFisher Scientific Inc	www.fisher.co.uk
Vector Laboratories Ltd	www.vectorlabs.com
VWR international	www.vwr.com
Whitehead Institute for Biomedical	www.wi.mit.edu

Appendix II

Stock solutions

General Solutions:

Phosphate Buffered Saline (PBS)

137mM NaCl, 2.7mM KCl, 3.2mM Na₂HPO₄ and 147mM KH₂PO₄, pH7.2 in dH₂O.
Prepared from tablets (Sigma; P4417) and autoclaved.

Tris Buffered Saline (TBS)

50mM Tris-HCl (pH7.4) and 150mM NaCl in dH₂O

PBSc

0.5mM MgCl₂ and 0.9mM CaCl₂ in PBS.

Cell culture solutions:

Collagenase IV (Sigma; C5138)

Diluted in 20,000U in 100ml of Hank's Balanced Salt's Solution (HBSS)(without Ca²⁺ and Mg²⁺) and containing 10mM HEPES (Invitrogen).

Stripper Medium

500ml of HBSS (without Ca²⁺ and Mg²⁺), 10mM HEPES, 500,000 Kallikrein inactivating units (KIU) Trasylol (Bayer) and 0.1% (w/v) EDTA.

Transport Medium

500ml of HBSS (without Ca²⁺ and Mg²⁺), 10mM HEPES, 500,000 Kallikrein inactivating units (KIU) Trasylol.

Molecular Biology Solutions:

Luria Broth (LB)

10g Tryptone, 10g NaCl, 5g of Yeast extract to 1l of dH₂O, pH7.0 and autoclaved immediately.

LB-Agar

LB containing 2% (w/v) agar and utoclaved immediately.

10x TBE Buffer

0.9M Tris, 0.9M Boric acid, 25mM EDTA in dH₂O. Diluted 1:10 in dH₂O prior to use.

Western Blotting Solutions:

2x SDS lysis buffer

125mM Tris-HCl (pH6.8), 20% (w/v) glycerol, 2% (w/v) SDS, 200mM Sodium fluoride, 2mM Sodium Orthovanadate, 40mM Tetra-sodium pyrophosphate and made to 50ml in dH₂O.

“Towbin” Transfer Buffer

12mM Tris, 38mM Glycine, 20% (v/v) Methanol made to 1l in dH₂O.

Immunofluorescence Solutions:

DABCO/Glycerol Antifade Mountant

0.01M NaHCO₃ and 2.5% (w/v) 1,3 diazobicyclo (2,2,2)-octane in glycerol, pH 8.0.

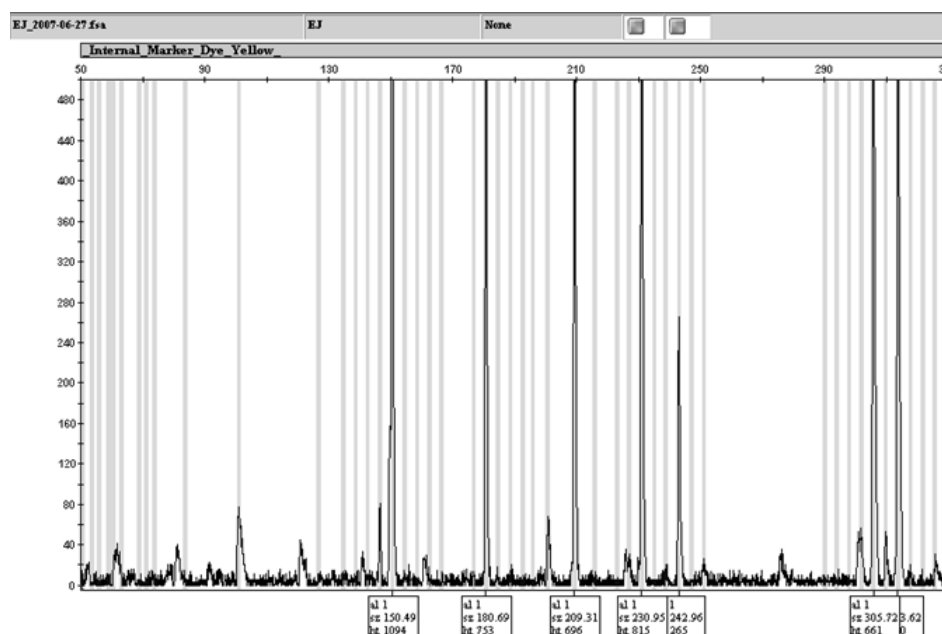
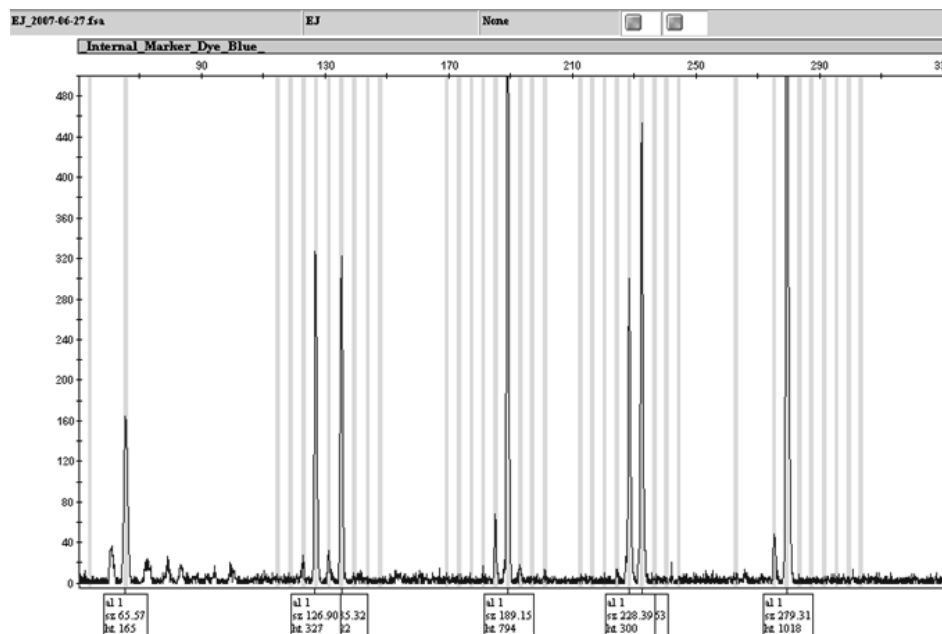
Appendix III

Y-Number Tissue Information

Y-number	Operation	Tissue	Sex	Age
Y372	Nephrectomy	Ureter	-	-
Y387	Nephrectomy	Ureter	F	44
Y579	Nephrectomy	Ureter	F	33
Y676	TURP	Bladder	M	78
Y878	Pyeloplasty	Renal Pelvis	-	-
Y919	Nephrectomy	Ureter	M	67
Y924	Nephrectomy	Ureter	M	63
Y970	Re-implant ureter	Ureter	-	-
Y1056	Renal transplant	Ureter	F	62

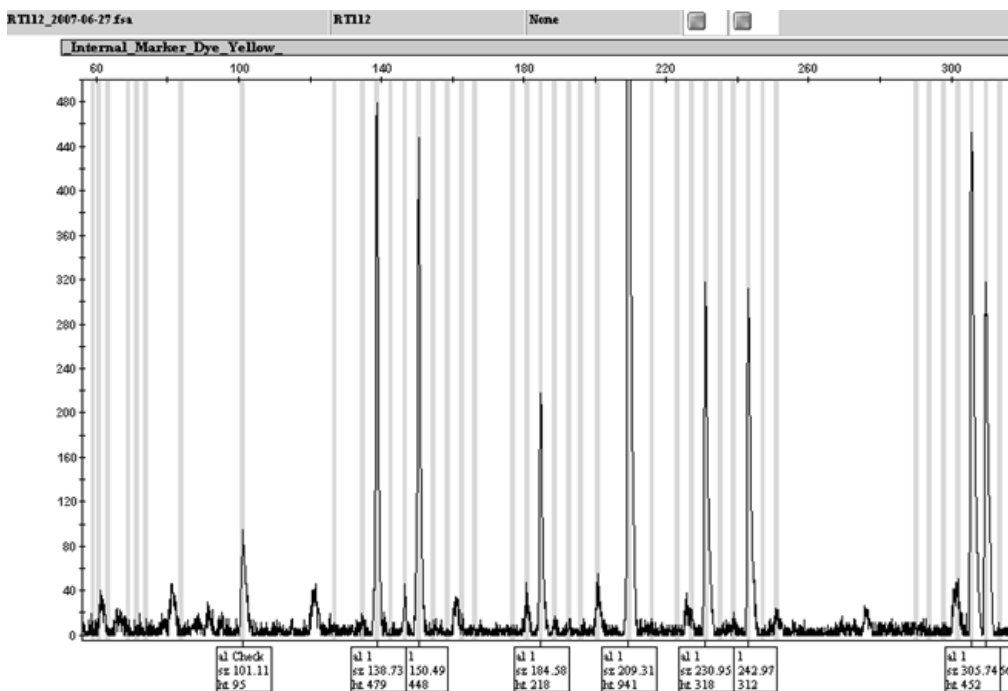
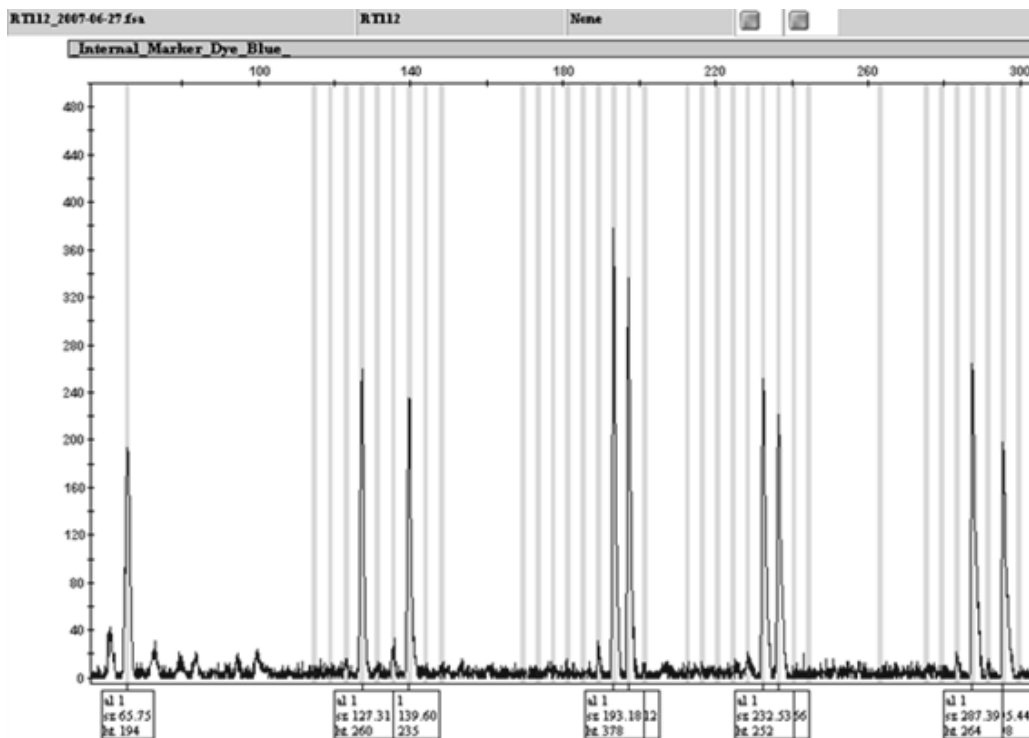
Appendix IV

Genotyping



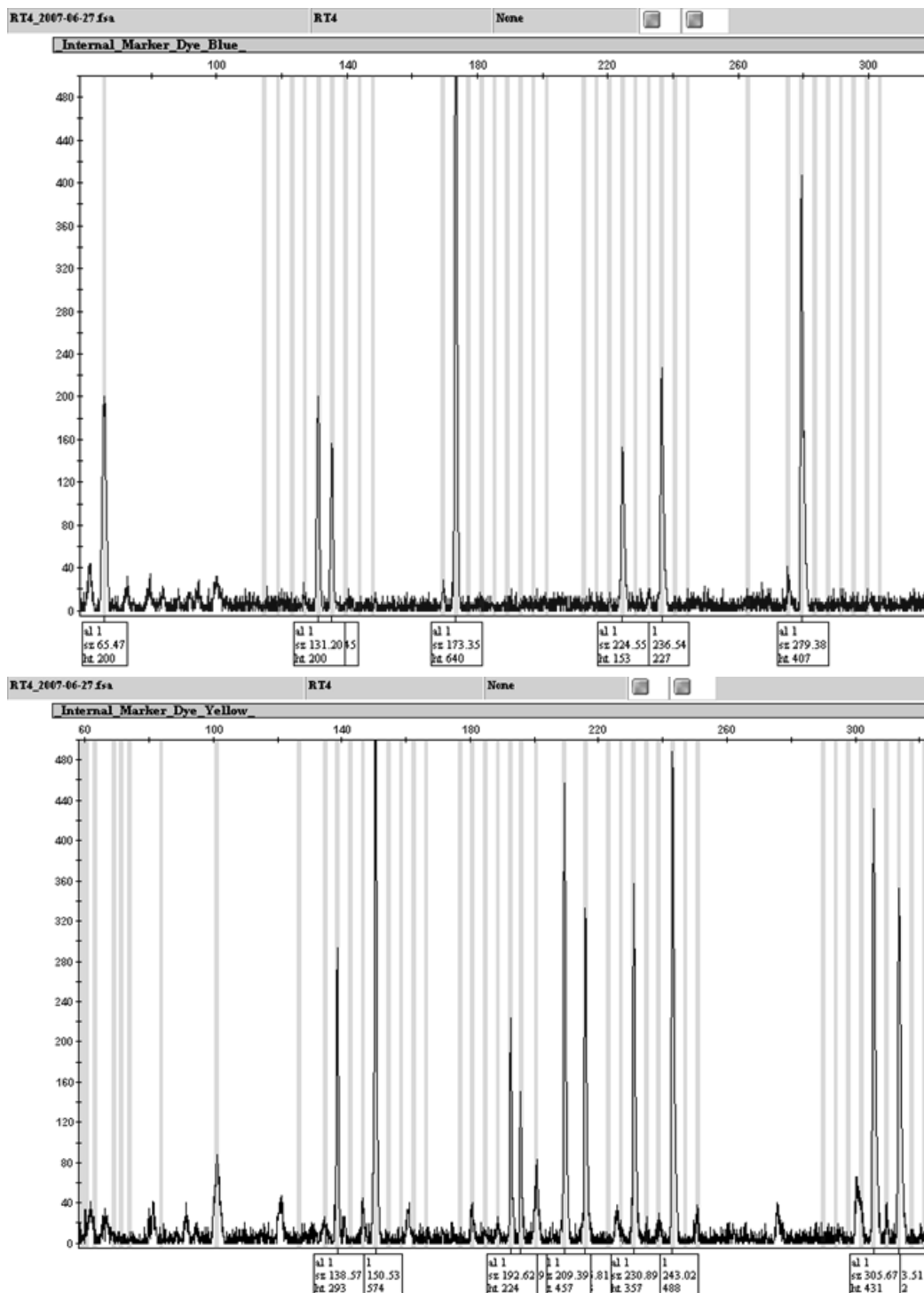
Electropherograms for EJ cell line

DNA (STR) profile for EJ cell line was as published by ATCC (Amelogenin: XCSF1PO: 10,12 D13S317: 12 D16S539: 9 D5S818: 10,12 D7S820: 10,11 TH01: 6 TPOX: 8,11 vWA: 17).



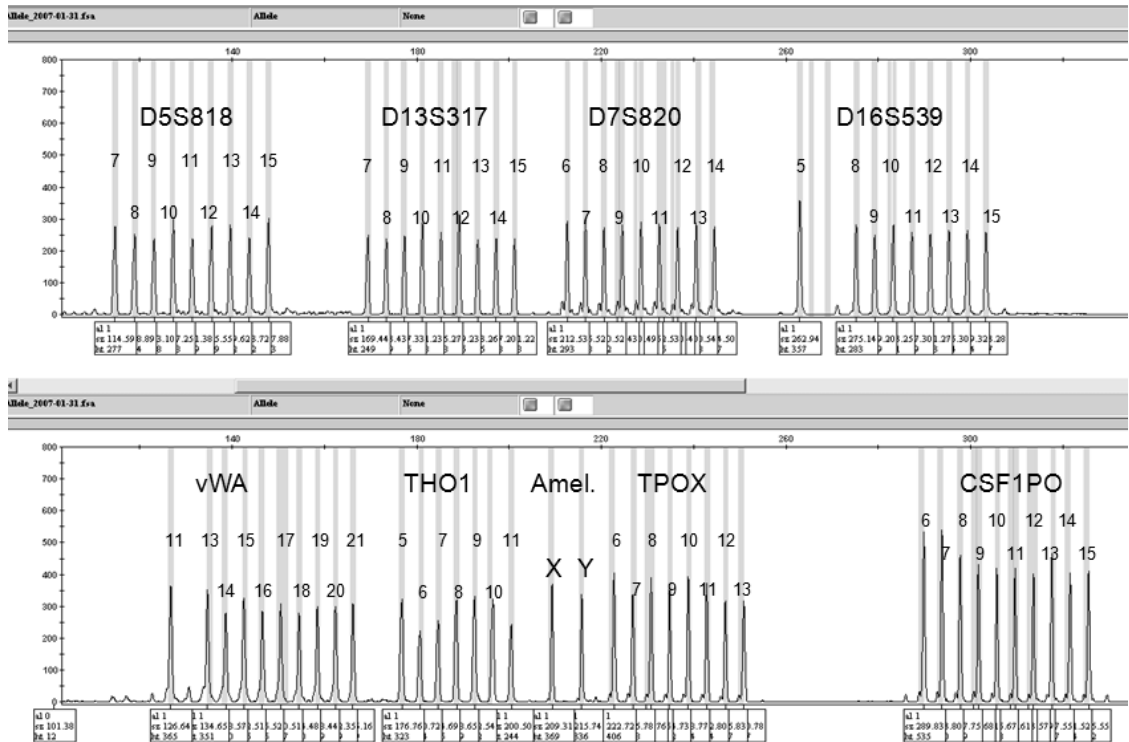
Electropherograms for RT112 cell line

DNA (STR) profile for RT112 cell line was as published by Sigma-Aldrich (Amelogenin: XCSF1PO: 10,11 D13S317: 13,14 D16S539: 11,13 D5S818: 10,13 D7S820: 11,12 THO1: 7 TPOX: 8,11 vWA: 14,17).



Electropherograms for RT4 cell line

DNA (STR) profile for RT112 cell line was as published by Sigma-Aldrich (Amelogenin: X,Y
 CSF1PO: 10,12 D13S317: 8 D16S539: 9 D5S818: 11,12 D7S820: 9,12 TH01: 9,9.3 TPOX: 8,1
 vWA: 14,17).



Allelic ladder

Appendix V

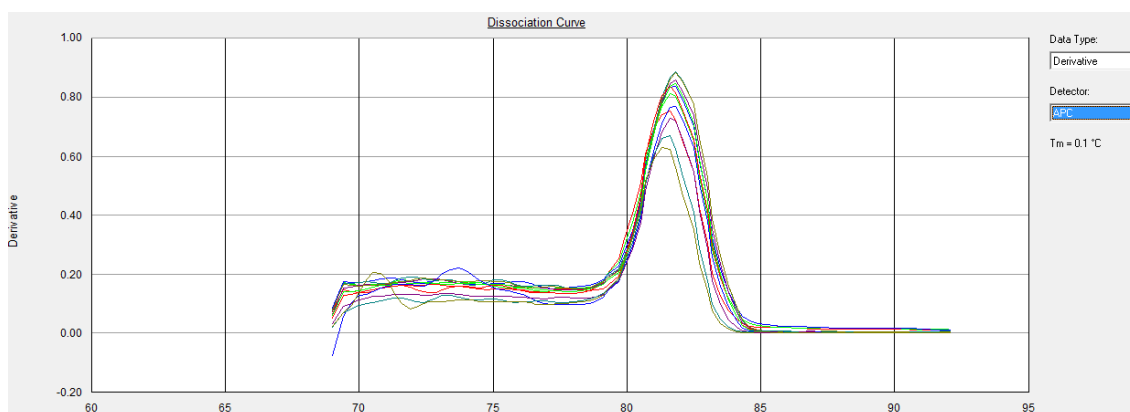
Primers

Gene	FWD 5' → 3'	REV 5' → 3'
APC	GGAGCCAAGCCATCTGTGAA	TGCTTTACTTGACCCACCTATTTG
Axin2	CAAGGGCCAGGTCACCAA	CCCCCAACCCATCTTCGT
c-MYC	GAGGAGACATGGTGAACCAGAGT	TCCTGGATGATGATGTTTTTGATG
CyclinD1	CGTGGCCTCTAAGATGAAGGA	TGTCGGTGTAGATGCACAGCTT
DKK3	GGGTCTTTGTCGCGATGGTA	GTTCTTGATAGCGTTGGAATTGAG
CDH1	AATCTGAAAGCGGCTGATACTGA	CGGAACCGCTTCCTTCATAG
Fzd2	CCAGTTCTATCCGCTGGTGAA	GCGTACATGGAGCACAGGAA
Fzd4	GTCTCAGTCTGGGGTTGCTC	GGATGAGCGGTGTGAAAGTT
Fzd6	CGGAACCAAGAAAACTAAAGAAATT	ATAGACGTAACATCCGAGAAGTGT
GAPDH	CAAGGTCATCCATGACAACCTTTG	GGGCCATCCACAGTCTTCTG
Lef1	GGACGAGATGATCCCCTTCA	CTTCCTCTTCGGGATGACTGAT
MKI67	CAAGAGCATCAGAACGTTTAAGGA	TTCTTGGCCACTTCTTCATTCC
ROR2	CCGGTTTGGGAAAGTCTACA	CGTGCGAACAGTAGCTGAAG
UPK2	CAGTGCCTCACCTTCCAACA	TGGTAAAATGGGAGGAAAGTCAA
UPK3a	CGGAGGCATGATCGTCAT	CAGCAAAACCCACAAGTAGAAAGA
Wif1	GGCACCTTTTACACATGATTTTCAG	TGGAATGGATATTGACAGGAATAG
Wnt3	AAGGGACCGGACTTGCAAT	GGCCACAGCAGAGCAGATC
Wnt3a	CTGGCAGCTGTGAAGTGAAG	TGGGTGAGGCCTCGTAGTAG
Wnt5a	CTGGCTCCTGTAGCCTCAAG	AATCTCCGTGCACTTCTTGC
Wnt5a	AACTCGCCCACCACACAAG	TCATTGCGCACGCAGTAGTC
Wnt7a	GGCCACCTTCTGAAGATC	GTACACCAGGTCCGTGTCCAT
Wnt11	GGGAGGATGTGCGGACAA	GAAAACCTTGCCCCCATGA
Wnt14	GGAGGCCGTGAGCATGAGT	TGCAGTTCAGCGCTCAA

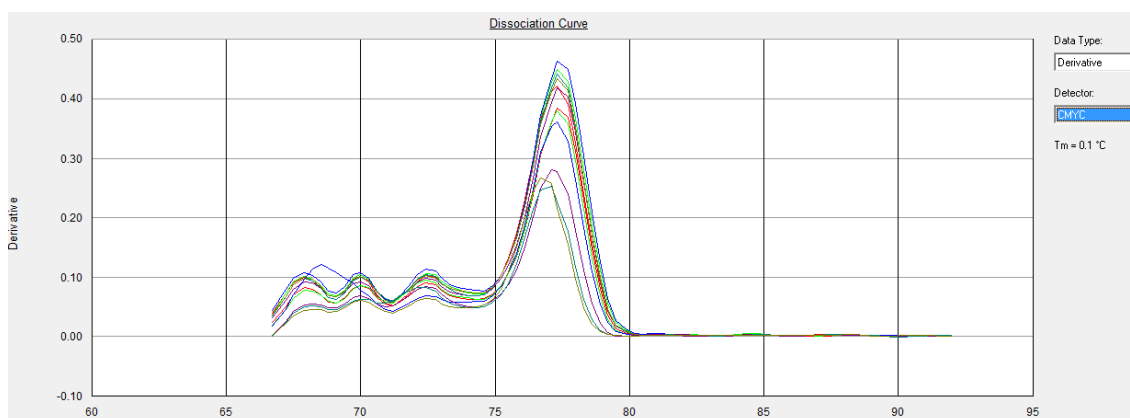
Appendix VI

Dissociation curves

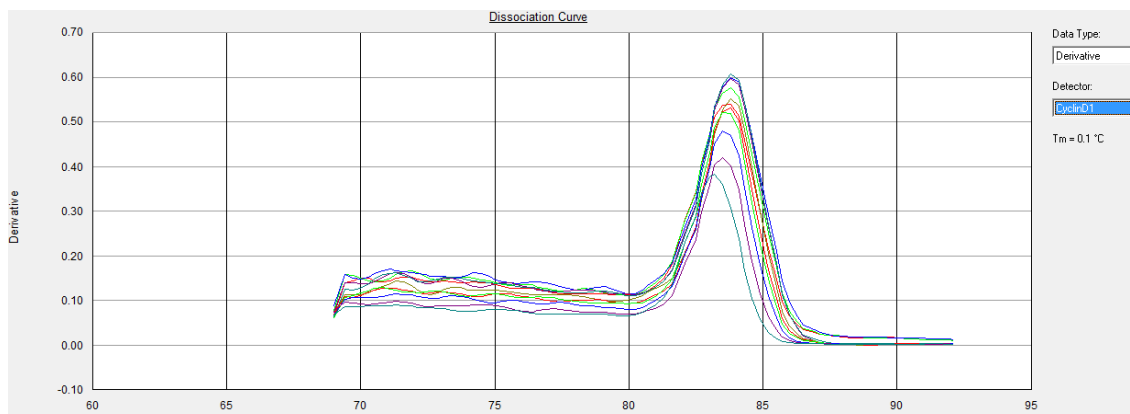
APC



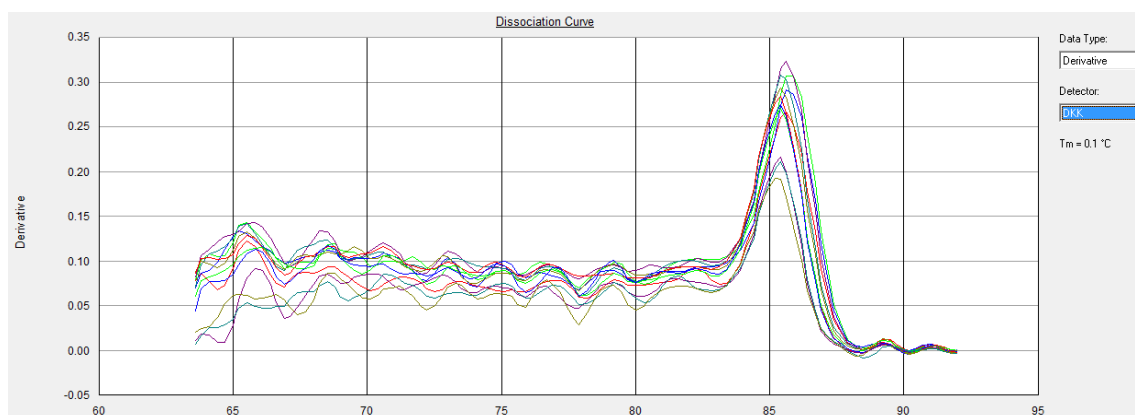
c-MYC



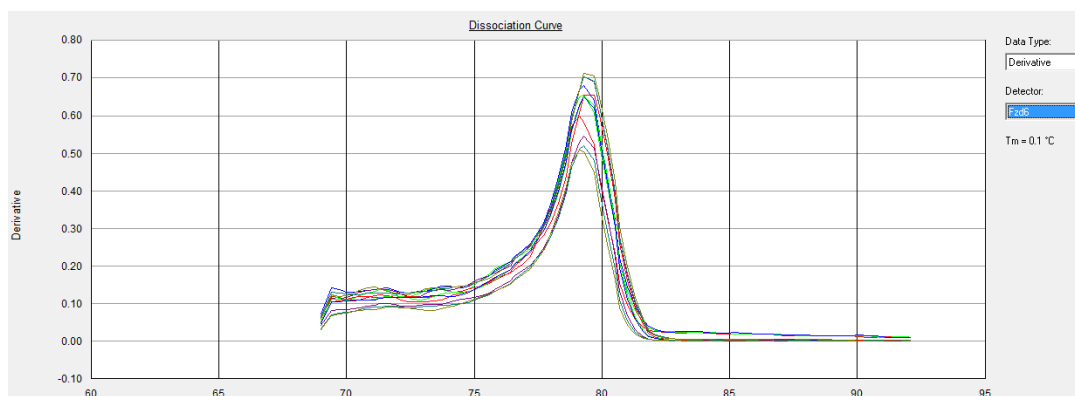
CyclinD1

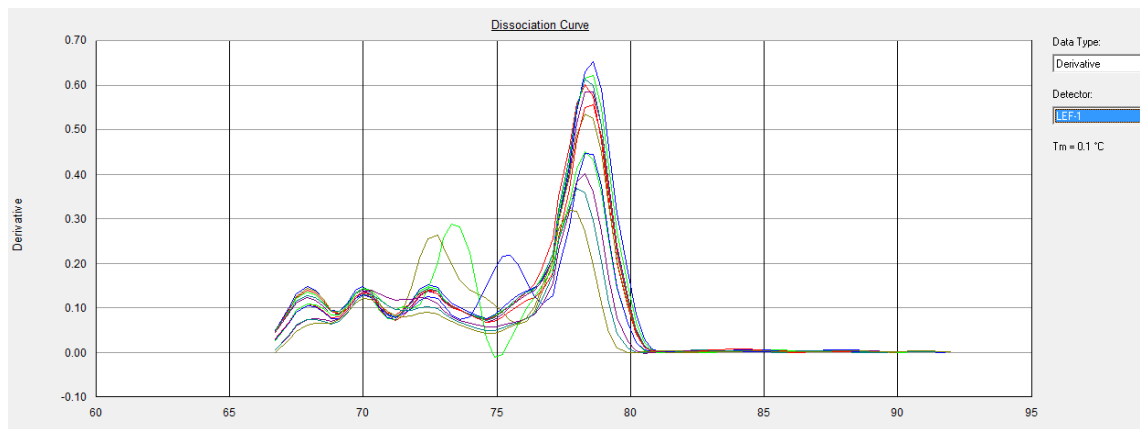
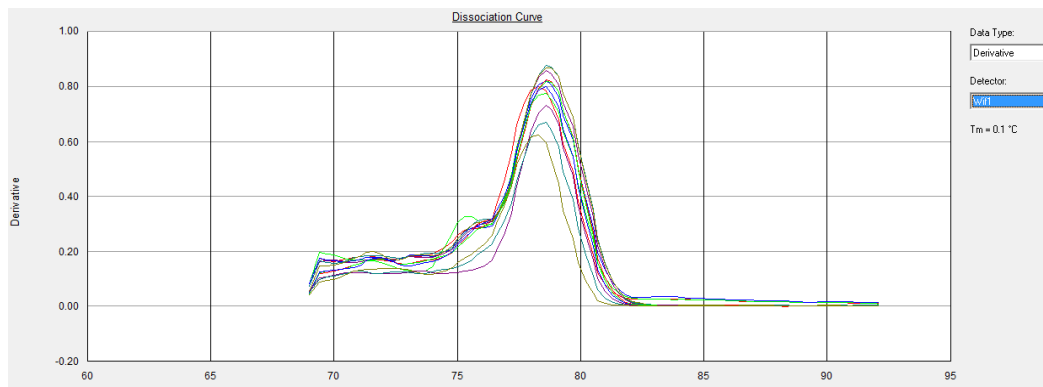
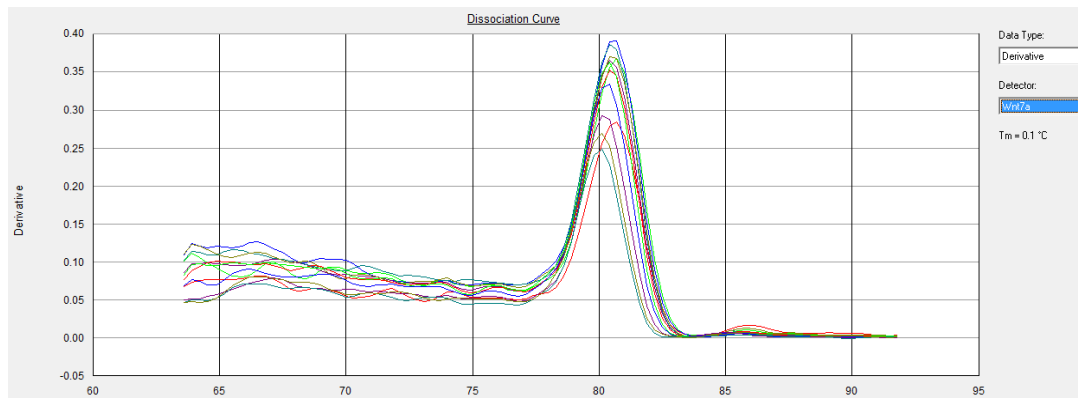


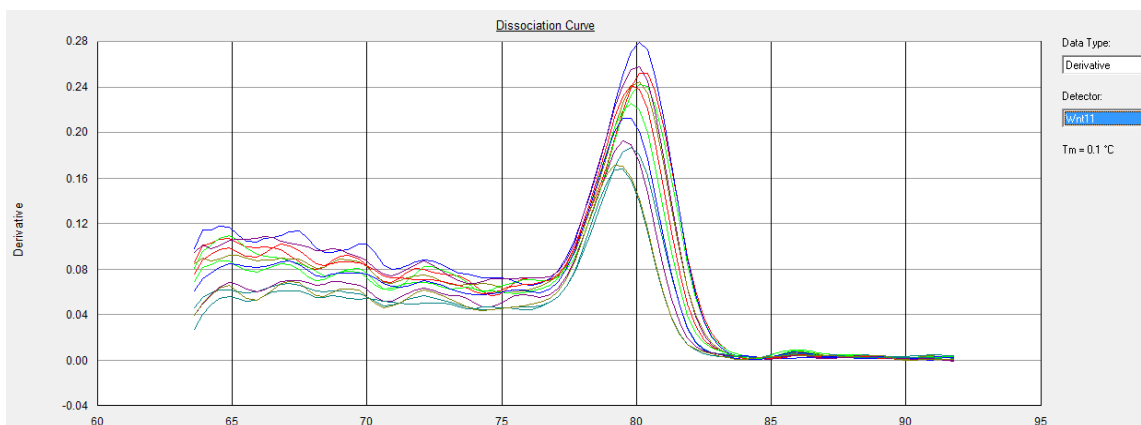
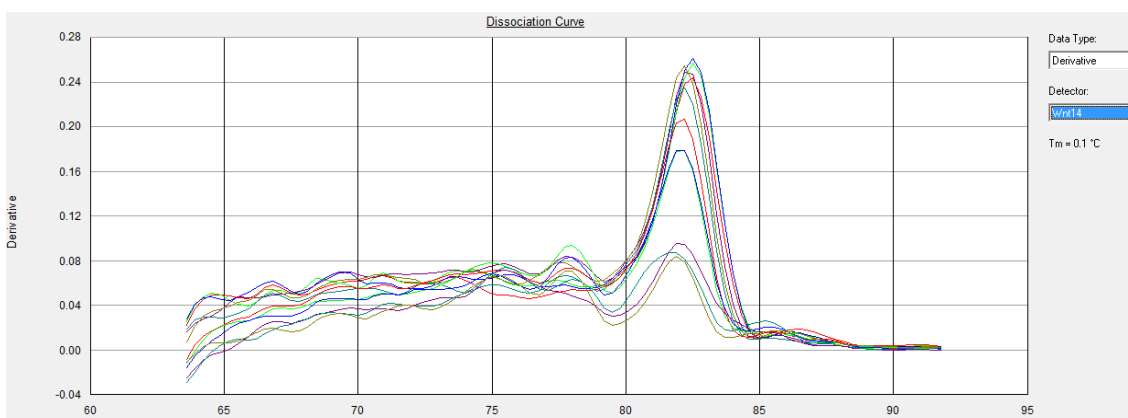
DKK3



Fzd6



Lef1**Wif1****Wnt7a**

Wnt11**Wnt14**

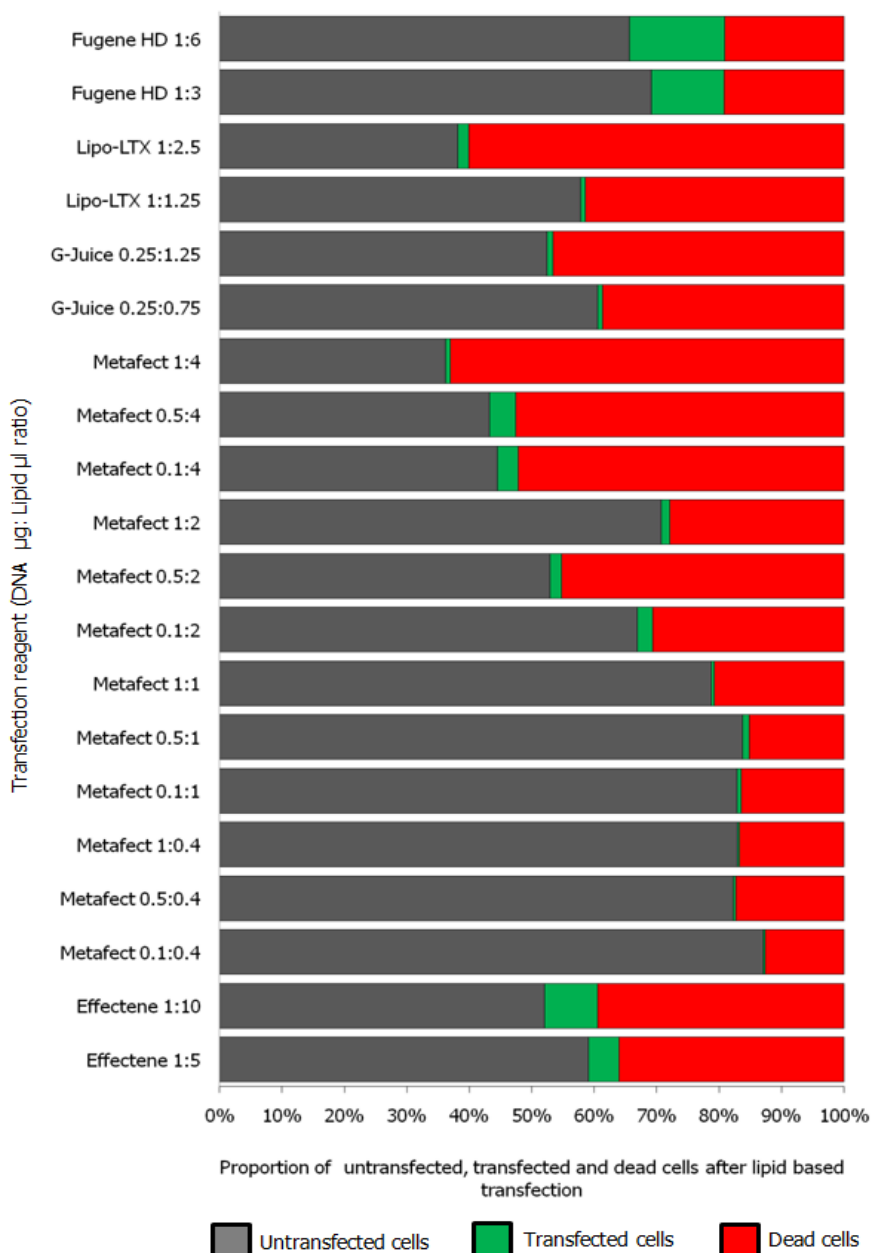
Appendix VII

FACS analysis

Transfection Reagent	Amount of DNA (μg)	Amount of Reagent (μl)	% Alive	% Dead	% of alive cells transfected	% of alive cells untransfected	% of transfected cells from total population	
Effectene®	1	5	64.0	36.0	7.7	59.1	4.9	
	1	10	60.5	39.5	14.1	52.0	8.5	
Metafectene®	0.1	0.4	87.3	12.7	0.3	87.1	0.2	
	0.5	0.4	82.7	17.3	0.6	82.3	0.5	
	1	0.4	83.3	16.7	0.4	83.0	0.3	
	0.1	1	83.6	16.4	0.9	82.8	0.8	
	0.5	1	84.8	15.2	1.2	83.8	1.0	
	1	1	79.3	20.7	0.7	78.7	0.6	
	0.1	2	69.4	30.6	3.6	66.9	2.5	
	0.5	2	54.8	45.2	3.4	53.0	1.9	
	1	2	72.1	27.9	1.9	70.7	1.4	
	0.1	4	47.9	52.1	7.0	44.5	3.3	
	0.5	4	47.4	52.6	8.8	43.3	4.1	
	1	4	37.0	63.0	2.2	36.2	0.8	
	GeneJuice®	0.25	0.75	61.4	38.6	1.4	60.5	0.8
		0.25	1.5	53.5	46.5	1.9	52.4	1.0
Lipofectamine™ LTX	1	1.25	58.6	41.4	1.4	57.8	0.8	
	1	2.5	39.9	60.1	4.6	38.1	1.8	
Fugene®HD	1	3	80.9	19.2	14.5	69.2	11.7	
	1	6	80.9	19.1	18.8	65.7	15.2	

Optimising NHU cell transfection using lipid based reagents

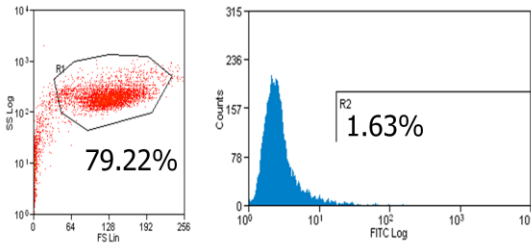
NHU Y924 (P3) cells were transfected with between 0.1-1 μg of pBabe-EGFP using 5 different lipid base transfection reagents as outlines in the table. 48 hours post-transfection cells were analysed via FACS for percentage viability and GFP expression.



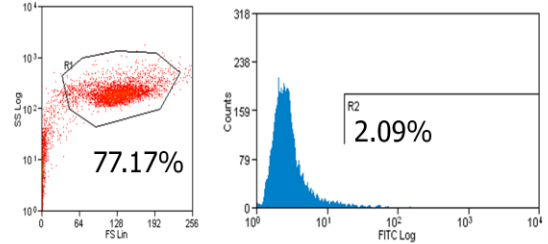
Comparison of lipid-based transfection reagents in NHU cells

NHU Y924 (P3) cells seeded into a 24-well Primaria® plate at 4×10^4 cells per well were transfected 24-hours after seeding with between 0.1-1 μ g of pBabe-EGFP using 5 different lipid based transfection reagents. Cells were assayed 48-hours post-transfection using FACS. Percentage of viable to non-viable cells was calculated using forward and side scatter dot blots versus a non-transfected control. Percentage of transfected cells was calculated using EGFP expression. 10,000 events were collected per sample.

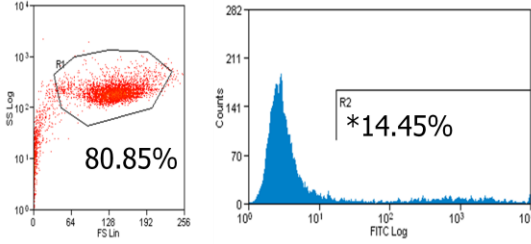
A) Fugene 3µl negative control



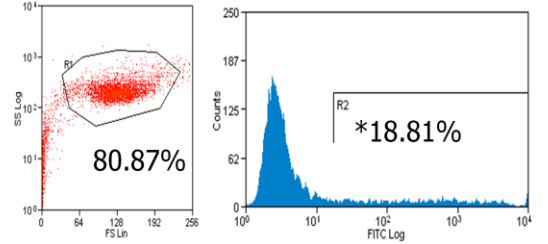
B) Fugene 6µl negative control



C) Fugene 3µl:1µg DNA

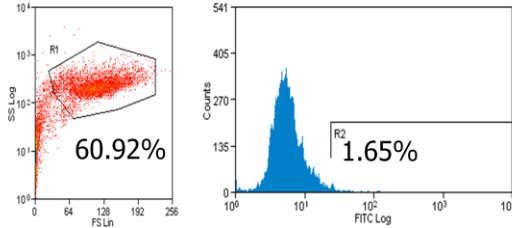


D) Fugene 6µl:1µg DNA

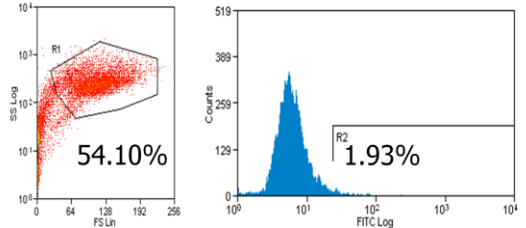


Scatter plots and histograms for Fugene

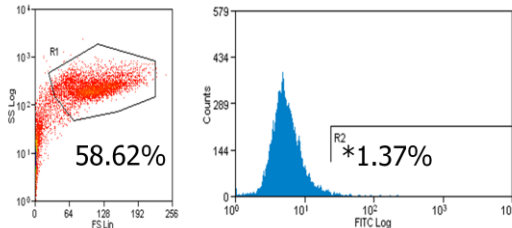
A) Lipofectamine LTX 1.25µl negative control



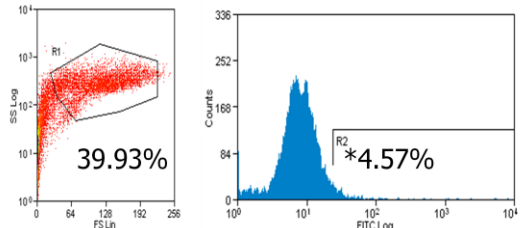
B) Lipofectamine LTX 2.5µl negative control



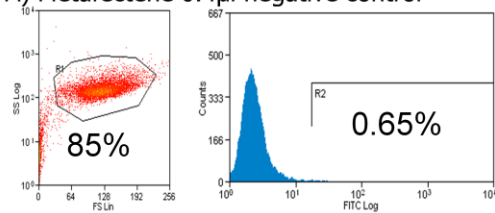
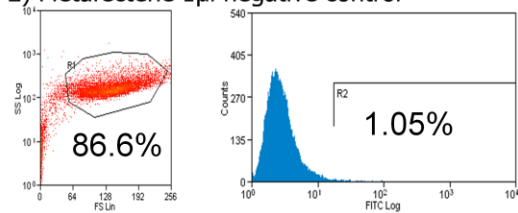
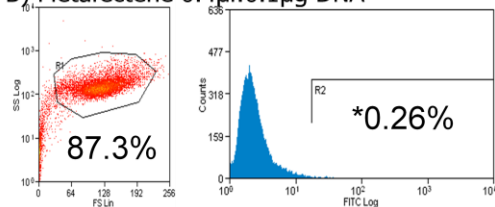
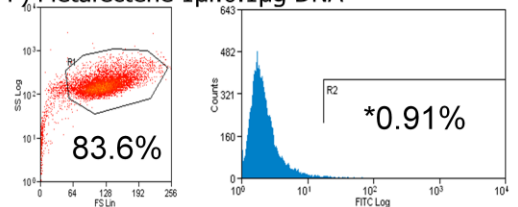
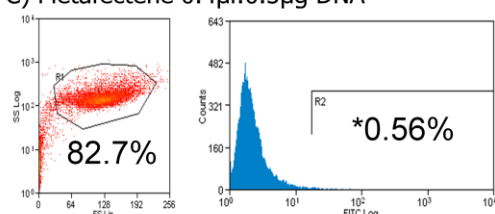
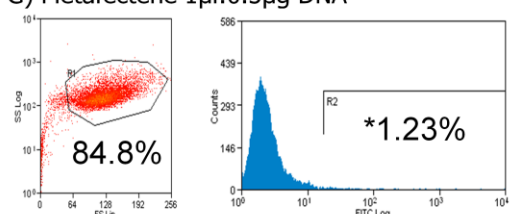
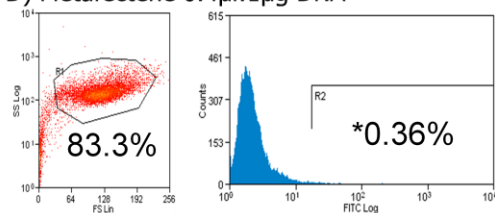
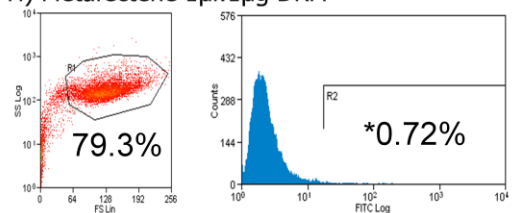
C) Lipofectamine LTX 1.25µl:1µg DNA



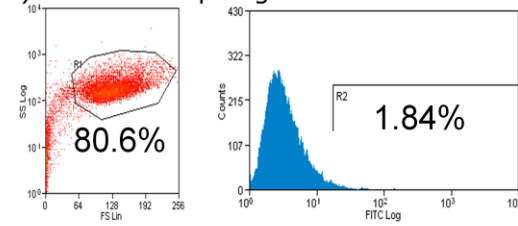
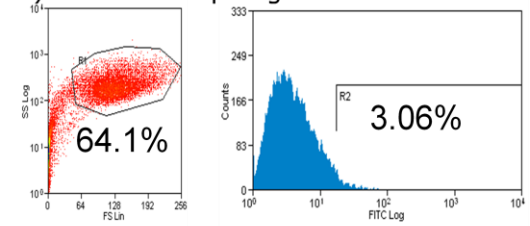
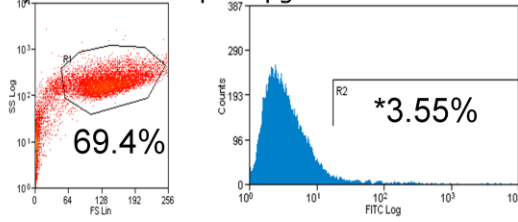
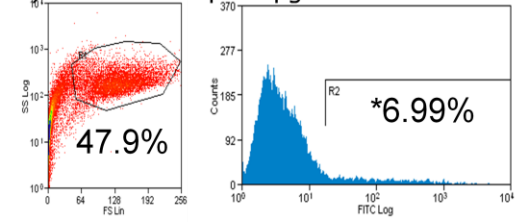
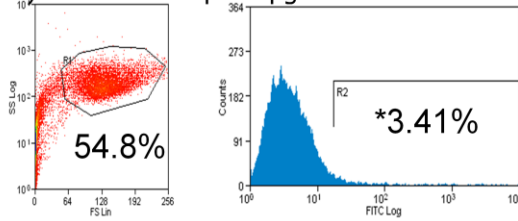
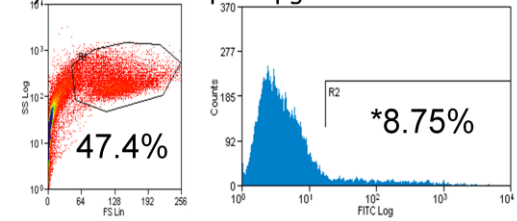
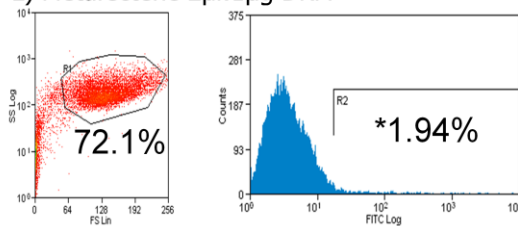
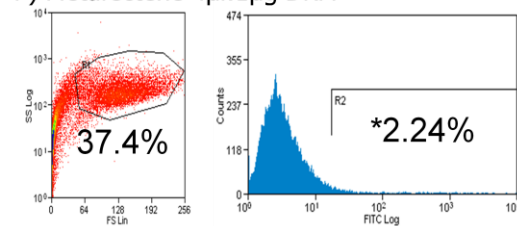
D) Lipofectamine LTX 2.5µl:1µg DNA



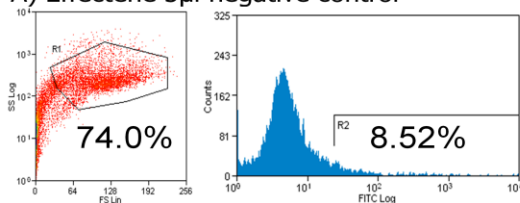
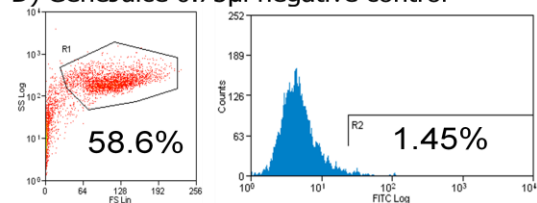
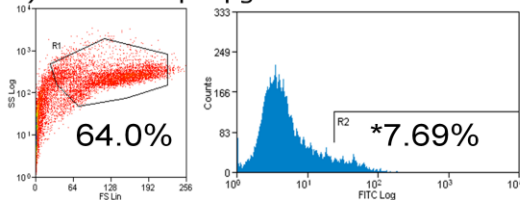
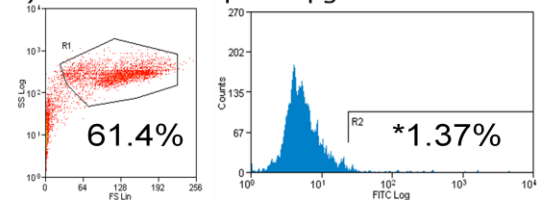
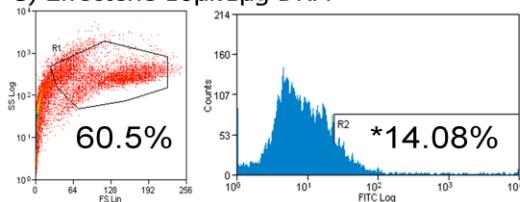
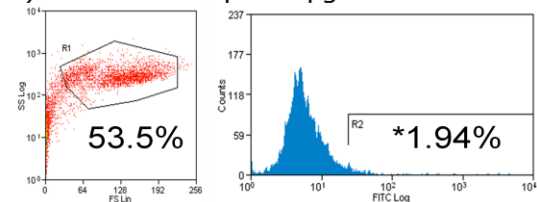
Scatter plots and histograms for Lipofectamine

A) Metafectene 0.4 μ l negative controlE) Metafectene 1 μ l negative controlB) Metafectene 0.4 μ l:0.1 μ g DNAF) Metafectene 1 μ l:0.1 μ g DNAC) Metafectene 0.4 μ l:0.5 μ g DNAG) Metafectene 1 μ l:0.5 μ g DNAD) Metafectene 0.4 μ l:1 μ g DNAH) Metafectene 1 μ l:1 μ g DNA

Scatter plots and histograms for Metafectene

I) Metafectene 2 μ l negative controlM) Metafectene 4 μ l negative controlJ) Metafectene 2 μ l:0.1 μ g DNAN) Metafectene 4 μ l:0.1 μ g DNAK) Metafectene 2 μ l:0.5 μ g DNAO) Metafectene 4 μ l:0.5 μ g DNAL) Metafectene 2 μ l:1 μ g DNAP) Metafectene 4 μ l:1 μ g DNA

Scatter plots and histograms for Metafectene

A) Effectene 5 μ l negative controlD) GeneJuice 0.75 μ l negative controlB) Effectene 5 μ l:1 μ g DNAE) GeneJuice 0.75 μ l:0.25 μ g DNAC) Effectene 10 μ l:1 μ g DNAF) GeneJuice 1.25 μ l:0.25 μ g DNA

Scatter plots and histograms for Effectene and GeneJuice

Appendix VIII

TOPFLASH/FOPFLASH promoter sequence

TOPFLASH TCF-specific promoter:

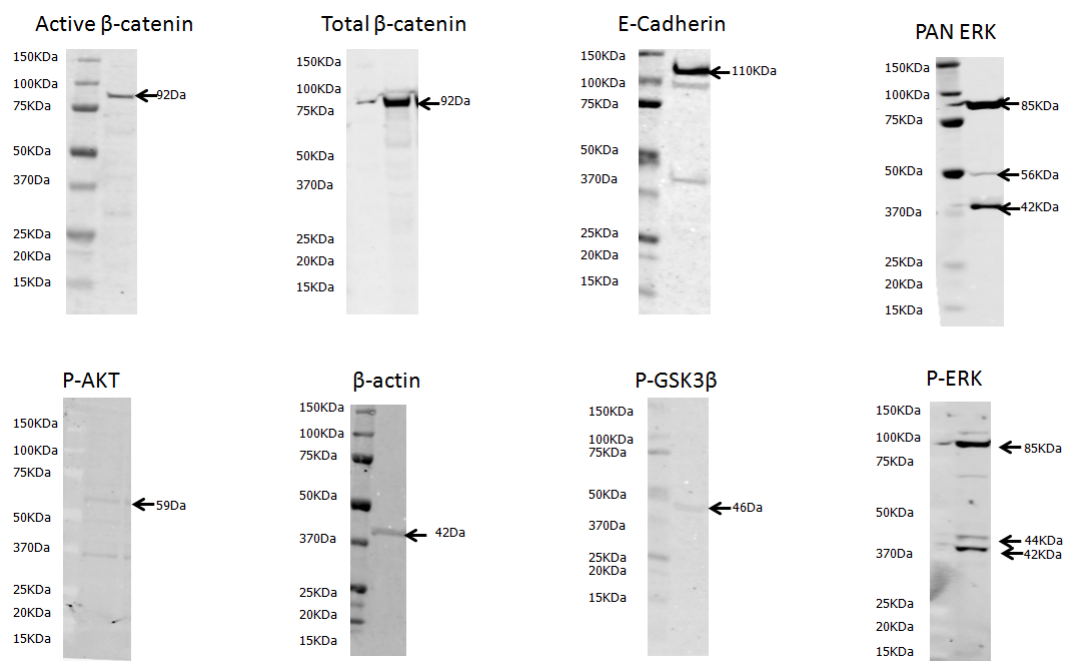
AAGATCAAAGGGGGTAAGATCAAAGGGGGTAAAATCAAAGGGGGCCCCCTTTGATCT
TACCCCTTTGATCTTACCCCTTTGATCTTA

FOPFLASH mutant TCF promoter:

GCCAAAGGGGGTAAGGCCAAAGGGGGTAAGGCCAAAGGGGGCCCCCTTTGGCCTTA
CCCCCTTTGGCCTTACCCCTTTGGCCTT

Appendix IX

Western blots



Western blots for: Active β -catenin (8E7), Total β -catenin(C2206), E-Cadherin (HECD1), PAN-ERK (16), P-AKT (D9E), β -actin, P-GSK3 β (AB30619), P-ERK (D13.14.4E)

Appendix X

β -catenin shRNA sequence

Adapted from (206).

FWD

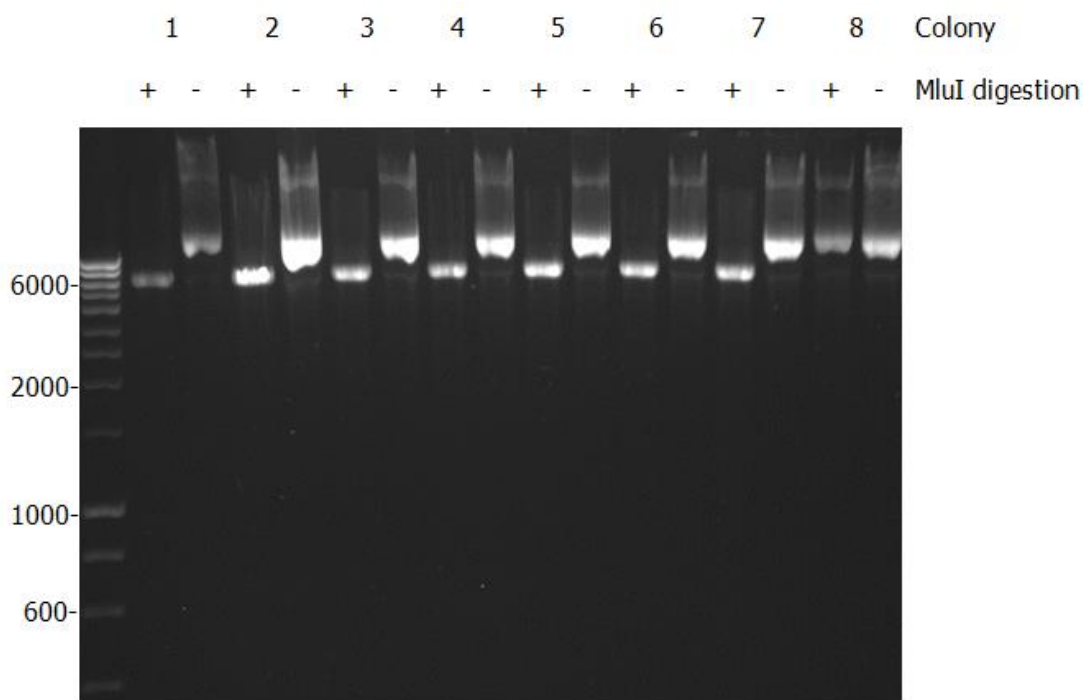
5'gatccAAGTCCTGTATGAGTGGGAACTTCAAGAGAGTTCCCACTCATACAGGACTTT
TTTTTACGCGTg 3'

REV

5'aattcACGCGTAAAAAAAGTCCTGTATGAGTGGGAACTCTCTTGAAGTTCCCACTCA
TACAGGACTTg 3'

Appendix XI

Verification of the β -Catenin shRNA pSIREN RetroQ retroviral vector

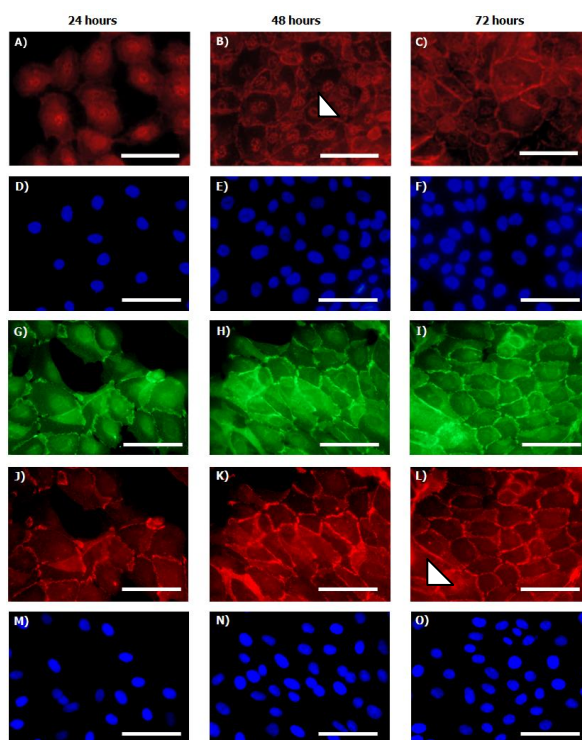


Verification of the β -Catenin shRNA pSIREN RetroQ retroviral vector

An shRNA hairpin was designed, annealed and ligated into the retroviral vector pSIREN RetroQ using the *EcoRI* and *BamHI* restriction sites present in the multiple cloning site (MCS). To verify the presence of the shRNA sequence, plasmid DNA was digested with the restriction enzyme *MluI* and the resulting DNA fragments were separated on an ethidium bromide stained 1% (w/v) agarose gel using gel electrophoresis. Undigested plasmid was run alongside for comparison as well as empty pSIREN RetroQ plasmid (clone 8). Clones carrying the β -catenin shRNA sequence cut with the restriction enzyme *MluI* to give a linear product at 6.4kb. Undigested plasmid and plasmid not containing the shRNA sequence ran as supercoiled DNA above the 10kb marker. DNA marker: Hyperladder I.

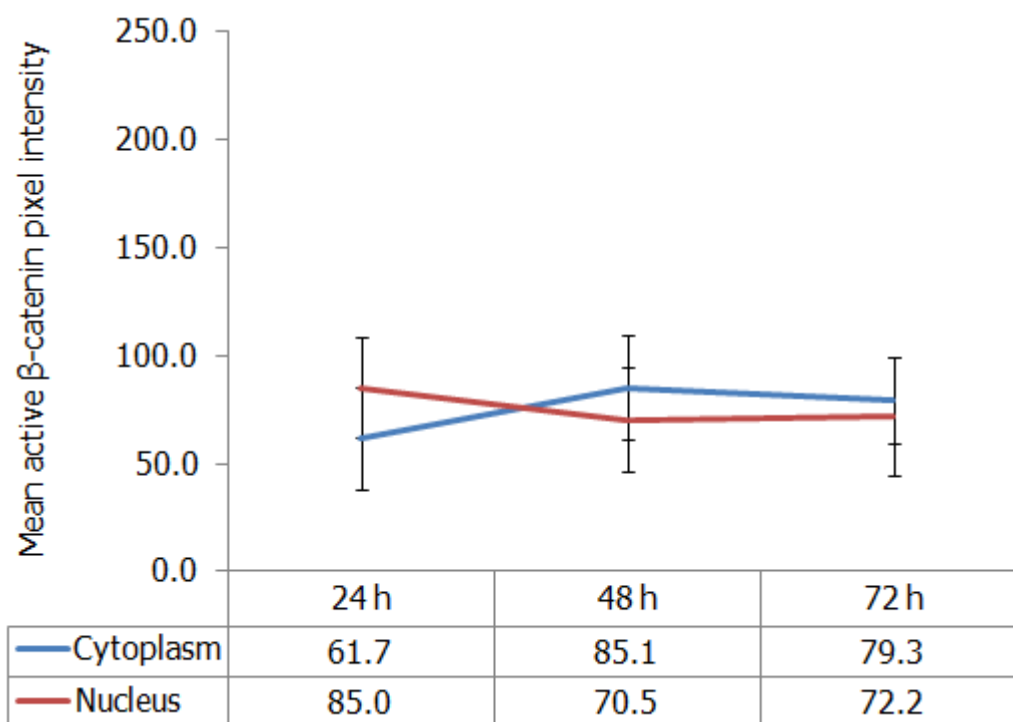
Appendix XII

β -catenin expression in NHU cultured in physiological calcium and PD153035



Expression and localisation of β -catenin in NHU cells cultured in KSFMc supplemented with physiological calcium concentrations and 1 μ M PD153035

NHU cells (Y919) at P4 were cultured for 24 hours, 48 hours and 72 hours in KSFMc+2mM CaCl₂. Slides were fixed and immunolabelled with; active β -catenin antibody (8E7) and rabbit anti-mouse IgG-Alexa 594 secondary antibody, total β -catenin (C2206) and goat anti-rabbit IgG Alexa 488 secondary antibody or E-cadherin antibody (HECD1) and anti-mouse IgG-Alexa 594. All slides were stained with Hoechst 33258 to delineate the nucleus and labelling was visualised under epi-fluorescent illumination. Photo-micrographs are of NHU cells labelled with anti-active β -catenin (A-C) with the corresponding Hoechst stain underneath (D-F), total β -catenin labelling (G-I) and E-cadherin (J-L) with the matched Hoechst staining below (M-O). Scale bar:100 μ M. Arrows denote unusual nuclear labelling with both active and total β -catenin antibodies at 48 hours post seeding.



Quantification of nuclear and cytoplasmic active β -catenin in NHU cells over time when cultured in KSFMc supplemented with physiological calcium concentrations and PD153035

Line graph represents nuclear and cytoplasmic active β -catenin pixel intensities and standard deviations as quantified from each micrograph using Adobe Photoshop[®] software.

Glossary

Abbreviation	
µg	micro gram
µl	micro litre
µM	micro molar
ABS	Adult bovine serum
AJ	Adherens junction
AKT	Murine thymoma viral oncogene (protein kinase B)
AML	Acute Myelogenous Leukaemia
AMP	Ampicillin
APC	Adenomatous Polyposis Coli
Asn	Asparagine
ATP	Adenosine triphosphate
AUM	Asymmetric unit membrane
Bad	BCL2-associated agonist of cell death
BLAST	Basic Local Alignment and Search Tool
bp	Base pair
BPE	Bovine pituitary extract
BrdU	5-bromo-2'-deoxyuridine
BUB1	Budding uninhibited by benzimidazoles 1 homolog
CD	Cluster of Differentiation
CDH1	Epithelial cadherin
CDK	Cyclin-dependant kinase
cDNA	complementary Deoxyribonucleic Acid
CIS	Carcinoma in situ
CK	Cytokeratin
CKI	Casein Kinase Ia
CLDN	Claudin
cm	centimetre
CRD	Cysteine rich domain
CSDA	Cold shock domain protein A
CT	Cholera toxin
Cxs	Connexins
Cys	Cysteine
DEPC	Diethyl Pyrocarbonate
DKK	Dickkopf
DMEM	Dulbecco's Modified Eagle's Medium
DMSO	Dimethylsulphoxide
DNA	Deoxyribonucleic Acid
dNTP	Deoxynucleotide triphosphate
Dsh	Dishevelled

E.coli	Escherichia coli
ECM	Extracellular Matrix
EDTA	Ethylene Diaminetetraacetic Acid
EGF	Epidermal growth factor
EGFR	Epidermal growth factor receptor
ER	Endoplasmic Reticulum
ERK	Extracellular regulated kinase 1/2
FACS	Fluorescence-activated cell sorting
FBS	Fetal bovine serum
FGF	Fibroblast growth factor
FGFR3	Fibroblast growth factor receptor 3
Fzd	Frizzled
g	gram
GAPDH	Glyceraldehyde-3-phosphate dehydrogenase
GDP	guanosine diphosphate
GEF	guanine nucleotide exchange factors
GPCR	G-protein coupled receptors
GSK3β	glycogen synthase kinase 3 β
GTP	guanosine triphosphate
h	hour
HB-EGF	heparin-binding Epidermal growth factor
HBSS	Hank's balance salt solution
HEPES	4-(2-Hydroxyethyl)piperazine-1-ethanesulfonic acid sodium
HGF	Hepatocyte growth factor
Hh	Hedgehog
HPACC	Health Protection Agency Culture Collection
hTERT	Human telomerase
IC	Interstitial Cystitis
IC₅₀	Half maximal inhibitory concentration
ICAT	beta-catenin-interacting protein 1
IGF	Insuli-like growth factor
ILK	Integrin-linked kinase
IRS	Insulin receptor substrate
ISUP	International Society for Urological Pathology
JAK	Janus kinase
JAM	Junctional adhesion molecule
JNK	c-Jun N-terminal kinase
Kb	Kilo base pair
KDa	Kilo Dalton
KIU	Kallikrein inactivating units
KSFM	keratinocyte serum-free medium
KSFMc	keratinocyte serum-free medium (complete)
LB	Luria Broth

LBA	Luria Broth Agar
LEF	lymphoid enhancer-binding factor
LRP	Low density lipoprotein receptor
M	Molar
mAb	Monoclonal antibody
MAGUK	Membrane-associated guanylate kinases
MAPK	Mitogen-activated protein kinases
Me:Ac	Methanol:Acetone
Min	Minute
MKI67	Antigen Ki-67
mL	Millilitre
mM	Millimolar
mRNA	messenger Ribonucleic Acid
mTOR	mechanistic target of rapamycin
MTT	Methylthiazolyldiphenyl-tetrazolium bromide
NFAT	Nuclear factor of activated T-cells
NHU	Normal Human Urothelial cells
NLK	Nemo-like kinase
nM	nanomolar
P	Passage number
pAKT	phospho-activated Murine thymoma viral oncogene
PBS	Phosphate buffered saline
PBSc	Phosphate buffered saline with calcium
PCNA	Proliferating cell nuclear antigen
PCR	Polymerase chain reaction
PD	PD153035
PDK	phosphoinositide dependent kinase-1
pERK	phospho-activated Extracellular regulated kinase 1/2
PGK	Phosphoglycerate kinase
pGSK3	phospho-inhibited glycogen synthase kinase 3 β
PI3K	Phosphatidyl inositol-3 kinase
PIP₂	phosphatidylinositol (4,5) triphosphate
PIP₃	phosphatidylinositol (3,4,5) triphosphate
PLC	Public limited company
PORCN	porcupine homolog
PPARγ	peroxisome proliferator activated receptor- γ
PPRE	peroxisome proliferator response elements
pTEN	phosphatase and tensin homolog
Puro	Puromycin
Raf	Murine leukemia viral oncogene homolog
RAS	Rat sarcoma viral oncogene homolog
Rb	Retinoblastoma
rhEGF	Recombinant human epidermal growth factor

RNA	Ribonucleic Acid
RNase	Ribonuclease
ROR	receptor tyrosine kinase-like orphan receptors
rpm	revolutions per minute
RT	Reverse transcriptase
RTq-PCR	Reverse transcriptase quantitative polymerase chain reaction
RXR	retinoid X receptor α
SC	squamous carcinoma
Ser	Serine
sFrp	Secreted frizzled related protein
SH	Src homologue
Shh	Sonic hedgehog
SMOH	Smoothed
SNAI1	Snail homolog 1
SOS	Son of Sevenless
STAT	signal transducers and activators of transcription
SVX	Ser/Thr-X(any amino acid)-Val motif
TCF	T-cell factor
TGF	Transforming growth factor
TGN	trans-Golgi network
Thr	Threonine
TJ	Tight junction
TNM	Tumor-Nodes-Metastasis
Tyr	Tyrosine
TZ	Troglitazone
UC	urothelial carcinoma
UPK	Uroplakin
UV	Ultra violet
WHO	World Health Organisation
Wif	Wnt inhibitory factor
WLS	Wntless
ZO	Zonular occludin
β-TrCP	β -transducin repeat-containing protein

Bibliography

1. Ellis H. *Clinical anatomy: a revision and applied anatomy for clinical students*. 10th ed. ed. Oxford: Blackwell Science; 2002.
 2. de Groat WC, Yoshimura N. Pharmacology of the lower urinary tract. *Annu Rev Pharmacol Toxicol*. 2001 41:691-721.
 3. de Groat WC. Anatomy and physiology of the lower urinary tract. *Urol Clin North Am*. 1993 20(3):383-401.
 4. Jost SP, Gosling JA, Dixon JS. The morphology of normal human bladder urothelium. *J Anat*. 1989 167:103-15.
 5. Hicks RM. The mammalian urinary bladder: an accommodating organ. *Biol Rev Camb Philos Soc*. 1975 50(2):215-46.
 6. Staack A, Hayward SW, Baskin LS, Cunha GR. Molecular, cellular and developmental biology of urothelium as a basis of bladder regeneration. *Differentiation*. 2005 73(4):121-33.
 7. Southgate J, Kennedy W, Hutton KA, Trejdosiewicz LK. Expression and in vitro regulation of integrins by normal human urothelial cells. *Cell Adhes Commun*. 1995 3(3):231-42.
 8. Wu XR, Manabe M, Yu J, Sun TT. Large scale purification and immunolocalization of bovine uroplakins I, II, and III. Molecular markers of urothelial differentiation. *J Biol Chem*. 1990 265(31):19170-9.
 9. Wu XR, Lin JH, Walz T, Haner M, Yu J, Aebi U, Sun TT. Mammalian uroplakins. A group of highly conserved urothelial differentiation-related membrane proteins. *J Biol Chem*. 1994 269(18):13716-24.
 10. Yu J, Lin JH, Wu XR, Sun TT. Uroplakins Ia and Ib, two major differentiation products of bladder epithelium, belong to a family of four transmembrane domain (4TM) proteins. *J Cell Biol*. 1994 125(1):171-82.
 11. Sun TT, Liang FX, Wu XR. Uroplakins as markers of urothelial differentiation. *Adv Exp Med Biol*. 1999 462(7):103-14.
 12. Lobban ED, Smith BA, Hall GD, Harnden P, Roberts P, Selby PJ, Trejdosiewicz LK, Southgate J. Uroplakin gene expression by normal and neoplastic human urothelium. *Am J Pathol*. 1998 153(6):1957-67.
 13. Deng FM, Liang FX, Tu L, Resing KA, Hu P, Supino M, Hu CC, Zhou G, Ding M, Kreibich G, Sun TT. Uroplakin IIIb, a urothelial differentiation marker, dimerizes with uroplakin Ib as an early step of urothelial plaque assembly. *J Cell Biol*. 2002 159(4):685-94.
 14. Olsburgh J, Harnden P, Weeks R, Smith B, Joyce A, Hall G, Poulson R, Selby P, Southgate J. Uroplakin gene expression in normal human tissues and locally advanced bladder cancer. *J Pathol*. 2003 199(1):41-9.
 15. Wu XR, Medina JJ, Sun TT. Selective interactions of UPIa and UPIb, two members of the transmembrane 4 superfamily, with distinct single transmembrane-domained proteins in differentiated urothelial cells. *J Biol Chem*. 1995 270(50):29752-9.
-

16. Hu CC, Liang FX, Zhou G, Tu L, Tang CH, Zhou J, Kreibich G, Sun TT. Assembly of urothelial plaques: tetraspanin function in membrane protein trafficking. *Mol Biol Cell*. 2005 16(9):3937-50.
 17. Hu P, Deng FM, Liang FX, Hu CM, Auerbach AB, Shapiro E, Wu XR, Kachar B, Sun TT. Ablation of uroplakin III gene results in small urothelial plaques, urothelial leakage, and vesicoureteral reflux. *J Cell Biol*. 2000 151(5):961-72.
 18. Hu P, Meyers S, Liang FX, Deng FM, Kachar B, Zeidel ML, Sun TT. Role of membrane proteins in permeability barrier function: uroplakin ablation elevates urothelial permeability. *Am J Physiol Renal Physiol*. 2002 283(6):F1200-7.
 19. Kong XT, Deng FM, Hu P, Liang FX, Zhou G, Auerbach AB, Genieser N, Nelson PK, Robbins ES, Shapiro E, Kachar B, Sun TT. Roles of uroplakins in plaque formation, umbrella cell enlargement, and urinary tract diseases. *J Cell Biol*. 2004 167(6):1195-204.
 20. Schneeberger EE, Lynch RD. The tight junction: a multifunctional complex. *Am J Physiol Cell Physiol*. 2004 286(6):C1213-28.
 21. Varley CL, Garthwaite MA, Cross W, Hinley J, Trejdosiewicz LK, Southgate J. PPARgamma-regulated tight junction development during human urothelial cytodifferentiation. *J Cell Physiol*. 2006 208(2):407-17.
 22. Southgate J, Harnden P, Trejdosiewicz LK. Cytokeratin expression patterns in normal and malignant urothelium: a review of the biological and diagnostic implications. *Histol Histopathol*. 1999 14(2):657-64.
 23. Achtstatter T, Moll R, Moore B, Franke WW. Cytokeratin polypeptide patterns of different epithelia of the human male urogenital tract: immunofluorescence and gel electrophoretic studies. *J Histochem Cytochem*. 1985 33(5):415-26.
 24. Moll R, Achtstatter T, Becht E, Balcarova-Stander J, Ittensohn M, Franke WW. Cytokeratins in normal and malignant transitional epithelium. Maintenance of expression of urothelial differentiation features in transitional cell carcinomas and bladder carcinoma cell culture lines. *Am J Pathol*. 1988 132(1):123-44.
 25. Moll R, Lowe A, Laufer J, Franke WW. Cytokeratin 20 in human carcinomas. A new histodiagnostic marker detected by monoclonal antibodies. *Am J Pathol*. 1992 140(2):427-47.
 26. Minsky BD, Chlapowski FJ. Morphometric analysis of the translocation of luminal membrane between cytoplasm and cell surface of transitional epithelial cells during the expansion-contraction cycles of mammalian urinary bladder. *J Cell Biol*. 1978 77(3):685-97.
 27. Truschel ST, Ruiz WG, Shulman T, Pilewski J, Sun TT, Zeidel ML, Apodaca G. Primary uroepithelial cultures. A model system to analyze umbrella cell barrier function. *J Biol Chem*. 1999 274(21):15020-9.
 28. Truschel ST, Wang E, Ruiz WG, Leung SM, Rojas R, Lavelle J, Zeidel M, Stoffer D, Apodaca G. Stretch-regulated exocytosis/endocytosis in bladder umbrella cells. *Mol Biol Cell*. 2002 13(3):830-46.
-

29. Fromter E, Diamond J. Route of passive ion permeation in epithelia. *Nat New Biol.* 1972 235(53):9-13.
 30. Parsons CL, Schmidt JD, Pollen JJ. Successful treatment of interstitial cystitis with sodium pentosanpolysulfate. *J Urol.* 1983 130(1):51-3.
 31. Southgate J, Varley CL, Garthwaite MA, Hinley J, Marsh F, Stahlschmidt J, Trejdosiewicz LK, Eardley I. Differentiation potential of urothelium from patients with benign bladder dysfunction. *BJU Int.* 2007 99(6):1506-16.
 32. Limas C. Proliferative state of the urothelium with benign and atypical changes. Correlation with transferrin and epidermal growth factor receptors and blood group antigens. *J Pathol.* 1993 171(1):39-47.
 33. Varley C, Hill G, Pellegrin S, Shaw NJ, Selby PJ, Trejdosiewicz LK, Southgate J. Autocrine regulation of human urothelial cell proliferation and migration during regenerative responses in vitro. *Exp Cell Res.* 2005 306(1):216-29.
 34. Baskin LS, Sutherland RS, Thomson AA, Nguyen HT, Morgan DM, Hayward SW, Hom YK, DiSandro M, Cunha GR. Growth factors in bladder wound healing. *J Urol.* 1997 157(6):2388-95.
 35. Lajtha LG, Gilbert CW, Porteous DD, Alexanian R. Kinetics of a Bone-Marrow Stem-Cell Population. *Ann N Y Acad Sci.* 1964 113:742-52.
 36. Mimeault M, Batra SK. Recent progress on tissue-resident adult stem cell biology and their therapeutic implications. *Stem Cell Rev.* 2008 4(1):27-49.
 37. Nielsen CM, Williams J, van den Brink GR, Lauwers GY, Roberts DJ. Hh pathway expression in human gut tissues and in inflammatory gut diseases. *Lab Invest.* 2004 84(12):1631-42.
 38. van de Wetering M, Sancho E, Verweij C, de Lau W, Oving I, Hurlstone A, van der Horn K, Batlle E, Coudreuse D, Haramis AP, Tjon-Pon-Fong M, Moerer P, van den Born M, Soete G, Pals S, Eilers M, Medema R, Clevers H. The beta-catenin/TCF-4 complex imposes a crypt progenitor phenotype on colorectal cancer cells. *Cell.* 2002 111(2):241-50.
 39. Fierabracci A, Caione P, Di Giovine M, Zavaglia D, Bottazzo GF. Identification and characterization of adult stem/progenitor cells in the human bladder (bladder spheroids): perspectives of application in pediatric surgery. *Pediatr Surg Int.* 2007 23(9):837-9.
 40. Gaisa NT, Graham TA, McDonald SA, Canadillas-Lopez S, Poulson R, Heidenreich A, Jakse G, Tadrous PJ, Knuechel R, Wright NA. The human urothelium consists of multiple clonal units, each maintained by a stem cell. *J Pathol.* 2011 225(2):163-71.
 41. Kurzrock EA, Lieu DK, Degraffenried LA, Chan CW, Isseroff RR. Label-retaining cells of the bladder: candidate urothelial stem cells. *Am J Physiol Renal Physiol.* 2008 294(6):F1415-21.
 42. Shin K, Lee J, Guo N, Kim J, Lim A, Qu L, Mysorekar IU, Beachy PA. Hedgehog/Wnt feedback supports regenerative proliferation of epithelial stem cells in bladder. *Nature.* 2011 472(7341):110-4.
-

43. Chopra B, Hinley J, Oleksiewicz MB, Southgate J. Trans-species comparison of PPAR and RXR expression by rat and human urothelial tissues. *Toxicol Pathol.* 2008 36(3):485-95.
44. CRUK. Cancer statistics UK December 2011. Cancer Research UK; 2011 [updated 2011; cited]; Available from: <http://publications.cancerresearchuk.org/cancerstats/statsincidence/incidence.html>.
45. Mostafa MH, Sheweita SA, O'Connor PJ. Relationship between schistosomiasis and bladder cancer. *Clin Microbiol Rev.* 1999 12(1):97-111.
46. Kamat MR, Kulkarni JN, Tongaonkar HB. Adenocarcinoma of the bladder: study of 14 cases and review of the literature. *Br J Urol.* 1991 68(3):254-7.
47. Eble JN. Pathology and genetics of tumours of the urinary system and male genital organs. Lyon: IARC Press ; Oxford : Oxford University Press [distributor]; 2004.
48. MacLennan GT, Kirkali Z, Cheng L. Histologic grading of noninvasive papillary urothelial neoplasms. *Eur Urol.* 2007 51(4):889-97; discussion 97-8.
49. Sobin LH, Gospodarowicz MK, Wittekind C. TNM classification of malignant tumours. 7th ed. ed. Oxford: Wiley-Blackwell; 2010.
50. Harnden P, Parkinson M. Transitional cell carcinoma of the bladder: diagnosis and prognosis. *Current diagnostic pathology.* 1996 3(1):109-21.
51. Oosterlinck W, Lobel B, Jakse G, Malmstrom PU, Stockle M, Sternberg C. Guidelines on bladder cancer. *Eur Urol.* 2002 41(2):105-12.
52. Bladder cancer:diagnostic criteria. *biomedical journal*; 2011 [updated 2011; cited 01/04/2011]; Available from: <http://bestpractice.bmj.com/best-practice/monograph/980/dignosis/criteria.html>.
53. Spruck CH, 3rd, Ohneseit PF, Gonzalez-Zulueta M, Esrig D, Miyao N, Tsai YC, Lerner SP, Schmutte C, Yang AS, Cote R, et al. Two molecular pathways to transitional cell carcinoma of the bladder. *Cancer Res.* 1994 54(3):784-8.
54. Hartmann A, Schlake G, Zaak D, Hungerhuber E, Hofstetter A, Hofstaedter F, Knuechel R. Occurrence of chromosome 9 and p53 alterations in multifocal dysplasia and carcinoma in situ of human urinary bladder. *Cancer Res.* 2002 62(3):809-18.
55. Knowles MA. What we could do now: molecular pathology of bladder cancer. *Mol Pathol.* 2001 54(4):215-21.
56. Wu XR. Urothelial tumorigenesis: a tale of divergent pathways. *Nat Rev Cancer.* 2005 5(9):713-25.
57. Rieger-Christ KM, Mourtzinos A, Lee PJ, Zaghera RM, Cain J, Silverman M, Libertino JA, Summerhayes IC. Identification of fibroblast growth factor receptor 3 mutations in urine sediment DNA samples complements cytology in bladder tumor detection. *Cancer.* 2003 98(4):737-44.
58. Hart KC, Robertson SC, Donoghue DJ. Identification of tyrosine residues in constitutively activated fibroblast growth factor receptor 3

- involved in mitogenesis, Stat activation, and phosphatidylinositol 3-kinase activation. *Mol Biol Cell*. 2001 12(4):931-42.
59. Cilento BG, Freeman MR, Schneck FX, Retik AB, Atala A. Phenotypic and cytogenetic characterization of human bladder urothelia expanded in vitro. *J Urol*. 1994 152(2 Pt 2):665-70.
60. Freeman MR, Yoo JJ, Raab G, Soker S, Adam RM, Schneck FX, Renshaw AA, Klagsbrun M, Atala A. Heparin-binding EGF-like growth factor is an autocrine growth factor for human urothelial cells and is synthesized by epithelial and smooth muscle cells in the human bladder. *J Clin Invest*. 1997 99(5):1028-36.
61. Bindels EM, van der Kwast TH, Izadifar V, Chopin DK, de Boer WI. Functions of epidermal growth factor-like growth factors during human urothelial reepithelialization in vitro and the role of erbB2. *Urol Res*. 2002 30(4):240-7.
62. Daher A, de Boer WI, El-Marjou A, van der Kwast T, Abbou CC, Thiery JP, Radvanyi F, Chopin DK. Epidermal growth factor receptor regulates normal urothelial regeneration. *Lab Invest*. 2003 83(9):1333-41.
63. Prenzel N, Fischer OM, Streit S, Hart S, Ullrich A. The epidermal growth factor receptor family as a central element for cellular signal transduction and diversification. *Endocr Relat Cancer*. 2001 8(1):11-31.
64. Cantley LC. The phosphoinositide 3-kinase pathway. *Science*. 2002 296(5573):1655-7.
65. Vivanco I, Sawyers CL. The phosphatidylinositol 3-Kinase AKT pathway in human cancer. *Nat Rev Cancer*. 2002 2(7):489-501.
66. Schindler C, Darnell JE, Jr. Transcriptional responses to polypeptide ligands: the JAK-STAT pathway. *Annu Rev Biochem*. 1995 64:621-51.
67. Leaman DW, Leung S, Li X, Stark GR. Regulation of STAT-dependent pathways by growth factors and cytokines. *FASEB J*. 1996 10(14):1578-88.
68. Nelson CM, Chen CS. Cell-cell signaling by direct contact increases cell proliferation via a PI3K-dependent signal. *FEBS Lett*. 2002 514(2-3):238-42.
69. Shapiro L, Fannon AM, Kwong PD, Thompson A, Lehmann MS, Grubel G, Legrand JF, Als-Nielsen J, Colman DR, Hendrickson WA. Structural basis of cell-cell adhesion by cadherins. *Nature*. 1995 374(6520):327-37.
70. Georgopoulos NT, Kirkwood LA, Walker DC, Southgate J. Differential regulation of growth-promoting signalling pathways by E-cadherin. *PLoS One*. 2010 5(10):e13621.
71. Jamora C, Fuchs E. Intercellular adhesion, signalling and the cytoskeleton. *Nat Cell Biol*. 2002 4(4):E101-8.
72. Thievensen I, Seifert HH, Swiatkowski S, Florl AR, Schulz WA. E-cadherin involved in inactivation of WNT/beta-catenin signalling in urothelial carcinoma and normal urothelial cells. *Br J Cancer*. 2003 88(12):1932-8.
73. Garcia del Muro X, Torregrosa A, Munoz J, Castellsague X, Condom E, Vignes F, Arance A, Fabra A, Germa JR. Prognostic value of the expression of E-cadherin and beta-catenin in bladder cancer. *Eur J Cancer*. 2000 36(3):357-62.
-

74. Kashibuchi K, Tomita K, Schalken JA, Kume H, Yamaguchi T, Muto S, Horie S, Kitamura T. The prognostic value of E-cadherin, alpha-, beta-, and gamma-catenin in urothelial cancer of the upper urinary tract. *Eur Urol.* 2006 49(5):839-45; discussion 45.
 75. Nakopoulou L, Zervas A, Gakiopoulou-Givalou H, Constantinides C, Doumanis G, Davaris P, Dimopoulos C. Prognostic value of E-cadherin, beta-catenin, P120ctn in patients with transitional cell bladder cancer. *Anticancer Res.* 2000 20(6B):4571-8.
 76. Shimazui T, Schalken JA, Girolodi LA, Jansen CF, Akaza H, Koiso K, Debruyne FM, Bringuier PP. Prognostic value of cadherin-associated molecules (alpha-, beta-, and gamma-catenins and p120cas) in bladder tumors. *Cancer Res.* 1996 56(18):4154-8.
 77. Kastritis E, Murray S, Kyriakou F, Horti M, Tamvakis N, Kavantzias N, Patsouris ES, Noni A, Legaki S, Dimopoulos MA, Bamias A. Somatic mutations of adenomatous polyposis coli gene and nuclear b-catenin accumulation have prognostic significance in invasive urothelial carcinomas: evidence for Wnt pathway implication. *Int J Cancer.* 2009 124(1):103-8.
 78. Marsit CJ, Karagas MR, Andrew A, Liu M, Danaee H, Schned AR, Nelson HH, Kelsey KT. Epigenetic inactivation of SFRP genes and TP53 alteration act jointly as markers of invasive bladder cancer. *Cancer Res.* 2005 65(16):7081-5.
 79. Urakami S, Shiina H, Enokida H, Kawakami T, Tokizane T, Ogishima T, Tanaka Y, Li LC, Ribeiro-Filho LA, Terashima M, Kikuno N, Adachi H, Yoneda T, Kishi H, Shigeno K, Konety BR, Igawa M, Dahiya R. Epigenetic inactivation of Wnt inhibitory factor-1 plays an important role in bladder cancer through aberrant canonical Wnt/beta-catenin signaling pathway. *Clin Cancer Res.* 2006 12(2):383-91.
 80. Urakami S, Shiina H, Enokida H, Kawakami T, Kawamoto K, Hirata H, Tanaka Y, Kikuno N, Nakagawa M, Igawa M, Dahiya R. Combination analysis of hypermethylated Wnt-antagonist family genes as a novel epigenetic biomarker panel for bladder cancer detection. *Clin Cancer Res.* 2006 12(7 Pt 1):2109-16.
 81. Tang Y, Simoneau AR, Liao WX, Yi G, Hope C, Liu F, Li S, Xie J, Holcombe RF, Journak FA, Mercola D, Hoang BH, Zi X. WIF1, a Wnt pathway inhibitor, regulates SKP2 and c-myc expression leading to G1 arrest and growth inhibition of human invasive urinary bladder cancer cells. *Mol Cancer Ther.* 2009 8(2):458-68.
 82. Ahmad I, Morton JP, Singh LB, Radulescu SM, Ridgway RA, Patel S, Woodgett J, Winton DJ, Taketo MM, Wu XR, Leung HY, Sansom OJ. beta-Catenin activation synergizes with PTEN loss to cause bladder cancer formation. *Oncogene.* 2008 30(2):178-89.
 83. Ahmad I, Patel R, Liu Y, Singh LB, Taketo MM, Wu XR, Leung HY, Sansom OJ. Ras mutation cooperates with beta-catenin activation to drive bladder tumorigenesis. *Cell Death Dis.* 2011 2:e124.
-

84. Southgate J, Hutton KA, Thomas DF, Trejdosiewicz LK. Normal human urothelial cells in vitro: proliferation and induction of stratification. *Lab Invest.* 1994 71(4):583-94.
85. Freshney RI, Freshney MG. *Culture of epithelial cells.* 2nd ed. / editors, R. Ian Freshney and Mary G. Freshney. ed. New York: Wiley-Liss; 2002.
86. Becton-Dickenson. Primaria flasks. 2011 [updated 2011; cited]; Available from: www.bdbiosciences.com/cellculture/surfaces/surfacetypes/tc/jsp.
87. Hutton KA, Trejdosiewicz LK, Thomas DF, Southgate J. Urothelial tissue culture for bladder reconstruction: an experimental study. *J Urol.* 1993 150(2 Pt 2):721-5.
88. Reznikoff CA, Yeager TR, Belair CD, Savelieva E, Puthenveetil JA, Stadler WM. Elevated p16 at senescence and loss of p16 at immortalization in human papillomavirus 16 E6, but not E7, transformed human uroepithelial cells. *Cancer Res.* 1996 56(13):2886-90.
89. Chapman EJ, Hurst CD, Pitt E, Chambers P, Aveyard JS, Knowles MA. Expression of hTERT immortalises normal human urothelial cells without inactivation of the p16/Rb pathway. *Oncogene.* 2006 25(36):5037-45.
90. Georgopoulos NT, Kirkwood LA, Varley CL, MacLaine NJ, Aziz N, Southgate J. Immortalisation of normal human urothelial cells compromises differentiation capacity. *Eur Urol.* 2011 60(1):141-9.
91. Chapman EJ, Kelly G, Knowles MA. Genes involved in differentiation, stem cell renewal, and tumorigenesis are modulated in telomerase-immortalized human urothelial cells. *Mol Cancer Res.* 2008 6(7):1154-68.
92. Scriven SD, Booth C, Thomas DF, Trejdosiewicz LK, Southgate J. Reconstitution of human urothelium from monolayer cultures. *J Urol.* 1997 158(3 Pt 2):1147-52.
93. Varley CL, Stahlschmidt J, Smith B, Stower M, Southgate J. Activation of peroxisome proliferator-activated receptor-gamma reverses squamous metaplasia and induces transitional differentiation in normal human urothelial cells. *Am J Pathol.* 2004 164(5):1789-98.
94. Cross WR, Eardley I, Leese HJ, Southgate J. A biomimetic tissue from cultured normal human urothelial cells: analysis of physiological function. *Am J Physiol Renal Physiol.* 2005 289(2):F459-68.
95. Varley CL, Stahlschmidt J, Lee WC, Holder J, Diggle C, Selby PJ, Trejdosiewicz LK, Southgate J. Role of PPARgamma and EGFR signalling in the urothelial terminal differentiation programme. *J Cell Sci.* 2004 117(Pt 10):2029-36.
96. Willert K, Brown JD, Danenberg E, Duncan AW, Weissman IL, Reya T, Yates JR, 3rd, Nusse R. Wnt proteins are lipid-modified and can act as stem cell growth factors. *Nature.* 2003 423(6938):448-52.
97. Willert KH. Isolation and application of bioactive Wnt proteins. *Methods Mol Biol.* 2008 468:17-29.
98. Capes-Davis A, Theodosopoulos G, Atkin I, Drexler HG, Kohara A, MacLeod RA, Masters JR, Nakamura Y, Reid YA, Reddel RR, Freshney RI.

- Check your cultures! A list of cross-contaminated or misidentified cell lines. *Int J Cancer*. 2010 127(1):1-8.
99. EMBL-EBI, Centre S. Ensembl database. 2000-2011 [updated 2000-2011; cited 2011 01/04/2011]; Available from: www.ensembl.org/index.html.
100. Appliedbiosystems. Guide to Performing Relative Quantitation of Gene Expression Using Real-Time Quantitative PCR. 2011 [updated 2011; cited]; Available from: www.appliedbiosystems.com/cms/group/mcb_support/documents/generaldocuments/cms_042380.pdf.
101. Hubbell E, Liu WM, Mei R. Robust estimators for expression analysis. *Bioinformatics*. 2002 18(12):1585-92.
102. Kirkeby S, Thomsen CE. Quantitative immunohistochemistry of fluorescence labelled probes using low-cost software. *J Immunol Methods*. 2005 301(1-2):102-13.
103. Korinek V, Barker N, Willert K, Molenaar M, Roose J, Wagenaar G, Markman M, Lamers W, Destree O, Clevers H. Two members of the Tcf family implicated in Wnt/beta-catenin signaling during embryogenesis in the mouse. *Mol Cell Biol*. 1998 18(3):1248-56.
104. Huelsken J, Birchmeier W. New aspects of Wnt signaling pathways in higher vertebrates. *Curr Opin Genet Dev*. 2001 11(5):547-53.
105. Peters JM, McKay RM, McKay JP, Graff JM. Casein kinase I transduces Wnt signals. *Nature*. 1999 401(6751):345-50.
106. Song DH, Dominguez I, Mizuno J, Kaut M, Mohr SC, Seldin DC. CK2 phosphorylation of the armadillo repeat region of beta-catenin potentiates Wnt signaling. *J Biol Chem*. 2003 278(26):24018-25.
107. Sun TQ, Lu B, Feng JJ, Reinhard C, Jan YN, Fantl WJ, Williams LT. PAR-1 is a Dishevelled-associated kinase and a positive regulator of Wnt signalling. *Nat Cell Biol*. 2001 3(7):628-36.
108. Li L, Yuan H, Weaver CD, Mao J, Farr GH, 3rd, Sussman DJ, Jonkers J, Kimelman D, Wu D. Axin and Frat1 interact with dvl and GSK, bridging Dvl to GSK in Wnt-mediated regulation of LEF-1. *EMBO J*. 1999 18(15):4233-40.
109. Glinka A, Wu W, Delius H, Monaghan AP, Blumenstock C, Niehrs C. Dickkopf-1 is a member of a new family of secreted proteins and functions in head induction. *Nature*. 1998 391(6665):357-62.
110. Mao B, Wu W, Li Y, Hoppe D, Stannek P, Glinka A, Niehrs C. LDL-receptor-related protein 6 is a receptor for Dickkopf proteins. *Nature*. 2001 411(6835):321-5.
111. Semenov MV, Tamai K, Brott BK, Kuhl M, Sokol S, He X. Head inducer Dickkopf-1 is a ligand for Wnt coreceptor LRP6. *Curr Biol*. 2001 11(12):951-61.
112. Bhanot P, Brink M, Samos CH, Hsieh JC, Wang Y, Macke JP, Andrew D, Nathans J, Nusse R. A new member of the frizzled family from *Drosophila* functions as a Wingless receptor. *Nature*. 1996 382(6588):225-30.
113. Ishitani T, Ninomiya-Tsuji J, Nagai S, Nishita M, Meneghini M, Barker N, Waterman M, Bowerman B, Clevers H, Shibuya H, Matsumoto K. The

- TAK1-NLK-MAPK-related pathway antagonizes signalling between beta-catenin and transcription factor TCF. *Nature*. 1999 399(6738):798-802.
114. Tago K, Nakamura T, Nishita M, Hyodo J, Nagai S, Murata Y, Adachi S, Ohwada S, Morishita Y, Shibuya H, Akiyama T. Inhibition of Wnt signaling by ICAT, a novel beta-catenin-interacting protein. *Genes Dev*. 2000 14(14):1741-9.
115. Whitfield ML, George LK, Grant GD, Perou CM. Common markers of proliferation. *Nat Rev Cancer*. 2006 6(2):99-106.
116. GeneCards. Geneannot.: Weizmann Institute; 2011 [updated 2011; cited 2011 01/04/2011]; Available from: www.genecards.weizmann.ac.il/geneannot/index.shtml.
117. Shiina H, Igawa M, Shigeno K, Terashima M, Deguchi M, Yamanaka M, Ribeiro-Filho L, Kane CJ, Dahiya R. Beta-catenin mutations correlate with over expression of C-myc and cyclin D1 Genes in bladder cancer. *J Urol*. 2002 168(5):2220-6.
118. Fleming J. Regulation of growth and differentiation in human urothelium. York: University of York; 2008.
119. Katoh M. Molecular cloning and characterization of human WNT3. *Int J Oncol*. 2001 19(5):977-82.
120. Kim M, Lee HC, Tsedensodnom O, Hartley R, Lim YS, Yu E, Merle P, Wands JR. Functional interaction between Wnt3 and Frizzled-7 leads to activation of the Wnt/beta-catenin signaling pathway in hepatocellular carcinoma cells. *J Hepatol*. 2008 48(5):780-91.
121. Carmon KS, Loose DS. Secreted frizzled-related protein 4 regulates two Wnt7a signaling pathways and inhibits proliferation in endometrial cancer cells. *Mol Cancer Res*. 2008 6(6):1017-28.
122. Carmon KS, Loose DS. Wnt7a interaction with Fzd5 and detection of signaling activation using a split eGFP. *Biochem Biophys Res Commun*. 2008 368(2):285-91.
123. Mikels AJ, Nusse R. Purified Wnt5a protein activates or inhibits beta-catenin-TCF signaling depending on receptor context. *PLoS Biol*. 2006 4(4):e115.
124. Melchior K, Weiss J, Zaehres H, Kim YM, Lutzko C, Roosta N, Hescheler J, Muschen M. The WNT receptor FZD7 contributes to self-renewal signaling of human embryonic stem cells. *Biol Chem*. 2008 389(7):897-903.
125. Mao B, Wu W, Davidson G, Marhold J, Li M, Mechler BM, Delius H, Hoppe D, Stannek P, Walter C, Glinka A, Niehrs C. Kremen proteins are Dickkopf receptors that regulate Wnt/beta-catenin signalling. *Nature*. 2002 417(6889):664-7.
126. Wu W, Glinka A, Delius H, Niehrs C. Mutual antagonism between dickkopf1 and dickkopf2 regulates Wnt/beta-catenin signalling. *Curr Biol*. 2000 10(24):1611-4.
127. Mao B, Niehrs C. Kremen2 modulates Dickkopf2 activity during Wnt/LRP6 signaling. *Gene*. 2003 302(1-2):179-83.
-

128. Li FQ, Mofunanya A, Harris K, Takemaru K. Chibby cooperates with 14-3-3 to regulate beta-catenin subcellular distribution and signaling activity. *J Cell Biol.* 2008 181(7):1141-54.
129. Gottardi CJ, Gumbiner BM. Role for ICAT in beta-catenin-dependent nuclear signaling and cadherin functions. *Am J Physiol Cell Physiol.* 2004 286(4):C747-56.
130. Li J, Ying J, Fan Y, Wu L, Ying Y, Chan AT, Srivastava G, Tao Q. WNT5A antagonizes WNT/beta-catenin signaling and is frequently silenced by promoter CpG methylation in esophageal squamous cell carcinoma. *Cancer Biol Ther.* 2010 10(6):617-24.
131. Jho EH, Zhang T, Domon C, Joo CK, Freund JN, Costantini F. Wnt/beta-catenin/Tcf signaling induces the transcription of Axin2, a negative regulator of the signaling pathway. *Mol Cell Biol.* 2002 22(4):1172-83.
132. Hughes TA, Brady HJ. E2F1 up-regulates the expression of the tumour suppressor axin2 both by activation of transcription and by mRNA stabilisation. *Biochem Biophys Res Commun.* 2005 329(4):1267-74.
133. Hughes TA, Brady HJ. Cross-talk between pRb/E2F and Wnt/beta-catenin pathways: E2F1 induces axin2 leading to repression of Wnt signalling and to increased cell death. *Exp Cell Res.* 2005 303(1):32-46.
134. Zhang T, Otevrel T, Gao Z, Ehrlich SM, Fields JZ, Boman BM. Evidence that APC regulates survivin expression: a possible mechanism contributing to the stem cell origin of colon cancer. *Cancer Res.* 2001 61(24):8664-7.
135. Howe LR, Watanabe O, Leonard J, Brown AM. Twist is up-regulated in response to Wnt1 and inhibits mouse mammary cell differentiation. *Cancer Res.* 2003 63(8):1906-13.
136. Tetsu O, McCormick F. Beta-catenin regulates expression of cyclin D1 in colon carcinoma cells. *Nature.* 1999 398(6726):422-6.
137. Sansom OJ, Reed KR, van de Wetering M, Muncan V, Winton DJ, Clevers H, Clarke AR. Cyclin D1 is not an immediate target of beta-catenin following Apc loss in the intestine. *J Biol Chem.* 2005 280(31):28463-7.
138. van Tienen FH, Laeremans H, van der Kallen CJ, Smeets HJ. Wnt5b stimulates adipogenesis by activating PPARgamma, and inhibiting the beta-catenin dependent Wnt signaling pathway together with Wnt5a. *Biochem Biophys Res Commun.* 2009 387(1):207-11.
139. Shaw PC, Davies AF, Lau KF, Garcia-Barcelo M, Waye MM, Lovestone S, Miller CC, Anderton BH. Isolation and chromosomal mapping of human glycogen synthase kinase-3 alpha and -3 beta encoding genes. *Genome.* 1998 41(5):720-7.
140. Asuni AA, Hooper C, Reynolds CH, Lovestone S, Anderton BH, Killick R. GSK3alpha exhibits beta-catenin and tau directed kinase activities that are modulated by Wnt. *Eur J Neurosci.* 2006 24(12):3387-92.
141. Kerkela R, Kockeritz L, Macaulay K, Zhou J, Doble BW, Beahm C, Greytak S, Woulfe K, Trivedi CM, Woodgett JR, Epstein JA, Force T, Huggins GS. Deletion of GSK-3beta in mice leads to hypertrophic cardiomyopathy

- secondary to cardiomyoblast hyperproliferation. *J Clin Invest.* 2008 118(11):3609-18.
142. Hoeflich KP, Luo J, Rubie EA, Tsao MS, Jin O, Woodgett JR. Requirement for glycogen synthase kinase-3 β in cell survival and NF- κ B activation. *Nature.* 2000 406(6791):86-90.
143. Meijer L, Flajolet M, Greengard P. Pharmacological inhibitors of glycogen synthase kinase 3. *Trends Pharmacol Sci.* 2004 25(9):471-80.
144. Coghlan MP, Culbert AA, Cross DA, Corcoran SL, Yates JW, Pearce NJ, Rausch OL, Murphy GJ, Carter PS, Roxbee Cox L, Mills D, Brown MJ, Haigh D, Ward RW, Smith DG, Murray KJ, Reith AD, Holder JC. Selective small molecule inhibitors of glycogen synthase kinase-3 modulate glycogen metabolism and gene transcription. *Chem Biol.* 2000 7(10):793-803.
145. Klein PS, Melton DA. A molecular mechanism for the effect of lithium on development. *Proc Natl Acad Sci U S A.* 1996 93(16):8455-9.
146. Ueda M, Ouhtit A, Bito T, Nakazawa K, Lubbe J, Ichihashi M, Yamasaki H, Nakazawa H. Evidence for UV-associated activation of telomerase in human skin. *Cancer Res.* 1997 57(3):370-4.
147. Hoang BH, Kubo T, Healey JH, Yang R, Nathan SS, Kolb EA, Mazza B, Meyers PA, Gorlick R. Dickkopf 3 inhibits invasion and motility of Saos-2 osteosarcoma cells by modulating the Wnt-beta-catenin pathway. *Cancer Res.* 2004 64(8):2734-9.
148. Smith DG, Buffet M, Fenwick AE, Haigh D, Ife RJ, Saunders M, Slingsby BP, Stacey R, Ward RW. 3-Anilino-4-arylmaleimides: potent and selective inhibitors of glycogen synthase kinase-3 (GSK-3). *Bioorg Med Chem Lett.* 2001 11(5):635-9.
149. Ryves WJ, Harwood AJ. Lithium inhibits glycogen synthase kinase-3 by competition for magnesium. *Biochem Biophys Res Commun.* 2001 280(3):720-5.
150. Zhang F, Phiel CJ, Spece L, Gurvich N, Klein PS. Inhibitory phosphorylation of glycogen synthase kinase-3 (GSK-3) in response to lithium. Evidence for autoregulation of GSK-3. *J Biol Chem.* 2003 278(35):33067-77.
151. Davies SP, Reddy H, Caivano M, Cohen P. Specificity and mechanism of action of some commonly used protein kinase inhibitors. *Biochem J.* 2000 351(Pt 1):95-105.
152. Bain J, McLauchlan H, Elliott M, Cohen P. The specificities of protein kinase inhibitors: an update. *Biochem J.* 2003 371(Pt 1):199-204.
153. Tanaka K, Kitagawa Y, Kadowaki T. Drosophila segment polarity gene product porcupine stimulates the posttranslational N-glycosylation of wingless in the endoplasmic reticulum. *J Biol Chem.* 2002 277(15):12816-23.
154. Gonzalez F, Swales L, Bejsovec A, Skaer H, Martinez Arias A. Secretion and movement of wingless protein in the epidermis of the Drosophila embryo. *Mech Dev.* 1991 35(1):43-54.
-

155. Banziger C, Soldini D, Schutt C, Zipperlen P, Hausmann G, Basler K. Wntless, a conserved membrane protein dedicated to the secretion of Wnt proteins from signaling cells. *Cell*. 2006 125(3):509-22.
 156. Bartscherer K, Pelte N, Ingelfinger D, Boutros M. Secretion of Wnt ligands requires Evi, a conserved transmembrane protein. *Cell*. 2006 125(3):523-33.
 157. Komekado H, Yamamoto H, Chiba T, Kikuchi A. Glycosylation and palmitoylation of Wnt-3a are coupled to produce an active form of Wnt-3a. *Genes Cells*. 2007 12(4):521-34.
 158. Kurayoshi M, Yamamoto H, Izumi S, Kikuchi A. Post-translational palmitoylation and glycosylation of Wnt-5a are necessary for its signalling. *Biochem J*. 2007 402(3):515-23.
 159. Desbois-Mouthon C, Cadoret A, Blivet-Van Eggelpeel MJ, Bertrand F, Cherqui G, Perret C, Capeau J. Insulin and IGF-1 stimulate the beta-catenin pathway through two signalling cascades involving GSK-3beta inhibition and Ras activation. *Oncogene*. 2001 20(2):252-9.
 160. Papkoff J, Aikawa M. WNT-1 and HGF regulate GSK3 beta activity and beta-catenin signaling in mammary epithelial cells. *Biochem Biophys Res Commun*. 1998 247(3):851-8.
 161. da Costa LT, He TC, Yu J, Sparks AB, Morin PJ, Polyak K, Laken S, Vogelstein B, Kinzler KW. CDX2 is mutated in a colorectal cancer with normal APC/beta-catenin signaling. *Oncogene*. 1999 18(35):5010-4.
 162. Sutherland C, Leighton IA, Cohen P. Inactivation of glycogen synthase kinase-3 beta by phosphorylation: new kinase connections in insulin and growth-factor signalling. *Biochem J*. 1993 296 (Pt 1):15-9.
 163. Sutherland C, Cohen P. The alpha-isoform of glycogen synthase kinase-3 from rabbit skeletal muscle is inactivated by p70 S6 kinase or MAP kinase-activated protein kinase-1 in vitro. *FEBS Lett*. 1994 338(1):37-42.
 164. Cross DA, Alessi DR, Cohen P, Andjelkovich M, Hemmings BA. Inhibition of glycogen synthase kinase-3 by insulin mediated by protein kinase B. *Nature*. 1995 378(6559):785-9.
 165. Thornton TM, Pedraza-Alva G, Deng B, Wood CD, Aronshtam A, Clements JL, Sabio G, Davis RJ, Matthews DE, Doble B, Rincon M. Phosphorylation by p38 MAPK as an alternative pathway for GSK3beta inactivation. *Science*. 2008 320(5876):667-70.
 166. Stambolic V, Woodgett JR. Mitogen inactivation of glycogen synthase kinase-3 beta in intact cells via serine 9 phosphorylation. *Biochem J*. 1994 303 (Pt 3):701-4.
 167. Morali OG, Delmas V, Moore R, Jeanney C, Thiery JP, Larue L. IGF-II induces rapid beta-catenin relocation to the nucleus during epithelium to mesenchyme transition. *Oncogene*. 2001 20(36):4942-50.
 168. Lu Z, Ghosh S, Wang Z, Hunter T. Downregulation of caveolin-1 function by EGF leads to the loss of E-cadherin, increased transcriptional activity of beta-catenin, and enhanced tumor cell invasion. *Cancer Cell*. 2003 4(6):499-515.
-

169. Ding Q, Xia W, Liu JC, Yang JY, Lee DF, Xia J, Bartholomeusz G, Li Y, Pan Y, Li Z, Bargou RC, Qin J, Lai CC, Tsai FJ, Tsai CH, Hung MC. Erk associates with and primes GSK-3 β for its inactivation resulting in upregulation of beta-catenin. *Mol Cell*. 2005 19(2):159-70.
170. Muller T, Bain G, Wang X, Papkoff J. Regulation of epithelial cell migration and tumor formation by beta-catenin signaling. *Exp Cell Res*. 2002 280(1):119-33.
171. Ji H, Wang J, Nika H, Hawke D, Keezer S, Ge Q, Fang B, Fang X, Fang D, Litchfield DW, Aldape K, Lu Z. EGF-induced ERK activation promotes CK2-mediated disassociation of alpha-Catenin from beta-Catenin and transactivation of beta-Catenin. *Mol Cell*. 2009 36(4):547-59.
172. Sharma M, Chuang WW, Sun Z. Phosphatidylinositol 3-kinase/Akt stimulates androgen pathway through GSK3 β inhibition and nuclear beta-catenin accumulation. *J Biol Chem*. 2002 277(34):30935-41.
173. Ng SS, Mahmoudi T, Danenberg E, Bejaoui I, de Lau W, Korswagen HC, Schutte M, Clevers H. Phosphatidylinositol 3-kinase signaling does not activate the wnt cascade. *J Biol Chem*. 2009 284(51):35308-13.
174. Nishita M, Hashimoto MK, Ogata S, Laurent MN, Ueno N, Shibuya H, Cho KW. Interaction between Wnt and TGF-beta signalling pathways during formation of Spemann's organizer. *Nature*. 2000 403(6771):781-5.
175. Katoh M. Cross-talk of WNT and FGF signaling pathways at GSK3 β to regulate beta-catenin and SNAIL signaling cascades. *Cancer Biol Ther*. 2006 5(9):1059-64.
176. McManus EJ, Sakamoto K, Armit LJ, Ronaldson L, Shpiro N, Marquez R, Alessi DR. Role that phosphorylation of GSK3 plays in insulin and Wnt signalling defined by knockin analysis. *EMBO J*. 2005 24(8):1571-83.
177. Donaldson R, Calder M. Modelling and analysis of biochemical signalling pathway cross-talk. *Electronic Proceedings in Theoretical Computer Science*. 2010 19(1):40-54.
178. Furuse M, Hirase T, Itoh M, Nagafuchi A, Yonemura S, Tsukita S. Occludin: a novel integral membrane protein localizing at tight junctions. *J Cell Biol*. 1993 123(6 Pt 2):1777-88.
179. Furuse M, Fujita K, Hiiragi T, Fujimoto K, Tsukita S. Claudin-1 and -2: novel integral membrane proteins localizing at tight junctions with no sequence similarity to occludin. *J Cell Biol*. 1998 141(7):1539-50.
180. Martin-Padura I, Lostaglio S, Schneemann M, Williams L, Romano M, Fruscella P, Panzeri C, Stoppacciaro A, Ruco L, Villa A, Simmons D, Dejana E. Junctional adhesion molecule, a novel member of the immunoglobulin superfamily that distributes at intercellular junctions and modulates monocyte transmigration. *J Cell Biol*. 1998 142(1):117-27.
181. Fanning AS, Anderson JM. PDZ domains: fundamental building blocks in the organization of protein complexes at the plasma membrane. *J Clin Invest*. 1999 103(6):767-72.
182. Wu X, Hepner K, Castelino-Prabhu S, Do D, Kaye MB, Yuan XJ, Wood J, Ross C, Sawyers CL, Whang YE. Evidence for regulation of the PTEN

- tumor suppressor by a membrane-localized multi-PDZ domain containing scaffold protein MAGI-2. *Proc Natl Acad Sci U S A*. 2000 97(8):4233-8.
183. Balda MS, Garrett MD, Matter K. The ZO-1-associated Y-box factor ZONAB regulates epithelial cell proliferation and cell density. *J Cell Biol*. 2003 160(3):423-32.
184. Herve JC, Bourmeyster N, Sarrouilhe D, Duffy HS. Gap junctional complexes: from partners to functions. *Prog Biophys Mol Biol*. 2007 94(1-2):29-65.
185. Gooding JM, Yap KL, Ikura M. The cadherin-catenin complex as a focal point of cell adhesion and signalling: new insights from three-dimensional structures. *Bioessays*. 2004 26(5):497-511.
186. Chitaev NA, Troyanovsky SM. Adhesive but not lateral E-cadherin complexes require calcium and catenins for their formation. *J Cell Biol*. 1998 142(3):837-46.
187. Koch AW, Manzur KL, Shan W. Structure-based models of cadherin-mediated cell adhesion: the evolution continues. *Cell Mol Life Sci*. 2004 61(15):1884-95.
188. Adams CL, Nelson WJ, Smith SJ. Quantitative analysis of cadherin-catenin-actin reorganization during development of cell-cell adhesion. *J Cell Biol*. 1996 135(6 Pt 2):1899-911.
189. Obama H, Ozawa M. Identification of the domain of alpha-catenin involved in its association with beta-catenin and plakoglobin (gamma-catenin). *J Biol Chem*. 1997 272(17):11017-20.
190. Takeichi M. Morphogenetic roles of classic cadherins. *Curr Opin Cell Biol*. 1995 7(5):619-27.
191. Shibamoto S, Hayakawa M, Takeuchi K, Hori T, Oku N, Miyazawa K, Kitamura N, Takeichi M, Ito F. Tyrosine phosphorylation of beta-catenin and plakoglobin enhanced by hepatocyte growth factor and epidermal growth factor in human carcinoma cells. *Cell Adhes Commun*. 1994 1(4):295-305.
192. Muller T, Choidas A, Reichmann E, Ullrich A. Phosphorylation and free pool of beta-catenin are regulated by tyrosine kinases and tyrosine phosphatases during epithelial cell migration. *J Biol Chem*. 1999 274(15):10173-83.
193. Roura S, Miravet S, Piedra J, Garcia de Herreros A, Dunach M. Regulation of E-cadherin/Catenin association by tyrosine phosphorylation. *J Biol Chem*. 1999 274(51):36734-40.
194. Kinch MS, Clark GJ, Der CJ, Burrridge K. Tyrosine phosphorylation regulates the adhesions of ras-transformed breast epithelia. *J Cell Biol*. 1995 130(2):461-71.
195. Piedra J, Martinez D, Castano J, Miravet S, Dunach M, de Herreros AG. Regulation of beta-catenin structure and activity by tyrosine phosphorylation. *J Biol Chem*. 2001 276(23):20436-43.
196. Piedra J, Miravet S, Castano J, Palmer HG, Heisterkamp N, Garcia de Herreros A, Dunach M. p120 Catenin-associated Fer and Fyn tyrosine kinases regulate beta-catenin Tyr-142 phosphorylation and beta-catenin-alpha-catenin Interaction. *Mol Cell Biol*. 2003 23(7):2287-97.
-

197. Shibamoto S, Higano K, Takada R, Ito F, Takeichi M, Takada S. Cytoskeletal reorganization by soluble Wnt-3a protein signalling. *Genes Cells*. 1998 3(10):659-70.
 198. Hazan RB, Norton L. The epidermal growth factor receptor modulates the interaction of E-cadherin with the actin cytoskeleton. *J Biol Chem*. 1998 273(15):9078-84.
 199. Balsamo J, Arregui C, Leung T, Lilien J. The nonreceptor protein tyrosine phosphatase PTP1B binds to the cytoplasmic domain of N-cadherin and regulates the cadherin-actin linkage. *J Cell Biol*. 1998 143(2):523-32.
 200. Hellberg CB, Burden-Gulley SM, Pietz GE, Brady-Kalnay SM. Expression of the receptor protein-tyrosine phosphatase, PTPmu, restores E-cadherin-dependent adhesion in human prostate carcinoma cells. *J Biol Chem*. 2002 277(13):11165-73.
 201. Nawroth R, Poell G, Ranft A, Kloep S, Samulowitz U, Fachinger G, Golding M, Shima DT, Deutsch U, Vestweber D. VE-PTP and VE-cadherin ectodomains interact to facilitate regulation of phosphorylation and cell contacts. *EMBO J*. 2002 21(18):4885-95.
 202. Lickert H, Bauer A, Kemler R, Stappert J. Casein kinase II phosphorylation of E-cadherin increases E-cadherin/beta-catenin interaction and strengthens cell-cell adhesion. *J Biol Chem*. 2000 275(7):5090-5.
 203. Batlle E, Sancho E, Franci C, Dominguez D, Monfar M, Baulida J, Garcia De Herreros A. The transcription factor snail is a repressor of E-cadherin gene expression in epithelial tumour cells. *Nat Cell Biol*. 2000 2(2):84-9.
 204. Ciruna B, Rossant J. FGF signaling regulates mesoderm cell fate specification and morphogenetic movement at the primitive streak. *Dev Cell*. 2001 1(1):37-49.
 205. Peinado H, Quintanilla M, Cano A. Transforming growth factor beta-1 induces snail transcription factor in epithelial cell lines: mechanisms for epithelial mesenchymal transitions. *J Biol Chem*. 2003 278(23):21113-23.
 206. Deng J, Miller SA, Wang HY, Xia W, Wen Y, Zhou BP, Li Y, Lin SY, Hung MC. beta-catenin interacts with and inhibits NF-kappa B in human colon and breast cancer. *Cancer Cell*. 2002 2(4):323-34.
 207. MacLaine NJ. Growth and survival of normal and paramalignant human urothelial cells. York: University of York; 2005.
 208. Maher MT, Flozak AS, Hartsell AM, Russell S, Beri R, Peled ON, Gottardi CJ. Issues associated with assessing nuclear localization of N-terminally unphosphorylated beta-catenin with monoclonal antibody 8E7. *Biol Direct*. 2009 4:5.
 209. Nelson WJ, Nusse R. Convergence of Wnt, beta-catenin, and cadherin pathways. *Science*. 2004 303(5663):1483-7.
 210. Tan X, Apte U, Micsenyi A, Kotsagrelis E, Luo JH, Ranganathan S, Monga DK, Bell A, Michalopoulos GK, Monga SP. Epidermal growth factor receptor: a novel target of the Wnt/beta-catenin pathway in liver. *Gastroenterology*. 2005 129(1):285-302.
-

211. Yun MS, Kim SE, Jeon SH, Lee JS, Choi KY. Both ERK and Wnt/beta-catenin pathways are involved in Wnt3a-induced proliferation. *J Cell Sci.* 2005 118(Pt 2):313-22.
212. Rottinger E, Besnardeau L, Lepage T. A Raf/MEK/ERK signaling pathway is required for development of the sea urchin embryo micromere lineage through phosphorylation of the transcription factor Ets. *Development.* 2004 131(5):1075-87.
213. Kim D, Rath O, Kolch W, Cho KH. A hidden oncogenic positive feedback loop caused by crosstalk between Wnt and ERK pathways. *Oncogene.* 2007 26(31):4571-9.
214. Almeida M, Han L, Bellido T, Manolagas SC, Kousteni S. Wnt proteins prevent apoptosis of both uncommitted osteoblast progenitors and differentiated osteoblasts by beta-catenin-dependent and -independent signaling cascades involving Src/ERK and phosphatidylinositol 3-kinase/AKT. *J Biol Chem.* 2005 280(50):41342-51.
215. Rijsewijk F, Schuermann M, Wagenaar E, Parren P, Weigel D, Nusse R. The Drosophila homolog of the mouse mammary oncogene int-1 is identical to the segment polarity gene wingless. *Cell.* 1987 50(4):649-57.
216. Nusslein-Volhard C, Wieschaus E. Mutations affecting segment number and polarity in Drosophila. *Nature.* 1980 287(5785):795-801.
217. Reichsman F, Smith L, Cumberland S. Glycosaminoglycans can modulate extracellular localization of the wingless protein and promote signal transduction. *J Cell Biol.* 1996 135(3):819-27.
218. Zhai L, Chaturvedi D, Cumberland S. Drosophila wnt-1 undergoes a hydrophobic modification and is targeted to lipid rafts, a process that requires porcupine. *J Biol Chem.* 2004 279(32):33220-7.
219. Takada R, Satomi Y, Kurata T, Ueno N, Norioka S, Kondoh H, Takao T, Takada S. Monounsaturated fatty acid modification of Wnt protein: its role in Wnt secretion. *Dev Cell.* 2006 11(6):791-801.
220. Kadowaki T, Wilder E, Klingensmith J, Zachary K, Perrimon N. The segment polarity gene porcupine encodes a putative multitransmembrane protein involved in Wingless processing. *Genes Dev.* 1996 10(24):3116-28.
221. Caricasole A, Ferraro T, Rimland JM, Terstappen GC. Molecular cloning and initial characterization of the MG61/PORC gene, the human homologue of the Drosophila segment polarity gene Porcupine. *Gene.* 2002 288(1-2):147-57.
222. van den Heuvel M, Harryman-Samos C, Klingensmith J, Perrimon N, Nusse R. Mutations in the segment polarity genes wingless and porcupine impair secretion of the wingless protein. *EMBO J.* 1993 12(13):5293-302.
223. Kitajewski J, Mason JO, Varmus HE. Interaction of Wnt-1 proteins with the binding protein BiP. *Mol Cell Biol.* 1992 12(2):784-90.
224. Goodman RM, Thombre S, Firtina Z, Gray D, Betts D, Roebuck J, Spana EP, Selva EM. Sprinter: a novel transmembrane protein required for Wg secretion and signaling. *Development.* 2006 133(24):4901-11.
225. Bartscherer K, Boutros M. Regulation of Wnt protein secretion and its role in gradient formation. *EMBO Rep.* 2008 9(10):977-82.

226. Port F, Kuster M, Herr P, Furger E, Banziger C, Hausmann G, Basler K. Wingless secretion promotes and requires retromer-dependent cycling of Wntless. *Nat Cell Biol.* 2008 10(2):178-85.
227. Coudreuse DY, Roel G, Betist MC, Destree O, Korswagen HC. Wnt gradient formation requires retromer function in Wnt-producing cells. *Science.* 2006 312(5775):921-4.
228. Mikels AJ, Nusse R. Wnts as ligands: processing, secretion and reception. *Oncogene.* 2006 25(57):7461-8.
229. Wu CH, Nusse R. Ligand receptor interactions in the Wnt signaling pathway in *Drosophila*. *J Biol Chem.* 2002 277(44):41762-9.
230. Dann CE, Hsieh JC, Rattner A, Sharma D, Nathans J, Leahy DJ. Insights into Wnt binding and signalling from the structures of two Frizzled cysteine-rich domains. *Nature.* 2001 412(6842):86-90.
231. Povelones M, Nusse R. The role of the cysteine-rich domain of Frizzled in Wingless-Armadillo signaling. *EMBO J.* 2005 24(19):3493-503.
232. Nusse R. Wnt Homepage. 1997-2010 [updated 1997-2010; cited 2011]; Available from: www.stanford.edu/group/nusselab/cgi-bin/wnt/.
233. Gazit A, Yaniv A, Bafico A, Pramila T, Igarashi M, Kitajewski J, Aaronson SA. Human frizzled 1 interacts with transforming Wnts to transduce a TCF dependent transcriptional response. *Oncogene.* 1999 18(44):5959-66.
234. Lu W, Yamamoto V, Ortega B, Baltimore D. Mammalian Ryk is a Wnt coreceptor required for stimulation of neurite outgrowth. *Cell.* 2004 119(1):97-108.
235. Wei W, Chua MS, Grepper S, So SK. Soluble Frizzled-7 receptor inhibits Wnt signaling and sensitizes hepatocellular carcinoma cells towards doxorubicin. *Mol Cancer.* 2011 10:16.
236. Niemann S, Zhao C, Pascu F, Stahl U, Aulepp U, Niswander L, Weber JL, Muller U. Homozygous WNT3 mutation causes tetra-amelia in a large consanguineous family. *Am J Hum Genet.* 2004 74(3):558-63.
237. Golan T, Yaniv A, Bafico A, Liu G, Gazit A. The human Frizzled 6 (HFz6) acts as a negative regulator of the canonical Wnt. beta-catenin signaling cascade. *J Biol Chem.* 2004 279(15):14879-88.
238. Cong F, Schweizer L, Varmus H. Wnt signals across the plasma membrane to activate the beta-catenin pathway by forming oligomers containing its receptors, Frizzled and LRP. *Development.* 2004 131(20):5103-15.
239. Lyons JP, Mueller UW, Ji H, Everett C, Fang X, Hsieh JC, Barth AM, McCrea PD. Wnt-4 activates the canonical beta-catenin-mediated Wnt pathway and binds Frizzled-6 CRD: functional implications of Wnt/beta-catenin activity in kidney epithelial cells. *Exp Cell Res.* 2004 298(2):369-87.
240. Nishizuka M, Koyanagi A, Osada S, Imagawa M. Wnt4 and Wnt5a promote adipocyte differentiation. *FEBS Lett.* 2008 582(21-22):3201-5.
241. Kanazawa A, Tsukada S, Kamiyama M, Yanagimoto T, Nakajima M, Maeda S. Wnt5b partially inhibits canonical Wnt/beta-catenin signaling

- pathway and promotes adipogenesis in 3T3-L1 preadipocytes. *Biochem Biophys Res Commun*. 2005 330(2):505-10.
242. Kanazawa A, Tsukada S, Sekine A, Tsunoda T, Takahashi A, Kashiwagi A, Tanaka Y, Babazono T, Matsuda M, Kaku K, Iwamoto Y, Kawamori R, Kikkawa R, Nakamura Y, Maeda S. Association of the gene encoding wingless-type mammary tumor virus integration-site family member 5B (WNT5B) with type 2 diabetes. *Am J Hum Genet*. 2004 75(5):832-43.
243. Winn RA, Marek L, Han SY, Rodriguez K, Rodriguez N, Hammond M, Van Scoyk M, Acosta H, Mirus J, Barry N, Bren-Mattison Y, Van Raay TJ, Nemenoff RA, Heasley LE. Restoration of Wnt-7a expression reverses non-small cell lung cancer cellular transformation through frizzled-9-mediated growth inhibition and promotion of cell differentiation. *J Biol Chem*. 2005 280(20):19625-34.
244. Wang Z, Shu W, Lu MM, Morrisey EE. Wnt7b activates canonical signaling in epithelial and vascular smooth muscle cells through interactions with Fzd1, Fzd10, and LRP5. *Mol Cell Biol*. 2005 25(12):5022-30.
245. Yu J, Carroll TJ, Rajagopal J, Kobayashi A, Ren Q, McMahon AP. A Wnt7b-dependent pathway regulates the orientation of epithelial cell division and establishes the cortico-medullary axis of the mammalian kidney. *Development*. 2009 136(1):161-71.
246. Rajagopal J, Carroll TJ, Guseh JS, Bores SA, Blank LJ, Anderson WJ, Yu J, Zhou Q, McMahon AP, Melton DA. Wnt7b stimulates embryonic lung growth by coordinately increasing the replication of epithelium and mesenchyme. *Development*. 2008 135(9):1625-34.
247. Bui TD, O'Brien T, Crew J, Cranston D, Harris AL. High expression of Wnt7b in human superficial bladder cancer vs invasive bladder cancer. *Br J Cancer*. 1998 77(2):319-24.
248. Saitoh T, Mine T, Katoh M. Up-regulation of WNT8B mRNA in human gastric cancer. *Int J Oncol*. 2002 20(2):343-8.
249. Kirikoshi H, Sekihara H, Katoh M. Expression of WNT14 and WNT14B mRNAs in human cancer, up-regulation of WNT14 by IFN γ and up-regulation of WNT14B by beta-estradiol. *Int J Oncol*. 2001 19(6):1221-5.
250. Carroll TJ, Park JS, Hayashi S, Majumdar A, McMahon AP. Wnt9b plays a central role in the regulation of mesenchymal to epithelial transitions underlying organogenesis of the mammalian urogenital system. *Dev Cell*. 2005 9(2):283-92.
251. Kirikoshi H, Sekihara H, Katoh M. Up-regulation of WNT10A by tumor necrosis factor alpha and *Helicobacter pylori* in gastric cancer. *Int J Oncol*. 2001 19(3):533-6.
252. Adaimy L, Chouery E, Megarbane H, Mroueh S, Delague V, Nicolas E, Belguith H, de Mazancourt P, Megarbane A. Mutation in WNT10A is associated with an autosomal recessive ectodermal dysplasia: the odontonycho-dermal dysplasia. *Am J Hum Genet*. 2007 81(4):821-8.
-

253. Longo KA, Wright WS, Kang S, Gerin I, Chiang SH, Lucas PC, Opp MR, MacDougald OA. Wnt10b inhibits development of white and brown adipose tissues. *J Biol Chem*. 2004 279(34):35503-9.
254. Ugur SA, Tolun A. Homozygous WNT10b mutation and complex inheritance in Split-Hand/Foot Malformation. *Hum Mol Genet*. 2008 17(17):2644-53.
255. Majumdar A, Vainio S, Kispert A, McMahon J, McMahon AP. Wnt11 and Ret/Gdnf pathways cooperate in regulating ureteric branching during metanephric kidney development. *Development*. 2003 130(14):3175-85.
256. Maye P, Zheng J, Li L, Wu D. Multiple mechanisms for Wnt11-mediated repression of the canonical Wnt signaling pathway. *J Biol Chem*. 2004 279(23):24659-65.
257. Fear MW, Kelsell DP, Spurr NK, Barnes MR. Wnt-16a, a novel Wnt-16 isoform, which shows differential expression in adult human tissues. *Biochem Biophys Res Commun*. 2000 278(3):814-20.
258. GeneCards. The GeneCards Human Gene Database. Weizmann Institute; 1996-2012.
259. Spencer GJ, Utting JC, Etheridge SL, Arnett TR, Genever PG. Wnt signalling in osteoblasts regulates expression of the receptor activator of NFkappaB ligand and inhibits osteoclastogenesis in vitro. *J Cell Sci*. 2006 119(Pt 7):1283-96.
260. Hoang BH, Kubo T, Healey JH, Sowers R, Mazza B, Yang R, Huvos AG, Meyers PA, Gorlick R. Expression of LDL receptor-related protein 5 (LRP5) as a novel marker for disease progression in high-grade osteosarcoma. *Int J Cancer*. 2004 109(1):106-11.
261. Qiang YW, Hu B, Chen Y, Zhong Y, Shi B, Barlogie B, Shaughnessy JD, Jr. Bortezomib induces osteoblast differentiation via Wnt-independent activation of beta-catenin/TCF signaling. *Blood*. 2009 113(18):4319-30.
262. Zhang Y, Kuipers AL, Yerges-Armstrong LM, Nestlerode CS, Jin Z, Wheeler VW, Patrick AL, Bunker CH, Zmuda JM. Functional and association analysis of frizzled 1 (FZD1) promoter haplotypes with femoral neck geometry. *Bone*. 2007 46(4):1131-7.
263. Garthwaite MA. The molecular basis of urothelial function in health and disease. York: University of York; 2006.
264. Lustig B, Jerchow B, Sachs M, Weiler S, Pietsch T, Karsten U, van de Wetering M, Clevers H, Schlag PM, Birchmeier W, Behrens J. Negative feedback loop of Wnt signaling through upregulation of conductin/axin2 in colorectal and liver tumors. *Mol Cell Biol*. 2002 22(4):1184-93.
-
-